Mineralogical Magazine, May 2016, Vol. 80(3), pp. 415–545

REVIEW

OPEN ACCESS

A review of the structural architecture of tellurium oxycompounds

A. G. CHRISTY[1], S. J. MILLS[2,*] AND A. R. KAMPF[3]

[1] Research School of Earth Sciences and Department of Applied Mathematics, Research School of Physics and Engineering, Australian National University, Canberra, ACT 2601, Australia
[2] Geosciences, Museum Victoria, GPO Box 666, Melbourne, Victoria 3001, Australia
[3] Mineral Sciences Department, Natural History Museum of Los Angeles County, 900 Exposition Boulevard, Los Angeles, CA 90007, USA

[*Received 24 November 2015; Accepted 23 February 2016; Associate Editor: Mark Welch*]

ABSTRACT

Relative to its extremely low abundance in the Earth's crust, tellurium is the most mineralogically diverse chemical element, with over 160 mineral species known that contain essential Te, many of them with unique crystal structures. We review the crystal structures of 703 tellurium oxysalts for which good refinements exist, including 55 that are known to occur as minerals. The dataset is restricted to compounds where oxygen is the only ligand that is strongly bound to Te, but most of the Periodic Table is represented in the compounds that are reviewed. The dataset contains 375 structures that contain only Te^{4+} cations and 302 with only Te^{6+}, with 26 of the compounds containing Te in both valence states. Te^{6+} was almost exclusively in rather regular octahedral coordination by oxygen ligands, with only two instances each of 4- and 5-coordination. Conversely, the lone-pair cation Te^{4+} displayed irregular coordination, with a broad range of coordination numbers and bond distances. A threshold was applied for Te^{4+}–O links of ~2.45 Å or 0.3 valence units with some flexibility, as a criterion to define strongly bound Te–O polymers and larger structural units. Using this criterion, Te^{4+} cations display one-sided 3-, 4- or 5-coordination by oxygen (with rare examples of coordination numbers 2 and 6). For both valence states of Te, examples are known of Te_mO_n complexes which are monomeric ($m = 1$; neso), noncyclic finite oligomers (soro), rings (cyclo), infinite chains (ino), layers (phyllo) and frameworks (tecto tellurates). There is a clear analogy to the polymerization classes that are known for silicate anions, but the behaviour of Te is much richer than that of Si for several reasons: (1) the existence of two cationic valence states for Te; (2) the occurrence of multiple coordination numbers; (3) the possibility of edge-sharing by TeO_n polyhedra; (4) the possibility for oxygen ligands to be 3-coordinated by Te; and (5) the occurrence of Te_mO_n polymers that are cationic, as well as neutral or anionic. While most compounds contain only one or two symmetrically distinct types of Te atom, Pauling's Fifth Rule is frequently violated, and stoichiometrically simple compounds such as $CaTeO_3$ can have polymorphs with up to 18 distinct Te sites. There is a tendency for local symmetry features such as the threefold axis of a TeO_6 octahedron or the acentric symmetry of a $Te^{4+}O_n$ polyhedron to be inherited by the host structure; the latter in particular can lead to useful physical properties such as nonlinear optical behaviour. We develop for the first time a hierarchical taxonomy of Te-oxysalt structures, based upon (1) valence state of Te; (2) polymerization state of Te_mO_n complexes; (3) polymerization state of larger strongly-bound structural units that include non-Te cations. Structures are readily located and compared within this classification.

KEYWORDS: tellurium, oxysalt, crystal chemistry, polymerization, crystal structure, structural heirarchy.

Introduction

TELLURIUM (Te) is an unusual element in that its cosmic abundance is greater than that of any other

*E-mail: smills@museum.vic.gov.au
DOI: 10.1180/minmag.2016.080.093

element with an atomic number >40, as measured by relative number of atoms in C1 chondrite (Anders and Ebihara, 1982). Nevertheless, Te is one of the rarest elements in the Earth's crust (0.4–10 ppb; Parker, 1967; Levinson, 1974; Govett, 1983; McDonough and Sun, 1995; Reimann and de Caritat, 1998) and also in seawater (up to 0.0009 ppb; Andreae, 1984; Lee and Edmond, 1985). It is thus 3 to 5 orders of magnitude less abundant than other even-number elements that are nearby in the periodic table, such as tin and barium, and is in fact rarer than platinum or gold.

The extreme depletion of Te in the Earth's crust is probably due to its strongly siderophile character at high pressure, which resulted in much primeval Te being sequestered in the core, and the small amounts of Te in the outer layers of the Earth arriving after core formation in a "late veneer" (Wang and Becker, 2013). The extreme scarcity of Te makes it all the more remarkable that there are ~160 Te minerals described from Nature: ~3% of all known species. Christy (2016) showed that most chemical elements show a power-law dependence between their abundance in the Earth's crust and the number of mineral species in which they are essential constituents. Other elements that are major constituents of 150–200 species are much more abundant, such as Ce and Ni, present in the crust at 33 and 105 ppm, respectively, according to Taylor and McLennan (1985). Conversely, if Te followed the typical trend, there would be only seven Te minerals. Tellurium is, in fact, the most extreme example of an element that forms an anomalously large number of distinct species in the Earth's crust. Telluride minerals, containing Te as an anion, are probably best known, and are well studied due to their association with gold in epithermal Au–Te deposits (cf. Cook and Ciobanu, 2005; Ciobanu *et al*., 2006), often related to alkaline magmatism (e.g. Jensen and Barton, 2000). Rare sulfosalts are also known in which cationic Te^{4+} plays a role analogous to As^{3+}, such as the tetrahedrite-group mineral goldfieldite, ideally $Cu_{10}\square_2(TeS_3)_4S$ (Trudu and Knittel, 1998). Hence, Te can adopt either anionic or cationic roles as a chalcophile element, like As and Sb. Also, like those elements, it oxidizes readily to form secondary oxycompounds under near-surface conditions. About half of the known Te minerals are such tellurites and tellurates.

The recent explosion of new secondary mineral species, particularly from Otto Mountain, California, has seen publication of descriptions for 14 new Te minerals from 2010 up to September, 2015 (Kampf *et al*., 2010*a*; Back *et al*., 2011; Housley *et al*., 2011; Pekov *et al*., 2010; Christy *et al*., 2016). This represents the greatest flurry of activity in the study of Te secondary minerals since the 1970s. The majority of these new minerals are also compounds new to inorganic chemistry, and possess new crystal-structure types. Crystal structures are now known for 55 of the ~80 Te oxyminerals. It is of particular interest that the Te oxyanions show a wide range of polymerization, somewhat analogous to silicates: examples range from isolated $[Te^{4+}O_3]^{2-}$ and $[Te^{6+}O_6]^{6-}$ anions to complex three-dimensional frameworks. The analogy to rock-forming silicates is strengthened by the observation that, in a locality with an unusually large number of tellurate species, there appears to be a correlation between polymerization state and both the early or late position of a mineral in the local paragenetic sequence, and the abundance of 'network-modifying' species such as Cu^{2+} (Christy *et al*., 2016).

A search of the Inorganic Crystal Structure Database (ICSD) and recent literature has found good-quality crystal structures for 703 compounds, in all. The number of structures referenced per year for the present study suggests that the rate of synthesis and structure refinement has been increasing through time, and that 40 new compounds and structures per year may now be typical (Fig. 1). Thus, the current interest in both synthetic and natural Te oxycompounds, along with the anomalously large number of the latter, justifies a review of their structural chemistry. It should be noted that new compounds appear in the literature constantly, but we had to stop updating our working list in mid-2015, in order to avoid repeated shuffling of the database and the associated risk of introducing errors.

Examination of the known structures of Te oxycompounds reveals extraordinary diversity due to a combination of factors, namely: (1) Te may occur as Te^{4+} or Te^{6+}, which are of comparable stability under atmospheric conditions, so compounds also occur with both oxidation states coexisting. (2) Te^{6+} is almost invariably octahedrally coordinated by oxygen (Christy and Mills, 2013). The $Te^{6+}O_6$ group is strongly bound, in that the average Te–O bond valence is unity. In contrast, Te^{4+} has a stereoactive lone electron pair, and may adopt a wide range of coordination geometries. Usually, three to four oxygens are strongly bound to form an asymmetric coordination polyhedron, but there may also be several other neighbours at longer distances (Christy and Mills, 2013). (3) As noted above, TeO_n polyhedra polymerize readily to form

https://doi.org/10.1180/minmag.2016.080.093 Published online by Cambridge University Press

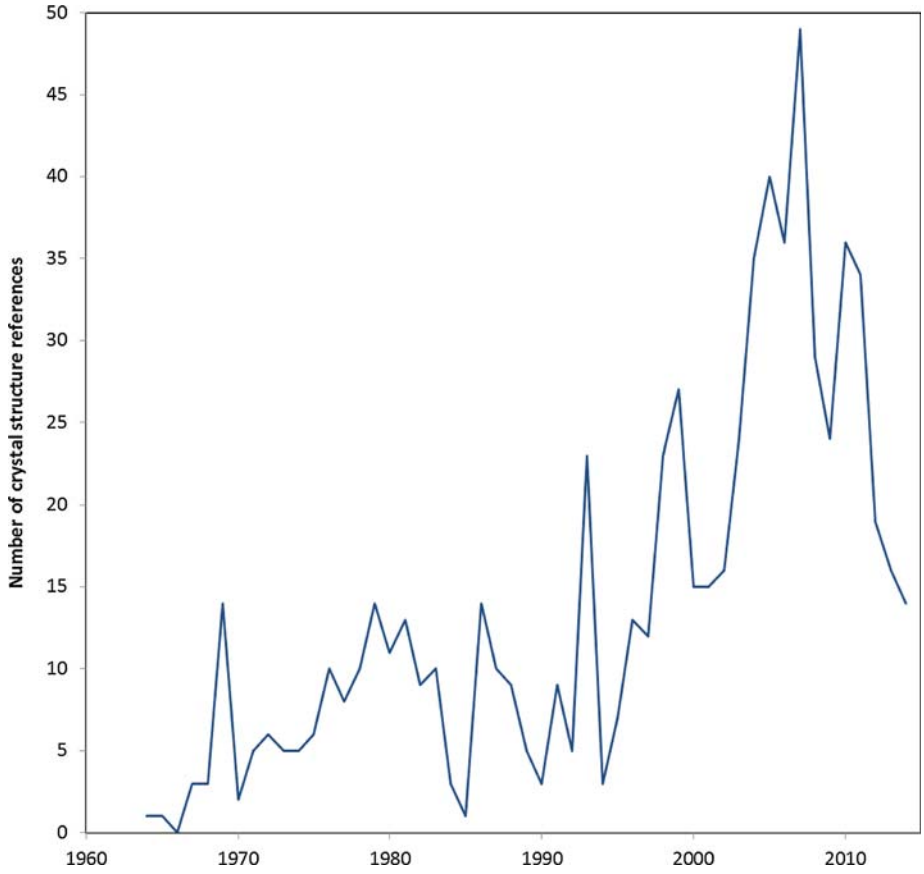

FIG. 1. Number of crystal structure references cited per year for the current study.

oligomers, chains, layers and frameworks. These units also link readily to other strongly-bonding cations to form heteropoly structural building units. (4) The geometries of TeO_n polymers are even more flexible than those of silicates, in that the polymers may contain Te with various coordination numbers, and may carry not just negative or zero net charge, but may also be positively charged in Te 'salts'. For example, a $[Te_2^{4+}O_3OH]^+$ infinite layer cation can be identified in $(Te_2O_3OH)(NO_3)$ (Anderson *et al*., 1980), while the $[Te^{4+}(OH)_3]^+$ ion has been recently identified in the structure of $Na_{11}H[Te(OH)_3]_8[SO_4]_{10}(H_2O)_{13}$ by Mills *et al*. (2016). (5) Te polyhedra readily share edges, as well as corners, in contrast to SiO_4 tetrahedra. (6) Oxygen may be coordinated by three Te^{4+}, as in winstanleyite, $TiTe_3O_8$ (Bindi and Cipriani, 2003). This possibility does not arise in conventional silicates because the short Si–O distance causes strong Si···Si repulsion, although edge-sharing of non-silicon tetrahedra and 3-coordination of oxygen atoms are seen in beryllosilicates and zincosilicates, where the lower cation valence decreases repulsion, and gives a small effective non-bonded radius relative to bond distances (O'Keeffe and Hyde, 1981). The longer bond distances make such geometries possible for Te–O polyhedra as well.

A structural hierarchy for silicates (Bragg, 1930; Zoltai, 1960; Liebau, 1985) is used widely to organize classic textbooks such as Deer *et al*. (1966). More recent schemes, such as those for borate (Hawthorne *et al*., 1996) and sulfate minerals (Hawthorne *et al*., 2000), render intelligible the diversity of these large, complex classes, highlight structure-composition-property relationships and facilitate comparison between species, and also aid in applying group nomenclature (Mills *et al*., 2009*b*). A major objective of the present study is to

https://doi.org/10.1180/minmag.2016.080.093 Published online by Cambridge University Press

create such a structural hierarchy for Te oxycompounds.

In NMR spectroscopy, a concise 'Q notation' to describe polymerization states of silicate species, in which 'Q^n' ($n = 0$–4) designates silicate tetrahedra with n bridging oxygen atoms and, by implication, 4-n non-bridging oxygen atoms (cf. Lippmaa *et al*., 1980). It would be convenient to use a similar notation in the present study for TeO_n polyhedra. However, the original symbology makes the assumptions that (1) the coordination of Si is always 4; (2) the coordination of O by Si is either 1 (non-bridging) or 2 (bridging) and, concomitantly; (3) the number of non-bridging oxygen atoms is the same as the number of next-nearest neighbour Si atoms. For Te, all three of these assumptions are invalid, as they are violated as a result of variable Te coordination number (CN), plus the possibilities of edge-sharing and CN3 oxygen. More information is needed to fully specify the polymerization state of a Te cation, including the numbers of oxygen ligands connected to 1, 2 or 3 Te cations, and the number of edges (i.e. 4-rings, Te–O–Te–O) shared between Te polyhedra. An extended notation Q^{abcz} can do this using four single-digit integers: a = number of CN1 oxygen atoms, b = number of CN2 oxygen atoms, c = number of CN3 oxygen atoms and z = number of shared edges. The total Te CN = $a + b + c$, the corresponding number of oxygen ligands per Te is $a + ½b + ⅓c$, and the number of next-nearest Te atoms is $b + 2c - z$. The original silicate Q^n would be written $Q^{(4-n)n00}$ in the extended notation ($Q^0 \equiv Q^{4000}$, $Q^1 \equiv Q^{3100}$… $Q^4 \equiv Q^{0400}$). Note that $0 \leq z \leq ½p(p-1)$, where $p = b + c$.

A very large number of different Q^{abcz} states can occur. For 4-coordinate Te alone, there are 80 possibilities, and 17 of these are found in the structures of the present study. In order to illustrate the value of the notation, the corresponding topologies are shown very diagrammatically in Fig. 2.

Te–O bond length and polyhedral geometry

'Bond valence' is a parameter that expresses the strength of a chemical bond between a cation and an anion in terms of the effective number of electron pairs involved in bonding. It is thus a generalization of the concept of 'bond order', well entrenched in organic chemistry (IUPAC, 1997), and of the "electrostatic bond strength" of Pauling (1929). The bond-valence model relates bond distance, r, to bond valence, s, for a given cation–anion pair via a smoothly varying function of two parameters. The equation most often used is $r = r_0 - b\ln s$, where: r_0 is the distance at unit bond valence, and b, a 'softness' parameter (Brown and Altermatt, 1985; Brese and O'Keeffe, 1991; Brown, 2002). Bond valences and their sums on a central atom are powerful crystallographic tools for distinguishing species of similar scattering factor, but different valence, and for identifying species such as O^{2-}, OH^- and H_2O and hydrogen bonds when H cannot be located in structure refinements.

While a universal softness value $b = 0.37$ Å is often assumed (e.g. Brown and Altermatt, 1985; Brese and O'Keeffe, 1991), it has become apparent that this does not model the bonding behaviour well for many heavier atoms. Several alternative parametrizations for particular species have been published in recent years [e.g. for Pb^{2+} by Krivovichev and Brown (2001); U^{6+} by Burns *et al*. (1997); Tl^{1+} by Locock and Burns (2004); and Sb^{3+} and Sb^{5+} by Palenik *et al*. (2005), Sidey *et al*. (2009) and Mills *et al*. (2009*a*)], and we examined the available structural data for Te^{4+}–O, Te^{4+}–Cl and Te^{6+}–O bonds in a recent paper (Mills and Christy, 2013). For Te^{4+}–O, we obtained the parameters $r_0 = 1.9605$ Å and $b = 0.41$ Å, while for Te^{6+}–O, we obtained the parameters $r_0 = 1.921$ Å and $b = 0.56$ Å. We considered all Te–O distances out to 3.5 Å as at least weakly bonded. Conversely, Te^{4+} showed a broad distribution of coordination numbers from 3 to 12, with two modes at CN6 and CN8 (fig. 1 in Mills and Christy, 2013). The distribution of Te^{4+}–O bond distances is also bimodal (Fig. 3). Thus, the oxygen neighbours of Te^{4+} separate into two groups: strongly-bound ligands on the opposite side of the Te from its stereoactive lone electron pair, with bond valences typically 0.3–1.3 valence units (vu) (corresponding to a distance of 1.85–2.45 Å), and more distant ligands, with bond valences usually < 0.15 vu (2.74 Å). When three short Te^{4+}–O bonds are present, the $Te^{4+}O_3$ geometry is invariably a rather symmetrical trigonal pyramid, with oxygen atoms at three of the four corners of a tetrahedron, and the lone pair of the Te directed towards the fourth vertex (Fig. 4*a*); any more distant oxygen atoms are on the same side of the Te as the lone pair. An apparently unique alternative to this geometry for 3-coordination is seen in $Nd[Te_2O_5]Br$, where the three Te–O bonds are coplanar, forming a 'T'-shape (Tarasov *et al*., 1996; described as structure **#285** below). $Te^{4+}O_4$ may be either square pyramidal, with four O–Te–O angles approximately equal (Fig. 4*b*), or have the oxygen atoms at the apices and two

https://doi.org/10.1180/minmag.2016.080.093 Published online by Cambridge University Press

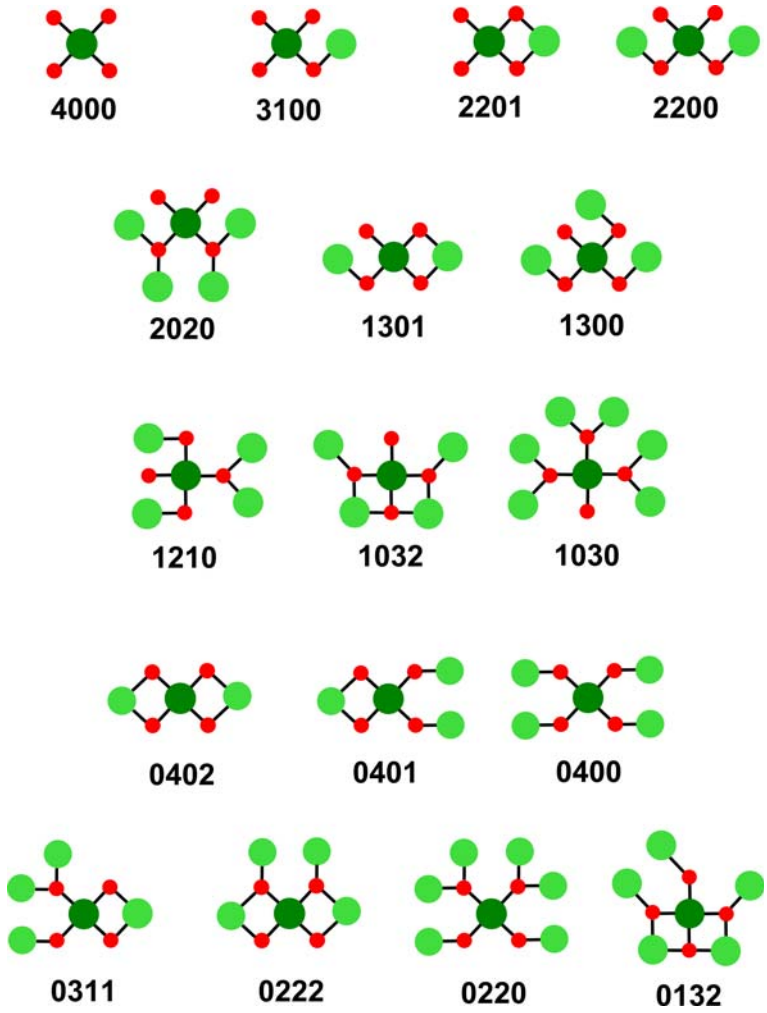

FIG. 2. The 17 distinct Q^{abcz} states that are observed for 4-coordinate Te in this study. The central Te atom is dark green, next-nearest neighbour Te atoms are light green and oxygen atoms are red. Examples of all of these in real structures will be depicted in later figures. In some cases, the topology corresponding to the Q number is not unique: for example, there is a different Q^{0132} configuration to that shown in which an edge is shared between a CN2 oxygen atom and one of the CN3 oxygen atoms.

equatorial positions of a trigonal bipyramid, with the lone pair replacing the missing ligand (Fig. 4*c*). The rarer examples of $Te^{4+}O_5$ approximate octahedra with the lone pair replacing one ligand (Fig. 4*d*).

Subsequent investigation of the $Te^{4+}O_6$ subset of these data by Christy and Mills (2013) showed that, although the Te–O distances within a given polyhedron could show a large variance, the oxygen atoms of a $Te^{4+}O_6$ polyhedron (including long bonds) generally fall very nearly on the surface of a sphere, not centred on the Te, but on a point ~1 Å away from the Te atom, which is consistent with the centre of lone-pair electron density. However, the Te–O distances within a given polyhedron could show a large variance, and the radius of the sphere of oxygen atoms increased linearly with the tellurium lone-pair distance (Christy and Mills, 2013). The volume of the $Te^{4+}O_6$ polyhedron varied, depending on both the sphere radius and the uniformity of the distribution of oxygen atoms over the sphere's surface. The polyhedra ranged in volume from nearly twice that

https://doi.org/10.1180/minmag.2016.080.093 Published online by Cambridge University Press

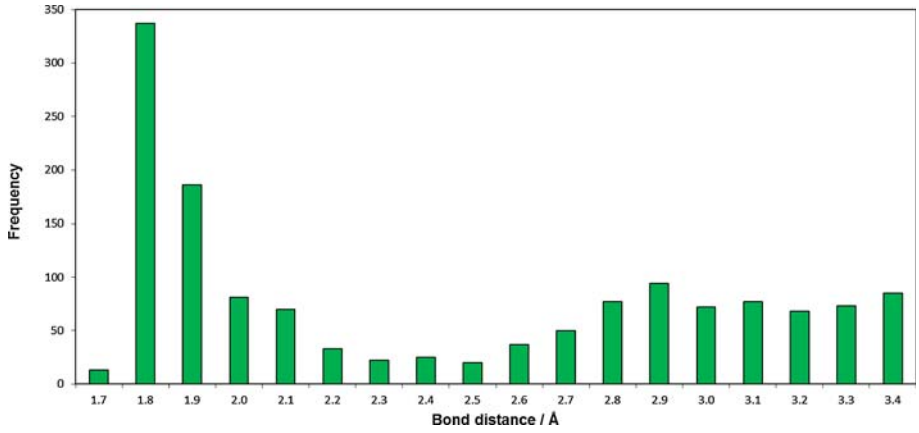

FIG. 3. Overall distribution of Te^{4+}–O bond distances for the data of Mills and Christy (2013).

predicted for a regular $Te^{4+}O_6$ octahedron, when the oxygen atoms are uniformly distributed and the lone pair is highly stereoactive, to 20% less than that of a regular octahedra, when the oxygen atoms are crowded on one side of the sphere. Extreme flexibility in the volume of coordination polyhedron is, thus, another feature of lone-pair cations, such as Te^{4+}, which can contribute to their accommodation in a wide range of crystal structures.

A further unusual feature, occasionally noted, is that bonding interactions of lone-pair cations are not limited to those of the conventional cation–anion type. Christy and Mills (2013) found that the most compressed $Te^{4+}O_6$ polyhedra also showed short distances between the lone pair and large cations, such as K or Ba and/or other Te^{4+} cations, suggesting that weak monopole–dipole (K,Ba)–lone-pair and dipole–dipole Te^{4+}–lone-pair interactions also help to stablize the relevant structures. These non-classical 'bonds' complicate the application of the bond-valence model to structures containing stereoactive lone pairs.

Mills and Christy (2013) verified the strong preference of Te^{6+} for octahedral geometry: that dataset included 100 examples of $Te^{6+}O_6$ octahedra, plus another five where six additional oxygen atoms lay near the cut-off distance, but only 13 examples of other coordinations. Examples of polyhedra with CN4–6 are shown in Fig. 4*e–g*.

The chemical and structural diversity of Te oxycompounds

In the current study, we examine the 703 Te oxycompounds for which good structure refinements are available. Where multiple refinements were available for a compound, one of the better ones was selected. Structures with obvious errors or that were of solid-solution variants of a pure end-member were usually rejected. The dataset includes 55 mineral species, about two-thirds of those described to date.

Chemical constituents

The frequency of occurrence of specific elements as essential constituents in these 703 compounds is shown on periodic tables in Fig. 5. Apart from Te and O, the most common constituents in the mineral species are Cu and Pb (22 out of 55), H (21), Cl (9), Fe (8) and Zn (6). While H, Cu, Cl and Pb are also important in the dataset as a whole, including synthetic compounds (223, 70, 68 and 42 compounds respectively out of 703), many of the latter also include Mo (77), Na (73), K (65), N (49), Ba (48) and P (38). The alkali metals Na and K are common as counteranions in many laboratory-crystallized Te oxysalts; while the number of N compounds is boosted by the analogous use of the ammonium ion, NH_4^+. The anomalously large number of Mo compounds is due to the large number of salts of the tellurohexamolybdate anion, $[Te^{6+}Mo_6^{6+}O_{24}]^{6-}$, that have been prepared, while the majority of P compounds are hydrogen-bonded adducts of $Te(OH)_6$ with alkalis and various phosphate anions.

The large proportion of Cu, Pb and H minerals is consistent with these elements, like Te, showing unusually high mineral diversity (Christy, 2015), and the common association of primary telluride minerals with sulfides of Cu and Pb. It is surprising

https://doi.org/10.1180/minmag.2016.080.093 Published online by Cambridge University Press

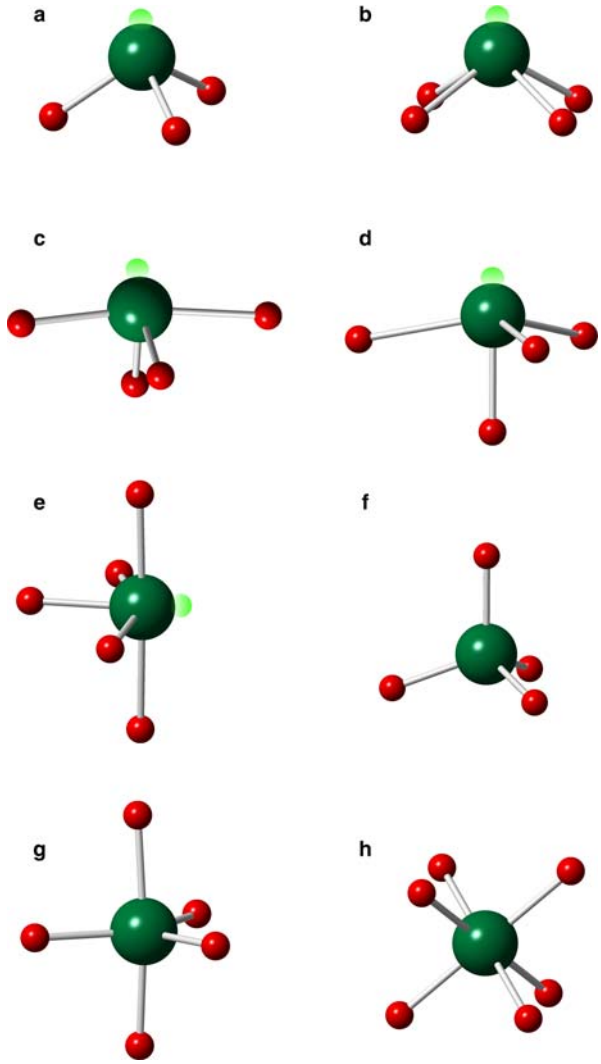

FIG. 4. Monomeric TeO_n anions. Lone-pair electron concentrations on Te^{4+} cations are depicted by small light-green spheres, reflecting their stereochemical role as 'pseudo-anions'. (*a*) $[Te^{4+}O_3]^{2-}$ in teineite, $CuTeO_3 \cdot 2H_2O$ (Effenberger, 1977); (*b*) square pyramidal $[Te^{4+}O_4]^{4-}$ in nabokoite, $K[Cu_7(TeO_4)(SO_4)_5]Cl$ (Pertlik and Zemann, 1988); (*c*) 'trigonal prism-1' coordinated $[Te^{4+}O_4]^{4-}$ in tellurite, TeO_2 (Kholodkovskaya *et al*., 1995); (*d*) Capped trigonal pyramid $[Te^{4+}O_4]^{4-}$ deduced to be a component of a layer anion in $BiTe_2O_5Cl$ (Berdonosov *et al*., 2007); (*e*) 'octahedron-1' coordinated $[Te^{4+}O_5]^{6-}$ in $Ba_2Te(PO_4)_2O$ (Kim *et al*., 2010); (*f*) Tetrahedral $[Te^{6+}O_4]^{2-}$ in Cs_2TeO_4 (Weller *et al*., 1999); (*g*) trigonal bipyramidal $[Te^{6+}O_5]^{4-}$ in $Cs_2K_2TeO_5$ (Untenecker and Hoppe, 1986*a*); and (*h*) octahedral $[Te^{6+}O_6]^{6-}$ in mcalpineite, Cu_3TeO_6 (Falck *et al*., 1978*a*).

that so few secondary Te minerals containing As, Sb and Bi are known, as these are also mineralogically diverse chalcophile elements. Syntheses of many Cu and Pb tellurates were probably attempted because of the importance of such phases as minerals.

Definition of Te^{4+} coordination and structural unit

Mills and Christy (2013) chose 3.5 Å as a cutoff distance for inclusion of weak bonds to oxygen in the Te^{4+} coordination sphere. The corresponding

https://doi.org/10.1180/minmag.2016.080.093 Published online by Cambridge University Press

a

	1	2	3	4	5	6	7	8	9	10	11	12	13	14	15	16	17	18
1	1 H																	2 He
2	3 Li	4 Be											5 B	6 C	7 N	8 O	9 F	10 Ne
3	11 Na	12 Mg											13 Al	14 Si	15 P	16 S	17 Cl	18 Ar
4	19 K	20 Ca	21 Sc	22 Ti	23 V	24 Cr	25 Mn	26 Fe	27 Co	28 Ni	29 Cu	30 Zn	31 Ga	32 Ge	33 As	34 Se	35 Br	36 Kr
5	37 Rb	38 Sr	39 Y	40 Zr	41 Nb	42 Mo	43 Tc	44 Ru	45 Rh	46 Pd	47 Ag	48 Cd	49 In	50 Sn	51 Sb	52 Te	53 I	54 Xe
6	55 Cs	56 Ba	57-71*	72 Hf	73 Ta	74 W	75 Re	76 Os	77 Ir	78 Pt	79 Au	80 Hg	81 Tl	82 Pb	83 Bi	84 Po	85 At	86 Rn
7	87 Fr	88 Ra	89-103 **	104 Rf	105 Db	106 Sg	107 Bh	108 Hs	109 Mt	110 Ds	111 Rg	112 Cn	113 Uut	114 Fl	115 Uup	116 Lv	117 Uus	118 Uuo

6*	57 La	58 Ce	59 Pr	60 Nd	61 Pm	62 Sm	63 Eu	64 Gd	65 Tb	66 Dy	67 Ho	68 Er	69 Tm	70 Yb	71 Lu
7**	89 Ac	90 Th	91 Pa	92 U	93 Np	94 Pu	95 Am	96 Cm	97 Bk	98 Cf	99 Es	100 Fm	101 Md	102 No	103 Lr

Occurs in % of mineral species				
0	< 5%	5–10%	10–20%	20–50%

b

	1	2	3	4	5	6	7	8	9	10	11	12	13	14	15	16	17	18
1	1 H																	2 He
2	3 Li	4 Be											5 B	6 C	7 N	8 O	9 F	10 Ne
3	11 Na	12 Mg											13 Al	14 Si	15 P	16 S	17 Cl	18 Ar
4	19 K	20 Ca	21 Sc	22 Ti	23 V	24 Cr	25 Mn	26 Fe	27 Co	28 Ni	29 Cu	30 Zn	31 Ga	32 Ge	33 As	34 Se	35 Br	36 Kr
5	37 Rb	38 Sr	39 Y	40 Zr	41 Nb	42 Mo	43 Tc	44 Ru	45 Rh	46 Pd	47 Ag	48 Cd	49 In	50 Sn	51 Sb	52 Te	53 I	54 Xe
6	55 Cs	56 Ba	57-71*	72 Hf	73 Ta	74 W	75 Re	76 Os	77 Ir	78 Pt	79 Au	80 Hg	81 Tl	82 Pb	83 Bi	84 Po	85 At	86 Rn
7	87 Fr	88 Ra	89-103 **	104 Rf	105 Db	106 Sg	107 Bh	108 Hs	109 Mt	110 Ds	111 Rg	112 Cn	113 Uut	114 Fl	115 Uup	116 Lv	117 Uus	118 Uuo

6*	57 La	58 Ce	59 Pr	60 Nd	61 Pm	62 Sm	63 Eu	64 Gd	65 Tb	66 Dy	67 Ho	68 Er	69 Tm	70 Yb	71 Lu
7**	89 Ac	90 Th	91 Pa	92 U	93 Np	94 Pu	95 Am	96 Cm	97 Bk	98 Cf	99 Es	100 Fm	101 Md	102 No	103 Lr

Occurs in % of all compounds					
0	< 2%	2–5%	5–10%	10–20%	20–50%

FIG. 5. Periodic table of elements, colour-coded according to the frequency of specific elements as essential constituents in all the crystal structures of this study (above) and in mineral species only (below). All structures include Te and O (black).

https://doi.org/10.1180/minmag.2016.080.093 Published online by Cambridge University Press

bond valence is ~0.023 vu. In contrast, the current study is concerned primarily with the strongest bonds of a structure, which define structural building units. For this study, we divide the 'primary' and 'secondary' Te^{4+}–O bonds at the minimum in the probability distribution between the two modes of Fig. 2. The threshold bond distance is thus 2.40–2.45 Å, corresponding to a bond valence of 0.34–0.30 vu, using the bond-valence parameters of Mills and Christy (2013). Note that this division is consistent with Hawthorne (2014) and references cited therein, who use a bond balance of ~0.30 vu to differentiate, in crystal structures, between the more strongly bound 'structural unit' and weakly bound 'interstitial complex'. The bond-valence threshold identifying bonds that form the structural unit is employed with some flexibility. The smaller divalent octahedral cations Mg, Zn, Fe^{2+} and Mn^{2+}, with bond-valence close to 0.33 vu, are part of the structural unit if they bond to tellurate oxygen atoms. However, for $Cu^{2+}O_{4+2}$ octahedra, elongated due to Jahn-Teller distortion, it was usually the case that only the four shortest bonds were strong enough to be included. Weaker bonds to these small cations were sometimes included, if needed to preserve the integrity of a well-defined coordination polyhedron. Conversely, the larger divalent cations Ca, Sr, Ba and Cd typically occurred with CN > 6 or a mixture of sixfold and higher coordination numbers, and were not generally included, unless they occurred on sites that were occupied by small cations in isostructural compounds. Other large cations with CN ≥ 7 (e.g. REE^{3+}, Zr^{4+} and Th^{4+}) or highly irregular coordination (Pb^{2+} or Bi^{3+}) were similarly excluded from the structural unit, except for $U^{6+}O_n$ polyhedra (n = 6–8). The dimensionality of the heteropoly structural unit was often higher than that of the Te oxyanion alone, as is apparent below.

When long bonds are excluded, the ranges of coordination numbers for the Te–O bonds included in the present study were between 2 and 6 for Te^{4+} and between 4 and 6 for Te^{6+}. The '2-coordinate' Te^{4+} of $Bi_2(TeO_3)_2O$ has additional ligands at just over 2.5 Å (Mercurio *et al*., 1998), while the 6-coordinate examples have the pyrochlore structure type, with Te^{4+} in octahedral coordination (Loopstra and Goubitz, 1986; Weber and Schleid, 2000). The other polyhedra are all of the types shown in Fig. 3 above. For 428 symmetrically distinct $Te^{6+}O_n$ polyhedra, frequencies were 2, 2 and 424 for n = 4, 5 and 6, respectively. For 846 symmetrically distinct $Te^{4+}O_n$ polyhedra, frequencies were 1, 535, 271, 37 and 2 for n = 2, 3, 4, 5 and 6, respectively, although it should be noted that, while the distribution is little changed for Te^{4+}-only compounds (for which the numbers are, respectively, 1, 530, 257, 24, 1), the small sample of mixed-valence compounds show a much greater preference for 4- and 5-coordination (frequencies for CN = 2, 3, 4, 5 and 6 are 0, 5, 14, 13 and 1, respectively).

We have classified the diverse Te-bearing moieties using a set of nested criteria, as follows: (1) Structures are separated into three oxidation-state taxa: those that contain only Te^{4+} as an essential major constituent, those that contain only Te^{6+}, and those that necessarily contain both Te^{4+} and Te^{6+}. (2) Within each oxidation-state taxon, we consider only the Te and its strongly-bound oxygen atoms. The next level of subdivision is on the basis of dimensionality of the Te_mO_n species. By analogy with the silicates (e.g. Deer *et al*., 1966), we use the categories (dimensionality taxa): neso (m = 1), soro (non-cyclic finite groups with m > 1), cyclo (finite groups containing a ring of at least 3 Te), ino (infinite chains), phyllo (infinite layers) and tecto (infinite frameworks). When more than one distinct type of Te_mO_n group is present, the highest-dimensional group with largest m and n determines the classification. (3) Within each dimensionality taxon, species are arranged in an order that facilitates further subdivison, if justified. Cyclo-, ino- and phyllotellurates are first separated depending on whether there is a single or multiple ring/chain/layer. They, along with neso/soro/tecto cases, are then ordered according to the number of Te and anions in the finite complex or, for infinite polymers, the translational repeat unit. (4) Finally, we consider linkage to non-tellurium cations to make larger heteropolymeric 'structural units'.

Note that consistent focus on Te oxyanions sometimes leads to rather counterintuitive divisions between the 'Te oxyanion' and the 'rest of the structural unit'. For example, on the basis of highest-valence bonds, the structure of mroseite, $Ca_2Te_2^{4+}O_4(CO_3)_2$, can be divided into two weakly-bonding Ca^{2+} cations, two carbonate groups and a neutral $[Te_2O_4]^0$ residual complex that consists of a pair of edge-sharing TeO_3 pyramids (cf. Fischer *et al*., 1975). The formula as written above emphasizes this analysis. However, one oxygen atom of each carbonate triangle also links to a Te via a bond that is strong enough to fall within the bond-valence threshold, to make a larger structural unit that is a finite carbonatotellurite cluster $[Te_2C_2O_{10}]^{4-}$. This can be written hierarchically so as to emphasize the carbonate groups, while not showing the full Te coordination, as $[(Te_2O_4)$

https://doi.org/10.1180/minmag.2016.080.093 Published online by Cambridge University Press

$(CO_3)_2]^{4-}$, or alternatively, so as to show the Te coordination, but breaking up the carbonate groups, $[(CO_2)_2(Te_2O_6)]^{4-}$. In the Tables below, mroseite is classified as having an edge-sharing $[Te_2O_6]^{4-}$ dimer, but both versions of the structural formula are used in the tables and text below, depending on context. Other compounds, in which oxygen atoms are shared by Te and other high bond-valence cations, are treated similarly, that is, with more intuitive or compact versions of formulae alongside structural formulae that emphasize Te environments.

Because the C–O links in mroseite have very high bond valence (~1.33 vu), in order to avoid overbonding of the oxygen, the bond from Te to the carbonate oxygen atom is longer and weaker than the other Te–O bonds: 2.313 Å = 0.42 vu using the parameters of Mills and Christy (2013), as opposed to 0.80–1.32 vu for the other Te–O bonds. Similar weak bonding is observed when Te shares an oxygen atom with other high bond-valence cations, and the need to reduce bond valence can increase the Te coordination number. Out of the 24 examples of TeO_5 polyhedra in Te^{4+}-only compounds, 16 (67%) have Te^{4+}–O–P^{5+}, Te^{4+}–O–As^{5+} or Te^{4+}–O–Se^{4+} links, where the non-Te cation makes a bond of 1.25–1.33 vu. Interestingly, Te^{4+} compounds with S^{6+} and V^{5+} do not show the same trend, because they tend instead to have very strongly bonded CN1 oxygen atoms on the non-Te cation, thus reducing the valence of the bond to the bridging oxygen atom.

Crystal structure symmetry and complexity

The Te oxysalts in the present study show a nearly even split between Te valences: the dataset contains 375 structures with Te^{4+} only, 302 with Te^{6+} only, and 26 with Te in both valence states. Interestingly, the distribution of structures between different crystal systems is quite distinct for the different valence states. As shown in Fig. 6, structures with only Te^{4+} are significantly more likely than average to be monoclinic or orthorhombic, and less likely to be trigonal, while the converse is true for structures that have only Te^{6+}. Structures that include both valences are particularly likely to be orthorhombic, while having surprisingly few triclinic examples. These differences suggest that, to a degree, the symmetry of the overall structure inherits (or at least is influenced by) the point symmetry of the Te oxyanion. The low symmetry of coordination polyhedra such as those of Figs 4*c–d* may make low-symmetry Te^{4+} structures more numerous, while TeO_6 octahedra (Fig. 4*h*) are likely to have at least one threefold rotation axis, which enhances the number of trigonal and cubic Te^{6+} phases.

The polarity due to lone-pair stereoactivity in Te^{4+}, in combination with the capacity for local symmetry inheritance by the structure, suggested that there might be a dependence of centrosymmetry on Te valence. However, the percentages of Te^{4+} and Te^{6+} structures lacking a centre of inversion were, respectively, 18.9% (71 out of 375) and 17.5% (53 out of 302), not significantly different from each other or the overall average of 18.6%. A higher proportion of acentric structures did occur for the mixed-valence structures (7 out of 26 = 26.9%), but this is also insignificant, given the small sample size. Further subdivision of the dataset by Te polymerization and coordination number did reveal two small groups with significantly high proportions of acentric structures. This was the case for eight out of 24 of the structures with isolated $Te^{4+}O_{4-5}$ polyhedra and five out of nine structures with mixed-valence layer anions, suggesting that there is a slight tendency to inheritance of polarity.

The structures in the present study markedly violate 'Pauling's Fifth Rule' that "the number of essentially different kinds of constituents in a crystal tends to be small" (Pauling, 1929), although Burdett and McLarnan (1984) noted that there is no *a priori* reason for such parsimony, except as an indirect corollary of some of Pauling's other rules. For both Te^{4+} and Te^{6+}, the average number of symmetrically distinct polyhedra per structure is greater than unity, there being a total of 846 + 428 = 1274 distinct polyhedra for the 703 structures. Fig. 7 shows the percentages of the 375 Te^{4+}-only, 302 Te^{6+}-only and 26 mixed-valence structures that have different numbers of symmetrically distinct Te sites. Structures with larger numbers of distinct sites are generally less numerous, although a quarter of Te^{4+}-only compounds still have between 3 and 5 distinct Te sites. The Te^{4+}-only compounds also include one example each of structures with 9, 10 and 18 distinct Te sites. The last of these is a polymorph of $CaTeO_3$ (Stöger *et al.*, 2009), dramatically demonstrating that simplicity of formula does not imply simplicity of structure.

Detailed tabulation and descriptions of Te oxysalt structures

Te–O complexes

The diversity of Te_mO_n polymers is summarized in Tables 1 through 7, which order the different Te–O

https://doi.org/10.1180/minmag.2016.080.093 Published online by Cambridge University Press

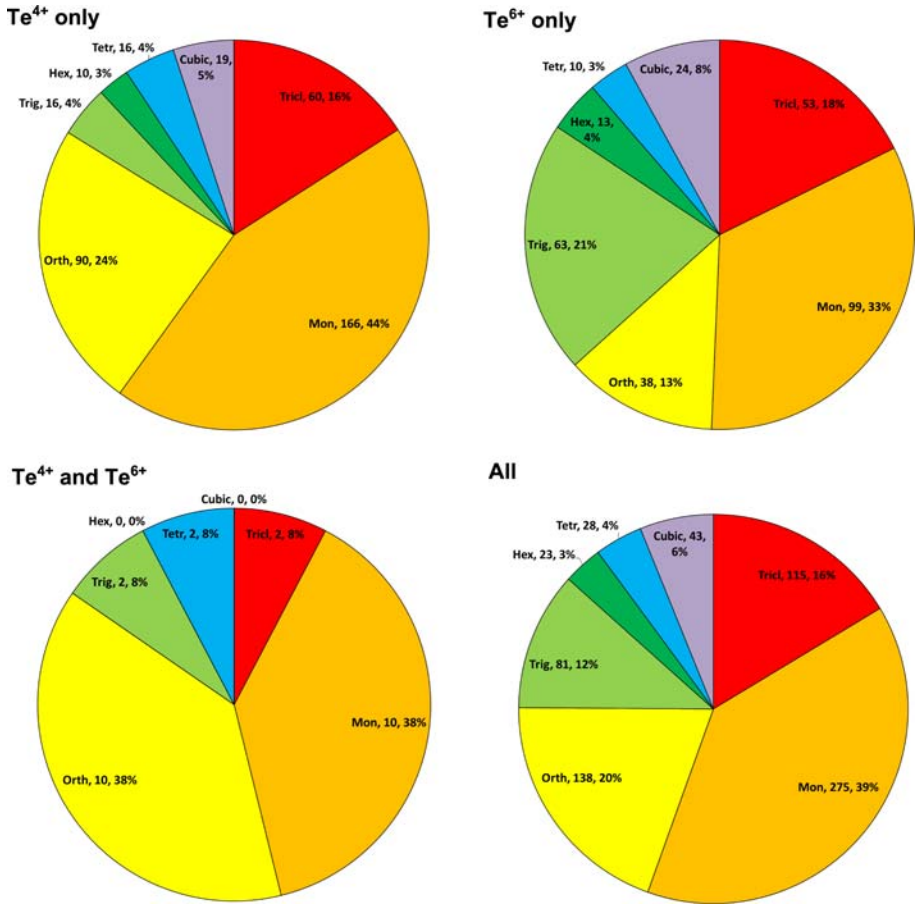

FIG. 6. Distribution of crystal structures among crystal systems for structures with Te^{4+} only, Te^{6+} only, both valences and all structures. Key: Hex = hexagonal; Tetr = tetragonal; Trig = trigonal; Tricl = triclinic; Mon = monoclinic; Orth = orthorhombic.

topologies according to the hierarchical principles given above. These tables serve, additionally, as an index for the listings of individual structures that follow in Tables 8–26. These tables have been deposited with the Principal Editor of *Mineralogical Magazine* and are available from www.minersoc.org/pages/e_journals/dep_mat_mm.html. Note that the tables separate $Te^{6+}X_6$ monomers into two groups: compounds that contain anionic $[TeO_{6-x}(OH)_x]^{(6-x)-}$ groups and those that contain neutral $Te(OH)_6$ molecules which form hydrogen-bonded structures with cations, anions, H_2O and polar organic molecules. For conciseness, specific structures are referenced below by the unique ordinal number that they are assigned in Tables 8–26 (deposited), where the corresponding literature reference is cited. These structure numbers will be prefixed with '#' and highlighted in **boldface**.

The finite oligomeric (soro and cyclo) Te^{4+} oxyanions of Table 1 have the topologies shown in Fig. 8. The numbers of Te atoms in these complexes range from 2 to 8, although the structure number ranges of Table 1 make it clear that some configurations are strongly preferred: we have 20 examples of the trimer Te_3X_8 (Fig. 8*g*), 16 of the simple dimer Te_2X_5 (Fig. 8*a*) and 14 of Te_4X_{11} (Fig. 8*k*). All of these groups are finite linear chains of corner-sharing TeO_n polyhedra, but while the dimer has Te in only 3-coordination, the other common anions show a tendency to alternate between 3-coordinated and 4-coordinated Te, which is also widespread among the less usual polymers (cf. Figs 8*c*,*g*,*j*,*k*,*m*,*o*). Tellurium in five-fold coordination is rare, and seems to be a characteristic of compounds that contain other highly electronegative cations such as P, As and Se (Figs 8*e*, *f*,*i*). Corner-linkage of TeO_n polyhedra through a

https://doi.org/10.1180/minmag.2016.080.093 Published online by Cambridge University Press

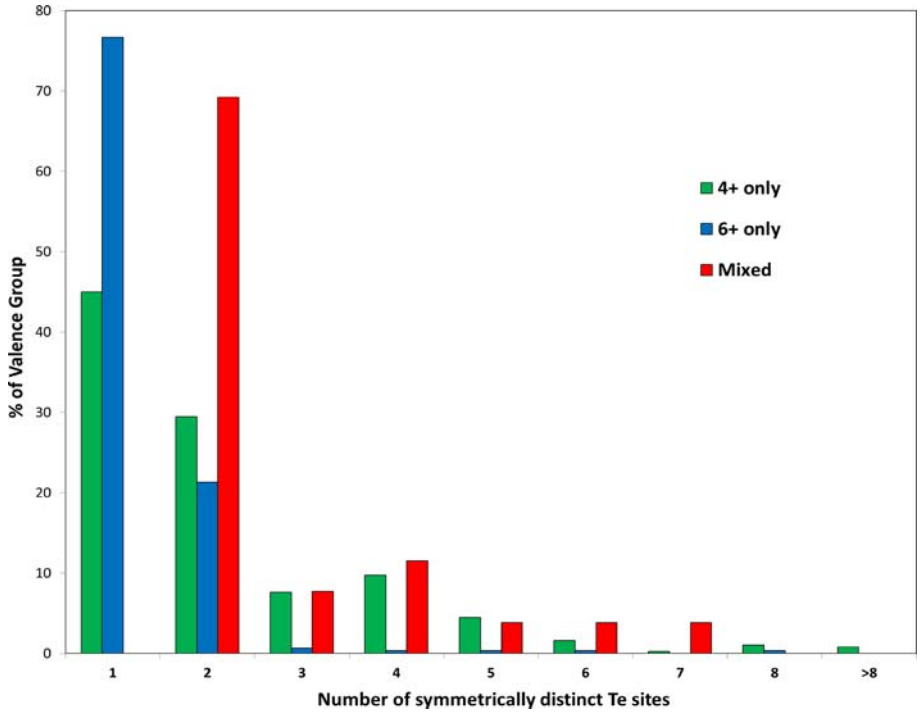

FIG. 7. Frequencies of structures with different numbers of distinct Te sites for Te^{4+}-only, Te^{6+}-only and mixed-valence compounds.

2-coordinate bridging oxygen atom is by far the most common polymerization mechanism, but there are also examples of edge-sharing through two such oxygen atoms (Figs 8*b*,*e*,*j*,*o*) and linkage through 3-coordinate oxygen atoms (Fig. 8*h*). The wide range of possibilities available allows formation of isomers with the same composition, but different topologies – Figs 8*b* and 8*c* provide an example. Most of the polymers are unbranched soro chains, although Fig. 8*l* shows an open-branched pentamer, Fig. 8*n* is a cyclo 6-ring, and Fig. 8*i* defies classification in the scheme of Liebau (1985), because its three CN5 Te atoms are Q^{3111} in our extended Q notation, joined through a mutually shared CN3 oxygen atom, as well as through additional bridging oxygen atoms of the conventional CN2 type.

The increased diversity of Te_mX_n polymer topologies relative to silicates is further evidenced by the chain structures collected in the present study. Single-chain topologies are listed in Table 2 and depicted in Fig. 9. Note that although the first entry in Table 2 appears to be a simple *einer* chain TeX_3 in the terminology of Liebau (1985), with all Te atoms translationally equivalent (**#281**), the bridging oxygen atom is split between two half-occupied positions, suggesting that the crystal structure as published shows an average of disordered *zweier* chains Te_2X_6. The stoichiometrically simplest chain type that occurs is a *zweier* edge-sharing chain of CN4 Te, Te_2X_4. Note that if all cations are Te^{4+} and all *X* are O^{2-}, then this is a neutral complex $[Te_2O_4]^0$ rather than a chain anion, as is the case in the example $Ag(TeO_2)(NO_3)$ of Fig. 2*a* (**#282**). The mineral telluroperite, $Pb_3TeO_4Cl_2 = Pb_2(PbTeO_4)Cl_2$, contains topologically similar chains in which the cations Pb^{2+} and Te^{4+} are disordered in a 1 : 1 ratio to give an anionic chain $[PbTeO_4]^-$ (**#283**).

The most common coordination of Te in the chains is 4. However, CN3 also occurs in Figs 7*b*,*e*, *g*,*h*,*j*,*k*,*m*,*o* and CN5 in Figs 9*d*,*j*,*m*,*n*. Although polymerization is usually achieved through CN2 bridging oxygen atoms, the chains of Figs 9*f* and 9*l* also feature edge-sharing. The repeat unit along the chain backbone is most often 2 (*zweier*), although the chain of Fig. 9*h* is *dreier*, and others are *vierer* (Figs 9*e*,*f*,*j*,*m*,*n*) or *sechser* (Figs 9*k*,*l*,*o*). The chains in Figs 9*i*,*m*,*n*,*o* have open branches, which attach

https://doi.org/10.1180/minmag.2016.080.093 Published online by Cambridge University Press

TABLE 1. Te_mO_n monomers and finite polymers with Te^{4+} only, found in the current study, classified by the most complex Te anion if more than one type is present.

Class	Stoichiometry	Descriptive notes	Fig. #	Structural unit heteropolymerization	Structure #
neso	TeX_3	(trigonal pyramid)	4*a*	none, clusters, chains, layers, frameworks	**1–171**
	TeX_4	(square pyramid)	4*b*	none, layers	**172**
	TeX_4	(trigonal bipyramid -1 ligand)	4*c*	clusters, chains, layers, frameworks	**173–193**
	TeX_5	(octahedron -1 ligand)	4*d*	framework	**194**
soro	Te_2X_5	(Δ–Δ)	8*a*	chains, layers, frameworks	**195–206**
	Te_2X_6	(Δ–◇)	8*b*	none, chains, layers, frameworks	**207–213**
	Te_2X_6	(◇=◇)	8*c*	clusters, chains, layers, frameworks	**214–223**
	Te_2X_7	(◇–◇)	8*d*	layer	**224**
	Te_2X_8	(⌓=⌓)	8*e*	chains	**225–226**
	Te_2X_9	(⌓–⌓)	8*f*	framework	**227**
	Te_3X_8	(Δ–◇–Δ)	8*g*	none, chains, layers, frameworks	**228–247**
	Te_3X_9	(Δ–◇–◇)	8*h*	none	**248**
	Te_3X_{11}	3⌓, CN2 and CN3 bridging O	8*i*	layer	**249**
	Te_4X_{10}	(Δ–◇=◇–Δ)	8*j*	none, layers, frameworks	**250–255**
	Te_4X_{11}	(Δ–◇–◇–Δ)	8*k*	none, layers	**256–273**
	Te_5X_{12}	◇(–Δ)$_4$	8*l*	framework	**274**
	Te_5X_{13}	(Δ–◇–Δ–◇–Δ)	8*n*	none	**275–278**
	$Te_{10}X_{26}$	open-branched decamer	8*o*	framework	**279**
cyclo	Te_6X_{12}	[–Δ–Δ–Δ–Δ–Δ–Δ–]	8*n*	layer	**280**

'*X*' = (O,OH); other symbols are 'Δ' = TeO_3, '◇' = TeO_4, '⌓' = TeO_5, '○' = TeO_6, '–' = corner-sharing, ' = ' = edge-sharing, '[…]' = entities forming closed ring.

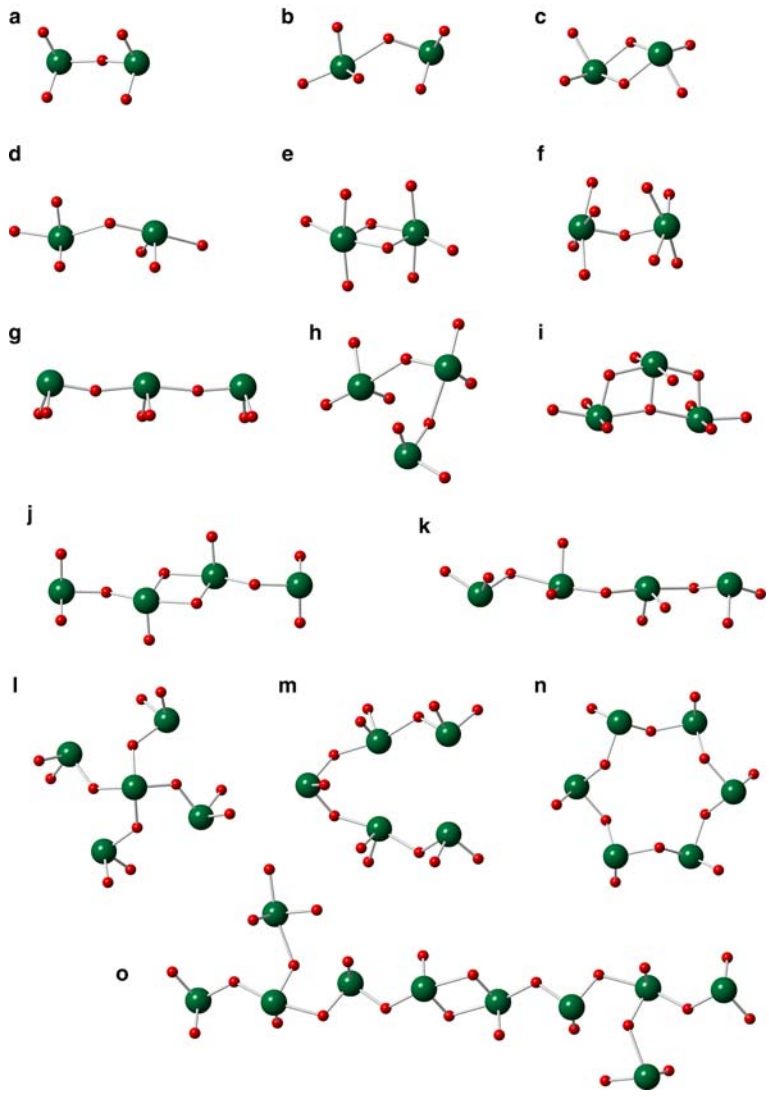

FIG. 8. Finite oxycomplexes containing only Te^{4+}. (*a*) Te_2X_5 (Q^{2100} Te) in $Cs_2Te_2O_5$ (**#195**); (*b*) mixed-coordination corner-sharing Te_2X_6 in poughite, $Fe_2(Te_2O_6)(SO_4) \cdot 3H_2O$ (**#211**); (*c*) four-coordinate edge-sharing Te_2X_6 (Q^{2201}) in $Pb_3(Te_2O_6)Br_2$ (**#215**); (*d*) Te_2X_7 (Q^{3100}) in $BaMo_2(Te_2O_7)O_4 \cdot H_2O$ (**#224**); (*e*) edge-sharing five-coordinate Te_2X_8 (Q^{3201}) in one polymorph of $Te(AsO_3OH)O$ (**#226**); (*f*) corner-sharing five-coordinate Te_2X_9 (Q^{4100}) in $Te_2(PO_4)_2O$ (**#227**); (*g*) Te_3X_8 in $Sr_4(Te_3O_8)Cl_4$ (**#228**); (*h*) Te_3X_9 in $Dy_4(Te_3O_9)(TeO_3)_3$ (**#248**) (*i*) Te_3X_{11} trimer linked through two CN2 and one CN3 bridging oxygen atoms in $Te_3(AsO_4)_2O_3$ (**#254**). The outer Te are Q^{3111} and the central one is Q^{2212}; (*j*) Te_4X_{10} in $Na_2(Te_2O_5) \cdot 2H_2O$ (**#255**); (*k*) Te_4X_{11} in $Yb_2(Te_4O_{11})$ (**#268**); (*l*) Te_5X_{12} open-branched pentamer in $Cu_4(Te_5O_{12})Cl_4$ (**#274**); (*m*) Te_5X_{13} in $Nd_5(Te_5O_{13})(TeO_3)_2(MoO_4)Cl_3$ (**#275**); (*n*) cyclo Te_6X_{12} in $(NH_4)_6[Mo_6(Te_6O_{12})(TeO_3)_2O_{18}][Mo_2O_7] \cdot H_2O$ (**#280**); (*o*) $Te_{10}X_{26}$ in $Nb_8[Te_{10}O_{26}](TeO_3)_6O_8$ (**#279**).

to a Te cation of the chain backbone through CN2 oxygen in most cases, but via a CN3 bridging oxygen for the chain of Fig. 9*i*. Figure 9*j* shows a loop-branched chain, in which a succession of 4-membered rings are united through common vertices.

Overall, the most common chain configurations are corner-sharing types with alternating CN3 and

https://doi.org/10.1180/minmag.2016.080.093 Published online by Cambridge University Press

https://doi.org/10.1180/minmag.2016.080.093 Published online by Cambridge University Press

TABLE 2. Te_mO_n single chains with Te^{4+} only (inotellurites), found in the current study.

Stoichiometry	Descriptive notes	Fig. #	Structural unit heteropolymerization	Structure #
TeX_3	see text	–	framework	**281**
Te_2X_4	(… = ◇ = ◇ = …)	9*a*	none	**282–283**
Te_2X_5	(…–Δ–◇–…)	9*b*	none, frameworks	**284–289**
Te_2X_6	(…–◇–◇–…)	9*c*	chains, layers	**290–298**
Te_2X_8	(…–⬠–⬠–…)	9*d*	frameworks	**299–301**
Te_4X_{10}	(…–Δ–◇–Δ–◇–…)	9*e*	none, chains, layers	**302–306**
Te_4X_{10}	(…–◇–◇–Δ–Δ–…)	9*f*	none	**307**
Te_4X_{10}	(…–◇ = ◇–◇ = ◇–…)	9*g*	frameworks	**308–311**
Te_4X_{10}	(…–(◇–Δ)–(◇–Δ)–…)	9*h*	none	**312**
Te_4X_{10}	(…–(◇–Δ)–◇–Δ–…)	9*i*	chain	**313**
Te_4X_{12}	(…–◇–◇–…) with branches on CN3 oxygen atoms	9*j*	layer	**314**
Te_6X_{14}	loop-branched *vierer* chain with Te CN = 3 and 5	9*k*	framework	**315**
Te_6X_{16}	(…–Δ–◇–◇–Δ–◇–◇–…)	9*l*	none	**316**
Te_6X_{16}	(…–◇–◇ = ◇–◇–◇ = ◇–…)	9*m*	frameworks	**317–322**
Te_6X_{18}	(…–◇–(Δ–⬠)–◇–(Δ–⬠)–…)	9*n*	framework	**323**
Te_6X_{22}	(…–(⬠–⬠)–◇–(⬠–⬠)–◇–…)	9*o*	framework	**324**
Te_8X_{22}	(…–(◇–Δ)–◇–◇–(◇–Δ)–◇–◇–…)	9*p*	none	**325**

Symbols as for Table 1, plus '(…###…)' = ### forming infinite chain, '(…##(#–#)##…)' chain with side branch inside additional parentheses.

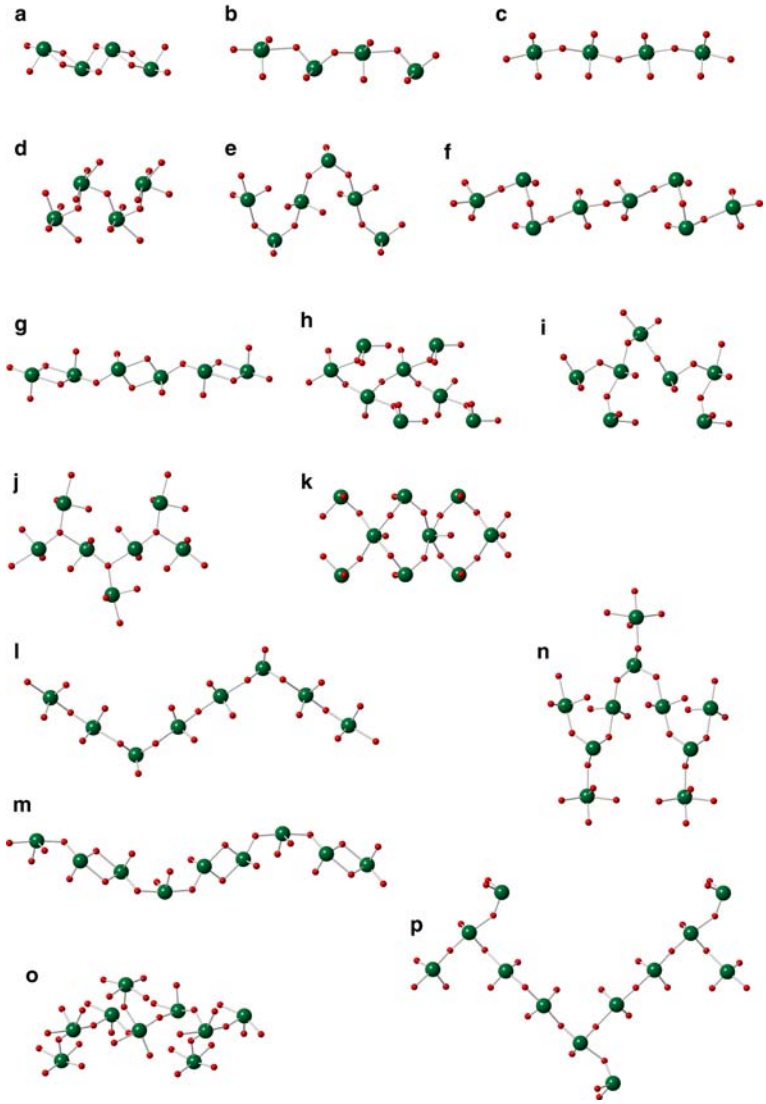

FIG. 9. Single-chain Te–O complexes containing only Te^{4+}. Chains all extend horizontally. The terms *zweier*, *dreier*, *vierer*, *sechser* imply chain backbone repeats of 2, 3, 4 and 6 Te atoms, respectively. The Q state is indicated where it is the same for all Te. More complex structures are discussed in the text. (*a*) Edge-sharing *zweier* Te_2X_4 (Q^{0402}) neutral complex in $Ag(TeO_2)(NO_3)$ (**#282**); (*b*) mixed-coordination corner-sharing *zweier* Te_2X_5 anion in rajite, $Cu(Te_2O_5)$ (**#284**); (*c*) four-coordinate corner-sharing *zweier* Te_2X_6 (Q^{2200}) in schmitterite, $(UO_2)(TeO_3)$ (**#292**); (*d*) five-coordinate *zweier* Te_2X_8 (Q^{3200}) in one of the $TeSeO_4$ dimorphs (**#300**); (*e*) corner-sharing *vierer* Te_4X_{10} in chekhovichite, $Bi_2(Te_2O_5)(TeO_3)_2$ (**#302**); (*f*) different order of CN3 and CN4 Te sharing corners in Te_4X_{10} of $Ho_2(Te_2O_5)Cl$ (**#307**); (*g*) corner- and edge-sharing *vierer* Te_4X_{10} (Q^{1301}) in denningite, $MnMn(Te_4O_{10})$ (**#310**); (*h*) open-branched *zweier* Te_4X_{10} in $K_2(Te_2O_5)$ (**#312**); (*i*) Open-branched *dreier* Te_4X_{10} in $Ba_2V^{5+}(Te_4O_9OH)O_3$ (**#313**); (*j*) open-branched *zweier* Te_4X_{12} with branches attached to CN3 bridging oxygen atoms in $(NH_4)_2W(Te_2O_6)O_2$ (**#314**); (*k*) loop-branched *vierer* Te_6X_{14} in $Ni_2(Te_3O_7)(TeO_3)$ (**#315**); (*l*) mixed-coordination *sechser* Te_6X_{16} in $Pb_2Te_3O_8$ (**#316**); (*m*) corner- and edge-sharing *sechser* Te_6X_{16} in spiroffite, $Mn_2Te_3O_8$ (**#318**); (*n*) open-branched *vierer* Te_6X_{18} in $Fe^{2+}Fe_2^{3+}(Te_3O_9)(TeO_3)$ (**#323**); (*o*) open-branched *vierer* Te_6X_{22} in $Te_3(PO_4)_2O_3$ (**#324**); (*p*) open-branched *sechser* Te_8X_{22} in $Ca_4(Te_4O_{11})(TeO_3)$ (**#325**).

https://doi.org/10.1180/minmag.2016.080.093 Published online by Cambridge University Press

TABLE 3. Te_mO_n multiple chains with Te^{4+} only (inotellurites), found in the current study.

Stoichiometry	Descriptive notes	Fig. #	Structural unit heteropolymerization	Structure #
Double chains				
Te_2X_4	*einer* with CN3 bridging oxygen atoms	10*a*	none	**326**
Te_5X_{12}	*zweier* with one CN3 oxygen and one chain loop-branched	10*b*	none	**327**
Te_6X_{14}	*zweier* open-branched chains	10*c*		**328–329**
Te_6X_{14}	*zweier* chains linked through (–◇ = ◇–) pair	10*d*	none	**330**
	dreier chains	10*e*	framework	**331**
Te_6X_{16}				
Te_8X_{18}	*zweier* chains linked through Te_4 double-triangle	10*f*	none	**332**
Triple chains				
Te_8X_{24}	*zweier* chains; outer two are open-branched	10*g*	layer	**333**
Quadruple chains				
$Te_{12}X_{26}$	outer chains are *zweier*, inner pair are *dreier* and share edges to make Te_4 double-triangles; CN3 oxygen atoms link extra Te to outer chains	10*h*	none	**334**

CN4 (eight instances of the *zweier* chain of Fig. 9*b*, four of the *vierer* chain of Fig. 9*e*) and CN4 chains with regularly-spaced edge-sharing links (four examples of the denningite-type *vierer* chain of Fig. 9*f* and six of the spiroffite-type *sechser* chain of Fig. 9*l*). Topographic isomers are common: the four different configurations Figs 9*e–h* all have the same Te_4X_{10} stoichiometry.

A chain is defined as multiple if it is possible to selectively remove some Te–O links so as to break it into two or more subchains that themselves remain continuous. The dataset of this study contains several types of double chain, as well as a triple chain and even a quadruple chain. These are listed in Table 3, and depicted in Fig. 10.

The simplest double chain found in this study is the uncharged *einer* double chain Te_2O_4 of $Bi_3(Te_2O_4)(TeO_3)_2Cl_5$ (**#326**). The bridging oxygen atoms of each subchain make a third Te–O bond, linking the two subchains together (Fig. 10*a*), to make a chain of Q^{1032} Te polyhedra that is almost an infinitely extended homologue of the finite trimer in Fig. 8*i*. All but one of the other multiple chains have *zweier* periodicity along the chain length, but show a remarkable range of complexity in the connection patterns between chains. One of the two inequivalent subchains of Fig. 10*b* can be regarded as loop-branched: backbone Te are Q^{1300}, but connect to additional Q^{2110} Te, making 3-rings, which, in turn, link to the unbranched subchain of Q^{2110} Te via the CN3 bridging oxygen. The zigzag pattern of 6-rings in Fig. 10*c* can be formed through conventional corner-linkage of open-branched subchains. This is also the case for the isomeric chain of Fig. 10*d*, except that the branches there do not link directly to the other subchain, but instead share edges to form a (Te = Te) pair that is not part of either backbone. The only *dreier* double chain (Fig. 10*e*) has unbranched subchains that corner-link directly to form a ribbon of 5-rings, reminiscent of the 6-rings of Fig. 10*c*. Both of these structures occur for Fe tellurates. The most complex double chain occurs for the chemically simple compound $Na_2Te_4O_9$ (**#332**; Fig. 10*f*). Each *zweier* subchain backbone can be regarded as loop-branched, so that the subchains are each made of linked 5-rings. However, the loops of the subchains join via a shared edge and two corner-linkages to form a cluster Te_4O_n in which two 3-rings are united at a common shared edge. An isolated cluster with the same topology occurs for Te^{6+} (Fig. 13*d*). It will be seen below that this 'double-triangle' moiety appears to be unusually stable, recurring as part of

https://doi.org/10.1180/minmag.2016.080.093 Published online by Cambridge University Press

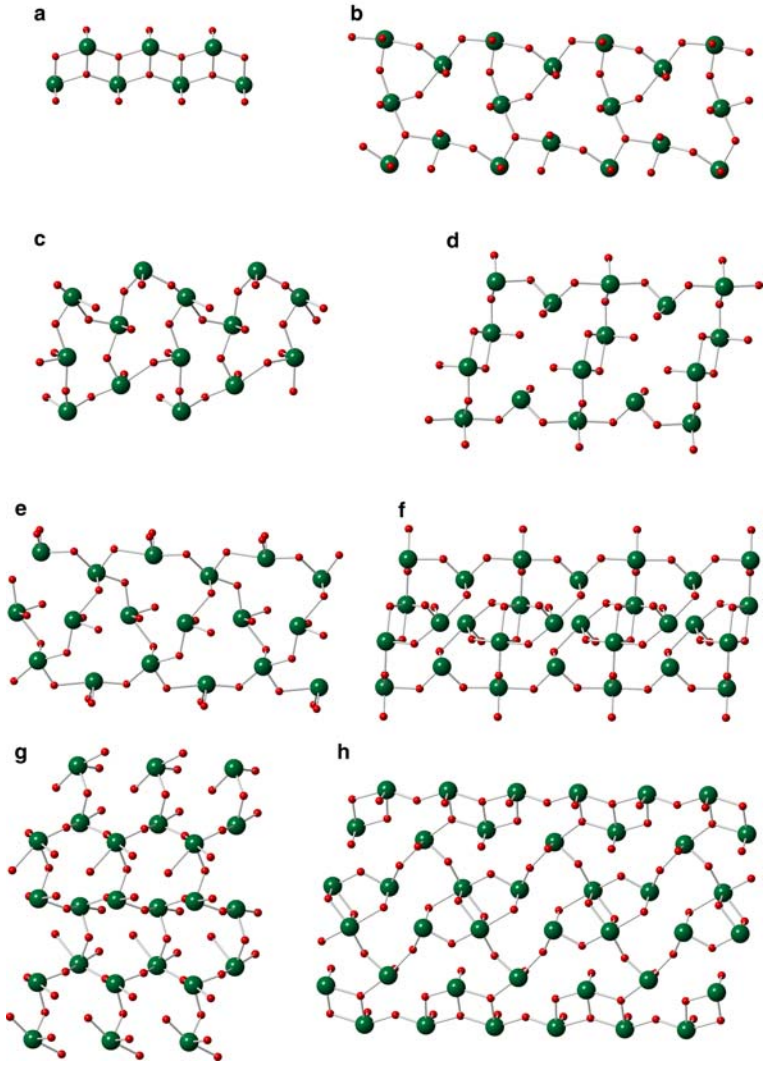

FIG. 10. Multiple-chain Te–O complexes containing only Te^{4+}. Chains all extend horizontally. (*a*) Four-coordinate Te make an *einer* Te_2X_4 neutral complex with CN3 bridging oxygen atoms in $Bi_3(Te_2O_4)(TeO_3)_2Cl_5$ (**#326**); (*b*) loop-branched and unbranched subchains join to make a *zweier* Te_5X_{12} double-chain anion in $Cd_7(Te_5O_{12})(Te_2O_5)Cl_8$ (**#327**); (*c*) open-branched subchains link to make *zweier* Te_6X_{14} with zigzag 6-rings in $Fe^{3+}(Te_3O_7)Cl$ (**#328**); (*d*) branches of subchains share edges to make isomeric *zweier* Te_6X_{14} in $Tl_2(Te_3O_7)$ (**#330**); (*e*) unbranched subchains link to form *dreier* Te_6X_{16} with ribbon of 5-rings in $Fe_4^{3+}(Te_6O_{16})(Te_2O_6)$ (**#331**); (*f*) loop-branched *zweier* subchains link to form Te_8X_{18} double chain with Te_4X_{12} 'double triangle' clusters between chain backbones in $Na_2(Te_4O_9)$ (**#332**); (*g*) open-branched *zweier* triple chain Te_8X_{24} in $Te_4(PO_4)_2O_5$ (**#333**); (*h*) quadruple chain $Te_{12}X_{26}$ with *zweier* and *dreier* subchains, CN3 bridging oxygen atoms and double-triangle clusters Te_4X_{10} where central subchains link in $Cd_4(Te_6O_{13})Cl_6$ (**#334**).

several larger polymers. The topology of the *zweier* triple chain of Fig. 10*g* is similar to that found in silicates for jimthompsonite and related 'biopyriboles' (Veblen and Burnham, 1978), but with additional side branches. Finally, Fig. 10*h* shows a quadruple chain which exhibits almost every complexity known in Te oxyanions. It contains Te with CN3, 4 and 5. While the two outer chains are *zweier*, the two central chains are *dreier*. Furthermore, the central chains join to each other

https://doi.org/10.1180/minmag.2016.080.093 Published online by Cambridge University Press

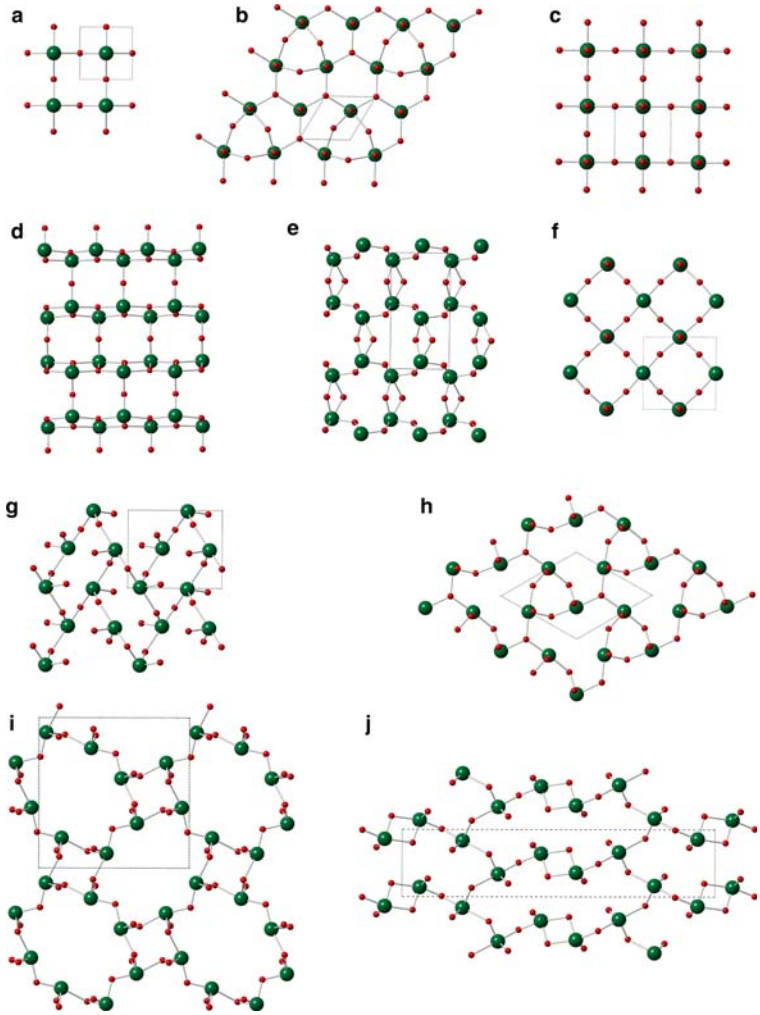

FIG. 11. Single-layer Te–O complexes containing only Te^{4+}. Unit-cell outlines are shown dashed when the projection direction is down a principal axis of the cell. The number of Te in the Te_mX_n formula unit corresponds to the translational repeat unit for the topology in its most symmetrical configuration; the repeat unit of the actual structure may be larger. (*a*) TeX_2 layer of square pyramids (Q^{0400} Te) in $Nd(Te_2O_4)OCl$ (**#335**); (*b*) most symmetrical local configuration for $TeX_{2.5}$ in the disordered structure of $Bi(Te_2O_5)Cl$ (**#337**); (*c*) TeX_3 with CN5 Te (Q^{1400}) in $Bi_2(TeO_3)(TeO_2)OBr_2$ (**#338**); (*d*) cationic $(Te,Sb)_2X_3$ layer (Q^{0132} Te) with 1 : 1 ratio of disordered Te^{4+} and Sb^{3+} in $Cu^{1+}(SbTeO_3)^{1+}Cl_2$ (**#339**); (*e*) cationic Te_2X_4 layer (Q^{0401}) in $(Te_2O_3OH)(NO_3)$ (**#340**); (*f*) Te_2X_5 layer with ordered CN4 and CN5 Te in $Bi_4(Te_2O_5)O_4Br_2$ (**#342**); (*g*) CN4 Te (Q^{1300}) forming Te_2X_5 layer with 6-rings in $Mg(Te_2O_5)$ (**#346**); (*h*) Te_3X_7 layer in which 3-rings are linked via CN3 bridging oxygen atoms (Q^{1210} Te) in $La_2(Te_3O_7)_2(WO_4)$ (**#349**); (*i*) Te_4X_{10} layer of Q^{1300} Te, with 4- and 8-rings in mackayite, $Fe^{3+}(Te_2O_5)OH$ (**#350**); (*j*) Te_4X_{10} layer of CN4 Te with 10-rings, edge-sharing pairs of Te having two rather than three bridging oxygen atoms, in one dimorph of $Li_2(Te_2O_5)$ (**#351**); (*k*) Te_4X_{10} layer of CN4 Te with 10-rings, edge-sharing pairs of Te having three bridging oxygen atoms, in $Tl_2(Te_2O_5)$ (**#352**); (*l*) Te_8X_{18} layer with 6-rings containing one or two CN3 Te, in $(NH_4)_2(Te_4O_9)$ (**#355**); (*m*) Te_8X_{18} layer with 6-rings containing zero or two CN3 Te, in $K_2(Te_4O_9) \cdot 3.2H_2O$ (**#356**); (*n*) convoluted $Te_{16}X_{36}$ layer with edge-sharing pairs of CN5 Te and corner-sharing CN3/CN4 Te, making 3-, 4- and 12-rings, in $(NH_4)Rb(Te_4O_9) \cdot 2H_2O$ (**#357**); (*o*) loop-branched $Te_{40}X_{100}$ layer in which tubes with 4-, 7- and 8-rings, running vertically on the page, are connected via sparser tubes with 9- and 10-rings, in $Ba_6(Te_{10}O_{25})Br_2$ (**#359**).

https://doi.org/10.1180/minmag.2016.080.093 Published online by Cambridge University Press

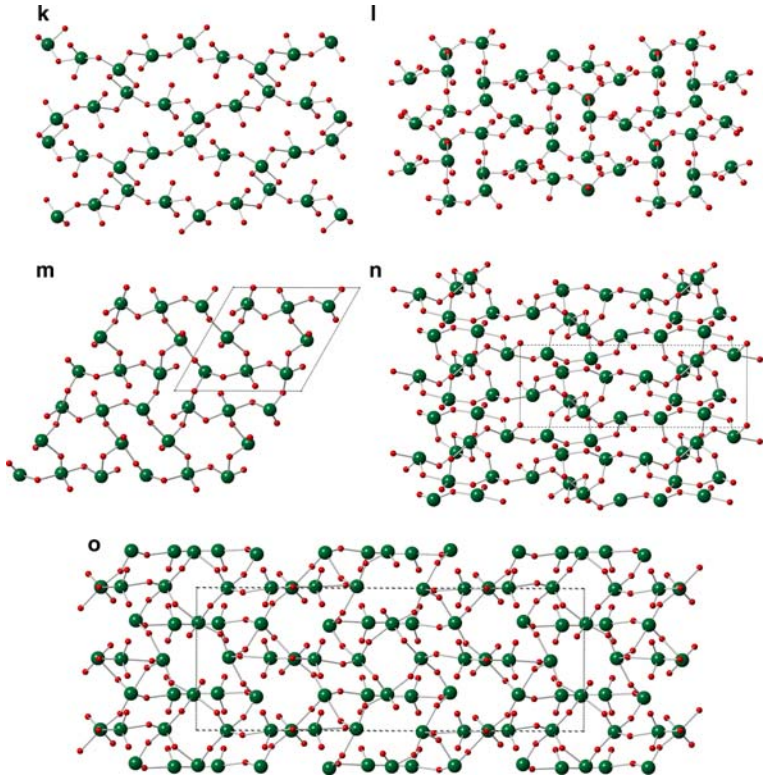

FIG. 11. Continued.

through Te–O polyhedra sharing edges and corners, to form again the 'double-triangle' cluster seen in Fig. 10*f*. Conversely, the central chains join to the outer chains less conventionally, via oxygen atoms which are CN3, as they also join to additional Te cations, so that the outer chains can be regarded as sequences of trimeric clusters resembling those of Fig. 8*i*.

Polyhedra $Te^{4+}X_n$ polymerize further to form layers, which may attain considerable complexity. The simplest single layers have TeX_4 square pyramids that link via corners to form a sheet TeX_2 (Fig. 11*a*), in which all Te are equivalent. All or half of these polyhedra may be capped by an additional ligand to form sheets with either TeX_3 (Fig. 11*c*) or Te_2X_5 (Fig. 11*f*) stoichiometry. A very different type of layer with Te:X = 2 : 5 is seen in Fig. 11*b*. This compound, ideally $Bi(Te_2O_5)Cl$ shows considerable structural disorder, and has all Te equivalent in its average structure. The Te shows short distances to one capping ligand (O1), three ~75%-occupied CN3 oxygen atoms (O2) and six ~25%-occupied CN2 oxygen atoms (O3). Short distances mean that O2 cannot be occupied simultaneously with its three nearest O3 sites, and O3 cannot be occupied simultaneously with its nearest O2 or its two nearest O3 sites. Figure 11*b* shows the most symmetrical way of satisfying these short-range order constraints, with ¾ of the Te in distorted 5-coordination (Q^{1220}) and ¼ in the capped pyramidal coordination of Fig. 3*d* (Q^{1030}). Figure 11*d* shows a $(Te_{0.5}Sb_{0.5})_2X_3$ sheet in which double chains of the type shown in Fig. 10*a*, featuring CN3 oxygen atoms, are connected through additional Te–O–Te links to produce a sheet with Q^{0132} cations $[(SbTe)O_3]^+$ that is positively charged, rather than anionic. The layer in Fig. 11*e* has Te_2X_4 stoichiometry. All Te are CN4 and all X are CN2, but each TeX_4 polyhedron shares one edge, so that it links to only three others (Q^{0401} configuration). Figure 11*e* shows the $[Te_2O_3OH]^+$ complex from $(Te_2O_3OH)(NO_3)$, which again is cationic rather than anionic. However, the neutral sheet $[Te_2O_4]^0$ of tellurite, TeO_2 (**#341**) has the

https://doi.org/10.1180/minmag.2016.080.093 Published online by Cambridge University Press

https://doi.org/10.1180/minmag.2016.080.093 Published online by Cambridge University Press

TABLE 4. Te_mO_n single layers with Te^{4+} only (phyllotellurites), found in the current study. The formula unit is the smallest possible translational repeat unit for the topology.

Stoichiometry	Descriptive notes	Fig. #	Structural unit heteropolymerization	Structure #
TeX_2	CN4 Te corner-linked to make 4-rings	11*a*	none	**335–336**
$TeX_{2.5}$	disordered CN4 and CN5 Te making 3-rings via CN2 and CN3 oxygen atoms	11*b*	none	**337**
TeX_3	CN5 Te corner-linked to make 4-rings	11*c*	none	**338**
$(Te,M)_2X_3$	CN4 Te linked via CN3 oxygen atoms into double chains and then via CN2 oxygen atoms into layer	11*d*	none	**339**
Te_2X_4	(>◇ = ◇<) pairs share corners to make 6-rings	11*e*	none	**340–341**
Te_2X_5	[–◇–⏢–◇–⏢–] 4-rings	11*f*	none	**342**
Te_2X_5	(–◇–) making 6-rings	11*g*	none, layer, frameworks	**343–348**
Te_3X_7	CN4 Te 3-rings linked via CN3 oxygen atoms to make 6-rings	11*h*	none	**349**
Te_4X_{10}	(◇–◇) making 8- and 4-rings	11*i*	framework	**350**
Te_4X_{10}	(–◇ = ◇–) link via (–◇–◇–◇–) to make 10-rings; each (–◇ = ◇–) pair shared by two rings	11*j*	none	**351**
Te_4X_{10}	(>◇ = ◇<) link via (–◇–◇–◇–) to make 10-rings; each (>◇ = ◇<) pair shared by four rings	11*k*	none	**352–353**
Te_8X_{18}	[–◇–◇–Δ–◇–◇–Δ–] and [–◇–◇–◇–◇–◇–Δ–] 6-rings	11*l*	none	**354–355**
Te_8X_{18}	[–◇–◇–Δ–◇–◇–Δ–] and [–◇–◇–◇–◇–◇–◇–] 6-rings	11*m*	none	**356**
$Te_{16}X_{36}$	(–◇–◇–Δ–◇–◇–Δ–) chains linked through (⏢ = ⏢) pairs to make 3-, 4- and 12-rings	11*n*	none	**357–358**
$Te_{40}X_{100}$	tubes with 4- 7- and 8-rings or 9- and 10-rings linked into looped sheet	11*o*	none	**359**

TABLE 5. Te_mO_n with Te^{4+} only in double layers (phyllotellurites) and frameworks (tectotellurites), found in the current study.

Stoichiometry	Descriptive notes	Fig. #	Structural unit heteropolymerization	Structure #
double layers (phyllo)				
Te_6X_{13}	[–◇–◇–◇–] 3-rings linked through CN3 oxygen to upper or lower Te of (◇ = ◇), to make 12-rings in each sublayer	12*a*	frameworks	**360–362**
Te_6X_{14}	[–⏢–◇–⏢–Δ–◇–⏢–◇–Δ–] 8–rings in sublayers, [–⏢–Δ–⏢–Δ–] and [–⏢–◇–Δ–⏢–◇–Δ–] bridging layers	12*b*	layer	**363**
frameworks (tecto)				
TeX_2	cristobalite type (CN4, Q^4)	12*c*	none	**364–365**
TeX_3	pyrochlore type (CN6, Q^6)	12*d*	none	**366**
Te_3X_7	Te links to four oxygen atoms with CN 1,2,2,3	12*e*	framework	**367**
Te_3X_7	Te links to four oxygen atoms with CN 1,2,2,3	12*f*	framework	**368**
Te_3X_8	Te links to four oxygen atoms with CN 1,1,3,3	12*g*	framework	**369–373**
Te_4X_9	4-rings [–◇–◇–◇–◇–] linked through pairs of Q^2-◇	12*h*	none	**374**
Te_5X_{11}	(◇ = ◇ = ◇ = ◇) linked through ◇ and CN3 oxygen to make chains of 6-rings, cross-linked by perpendicular chains (–◇–◇–) making 8- and 10-rings.	12*i*	none	**375**

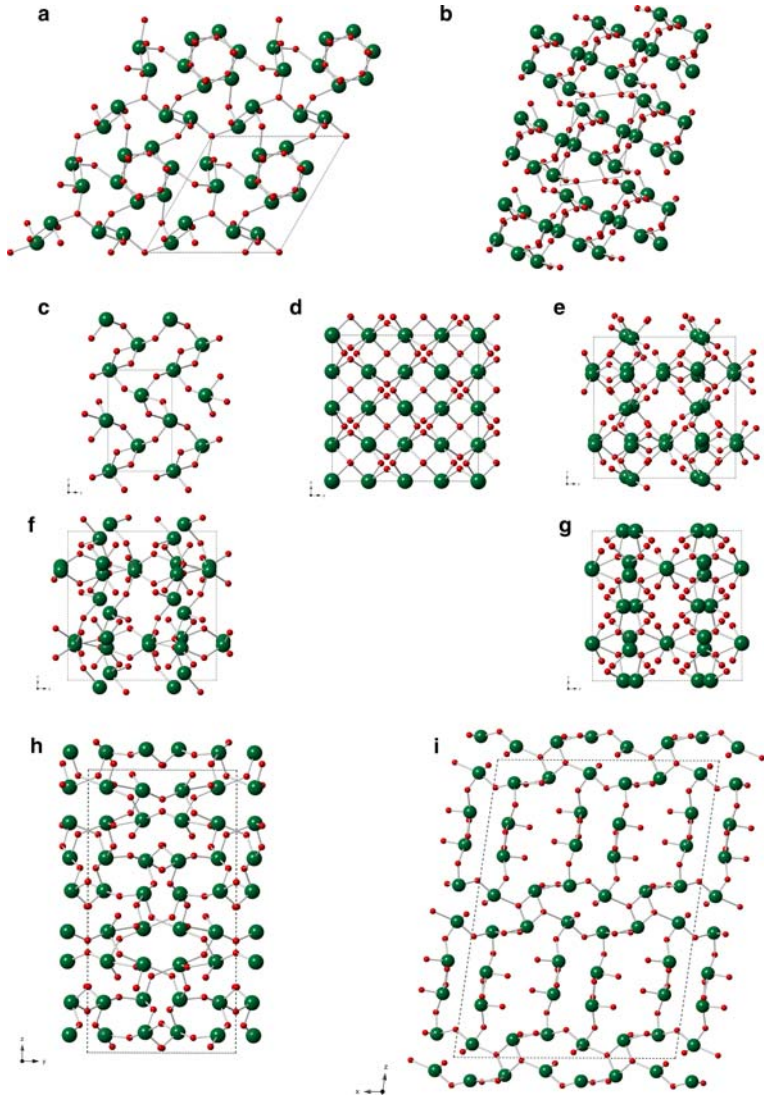

FIG. 12. Double-layer and framework Te–O complexes containing only Te^{4+}. Unit-cell outlines are shown dashed for the frameworks. (*a*) Te_6X_{13} double layer in $Zn(Te_6O_{13})$ (**#360**); (*b*) Te_6X_{14} double layer in $Te_3(SeO_3)O_5$ (**#363**); (*c*) TeX_2 framework (Q^{0400}) of the paratellurite polymorph of TeO_2 (**#364**); (*d*) pyrochlore framework TeX_3 (Q^{0600}) in $Pr_2(Te_2O_6)O$ (**#366**); (*e*) Te_3X_7 framework in $KGa(Te_6O_{14})$ (**#367**); (*f*) Te_3X_7 framework in cliffordite, $(UO_2)(Te_3O_7)$ (**#368**); (*g*) Te_3X_8 framework of winstanleyite, $Ti(Te_3O_8)$ (**#372**); (*h*) Te_4X_9 framework of $Cs_2(Te_4O_9)$ (**#374**); (*i*) Te_5X_{11} framework of $Pb(Te_5O_{11})$ (**#375**).

same topology, but is much more deeply corrugated. When TeX_4 polyhedra share three corners only (Q^{1300}) to form 6-rings, a Te_2X_5 sheet such as Fig. 11*g* is obtained, topologically similar to the silicate sheet of micas, but less regular geometrically. As is the case for phyllosilicates, the non-bridging oxygens can be distinguished between those that point 'up' and those that point 'down' relative to the overall plane of the layer, and different up/down ordering patterns of apical oxygen atoms may occur. In the present study, most examples (including that of Fig. 11*g*) show alternation of pairs of 'up' and pairs of 'down' polyhedral apices. However, one of the dimorphs of

https://doi.org/10.1180/minmag.2016.080.093 Published online by Cambridge University Press

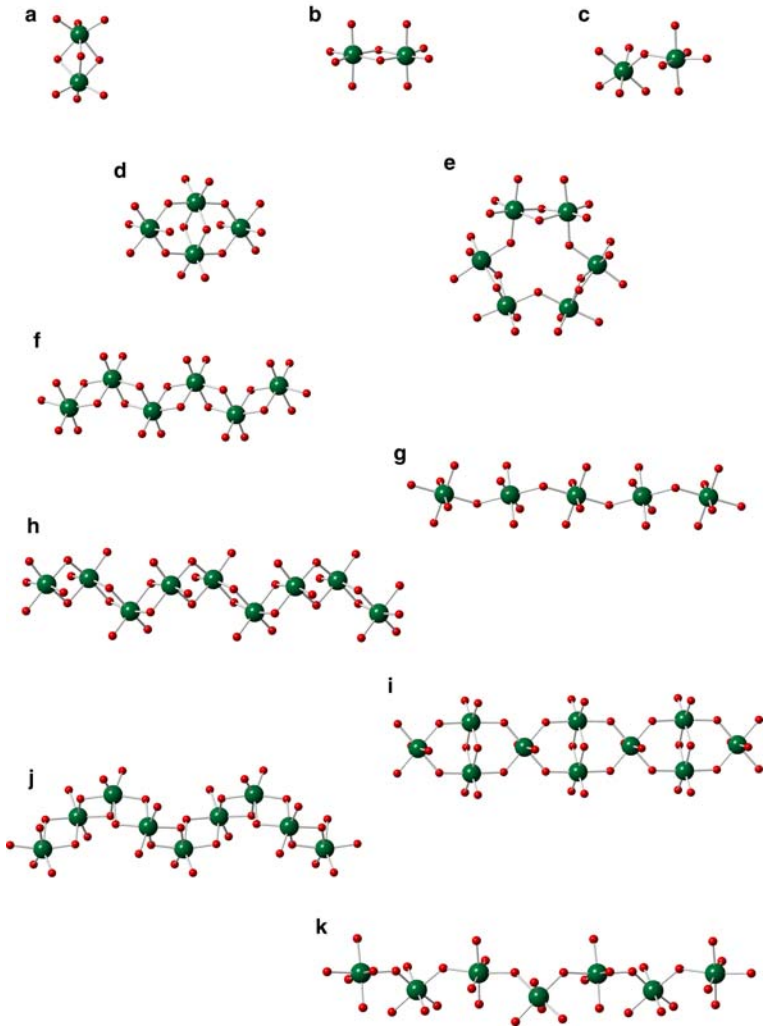

FIG. 13. Finite oligomers and chains containing only Te^{6+}. (*a*) Face-sharing dimer Te_2X_9 in $Ba_3(Te_2O_9)$ (**#619**); (*b*) edge-sharing Te_2X_{10} in eckhardite, $Ca_2Cu_2(Te_2O_{10}) \cdot 2H_2O$ (**#639**); (*c*) corner-sharing Te_2X_{11} in schieffelinite, $Pb_{10}(Te_2O_8(OH)_3)_2(TeO_2(OH)_4)_2(SO_4) \cdot 5H_2O$ **(#642)**; (*d*) 'double-triangle' tetramer Te_4X_{18} of $K_2(Te_4O_8(OH)_{10})$ **(#644)**; (*e*) cyclo 6-ring Te_6X_{27}, with alternation of edge- and corner-sharing in $K_{8.5}(H_3O)_{0.5}(Te_6O_{18}(OH)_9) \cdot 17H_2O$ (**#645**); (*f*) edge-sharing *zweier* chain Te_2X_8 in $CaTeO_4$ (**#648**); (*g*) corner-sharing *zweier* chain Te_2X_{10} in ottoite, $Pb_2(Te_2O_{10})$ (**#655**); (*h*) helical edge-sharing *dreier* chain Te_3X_{12} in $Ag_3(TeO_4)I$ **(#657)**; (*i*) loop-branched *zweier* chain of 'double-triangle' clusters Te_3X_{12} in $K_2(Te_3O_8(OH)_4)$ (**#658**); (*j*) helical edge-sharing *vierer* chain Te_4X_{16} in $Li_2(TeO_4)$ **(#662)**; (*k*) corner-sharing *vierer* chain Te_4X_{20} in housleyite, $Pb_6Cu(Te_4O_{18}(OH)_2)$ (**#663**).

$Li_2Te_2O_5$ (**#351**) has all apices oriented in the same direction, similar to the micas.

The trigonal Te_3X_7 sheet of Fig. 11*h* has CN2 oxygen atoms linking Te into 3-rings and additional CN3 oxygen atoms forming 6-rings (Q^{1210} configuration); note that the hybrid double chain of Fig. 10*b* is actually a slice of this structure. Figure 11*i* shows a Te_4X_{10} sheet with 4- and 8-rings, which again is strongly analogous to a well-known silicate structure, apophyllite (Colville *et al.*, 1971). The isomeric Te_4X_{10} structures of Figs 11*j* and 11*k* both have all Te 4-coordinated, but in 10-rings only, which requires some Te to link to only two others rather than three, and hence, for

https://doi.org/10.1180/minmag.2016.080.093 Published online by Cambridge University Press

some edges to be shared. In Fig. 11*j*, the edge-sharing Te are Q^{1301} and the others Q^{1300}, while in Fig. 11*k*, the edges are shared by Q^{0401} polyhedra and the others are Q^{2200}. The isomeric pair of Te_8X_{18} alkali tellurite sheets in Figs 11*l* and 11*m* have no shared edges, but both have ¼ of the Te in CN3 rather than CN4. The Te form 6-rings which contain one or two CN3 cations in Fig. 11*l*, but zero or two CN3 cations in the pseudohexagonal sheet of Fig. 11*m*. The much more complex and highly convoluted $Te_{16}X_{36}$ sheet of Fig. 11*n* has Te in 3-, 4- and 5-coordination, making 3-, 4- and 12-rings. The CN5 Te occur in edge-sharing pairs. Finally, Fig. 11*o* shows an extraordinarily complex sheet made by Q^{2200} Te cross-linking elliptical tubes which have 4-, 7- and 8-rings of CN4 Te.

Analogously to the case for chains, a phyllotellurate has a double layer if deletion of selected Te–O bonds can separate it into two distinct sublayers which themselves remain continuous. Our dataset contains two types of double layer, as seen in Table 5 and Fig. 12. The Te_6X_{13} double layer of Fig. 12*a* has all Te CN = 4, but half of them are Q^{1300}, sharing corners to form 3-rings, while the other half of the Te are branches off these rings, which share edges (Q^{0311}) to link the two sublayers. Oxygen atoms with CN3 link the edge-sharing dimers to complete each of the sublayers. Conversely, the Te_6X_{14} double layer of Fig. 12*b* has no edge-sharing or CN3 oxygen atoms, but has Te in three different coordination states (Q^{0300}, Q^{1300} and Q^{1400} configurations). Like many Te–O polymers containing CN5 Te, this thick double layer is braced by additional polyhedra containing other high-charge, low-CN cations ($Se^{4+}O_3$ in this case).

$Te^{4+}O_n$ polyhedra also form a range of infinite three-dimensional frameworks. Figure 12*c* shows the electrically neutral tetragonal framework of paratellurite, TeO_2, and its metastable orthorhombic distorted variant γ-TeO_2; these are polymorphs of tellurite, which has a layered structure of the type seen in Fig. 11*e*. The paratellurite framework is of interest in that it is isopuntal with the low-cristobalite form of SiO_2 (Dollase, 1965), and yet can also be derived from the structure of rutile (and the dense stishovite form of silica) by deformation of coordination octahedra $TeO_6 \rightarrow TeO_{4+2} \rightarrow TeO_4$. Note that the Q^{0400} Te polyhedra are much less symmetrical than SiO_4 tetrahedra. The paratellurite structure is thus a shared hettotype structure that could act as a transition state for diffusionless phase transformations between the low-density/high-temperature structure of high-cristobalite on the one hand, and the high-pressure stishovite structure on the other, analogous to the transformation mechanisms described in Christy (1993).

Figure 10*d* shows a rare example of Te^{4+} in Q^{0600} polyhedra that are nearly regular octahedra, with no lone-pair stereoactivity, and which link to form the pyrochlore framework. The frameworks of Figs 12*e–g* are all closely related, and like that of Fig. 12*d*, have cubic unit cells with $a \approx 10$ Å; all can ultimately be derived from $2 \times 2 \times 2$ superstructures of the fluorite type. The Te_3X_7 framework of KGa(Te_6O_{14}) (Fig. 10*e*) is formed when ¼ of the 'fluorite' cations are replaced by non-Te species and ⅛ of the anions omitted, to make a framework in which Te are in a Q^{1210} configuration, linked through $2 \times$ CN2 oxygen atoms and one CN3 oxygen atom. The isomeric cliffordite framework (Fig. 12*f*) has a similar range of oxygen CN and the same $Pa\bar{3}$ space-group symmetry, but the topology of linkage of the CN2 and CN3 oxygen atoms is different. The structure of the winstanleyite group, $M^{4+}(Te_3O_8)$, is a slightly distorted fluorite superstructure in which the Te framework has Q^{2020} Te linked through two CN3 oxygen atoms only; it can thus be represented as a 3-connected net with CN3 oxygen at the nodes and (TeO_2) groups decorating the links (Fig. 12*g*).

Figure 12*h* shows a more open tetragonal Te_4X_9 framework in which half the Te cations are Q^{0400}, forming Te_4O_{12} rings which are arranged on a *D* lattice complex (Fischer and Koch, 2006), analogous to the Ti atoms in anatase (TiO_2; Howard *et al*., 1991) or Ca in scheelite ($CaWO_4$; Zalkin and Templeton, 1964). These Te atoms are linked to form a framework through pairs of Q^{2200} Te atoms, making additional 4-rings. The Te_5X_{11} framework of Pb(Te_5X_{11}) is even more open (Fig. 12*i*). This structure has five distinct types of Te, all CN4, but in four distinct Q states. Te1 (Q^{0222}) and Te3 (Q^{0401}) form edge-sharing tetramers Te3 = Te1 = Te1 = Te3, while Q^{1210} Te2 links to Te3 of one tetramer and through CN3 oxygen to both Te1 of the next, so that Te1, Te2 and Te3 form continuous chains of 6-rings which run ‖ **x** and lie in layers ‖ (001). Between these layers and cross-connecting them are corner-sharing chains running ‖ **y** of Q^{1300} Te4 and Te5, where the chain backbones –Te4–O–Te5–O– have an asymmetrical crankshaft geometry, very similar to that of the Pb–O chains in massicot (Hill, 1985). Connections are so sparse that the smallest rings to include Te4 or Te5 have eight and ten members.

As noted above, the stereochemistry of Te^{6+} is much less diverse than that of Te^{4+}, so the range of

https://doi.org/10.1180/minmag.2016.080.093 Published online by Cambridge University Press

TABLE 6. Te_mO_n complexes with Te^{6+} only, found in the current study. '*M*' = another CN6 cation in solid solution with Te.

Class	Stoichiometry	Descriptive notes	Figure #	Structural unit heteropolymerization	Structure #
neso	TeX_4	tetrahedral	4*e*	none	**432, 434**
	TeX_5	trigonal bipyramidal	4*f*	none	**433–434**
	TeX_6	octahedral	4*g*	none, clusters, chains, layers, frameworks	**375–431** ($Te(OH)_6$ adducts) **435–618** (TeX_6 anions)
soro	Te_2X_9	(○ ≡ ○)	13*a*	none	**619–620**
	Te_2X_{10}	(○ = ○)	13*b*	none, chains, layers, frameworks	**621–641**
	Te_2X_{11}	(○–○)	13*c*	none	**642–643**
cyclo	Te_4X_{18}	'double triangle'	13*d*	none	**644**
	Te_6X_{27}	6-ring with alternating corner- and edge-sharing	13*e*	none	**645**
ino	Te_2X_8	edge-sharing	13*f*	none	**646–652**
	Te_2X_{10}	corner-sharing	13*g*	none, framework	**653–656**
	Te_3X_{12}	edge-sharing	13*h*	none	**657**
	Te_3X_{12}	loop-branched *zweier*	13*i*	none, layers	**658–661**
	Te_4X_{16}	edge-sharing	13*j*	none	**662**
	Te_4X_{20}	corner-sharing	13*k*	none	**663**
phyllo	$(Te,M)X_3$	edge-sharing, 6-rings (cation CN octahedral)	14*a*	layers	**664–666**
	$(Te,M)X_3$	edge-sharing, 6-rings (cation CN trigonal prismatic)	14*b*	layers	**667**
	TeX_4	corner-sharing, 4-rings	14*c*	none, framework	**668–670**
	Te_3X_{14}	corner-sharing, 8-rings	14*d*	none	**671**
tecto	$(Te,M)X_2$	distorted rutile (VO_2) type	14*e*	none	**672–673**
	TeX_3	distorted ReO_3 (FeF_3) type	14*f*	none	**674**
	Te_2X_7	weberite type	14*g*	none	**675–676**
	$(Te,M)_4X_{12}$	edge- and corner-sharing	14*h*	none	**677**

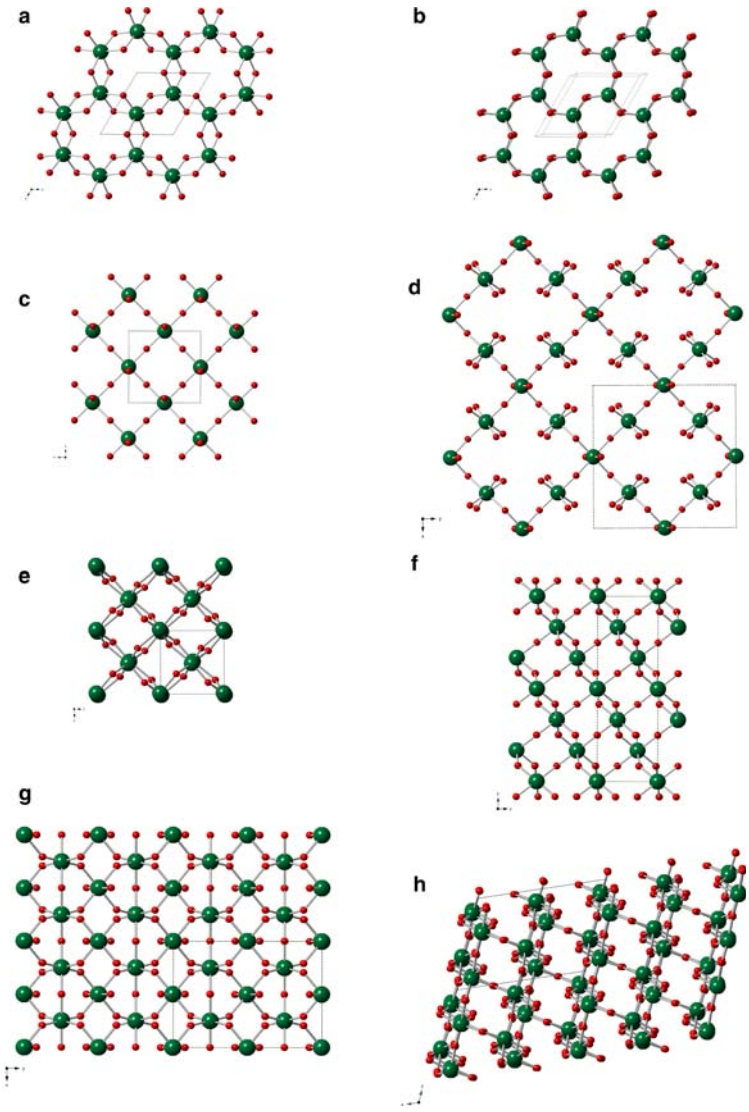

FIG. 14. Layers and frameworks containing only Te^{6+}. (*a*) Edge-sharing octahedral (Te,Fe)X_3 layer in burckhardtite, $Pb_3(Fe^{3+}Te^{6+}O_6)(AlSi_3O_8)$ (**#666**); (*b*) edge-sharing trigonal prismatic (Te,Mn)X_3 layer in $Sr(Mn^{4+}Te^{6+}O_6)$ (**#667**); (*c*) corner-sharing TeX_4 layer in $Bi_2(TeO_4)O_2$ (**#669**); (*d*) chiolite-type layer Te_3X_{14} of $Ca_5(Te_3O_{14})$ (**#671**); (*e*) distorted rutile framework (Te,Ni)X_2 of $(Ni^{2+}Te^{6+})O_4$ (**#673**); (*f*) FeF_3 (collapsed ReO_3 type) framework of TeO_3 (**#674**); (*g*) weberite-type framework Te_2X_7 of $Na_2(Te_2O_7)$ (**#675**); (*h*) strongly layered (Te,Fe)$_4X_{12}$ framework with edge-sharing in $Pb_3(Fe_2^{3+}Te_2^{6+}O_4)$ (**#677**).

polymeric complexes is also more restricted. Table 6 shows that the tetrahedral TeO_4^{2-} anion (Fig. 4*e*) and bipyramidal TeO_5^{4-} (Fig. 4*f*) occur in only three structures altogether, one of which contains both of them. Conversely, octahedral complexes TeX_6 (Fig. 4*h*) are extremely common. The neutral 'orthotelluric acid' molecule $Te(OH)_6$, with its ability to make a profusion of hydrogen bonds, is the defining Te species in 59 structures, while no less than 182 have less protonated octahedral anions as their most complex Te complex. Thus, isolated TeX_6 octahedra are the most complex Te complex in about one third of the total database. Only five types of finite oligomer are

https://doi.org/10.1180/minmag.2016.080.093 Published online by Cambridge University Press

TABLE 7. Te_mO_n monomers and finite polymers with mixed Te^{4+} and Te^{6+} found in the current study, classified by the most complex Te anion type.

Class	Stoichiometry	Descriptive notes	Fig.#	Structural unit heteropolymerization	Structure #
neso	$Te^{6+}X_6$	+ separate $Te^{4+}X_3$		framework	**678**
ino	$(MTe^{4+})Te^{6+}X_8$	loop-branched *zweier* (double triangles)	15*a*	none	**679**
	$Te^{4+}Te_2^{6+}X_{11}$	loop-branched *zweier* (3-rings)	15*b*	none	**680**
	$Te_2^{4+}Te_2^{6+}X_{12}$	loop-branched *zweier* (3-rings)	15*c*	none	**681**
phyllo	$Te^{4+}Te^{6+}X_6$	corner-sharing, 3-rings and 4-rings	15*d*	none	**682–684**
	$Te^{4+}Te^{6+}X_6$	corner-sharing, 3-rings and 5-rings	15*e*	none	**685**
	$Te^{4+}Te^{6+}X_6$	double triangles, 8-rings	15*f*	none	**686**
	$Te^{4+}Te^{6+}X_6$	double triangles, 4-rings	15*g*	none	**687**
	$Te^{4+}Te^{6+}X_7$	6-rings	15*h*	layers, frameworks	**688–694**
	$Te_3^{4+}Te^{6+}X_9$	3-, 4- and 6-rings	15*i*	none	**695**
tecto	$Te^{4+}Te^{6+}X_5$		16*a*	none	**696**
	$Te_2^{4+}Te^{6+}X_8$	Te^{6+} linked by edge-sharing dimers of Te^{4+}	16*b*	none	**697**
	$Te_2^{4+}Te^{6+}X_8$	cross-linked chains of double triangles	16*c*	none	**698**
	$Te_2^{4+}Te_2^{6+}X_{11}$	kagome $Te^{6+} + Te^{4+}$ layers cross-linked by edge-sharing dimers of Te^{4+}	16*d*	none	**699**
	$Te_3^{4+}Te^{6+}X_{12}$	ordered pyrochlore framework	16*e*	none	**700**
	$Te_3^{4+}Te^{6+}X_{12}$	modified pyrochlore framework	16*f*	none	**701**
	$Te_2^{4+}Te_3^{6+}X_{14}$	kagome Te^{6+} layers cross-linked by edge-sharing dimers of Te^{4+}	16*g*	none	**702**
	$Te_3^{4+}Te_5^{6+}X_{23}$	modified pyrochlore framework	16*h*	none	**703**

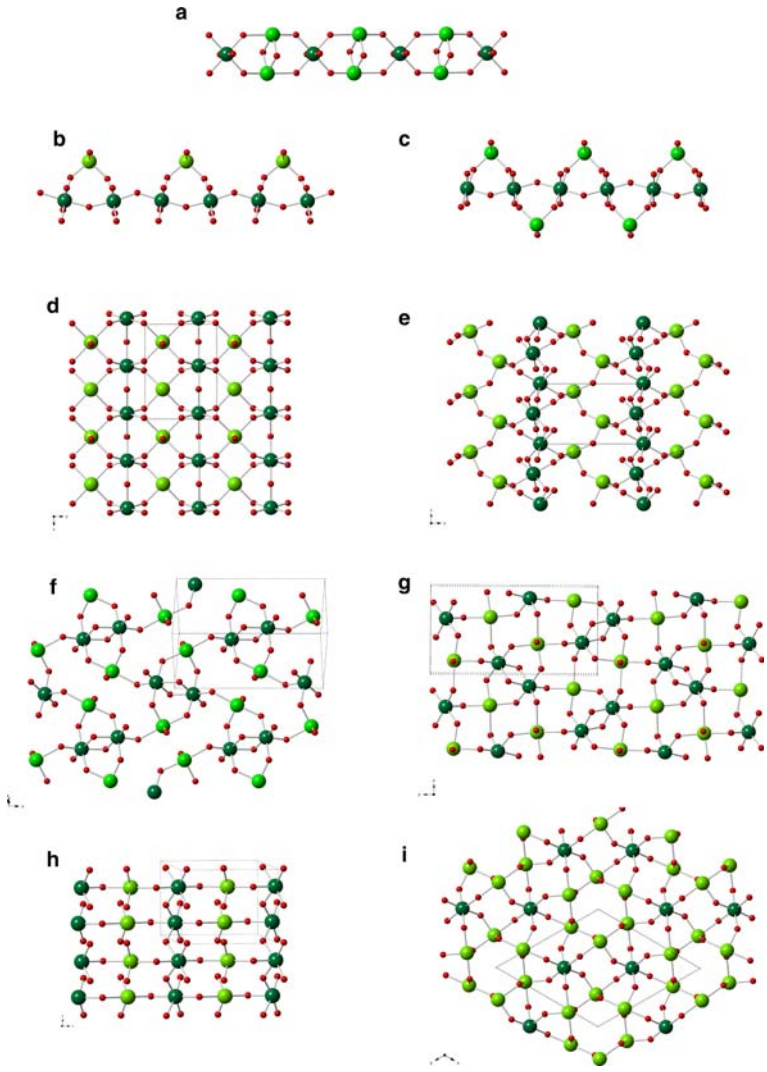

FIG. 15. Te–O chain and layer complexes containing both Te^{4+} (light green) and Te^{6+} (dark green). (*a*) Loop-branched *zweier* chain $(Te^{4+},Bi^{3+})_2Te^{6+}X_8$ containing 'double triangle' motifs in $Bi[(Bi^{3+}Te^{4+})Te^{6+}O_8]$ (**#679**); (*b*) loop-branched *zweier* chain with 3-rings $Te^{4+}Te^{6+}_2X_{11}$ in $Cd_2Te^{4+}Te^{6+}O_7 = Cd_4(Te^{4+}Te^{6+}_2O_{11})(Te^{4+}O_3)$ (**#680**); (*c*) loop-branched *zweier* chain with 3-rings $Te^{4+}_2Te^{6+}_2X_{12}$ in $Cd_4(Te^{4+}_2\ Te^{6+}_2\ O_{12})(Te^{4+}O_3)_2$ (**#681**); (*d*) layer with 3- and 4-rings in $(NH_4)(Te^{4+}Te^{6+}O_5(OH))$ (**#682**); (*e*) layer $Te^{4+}Te^{6+}X_6$ with Te^{4+} and Te^{6+} making 3- and 5-rings in $Te^{4+}Te^{6+}O_4(OH)_2$ (**#685**); (*f*) layer $Te^{4+}Te^{6+}X_6$ with double-triangle clusters and 8-rings in $Ag_2(Te^{4+}Te^{6+}O_6)$-I (**#686**); (*g*) layer $Te^{4+}Te^{6+}X_6$ with double-triangle clusters and 4-rings in $Ag_2(Te^{4+}Te^{6+}O_6)$-III (**#687**); (*h*) strongly corrugated layer $Te^{4+}Te^{6+}X_7$ of 6-rings in SrCu $(Te^{4+}Te^{6+}O_7)$ (**#688**); (*i*) 6-rings of Te^{4+} sharing corners through Te^{6+} in $Te^{4+}_3Te^{6+}O_9$ (**#695**).

documented. Octahedral dimers may share faces (Q^{3303} Te_2X_9, Fig. 13*a*), edges (Q^{4202} Te_2X_{10}, Fig. 13*b*) or corners (Q^{5101} Te_2X_{11}, Fig. 13*c*). The only larger oligomers are a bicyclic 'double triangle' tetramer Te_4X_{18} (Fig. 13*d*), which is a Te^{6+} analogue of the Te^{4+} clusters that occur as parts of more complex polymers in Figs 10*f* and 10*h*, and a 6-ring Te_6X_{27} with alternating corner-sharing and edge-sharing of octahedra (Fig. 13*e*).

Table 6 shows that the variety of infinite Te^{6+} chains is similarly limited. Only single chains are known. *Zweier* chains may be edge-sharing Te_2X_8

https://doi.org/10.1180/minmag.2016.080.093 Published online by Cambridge University Press

(Fig. 13*f*) or corner-sharing Te_2X_{10} (Fig. 13*g*). Edge-sharing *dreier* chains Te_3X_{12} occur (Fig. 13*h*), as do edge-sharing *vierer* Te_4X_{16} (Fig. 13*j*) and corner-sharing Te_4X_{20} (Fig. 13*k*). Note that the *vierer* periodicity of the latter is determined by having alternation of Q^{4200} octahedra with *cis* and *trans* bridging oxygen atoms, a type of variability that does not occur with coordination numbers below 5. Note that all the corner-sharing *zweier* chains of this study have *trans* bridging oxygen atoms. The most complex chain is a loop-branched dreier Te_3X_{12} isomer (Fig. 13*i*), which is made by polymerization of the 'double triangle' cluster of Fig. 13*d*.

The Te^{6+} polyhedra also link to form layers and frameworks, but again, the range of polymer types is restricted relative to that seen for Te^{4+}. Q^{0603} octahedra share edges to form TeX_3 sheets with the same topology as those of the $Al(OH)_3$ polymorphs, such as gibbsite (Saalfeld and Wedde, 1974; Fig. 14*a*). However, the Te in these octahedra appears always to be in solid solution with another cation of lower valence (Fe^{3+}, Ti^{4+}, Mn^{4+} or Ge^{4+}), which gives the layer an overall negative charge. The same is true for the single case where a sheet is formed through edge-sharing of trigonal prisms, rather than octahedra (Fig. 14*b*). Such charge reduction is not necessary when Q^{2400} octahedra share corners to form TeX_4 sheets with 4-rings (Fig. 14*c*). The most complex tellurate layer type has corner-sharing of Q^{2400} and Q^{4200} octahedra to form a layer with overall stoichiometry Te_3X_{14} (Fig. 14*d*), with the same topology as that seen in chiolite, $Na_5(Al_3F_{14})$ (Jacoboni *et al*., 1981).

Long-range disorder is shown by Te^{6+} with lower-valence cations again in $MTeO_4$ tellurates with a monoclinically distorted $(Te,M)X_2$ rutile framework, containg Q^{0062} octahedra (Fig. 14*e*). Here, disordered substitution with low-valence cations results in electroneutrality of the framework. Further analogies between Te–O and Al–F frameworks are provided by the rhombohedrally distorted ReO_3 structure of TeO_3 itself (Fig. 14*f*), collapsed so that the oxygen atoms approximate hexagonal close packing, which is shared with a polymorph of AlF_3 (Daniel *et al*., 1990), and the Te_2X_7 framework of Fig. 14*g*, which is that of weberite, $Na_2(MgAlF_7)$ (Knop *et al*., 1982). The weberite framework contains many 3- and 6-rings, similar to the pyrochlore framework of Fig. 12*d*, but half of the octahedra are not Q^{0600}, but are instead partly depolymerized to Q^{2400}, which allows extra anions to be included. The unique Te_4X_{12} framework of Fig. 14*h* also contains many 3- and 6-rings (as well as 4- and 8-rings), but there is also some edge-sharing: half the octahedra are Q^{0601} and the other half Q^{0602}. In this framework, dense zigzag columns || **z** share polyhedral edges in the **y** direction to define layers, which in turn are linked into a framework via relatively sparse Te–O–Te bridges. Again, this particular structure has Te mixed with another cation (Fe^{3+}) on all the octahedral sites, in order to give it an overall negative charge.

Last, we consider the 26 structures of the present study which contain both Te^{4+} and Te^{6+}. Only one of these structures (**#675**) has separate Te^{4+} and Te^{6+} polyhedra which are not linked by strong bonds. In all the rest, ino, phyllo or tecto polymers contain Te in both valence states. Given their different stereochemical preferences, Te^{4+} and Te^{6+} are always ordered on distinct sites. The three types of chains are all only *zweier* in backbone periodicity, but nevertheless, display other complexities. In Fig. 15*a*, Te^{4+} and Bi^{3+} are disordered in pairs of edge-sharing Q^{0401} polyhedra, which are linked through Q^{2400} Te^{6+} to make a chain of 'double triangles'. Figures 15*b* and *c* show chains in which Q^{2400} Te^{6+} backbones are decorated by Q^{2200} Te^{4+} to make 3-rings. Again, Cd demonstrates a tendency to be associated with structurally complex anions (cf. Fig. 10*b* and *h*). Figure 15*d* shows a relatively common type of $Te^{4+}Te^{6+}X_6$ layer (four examples known) in which Q^{1400} Te^{4+} and Q^{0600} Te^{6+} share corners to 3- and 4-rings. Other isomeric layers with the same stoichiometry are seen in Figs 13*e–g*. The layer of Fig. 15*e* features *zweier* chains of Q^{2400} $Te^{6+}O_6$. Unlike the *zweier* Te^{6+} chains of Fig. 13*g*, these strongly zigzag chains are *cis*-bridged. They are linked through massicot-like chains (cf. Hill, 1985) of Q^{0400} $Te^{4+}O_4$, to form 3- and 5-rings; the 3-rings on the Te^{6+} backbone form a loop-branched chain resembling that of Fig. 15*c*. The topologies of Figs 15*f* and 15*g* both feature edge-sharing between Te^{6+} octahedra to produce 'double triangle' clusters, but differ in coordination number of Te^{4+}, numbers of non-bridging oxygen atoms on Te^{6+}, and ring sizes in the layers. Note that the positions of Te^{6+} and Te^{4+} in the 'double triangles' are reversed here, relative to the chain of Fig. 15*a*. Figure 15*f* has Q^{1300} Te^{4+} and Q^{1501} Te^{6+} with 8-rings between the clusters, while Fig. 15*g* has Q^{1400} Te^{4+}, Q^{0601} Te^{6+} and 4-rings. One compound, $Ag_2(Te^{4+}Te^{6+}O_6)$, has three polymorphs 'I', 'II' and 'III', displaying, respectively, the topologies of Fig. 15*f*, *d* and *g* (**#686**, **684** and **687**). The most popular type of mixed-valence layer, with seven examples, is the $Te^{4+}Te^{6+}X_7$ topology of Fig. 15*h*. Here again, zigzag *cis*-bridged chains of Te^{6+} (Q^{2400}) are

https://doi.org/10.1180/minmag.2016.080.093 Published online by Cambridge University Press

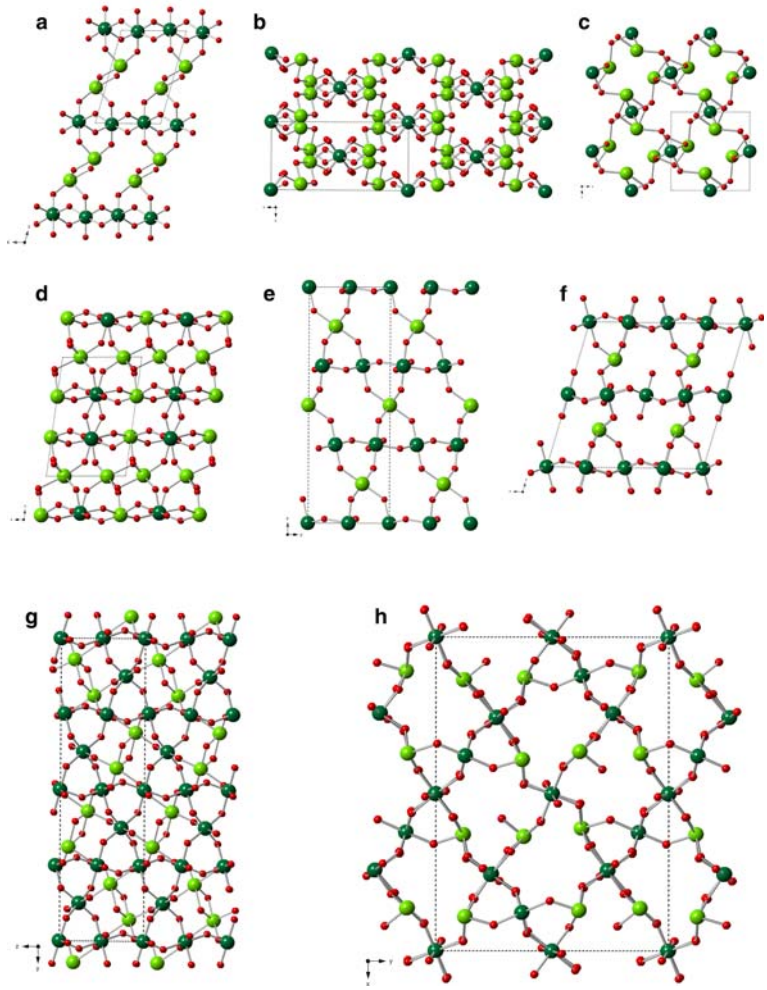

FIG. 16. Te–O frameworks containing both Te^{4+} and Te^{6+}. (*a*) Framework of $Te^{4+}Te^{6+}O_5$ (**#696**). (*b*) $Te_2^{4+}Te^{6+}X_8$ in carlfriesite, $Ca(Te_2^{4+}Te^{6+}O_8)$ (**#697**); (*c*) $Te_2^{4+}Te^{6+}X_8$ in $Sr(Te_2^{4+}Te^{6+}O_8)$, viewed down chains of double triangles (**#698**); (*d*) $Te_2^{4+}Te_2^{6+}X_{11}$ in $Ag_2(Te_2^{4+}Te_2^{6+}O_{11})$ (**#699**); (*e*) ordered pyrochlore framework $Te_3^{4+}Te^{6+}X_{12}$ in $Cs_2(Te^{4+}Te_3^{6+}O_{12})$ (**#700**); (*f*) sheared and depolymerized pyrochlore framework $Te_3^{4+}Te^{6+}X_{12}$ in $K_2(Te^{4+}Te_3^{6+}O_{12})$ (**#701**); (*g*) $Te_2^{4+}Te_3^{6+}X_{14}$ framework in $(Na_{1.6}Ag_{0.4})(Te_2^{4+}Te_3^{6+}O_{14})$, emphasizing kagome layers (**#702**); (*h*) modified pyrochlore framework $Te_3^{4+}Te_5^{6+}X_{23}$ of $Rb_4(Te_3^{4+}Te_5^{6+}O_{23})$ (**#703**).

connected through Te^{4+} (Q^{2200}), but the two non-bridging ligands on both types of cation give a greater *X*/Te ratio. The strong nonplanarity of the layer and small O–Te–O angles allow four 6-rings to meet at each Te^{6+}, in contrast to the three 6-rings meeting at each node in the more familiar mica-type layer (Fig. 11*g*). In Fig. 15*i*, a layer of stoichiometry $Te_3^{4+}Te^{6+}X_9$ is formed by 6-rings of Q^{0400} Te^{4+} linked through Q^{0600} Te^{6+} to make a sheet with additional 3- and 4-rings.

All the mixed-valence framework compounds have unique structures, although some of them are closely related to one another. In particular, most of them contain component layers with the well-known 'hexagonal tungsten bronze' or 'kagome' topology (O'Keeffe and Hyde, 1996), where 3- and 6-rings alternate around each node of the net in the order 3.6.3.6. Figure 16*a* shows the framework of $Te^{4+}Te^{6+}O_5$, in which corner-sharing layers (similar to Fig. 14*c*) of Q^{0600} Te^{6+} are cross-linked via

https://doi.org/10.1180/minmag.2016.080.093 Published online by Cambridge University Press

corner-sharing massicot-like chains of Q^{0400} Te^{4+}; cross-linkage produces 3-rings, as so often is seen in tellurate polymers. In carlfriesite, $Ca(Te_2^{4+}Te^{6+}O_8)$, Q^{2400} Te^{6+} are cross-linked through edge-sharing dimers of Q^{0401} Te^{4+} to make a trellis-like, nanoporous framework (Fig. 16*b*). The isomeric framework of $Sr(Te_2^{4+}Te^{6+}O_8)$ is also zeolite-like, but is formed by cross-linkage of chains similar to those of Fig. 15*a*, made from 'double-triangle' clusters containing Q^{0600} Te^{6+} and edge-sharing dimers of Q^{0501} Te^{4+} (Fig. 15*c*). Figure 16*d* shows another rather open framework of stoichiometry $Te_2^{4+}Te_2^{6+}X_{11}$, in which Q^{0500} Te^{4+} and Q^{0600} Te^{6+} define layers with a pseudohexagonal kagome net. Te^{6+}–O–Te^{6+} bridges link pairs of such layers, producing ladder-like double chains of Te^{6+}. Layer pairs are, in turn, linked into a framework through pairs of edge-sharing Q^{0501} polyhedra. Kagome layers are also found in the $Te_3^{4+}Te^{6+}X_{12}$ framework of Fig. 16*e*, which is that of pyrochlore and, thus, contains kagome nets in four different orientations. The framework, ideally cubic in symmetry, is rhombohedrally distorted as a result of Te^{4+}–Te^{6+} ordering. Like Fig. 12*d*, this is a rare example of Te^{4+} in octahedral coordination, with no evidence of a stereoactive lone pair: all Te cations are Q^{0600}. The K analogue of the Cs compound of Fig. 16*e* has the modified pyrochlore framework shown in Fig. 16*f*. Monoclinic shear of the structure is accompanied by breaking of some Te^{4+}–O–Te^{6+} links, so that Te^{4+} is now Q^{0500} (with a stereoactive lone pair) and one-sixth of the Te^{6+} are Q^{2400}. Kagome nets are also a major feature of the $Te_2^{4+}Te_3^{6+}X_{14}$ framework in Fig. 14*g*, where the Q^{0600} Te^{6+} form such layers, which are cross-linked via pairs of edge-sharing Q^{5001} Te^{4+}. As for the framework of Fig. 16*d*, the cross-linkage produces additional 3- and 4-rings. The orthorhombic $Te_3^{4+}Te_5^{6+}X_{23}$ framework is yet another modification of the pyrochlore type, in which the lone pairs of Te^{4+} are accommodated by breaking some Te^{4+}–O–Te^{4+} links, with complete elimination of $^1/_{24}$ of the oxygens. The ordering pattern of Te^{4+} and Te^{6+} is quite different from those of Figs 16*d* and 16*e*. Kagome layers are preserved in two orientations, but are not exclusively Q^{0600} Te^{6+}: alternate layers have $^1/_6$ or $^1/_3$ of their cations Q^{0500} Te^{4+}.

Descriptions of individual structures

Finite Te^{4+}–O complexes

Our descriptions of individual structures begin with those that contain finite Te^{4+}–O complexes (neso, soro and cyclo tellurites), **#1–280**. The various topologies that occur are summarized in Table 1 and depicted in Figs 4 and 8.

Structures with monomeric $Te^{4+}O_3$, no larger structural unit, and no other anions or water

Structures **#1**–**24** are listed in Table 8 (deposited), along with their full references. In $Li_2[TeO_3]$ (**#1**), helical columns of edge-sharing LiO_4 tetrahedra || **x** are cross-linked into layers || (002), with TeO_3 pyramids bracing the layers. Layers are held together only through weak Te···O interactions across the interlayer.

$Na_2[TeO_3]$ and $Ag_2[TeO_3]$ (**#2**–**3**) have a monoclinic $\sqrt{2} \times 3\sqrt{2} \times 1$ superstructure of the rocksalt type, with the Te coordination environment distorted to give only three close neighbours. $Tl_2[TeO_3]$ (**#4**) has an orthorhombic $3 \times 2 \times 1$ superstructure of rocksalt with a different cation ordering pattern. Short bonds form –Te–O–Tl–O–Tl–O– chains || **x**, with a crankshaft shape reminiscent of the Pb–O chains in the massicot form of PbO; such chains recur frequently in the structures of the present study, as noted above. Both Tl and Te have stereoactive lone pairs and only three close oxygen neighbours, making the structure strongly layered || (020). $AgTl[TeO_3]$ (**#5**) has similar cell dimensions but a different cation ordering pattern and space group. Again, the structure is layered, but this time || (200).

$K_2[TeO_3]$ and $Cs_2[TeO_3]$ (**#6**–**7**) have nearly-identical structures that are both oxygen-stuffed derivatives of the Ni_2In type; they are therefore TeO_3^{2-} analogues of the high-temperature K_2SO_4 structure (O'Keeffe and Hyde, 1985). The alkali cations are in 6–9 coordination. $Rb_2[TeO_3]$ (**#8**) appears to have a slight monoclinic distortion of the same structure, although the refinement is of poor quality.

$Ca[TeO_3]$ and $Sr[TeO_3]$ both occur in a large number of polymorphs with large unit cells and low symmetry (**#9**–**15**). All structures are packings of $(Ca,Sr)O_{6-8}$ polyhedra containing tunnels, with TeO_3 groups bracing the sides and the tunnels and lone pairs pointing into the central space. The two forms of $Ba[TeO_3]$ are quite different. One of them (**#16**) has the simple monoclinic structure of $KClO_3$ (Bats, 1978); the Ba and Te substructure resembles the CrB/TlI type (Helmholtz, 1936), and Ba is in 7 + 2 coordination by oxygen. $BaTeO_3$ is thus an oxygen-stuffed analogue of TlI, in the same way that baryte, $BaSO_4$, is an oxygen-stuffed derivative of the closely related FeB structure (O'Keeffe and

https://doi.org/10.1180/minmag.2016.080.093 Published online by Cambridge University Press

Hyde, 1985). The other dimorph (**#17**) has an approximately cubic close-packed (*ccp*) array of Ba + Te but a very complex ordering pattern, with Ba in 8–10 coordination.

There are also two synthetic polymorphs with known structures for $Pb[TeO_3]$; interestingly, these appear to be distinct from the two mineral species of this composition, triclinic fairbankite (Williams, 1979) and orthorhombic plumbotellurite (Spiridonov and Tananeyva, 1982), both of which remain poorly characterized. The tetragonal form (**#18**) has a structure very similar to that of scheelite ($CaWO_4$) but with ¼ of the oxygens removed in an ordered fashion. The coordination numbers are 6 and 3 for Pb and Te, as opposed to 8 and 4 for Ca and W. The lone pairs of both Pb^{2+} and Te^{4+} are directed into tunnels running || **z**. The more complex monoclinic structure of **#19** has a framework of $PbO_{4–6}$ and TeO_3, again with tunnels (this time || **y**) which act as micelles to contain the lone pairs.

$Cd[TeO_3]$ (**#20**) has Te filling interstices in an edge-sharing framework of irregular CdO_6 polyhedra. $Sc_2[TeO_3]_3$ (**#21**) has edge-sharing layers of $ScO_{6–7}$ polyhedra || (020), which are bridged by Te. In $Ce^{4+}[TeO_3]_2$ (**#22**), zigzag chains of edge-sharing CeO_8 are linked into a framework by Te. The Th and Pu analogues (**#23**–**24**) are isostructural.

Structures with monomeric $Te^{4+}O_3$ and no larger structural unit, but with additional anions or water

Structures **#25**–**46** are listed in Table 9 (deposited), along with their full references. In $Li_3[TeO_3](OH)$ (**#25**), LiO_3OH tetrahedra and TeO_3 pyramids form honeycomb-like double layers || (100), which are held together only by long Te···O and lone-pair interactions. Thus, the structure resembles that of the chemically similar but anhydrous phase **#1**. $Na_2[TeO_3] \cdot 5H_2O$ (**#26**) has three types of Na. Face-sharing trimers $(H_2O)_2Na1 \equiv (H_2O)_3 \equiv Na2 \equiv (H_2O)_3 \equiv Na1(H_2O)_2$ share corners with each other and with square-planar $Na3(H_2O)_2O_2$ to form a very open hydrogen-bonded framework in which TeO_3 is only loosely held. $KNa[TeO_3] \cdot 3H_2O$ (**#27**) has a denser, simpler structure with $K(H_2O)_6O_3$ and $Na(H_2O)_3O_3$ polyehdra sharing faces. The arrangement of K, Na and Te is a threefold ordering of the primitive hexagonal net, so this can be regarded as an O/H_2O-stuffed derivative of that archetype. The same is also true of $K_2[TeO_3] \cdot 3H_2O$ (**#28**), although the oxygen positions there are adjusted to give 8–13 coordination. Note that the anhydrous analogue (**#6**) is derived by oxygen-stuffing of a different but equally simple hexagonal arrangement of cations.

$MgTeO_3 \cdot 6H_2O \equiv [Mg(H_2O)_6][TeO_3]$ (**#29**) has a rhombohedral structure with angle $\alpha_{rh} = 97.4°$. It can be regarded as a derivative of the CsCl type, in which Cs^+ and $Cl^–$ anions are replaced by $[Mg(H_2O)_6]^{2+}$ and $[TeO_3]^{2–}$ complexes. As the lone pairs of the Te cations all point in the same direction along **z**, the structure is polar and ferroelectric, with point group *R*3. The structure of $Sr[TeO_3] \cdot H_2O$ (**#30**) is centrosymmetric but strongly anisotropic, with edge-sharing $SrO_6(H_2O)$ polyhedra defining layers || (100). The layers are held together via H-bonds and Te lone-pair/secondary bonding interactions. $Ba[TeO_3] \cdot H_2O$ (**#31**) is isostructural, although with **x** and **z** directions exchanged.

The structures of $A_3^{2+}[TeO_3]_2X_2$ (A = Sr or Ba; X = Cl or Br) have a large ($a \approx 16$ Å) cubic unit cell with the same space group $Fd\bar{3}m$ as diamond (**#32**–**34**). Clusters $[Sr_6Te_4O_{12}]^{4+}$ can be distinguished, in which Sr are at the vertices of an octahedron, linked by O along the octahedral edges, and braced by Te above four out of the eight octahedral faces. These clusters are arranged in the same fashion as the C atoms of diamond, and Sr_3 triangles of neighbouring clusters face each other to define a second type of octahedron between them. Halide anions centre both types of octahedron, and also occur in the largest remaining interstices of the structure with six Sr arranged in an almost planar hexagon at 3.6–4.4 Å and six Te above and below the plane at 3.3–3.8 Å. The structure can be regarded as a derivative of the pyrochlore type, with X replacing CN8 and CN6 cations of pyrochlore and A replacing the framework anions of pyrochlore. $Pb_3[TeO_3]Cl_4$ (**#35**) is quite different, in that one tellurate oxygen is tetrahedrally coordinated $OTePb_3$ and the others triangularly coordinated $OTePb_2$ to make a rod $[Pb_3TeO_4]^{4+}$ running || **z**. The rod has a rhombic cross-section with the Pb cations (bonded to only 2 or 3 oxygen atoms) on the exterior, and are arranged in a herringbone fashion. They are held together through four crystallographically distinct Cl anions, bonded to 3–5 Pb. Again, the structure is polar due to tilt of all TeO_3 groups in the same sense along the **z** direction.

In $Ho[TeO_3]Cl$ (**#36**), Ho^{3+} is in pentagonal bipyramidal coordination by five O and two Cl (one apical and one equatorial). The HoO_5Cl_2 polyhedra form edge-sharing ribbons || **y**, which are again arranged in herringbone fashion but are cross-liked through Te cations. The lone pairs of Te point into well-defined micellar channels that run || **y**, between

https://doi.org/10.1180/minmag.2016.080.093 Published online by Cambridge University Press

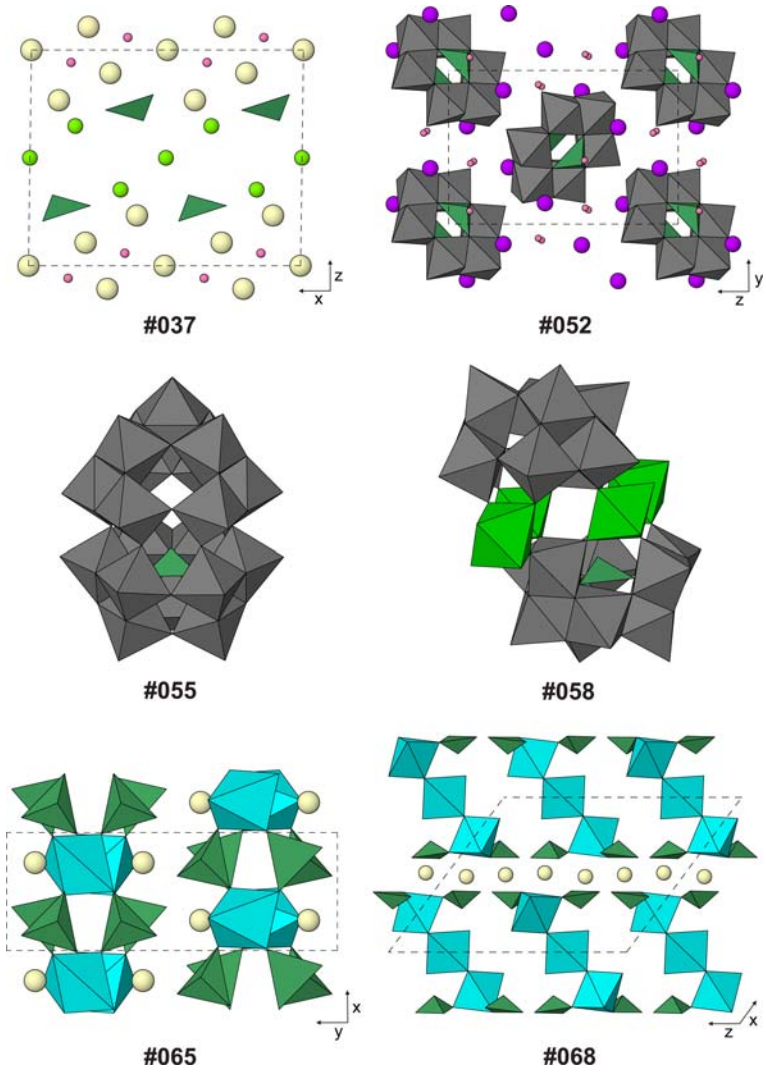

FIG. 17. Examples of structures with monomeric TeO_3 pyramids that are either weakly bound, or are part of larger structural units that are finite clusters or chains (Tables 9–10, deposited). Small spheres: O (dark pink), when not part of a polyhedron. Medium spheres: Cl (light green). Large spheres: K (purple), rare-earth cations Nd, Dy or Yb (light yellow). Polyhedra: Cu (cyan), Ni (light green), Mo or W (grey) and Te (dark green).

the ribbons. $Nd_5[TeO_3]_2O_4Cl_3$ (**#37**) has three types of Nd^{3+} polyhedra: NdO_8 cubes, irregular NdO_6Cl and NdO_5Cl_3 square antiprisms. These form thick layers ‖ (001), with Cl^- bridging the interlayer regions and Te bracing the outsides of the layers. The TeO_3 group is canted so that Te makes four long bonds to Cl at 3.19–3.40 Å (Fig. 17). $Na_2Lu_3[TeO_3]_4I_3$ (**#38**) has all the atoms except O in an approximately *ccp* array, with a layer sequence (Na_2Te_4), Lu_6, (Na_2Te_4), I_6 alternating along the **x** direction. Oxygen atoms define nearly-cubic LuO_8 polyhedra which share edges to form sheets ‖ (100). Some oxygen atoms are in tetrahedral coordination (OLu_2NaTe), while others are displaced away to tetrahedral sites so as to be in nearly plane triangular coordination by Lu_2Te, with a second Te much more distant at 3.15 Å. Thus, the structure can be regarded as a modified superstructure of the fluorite type (the cell parameters correspond to $2 \times 1 \times 3$ fluorite cubes).

https://doi.org/10.1180/minmag.2016.080.093 Published online by Cambridge University Press

Alternatively, it may be described as a structure in which thick Lu–O sheets are braced by Te^{4+}, with I^- occupying the interlayer region and NaO_4I_4 square antiprisms holding the sheets together. $Nd_4Cu^{1+}[TeO_3]_5Cl_3$ (**#39**) has a superficially similar stoichiometry but a quite different structure. NdO_8, NdO_7Cl and NdO_7 polyhedra share edges to form walls that surround two types of channel running || **y**; large and small channels alternate in a checkerboard fashion. The small channels contain one out of five distinct types of TeO_3, which again render the structure polar by all pointing in the same sense along the **y** direction. The large channels are lined by the rest of the Te atoms, but still contain enough space to accommodate a zigzag corner-sharing chain $[Cu_2Cl_6]^{4-}$ of $CuCl_4$ tetrahedra, held in place by Nd3–Cl3 links as well as each Cl making two to four long bonds to Te. $Bi_2[TeO_3]_2O$ (**#40**) has a defect fluorite superstructure (cf. **#38**) with a unit cell corresponding to 4 × 1 × 4 cubes of fluorite, with $^1/_8$ of the anions missing. Overall, Bi + Te form a *ccp* array. They are ordered into columns || **y**, with 1 × 1 and rectangular 2 × 3 blocks of Bi separating 2 × 1 and paralleogram-shaped 2 × 3 blocks of Te. If tetrahedral interstices are surrounded by Bi_4, then they are occupied by O. Bi_2Te_2 tetrahedra have oxygens displaced away from one Te or absent, $BiTe_3$ tetrahedra have oxygens linked only to 1 Bi + 1 Te, and Te_4 tetrahedra are unoccupied. Tellurium lone pairs point along ±**y** for the small Te blocks, but are directed into the interiors of the large blocks, which along with long Bi–O bonds mark the gap between weakly defined thick layers || (200). Te2 in this structure is our unique example of '2-coordinate' Te; however, if all Te–O distances out to 3.5 Å are considered, a square-pyramidal coordination polyhedron (Fig. 3*e*) is defined by oxygens at 1.865, 1.911, 2.519, 2.793 and 3.062 Å. It is possible that the O coordinates are not accurate in this structure, and that the true coordination polyhedron has a narrower spread of bond distances. Smirnite, $Bi_2[TeO_3]O_2$ (**#41**) has yet another defect fluorite superstructure with a unit cell corresponding to 2 × 3 × 1 fluorite cubes with $^1/_6$ of the anions missing, and many of the rest displaced so as to approximate plane triangular coordination by 3Bi or 2Bi + 1Te. The Te atoms are on the outsides of thick layers || (100), which are linked only through long Bi···O and Te···O bonds.

In $Ca_6[TeO_3]_5(NO_3)_2$ (**#42**), CaO_{6-8} polyhedra share edges to form undulating layers || (100) and also bridge these layers into a framework which contains large channels || **y**. TeO_3 pyramids decorate the sides of these channels, and the channels act as micelles which contain the Te lone pairs and also NO_3^- anions. The structure is thus strongly reminiscent of the nitrate-free tellurites **#9–15**. $Ca_5[TeO_3]_4(NO_3)_2 \cdot 2H_2O$ (**#43**) is rather similar, but the Ca layers || (200) remain completely separate, with no bridges connecting them. Tellurium lone pairs and nitrate groups point into continuous interlayer gaps.

$Sc_2[TeO_3](SeO_3)(SeO_4)$ (**#44**) has zigzag chains of edge-sharing ScO_7 polyhedra running || **x**. TeO_3 groups connect the chains into pairs, and the SeO_3 pyramids connect these further into layers || (002), while SeO_4 tetrahedra share oxygens with four different Sc to link the layers into a rather open framework.

$La_2[Si_6O_{13}][TeO_3]_2$ (**#45**) contains LaO_9 and TeO_3 polyhedra, forming layers || (100). These intercalate with a silicate sheet in which *dreier* double chains like those of okenite (Merlino, 1983) link to their neighbours to make a double layer in a disordered fashion, such that ⅔ of the Si are Q^4 and ⅓ are Q^3, giving an overall composition $[Si_6O_{13}]^{2-}$. A similar intercalation of La–Te and silicate sheets occurs in the triclinic structure of $La_4[Si_{5.2}Ge_{2.8}O_{18}][TeO_3]_4$ (**#46**) but here, the layers are || (010), La^{3+} cations have CN8–10, and the silicate–germanate anion is a loop-branched single sheet which is formed by cross-linking of narsarsukite-like tubes (Peacor and Buerger, 1962) running || **x**. Half of the (Si,Ge) are Q^3 and half are Q^4, and Ge > Si in two out of the eight tetrahedral sites.

Structures with monomeric $Te^{4+}O_3$ as part of a larger structural unit that is a finite cluster.

Details for structures **#47–62** are shown in Table 10 (deposited). $HgTeO_3 \equiv [Hg_2(TeO_3)_2]$ (**#47**) has two types of Hg in quite differently distorted coordination polyhedra. Hg1 has two oxygen nearest neighbours at 2.06–2.12 Å and four more oxygen atoms at 2.54–2.73 Å, while Hg2 has one close oxygen neighbour at 2.14 Å, one at 2.30 Å and three more at 2.40–2.46 Å. Using the parameters of Brese and O'Keeffe (1991), the Hg2 distances correspond to bond valences of 0.57, 0.37 and 0.28–0.24 vu, so a 'strong bond' threshold of 0.3 vu would make both Hg atoms 2-coordinate, with O–Hg2–O less symmetrical and less linear than O–Hg1–O. The strong bonds define a structural unit that is a neutral molecule in which Hg1 and Hg2 form a ring with two TeO_3 groups. These molecules lie in layers || (002) and are linked through long Hg···O and Te···O bonds. The complex structure of $Cd_4V_2^{5+}Te_3^{4+}O_{15} \equiv Cd_4[VO_3][(VO_3)(TeO_3)](TeO_3)_2$

https://doi.org/10.1180/minmag.2016.080.093 Published online by Cambridge University Press

(**#48**) contains several structure-building elements. Pyroxene-like zigzag vanadate chains $[V_2O_6]^{2-}$ run || **x**, although these do not contain Te. The most complex structural unit with Te is a cluster $[VTeO_6]^{3-}$ formed by corner-sharing of a VO_4^{3-} tetrahedron and a TeO_3^{2-} pyramid. The V-bearing structural units act as bridges between layers || (020) of relatively weakly-bound CdO_{6-8} polyhedra. The remaining TeO_3^{2-} are attached to the Cd–O layers, and all Te lone pairs point into channels than run || **x**, between the vanadate chains.

In $Pb_2[Pd^{2+}Cl_2(TeO_3)_2]$ (**#49**), two TeO_3 groups are linked through a PdO_2Cl_2 square to make an anionic complex *trans*-$[PdCl_2(TeO_3)_2]^{4-}$. These complexes form layers || (002) which are linked via irregular PbO_5 polyhedra, with the long axes of complexes oriented towards [120] and $[1\bar{2}0]$ in alternate layers. $Bi_2WTe_2O_{10} \equiv Bi_2[WO_4(TeO_3)_2]$ (**#50**) has two TeO_3 groups linked through a WO_6 octahedron to make a complex *cis*-$[WO_4(TeO_3)_2]^{6-}$. These V-shaped anions are linked through irregularly coordinated Bi^{3+} cations. The six shortest Bi–O bonds out to 2.58 Å define edge-sharing chains of distorted BiO_6 octahedra || **y**, which with the Te–W anions make layers || (200). However, longer Bi–O at 2.83 and 3.27 Å link the Bi chains into continuous sheets || (002), alternating with layers of Te–W anions. The cluster anion in $Nd_2W_2Te_2O_{13} \equiv Nd_2[W_2O_7(TeO_3)_2]$ (**#51**) has two TeO_3 linked to an edge-sharing pair of octahedra, W_2O_{10}. However, while Te1 is joined to both W atoms to form a 3-ring of cation-centred polyhedra, Te2 is attached only to W1, giving the overall stoichiometry $[W_2O_7(TeO_3)_2]^{6-}$. These anions lie in layers || $(10\bar{2})$, and are connected through CN8–9 Nd^{3+}.

$K_4[Mo_6Te_2O_{24}] \cdot 6H_2O$ (**#52**) and its isostructural Rb analogue (**#53**) are our first examples of a large family of salts (mainly telluropolymolybdates) in which the structural unit is a modified Anderson–Evans anion (Anderson, 1937; Evans, 1948, 1974). Six MoO_6 octahedra share edges to form a hexagonal ring, but instead of one Te occupying the vacant octahedral site at the ring centre, two pyramidally coordinated Te sit above and below the vacant octahedral position. The hexagonal heteropolyanions lie in layers parallel to $(10\bar{2})$, with their planes normal to either $[11\bar{1}]$ or $[1\bar{1}\bar{1}]$ directions. Water molecules and 8–9 coordinated alkali cations lie between them (Fig. 17).

$Cs_6Na_2[W_6Mo_3S_4O_{20}(H_2O)_3(W_9TeO_{33})] \cdot 11.7H_2O$ (**#54**) and the nearly isostructural $Cs_{7.15}Na_{1.85}[W_6Mo_3S_4O_{20}(H_2O)_2Cl(W_9TeO_{33})] \cdot 11.2H_2O$ (**#55**) have extremely complex heteropolyanions which can be derived from incomplete fragments of the cuboctahedral $TM_{12}O_{40}$ Keggin ion (Keggin, 1934), where T = a tetrahedral cation and M = an octahedral cation. The ion is composed of two dissimilar half-cuboctahedral fragments of the Keggin cage. One fragment has composition $[W_9O_{30}(TeO_3)]$, and has a TeO_3 pyramid rather than a TO_4 tetrahedron bracing a bowl-shaped cluster of WO_6 octahedra (Fig. 17). The other fragment is $[W_6Mo_3S_4O_{26}(H_2O,Cl)_3]$. It has no analogue of the central Te^{4+} cation, and has Mo^{6+} rather than W^{6+} as the cations on one triangular face of the cage. The four anions bonded to two to three Mo and no W are S^{2-} rather than O^{2-}, and the three anions bonded to one Mo only are (H_2O,Cl). The two half-cuboctahedra link through six oxygen atoms to form an ellipsoidal cluster that is similar but not identical to the Wells–Dawson cluster (Wells, 1947; Dawson, 1953; Baker and Figgis, 1970). The clusters are held together by additional water molecules and Cs^+ and Na^+ cations in a wide range of coordination states.

The heteropolyanion in $K_8Na_2[Pd_3(W_9TeO_{33})_2] \cdot 51H_2O$ (**#56**) consists of two half-Keggin subunits linked into a single, large dumbell-shaped anion through a set of three square-planar coordinated Pd^{2+} cations, to make an expanded version of the cluster in **#54–55**. These anions are packed around inverse tetrad axes and linked through $K(H_2O)_{7-9}$ and $Na(H_2O)_6$ polyhedra. $K_9Na[Cu_3(H_2O)_3(W_9TeO_{33})_2] \cdot 16H_2O \cdot$ (**#57**) is almost isostructural but has a much lower water content, and each of the bridging Cu^{2+} ions also has an H_2O molecule associated, to give it 5-fold rather than 4-fold coordination. Unusually, water molecules are included in the structural unit here and in the clusters below, when they are necessary to fully define the coordination environment of a cluster cation.

$[N(CH_3)_4]_2Na_6[Ni(H_2O)_2(Ni(H_2O)_3)_2(WO_2)(W_9TeO_{33})_2] \cdot 23H_2O$ (**#58**) and its analogue with Zn^{2+} replacing Ni^{2+} (**#59**) have slightly more complex clusters in which the W_9TeO_{33} fragments are not half-cuboctahedra but half-anticuboctahedra, in which two square faces share an edge (Fig. 17). These are linked through two $M^{2+}O_3(H_2O)_3$ octahedra and two octahedra that are 50% $M^{2+}O_4(H_2O)_2$ and 50% $W^{6+}O_6$. There is also a partially disordered cluster in $K_{14}[V_{12}^{5+}Mo_{12}^{6+}O_{69}(TeO_3)_2] \cdot 27H_2O$ (**#60**), in which two half-Keggin units each have an average composition $V_{4.5}Mo_{4.5}TeO_{33}$ and are linked through a ring of three VO_4 tetrahedra alternating with three MoO_6

https://doi.org/10.1180/minmag.2016.080.093 Published online by Cambridge University Press

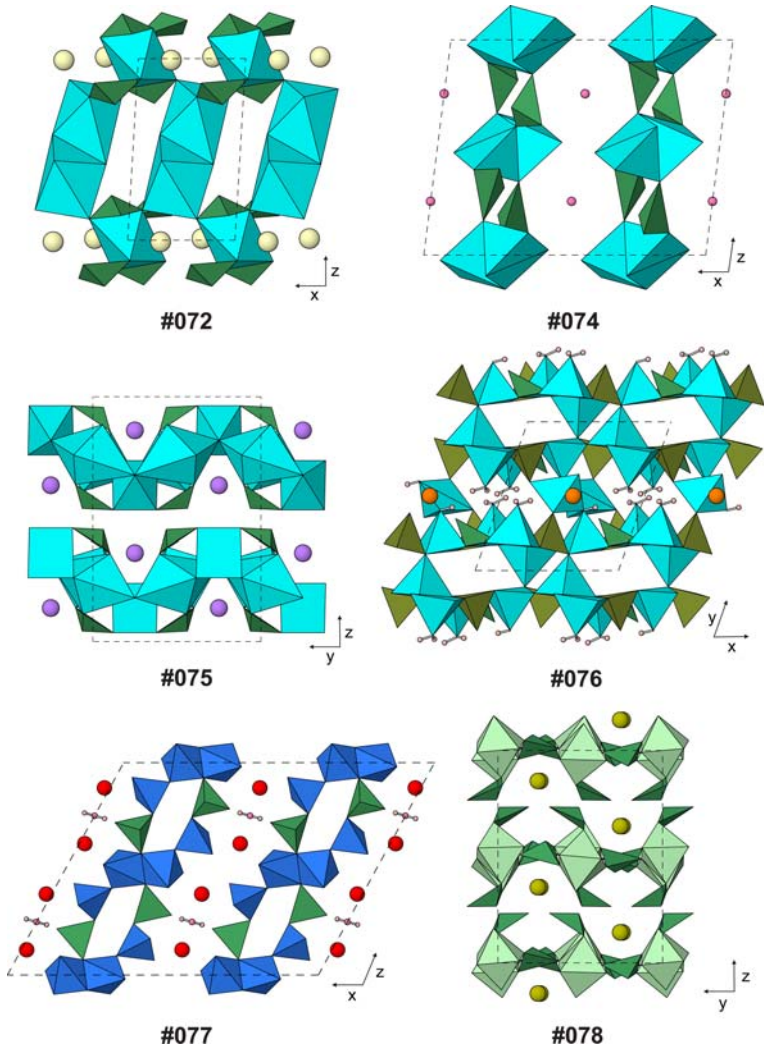

FIG. 18. Examples of structures with monomeric TeO_3 pyramids as part of larger structural units that are chains or layers (Tables 10–11, deposited). Small spheres: H (pale pink). Medium spheres: O (dark pink), when not part of a polyhedron. Large spheres: Bi (pale violet), Ca (orange), Na (dark yellow), Sr (red) and Yb (light yellow). Polyhedra: As (brown-green), Cu (cyan), Ga (light green), Te (dark green) and V (blue).

octahedra. $K_{10}[V_4(V_3Mo_{17}\square)O_{74}](TeO_3)] \cdot 15H_2O$ (**#61**) has a unique cluster that contains two different kinds of half-Keggin unit. One is $(V_3Mo_5\square)TeO_{33}$ with partial V–Mo disorder; this has the same topology as the half-Keggin units of **#54–57** and **#60**, with CN3 oxygen atoms centring the three triangular faces around the sides of the 'bowl' but not the bottom triangular face. The other half-Keggin unit is Mo_9VO_{35}, of the type found in the Wells–Dawson cluster, in which it is the bottom face that is centred, and with a VO_4 tetrahedron instead of a TeO_3 pyramid. Instead of the two 'bowls' facing towards each other, the vanadate bowl is inverted, so that the VO_4 tetrahedron is pointing away from the centre of the cluster. The two bowls are linked through a ring of alternating V and Mo, as for **#60**. The extraordinarily complex structural unit of $(NH_4)[H(Ru_4^{4+}O_6(H_2O)_9)_2(Fe^{3+}(H_2O)_2)_2(W_9TeO_{33})_2] \cdot 36H_2O$ (**#62**) has two half-anticuboctahedra W_9TeO_{33} similar to those of **#58–59**, linked through a pair of $FeO_4(H_2O)_2$ octahedra and also through three oxygen atoms each of two

https://doi.org/10.1180/minmag.2016.080.093 Published online by Cambridge University Press

tetrahedral clusters or corner-sharing RuX_6 octahedra, $Ru_4O_9(H_2O)_9$.

Structures with monomeric $Te^{4+}O_3$ as part of a larger structural unit that is a chain

The next 11 structures (**#63–73**, Table 10, deposited) have TeO_3 groups incorporated into infinite heteropolymeric anions. In magnolite, $[(Hg_2)(TeO_3)]$ (**#63**), each Hg atom is bonded to one other at 2.53 Å to make a $(Hg_2)^{2+}$ dimer, and has no other neighbours apart from one close oxygen at 2.06 Å and three more distant at 2.69–3.00 Å. The Hg dimers and TeO_3 groups form continuous chains –O–Te–O–Hg–Hg–O–Te–O– running || **y** and zigzagging in the (001) plane, with Te atoms at the apices of the bends. The chains are held together only by long Hg···O and Te···O bonds. $BaZn(TeO_3)Cl_2$ (**#64**), better written for our our purposes as $Ba_2[Zn_2Cl_3(TeO_3)_2]Cl$, has double chains || **y** resembling those of the amphibole minerals, in which TeO_3 pyramids instead of tetrahedra alternate with Q^3 ZnO_3Cl tetrahedra and Q^2 ZnO_2Cl_2. The chains lie in double layers || (002) with additional Cl^- and 6–7 coordinate Ba^{2+} between them. Dy $[CuCl(TeO_3)_2]$ and its analogues (**#65–67**) have a loop-branched structural unit, in which TeO_3 pyramids and CuO_4Cl pyramids make CuTeCuTe 4-rings, which link into a chain || **x** through the Cu atoms (Fig. 17). The chains form layers || (002), which are interconnected through zigzag chains of edge-sharing DyO_8. The Te lone pairs and Cl are located in channels which run between the Dy chains and the Cu–Te chains. The compound $Yb_3[Cu^{2+}Cl_2(TeO_3)_2]_2[Cu^{1+}Cl_2]$ (**#68**) has an open-branched chain || **y** in which pyramids $Cu^{2+}O_3Cl_2$ and TeO_3 alternate along the chain backbone, while a second type of TeO_3 acts as a branch sharing an oxygen atom with the Cu. These chains attach on either side of a layer || (100) of edge-sharing YbO_8 polyhedra, with isolated, linear $[Cu^{1+}Cl_2]^-$ anions in the interlayer gap (Fig. 17). $LaNbTeO_6 \equiv La[NbO_3(TeO_3)]$ (**#69**) has NbO_6 octahedra sharing trans corners to make *zweier* chains || **y**; oxygen atoms are shared with Te so as to make two differently oriented Nb_2Te 3-rings, which alternate along the chain. Chains are held together via long Te···O bonds and 8-coordinated La^{3+}. This compound is isostructural with $Pb[MoO_3(SeO_3)]$ (Oh *et al*., 2012).

$Tl_2[(UO_2)(TeO_3)_2]$-β (**#70**) has Te–U–Te–U 4-rings which link through UO_6 octahedra to make loop-branched chains || **x**. These pack in a herringbone fashion, and are linked through ribbons of edge-sharing $TlO_{5–7}$ polyhedra. The α polymorph has a layered structure (**#221**, below). $Sr_3(UO_2)(TeO_3)_4 \equiv Sr_3[(UO_2)(TeO_3)_2](TeO_3)_2$ (**#71**) has similar chains || **y**, all sharing a common attitude, and bridging layers || (200) of $SrO_{7–8}$ polyhedra. Additional isolated TeO_3 brace the Sr layers. The complex chain in $Yb_2[Cu_3Cl_4(TeO_3)_4]$ (**#72**) is again based on linked 4-rings, but the polyhedra are CuO_6 octahedra at the nodes and CuO_3Cl_2 on the loops. One of two types of TeO_3 acts as an additional bridge between two Cu, making Cu_2Te 3-rings, while the other type of TeO_3 shares an edge with CuO_6, so that the bridging oxygens in the Cu chain have CN3. These chains run || **x** and are linked through edge-sharing zigzag chains of YbO_8 to make thick layers || (001) (Fig. 18). The layers are held together only by long bonds to Te. $Bi_2W_3Te_2O_{16} \equiv Bi_2[W_3O_{10}(TeO_3)_2]$ (**#73**) again has loop-branched chains of 4-rings, but the polyhedra are all WO_6, giving a chain stoichiometry W_3O_{14}. TeO_3 groups share non-bridging oxygen atoms to make W_2Te 3-rings, similar to the Cu_2Te of **#72**, and giving a final chain composition $W_3Te_2O_{16}$. The chains run || **y** and lie in layers || (002), which cross-link sheets of BiO_8 polyhedra.

Structures with monomeric $Te^{4+}O_3$ as part of a larger structural unit that is a layer

Structures **#74–#112** (Table 11, deposited) have infinite two-dimensional structural units. $[Cu(NH_3)(TeO_3)](H_2O)$ (**#74**) has a 3-connected net with 4- and 8-rings, topologically similar to the 'apophyllite' layer of mackayite (Fig. 11*i*), but the polyhedra at the nodes are alternately TeO_3 and square-planar $CuO_3(NH_3)$ (Fig. 18). The polyhedra are tilted so that a very elongated octahedron around Cu is completed by another TeO_3 oxygen at 2.60 Å and the H_2O molecule at 3.07 Å. The layers are || (200), and are connected only through H bonds. $Bi[Cu_3O_2(TeO_3)_3]Cl$ (**#75**) has a complex layer in which a hexagonal honeycomb array of CN3 oxygen atoms are linked through the two bridging oxygen atoms of CuO_4 squares. The layer is corrugated because one type of Cu has *trans* bridging oxygen atoms while the other type has *cis*. A Te atom sits above or below each CN3 oxygen, sharing its own oxygens with two *trans* Cu and one *cis* Cu. Elongated octahedra around all Cu are completed by long bonds to Cl. The layers are || (002) and are connected through BiO_8 polyhedra and long Te···O bonds (Fig. 18). Juabite, $Ca[Cu_{10}(AsO_4)_4(TeO_3)_4(OH)_2] \cdot 4H_2O$ (**#76**) has a structure in which double layers || (010) are held

https://doi.org/10.1180/minmag.2016.080.093 Published online by Cambridge University Press

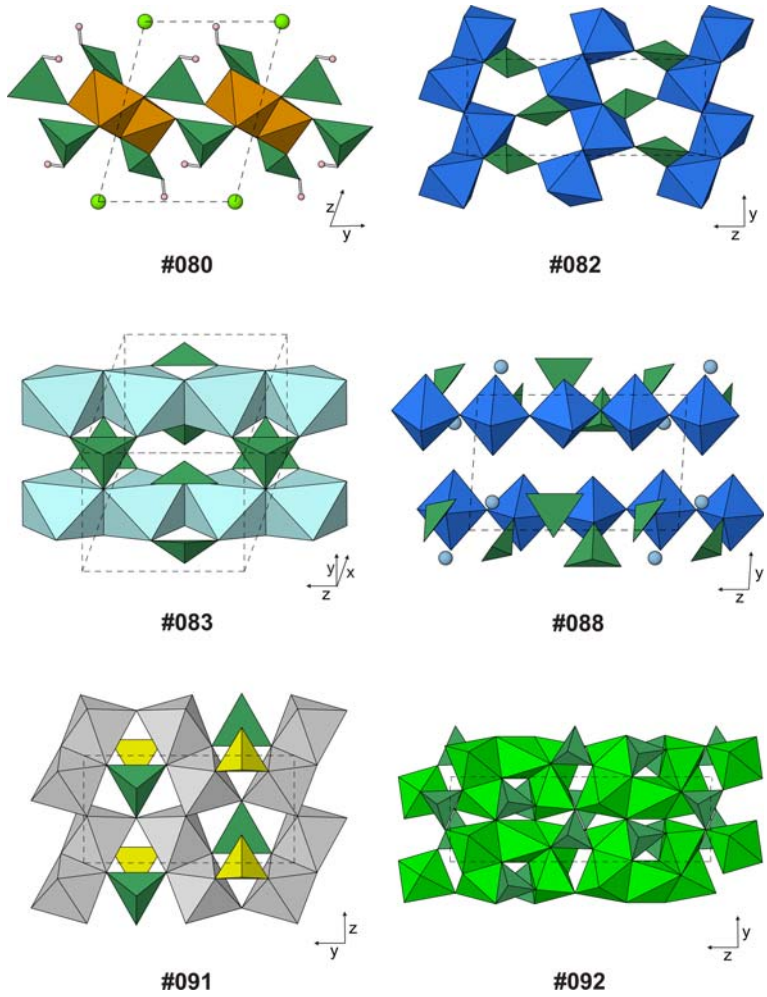

FIG. 19. Examples of structures with monomeric TeO_3 pyramids as part of larger structural units that are layers (Table 11, deposited). Small spheres: H (pale pink). Large spheres: Cl (yellow-green) and Li (pale blue). Polyhedra: Al (pale grey), Fe (orange-brown), In (pale blue), Ni (bright green), S (yellow), Te (dark green) and V (blue).

together only through long Te···O bonds. The two sublayers contain edge-sharing blocks OTe = Cu = O_2 = Cu = O_2 = TeO with long axes || [$10\bar{1}$], which are held together by sharing corners with continuous chains of more CuO_4 squares and AsO_4 tetrahedra (Fig. 18). The resulting net is approximately centred-rectangular, and has 8- and 3-rings. Two such sheets are linked by the inward-pointing apical oxygens of AsO_4 tetrahedra connecting to additional $Cu_2O_4(OH)_2$ dimers. Loosely bound H_2O and CN6 Ca^{2+} lie between the two sublayers.

$Sr_2V_4^{5+}Te_2O_{16} \cdot H_2O \equiv Sr_2[V_2O_5(TeO_3)]_2 \cdot H_2O$ (**#77**) has a structure in which CN5 V1 and CN4 V2 polyhedra share corners with TeO_3 to make chains –V1–V2–Te–V1–V2–Te– running || **z** and zigzagging in the (100) plane. Such chains at two different heights along **x** are linked by edge-sharing of VO_5 polyhedra to make a layer || (200) which is strongly corrugated but not topologically a double layer. Thus, the TeO_3 groups and can be regarded as linking $[V_4O_{14}]$ tetramers (Fig. 18). One oxygen atom of TeO_3 is directed at the interlayer gap, while the lone pair points into a deep fold in the layer. Water molecules and CN8 Sr^{2+} are between the layers.

In $Na[Ga(TeO_3)_2]$ (**#78**), edge-sharing pairs of GaO_6 octahedra are linked through corner-sharing

https://doi.org/10.1180/minmag.2016.080.093 Published online by Cambridge University Press

TeO_3 to make layers || (002) consisting exclusively of Ga–Te–Ga–Te 4-rings. A second type of TeO_3 shares the remaining oxygen atoms of the Ga octahedra, forming Ga–Te–Ga 3-ring loops, which occur in pairs to make a Ga_2Te_2 unit resembling the 'double triangle' tetrameric Te unit that occurs in many Te-only polymers (Figs 10*f*, 10*h*, 13*d*, 13*i*, 15*f*, 15*g* and 16*c*). Layers are linked through CN7 Na^+ ions (Fig. 18). $Na[Fe^{3+}(TeO_3)_2]$ (**#79**) is isostructural. Rodalquilarite, $Fe_2^{3+}Te_4O_9(OH)_3Cl \equiv [Fe_2(TeO_2OH)_3(TeO_3)]Cl$ (**#80**) also has Fe_2Te_2 'double triangles'. These share FeO_6 edges to form zigzag chains || **x**, which are cross-linked via a second type of TeX_3 into layers || (001). The Cl^- lie between the layers, and are weakly bonded to Te (Fig. 19). Oxygen atoms that are not bonded to Fe are 100% OH^- for Te1, 50% O^{2-} 50% OH^- for Te2 (Kampf and Mills, 2011). $[(Fe^{2+}Fe_4^{3+})(TeO_3)_6]Cl_2$ (**#81**) has three types of Fe polyhedra. $(Fe1)O_6$ octahedra share two *trans* corners with $(Fe3)O_5$. $(Fe2)O_6$, share two edges with each other to make zigzag chains || **x**, and a third edge with Fe3, linking all Fe polyhedra into an undulating layer || $(01\bar{1})$ with elongated 12-rings. The mean Fe–O distances are very similar for Fe1 and Fe2 (2.03 *vs.* 2.01 Å), implying that there is little ordering of Fe^{2+} and Fe^{3+}. Two types of TeO_3 share all oxygen atoms with Fe polyhedra, with lone pairs pointing into the interlayer space. As in rodalquilarite, interlayer Cl^- are weakly bonded to Te.

The phase α-$V^{4+}TeO_4 \equiv [VO(TeO_3)]$ (**#82**) is isopuntal with the raspite polymorph of $PbWO_4$ (Fujita *et al*., 1977). Edge-sharing, distorted VO_6 octahedra form V_2O_8 chains || **y**, analogous to the W_2O_8 chains of raspite. These are arranged similarly to the corresponding chains in ferberite, $FeWO_4$ (Ulku, 1967) but with an additional lattice shear so that (1) the anions no longer form a continuous hexagonal close-packed substructure, and (2) the Pb/Te polyhedra are no longer octahedra, but are very irregular (Fig. 19). The structure can be regarded as a distortion of the pucherite type, which is orthorhombic and has an anion array that is still hexagonal close-packed (see discussion of **#648–650** below). In raspite, Pb^{2+} has seven neighbours at 2.3–2.9 Å and no more within 3.2 Å, while $TeVO_4$ shows even less regularity: Te^{4+} has three strongly bound neighbours at 1.75, 2.00 and 2.25 Å, followed by four more within 3.4 Å, at 2.42, 2.59, 3.04 and 3.17 Å. As is typical for V^{4+}, there is one very short bond of 1.73 Å of one of the oxygen atoms that is not linked to Te, although this ligand is also only 2.04 Å from a second V atom. Note that Te^{6+} plays the V/W role in the raspite structure in **#650**, below. The β polymorph of $VTeO_4$ has a very different, layered structure (**#222**, below).

$[InCl(TeO_3)]$ (**#83**) and its Br analogue (**#84**) have edge-sharing chains of InO_4X_2 octahedra (X = Cl or Br) running || **z**, sharing oxygen atoms with TeO_3 groups to make In_2Te 3-rings. The resulting loop-branched chains (similar in topology to the Te chain of Fig. 15*c*), at two different x heights, are linked through the third oxygen ligand of Te to make a corrugated layer || (100), with layers connected only via long $Te\cdots X$ interactions (Fig. 19). $[BiI(TeO_3)]$ (**#85**) has the same space group and similar unit-cell parameters, but is not quite isostructural. The TeO_3 groups are differently oriented, so that they cross-link chains at the same x coordinate, and the structural unit can be described as a double layer rather than a highly corrugated single layer. The Bi coordination polyhedra are BiO_5I_2 rather than octahedra, and share corners along the chain direction **z** rather than edges, while making new shared-edge connections between sublayers.

$YV^{5+}Te_2O_8 \equiv Y[VO_2(TeO_3)](TeO_3)$ (**#86**) has two topological types of TeO_3. The first type (Te2 and Te3) share corners with VO_6 distorted octahedra to complete V_2Te 3-rings above and below a corner-sharing VO_4 layer with a square-net topology similar to those of Fig. 11*a*,*f*. Layers are || (002), and connect through TeO_3 sharing oxygen atoms with edge-sharing sheets of YO_8 polyhedra. The remaining Te1 and Te4 act as additional braces on the Y layer, and are not part of the larger structural unit.

$BaMo_2^{6+}TeO_9 \equiv Ba[Mo_2O_6(TeO_3)]$ (**#87**) has MoO_6 octahedra sharing corners to form zigzag *zweier* double chains || **y**, which are cross-linked via TeO_3 into double layers || (002). BaO_{10-11} polyhedra lie between the layers. $LiV_3^{5+}Te_2O_{12} \equiv Li[(V^{5+}O_2)_3(TeO_3)_2]$ (**#88**) has strips of distorted VO_6 octahedra sharing edges and CN3 oxygen atoms to form chains || **z** similar to the Te chain of Fig. 10*a*. Te1 shares three oxygen atoms with three V of one such chain, making clusters which include a Te_2V_2 'double triangle' motif, while Te2 shares oxygen ligands with V atoms of two chains, to link them into a double layer || (010). CN6 Li^+ cations sit within corrugations of the layer, and layers are held together through weak Li–O and Te–O bonds (Fig. 19). $(NH_4)V^{4+}V^{5+}TeO_7 \equiv (NH_4)[(V^{4+}O)V^{5+}O_3(TeO_3)]$ (**#89**) has extremely corrugated layers || (200) in which alternating $V^{4+}O_6$ octahedra and $V^{5+}O_4$ tetrahedra each share three corners to form 6-rings. TeO_3 shares the otherwise non-bridging oxygen ligand of V^{5+} and two of V^{4+}; the additional

https://doi.org/10.1180/minmag.2016.080.093 Published online by Cambridge University Press

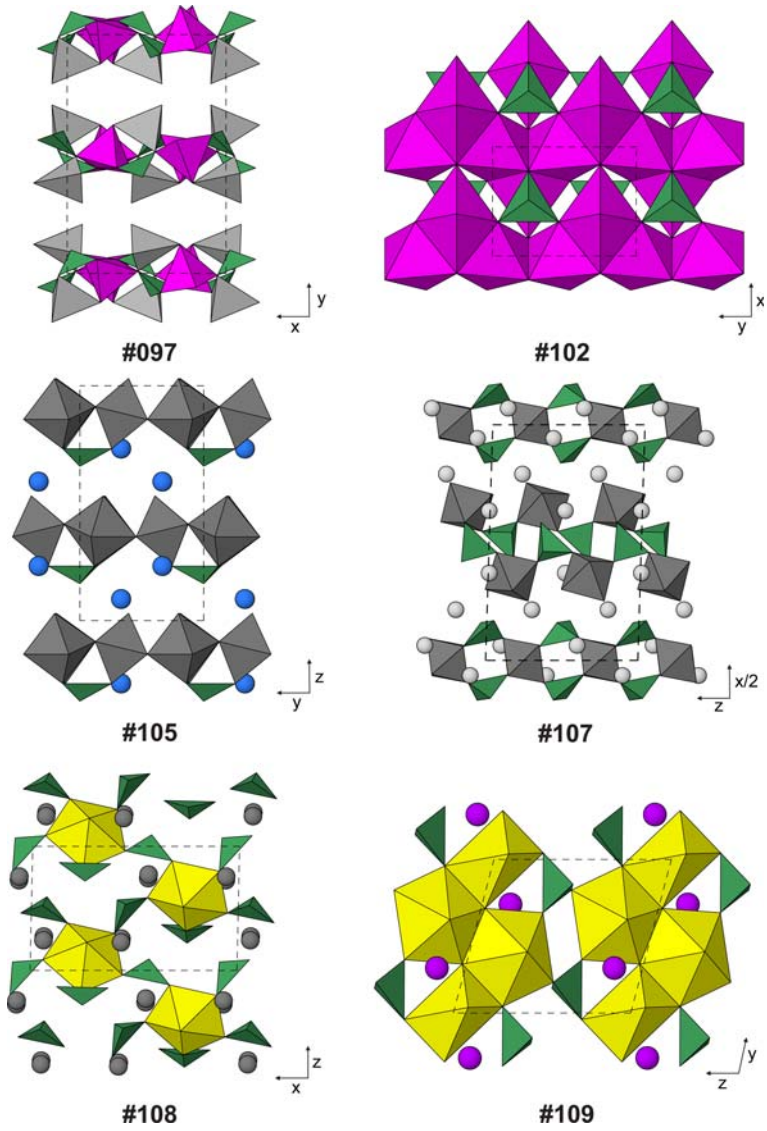

FIG. 20. Examples of structures with monomeric TeO_3 pyramids that are part of larger structural units that are layers (Table 11, deposited). Large spheres: Ag (pale grey), Cs (blue), K (purple) and Pb (dark grey). Polyhedra: Co (magenta), Mo or W (dark grey), Te (dark green), U (yellow) and Zn (pale grey).

connectivity means that the structural unit can be regarded as a double layer. The remaining ligand of V^{4+} is very close (1.61 Å), making a well-defined vanadyl group, $[V=O]^{2+}$. $(NH_4)^+$ ions are in the interlayer gap. $Cs_3[(V^{4+}O)V^{5+}O_3(TeO_3)]_2Cl$ (**#90**) has a closely related structure with similar unit-cell dimensions, in which chains $(V^{4+}V^{5+}O_8)$ || **z** of alternating $V^{4+}O_6$ and $V^{5+}O_4$ do not form continuous layers, but are linked into a single layer normal to **x** through TeO_3. There are four such layers per unit cell, which alternate in their facing direction. The apical oxygen atoms of V polyhedra point towards interlayers that contain Cs^+ ions only, while Te lone pairs point towards another type of interlayer, which contains both Cs^+ and Cl^-.

$[Al_2(TeO_3)(SO_4)(OH)_2]$ (**#91**) has zigzag edge-sharing ribbons of AlX_6 octahedra || **z**, which in turn share corners with each other to make continuous

https://doi.org/10.1180/minmag.2016.080.093 Published online by Cambridge University Press

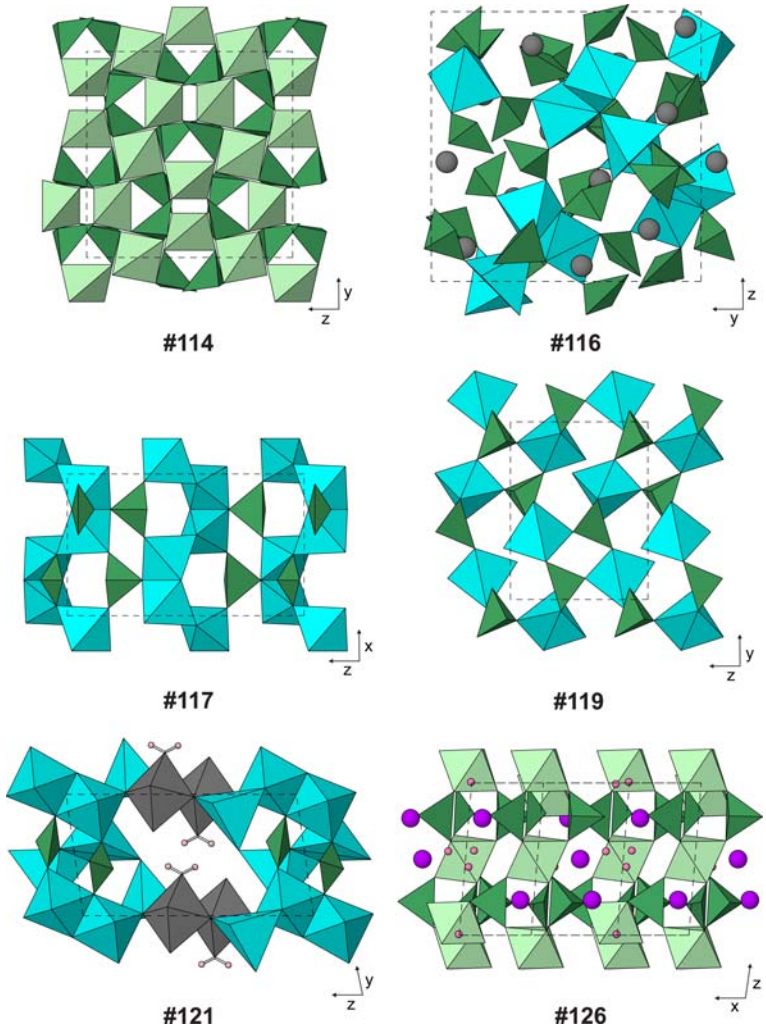

FIG. 21. Examples of structures with monomeric TeO_3 pyramids that are part of larger structural units that are frameworks (Table 12, deposited). Small spheres: H (pale pink) and O (dark pink), when not part of a polyhedron. Large spheres: K (purple) and Pb (dark grey). Polyhedra: Cu (cyan), Ga (pale green), Mo (dark grey) and Te (dark green).

sheets $Al_2O_5(OH)_2$ || (100). The sheets are braced by SO_4 tetrahedra sharing two oxygen atoms and TeO_3 pyramids sharing all three, and successive sheets are held together through very long Te···O bonds (Fig. 19). The compounds $[M_5X_2(TeO_3)_4]$ with M^{2+} = (Ni, Co or Mg), X^- = Cl and Br, (**#92–96**) all have a structure with rather dense layers of edge-sharing MO_6 and MO_5X octahedra || (200), braced by TeO_3 groups. Long Te···X bonds are important in holding the layers together (Fig. 19).

The compounds $[PTX_2(TeO_3)]$ with P^{2+} = (Co, Cu or Zn), T^{2+} = Zn and X^- = Cl and also $[ZnZnBr_2(TeO_3)]$ and $[CoCoBr_2(TeO_3)]$ (**#97–101**) have an orthorhombic structure in which PO_5X and TO_2X_2 polyhedra share corners to make layers || (020) (Fig. 20). Although these compounds are not known as minerals, they are isostructural with sophiite, $[Zn_2Cl_2(SeO_3)]$ (Semenova *et al.*, 1992). $[Co_2Cl_2(TeO_3)]$ (**#102**), the Cl analogue of **#101**, has a different, monoclinic structure with layers of edge-sharing CoO_4Cl_2 and CoO_3Cl_3 octahedra || (001). In both cases, layers are again braced by TeO_3 groups and held together through long Te···X bonds (Fig. 20). $[Cu_3Br_2(TeO_3)_2]$

https://doi.org/10.1180/minmag.2016.080.093 Published online by Cambridge University Press

(**#103**) has CuO_4 squares sharing all corners with edge-sharing pairs of CuO_4Br pyramids to make loop-branched chains || **y** which feature a Cu analogue of the 'double triangle' motif; these chains are bridged by TeO_3 groups to make layers || (001). Long Cu···Br bonds complete an elongated octahedron of ligands around square-coordinated Cu1, and long Te···Br bonds hold the layers together.

$(NH_4)_2Mo_3TeO_{12} \equiv (NH_4)_2[Mo_3O_9(TeO_3)]$ and its Cs analogue (**#104–105**) have a structure in which $Mo^{6+}O_6$ octahedra share four corners to form Mo_3O_{12} layers with the kagome net of 3- and 6-rings. Tellurium atoms share apical oxygen atoms of the Mo octahedra around each 3-ring, to make $[Mo_3O_9(TeO_3)]^{2-}$ layers || (002). Layers are connected through longer Te···O bonds (2.92–2.95 Å) which complete a very distorted octahedron around Te, as well as through interlayer NH_4^+ or Cs^+ ions (Fig. 20). The positions of Mo and Te atoms correspond to those of O atoms in the tridymite structure. Alternatively, the MoO_6 and TeO_{3+3} octahedra can be regarded as forming a hexagonal relative of the pyrochlore framework, in which half of the Mo_3 triangles link to Te above and below the centre of the triangle. The structure is polar (space group $P6_3$) as the TeO_3 pyramids always point in the same sense along **z**. $Rb_2[W_3O_9(TeO_3)]$ (**#106**) is almost isostructural, but with the symmetry reduced to $P31c$ due to slight collapse of the layers. $Ag_6W_3Te_4O_{16} \equiv Ag_6[W_2O_6(TeO_3)_2][WO_2(TeO_3)_2]$ (**#107**) has two types of infinite, strongly-bound structural unit: a layer $[W_2Te_2O_{12}]^{4-}$ and a chain $[WTe_2O_8]^{2-}$; for classification purposes, the layer takes precedence. The chains are loop-branched, with WO_6 octahedra sharing four corners with TeO_3 groups to make W–Te–W–Te 4-rings. They run || **z** and are stacked to make layers || (200), which alternate with the continuous W–Te sheets. The latter have WO_6 and TeO_3 polyhedra alternating in a 3-connected net of 4- and 8-rings with the 'apophyllite' topology (cf. Fig. 11*i*). Layers are held together through long Te···O links and also three types of interlayer Ag^+, in very irregular 5-coordination (Fig. 20).

$Pb_2[(UO_2)(TeO_3)_3]$ (**#108**) has a structure in which UO_7 pentagonal dipyramids share four equatorial oxygen atoms and two types of TeO_3 share two ligands to form layers || (020) of crumpled 8-rings in which Te and U cations alternate. A third type of TeO_3 shares the remaining equatorial oxygen ligand of U, and projects into the interlayer gap, where Pb^{2+} cations in irregular 7–8 coordination hold the structure together (Fig. 20).

In the compounds $A_2[(UO_2)_3O_2(TeO_3)_2]$ (A = K, Rb and Cs: **#109–111**), edge-sharing pairs of UO_7 polyhedra share both CN2 and CN3 oxygen atoms with UO_6 octahedra to form ribbons || **y**, which in turn are bridged by TeO_3 groups to form layers || $(10\bar{1})$, which are held together by CN7–8 interlayer A^+ cations (Fig. 20). $K_4[(UO_2)_5O_5(TeO_3)_2]$ (**#112**) has a similar structure in which broader edge-sharing ribbons ($4 \times UO_7$ and $1 \times UO_6$ polyhedra per asymmetric unit) are bridged by TeO_3 to form layers which are also oriented || $(10\bar{1})$, with 8-coordinated K^+ in the interlayer.

Structures with monomeric $Te^{4+}O_3$ as part of a larger structural unit that is a framework

The TeO_3^{2-} pyramid is incorporated into an infinite three-dimensional structural unit in compounds **#113–194** (Table 12, deposited). The first two examples are $Ga_2(TeO_3)_3$-α, which in this context is more appropriately written $[(Ga_{2.67}\square_{0.33})(TeO_3)_4]$, and $[(Ga_2Zn)(TeO_3)_4]$ (**#113–114**), which both have the structure of eulytine, $Bi_4(SiO_4)_3 \equiv Si_3(BiO_3)_4$ (Menzer, 1931). This framework is made by CN2 oxygen atoms linking one CN4 (Ga, Zn) atom and one CN3 Te atom (Fig. 21). The cation sublattice $(Ga,Zn)_3Te_4$ has the same arrangement as the Th_3P_4 structure (Meisel, 1939; O'Keeffe and Andersson, 1977; Hyde and Andersson, 1989). The much less dense β polymorph of $Ga_2(TeO_3)_3$ is described below (**#136**).

The mineral choloalite, ideally $Pb_3[(Cu^{2+}_{2.67}Sb^{5+}_{0.33})(TeO_3)_6]Cl$ is almost isostructural with $SrCu(TeO_3)_2 = Sr_3[Cu_3(TeO_3)_6]\square$ (**#115–116**). Again, the structure is cubic in symmetry, but rather complex. CuO_4 squares share all corners with Te, and TeO_3 groups share two corners with Cu, to form a framework with a large unit cell ($a \approx 12.5$ Å) and chiral symmetry ($P4_132$). The Cl^- anion, if present, is shared by three (Cu,Sb) atoms as a fifth ligand, while (Pb,Sr) is located in large interstices in irregular 9–12 coordination (Sr) or 6–9 (Pb) (Fig. 21). Balyakinite, $[Cu(TeO_3)]$ (**#117**) has a structure in which edge-sharing pairs CuO_5 square pyramids link corners to form zigzag chains || **x**, which are cross-linked in the **y** and **z** directions into a rather open framework by TeO_3 groups (Fig. 21). Structures **#142** and **#297** are polymorphs. Although the unit-cell parameters and stoichiometry of $[Zn(TeO_3)]$ (**#118**) are similar to those of balyakinite, the structure is different. It features edge-sharing pairs of ZnO_5, but they link with four neighbouring dimers through corners to form continuous corrugated layers || (002), with TeO_3

https://doi.org/10.1180/minmag.2016.080.093 Published online by Cambridge University Press

providing bridges between layers in the **z** direction. $Cu(SeO_3)$ is not isostructural with balyakinite, but one of its four polymorphs has the structure of Zn (TeO_3) (Effenberger, 1986; Hawthorne *et al*., 1986), and another has the perovskite-type structure of high-pressure $Cu(TeO_3)$ (**#142**) (Kohn *et al*., 1976). Teineite, $Cu(TeO_3) \cdot 2H_2O \equiv [Cu(H_2O)_2(TeO_3)]$ (**#119**), the dihydrate of balyakinite, also features square pyramids, although these are $CuO_3(H_2O)_2$, and do not link to each other. The Cu polyhedra share oxygens with Te so that Cu and Te define an open 3-connected framework in which their locations correspond respectively to Ca and half of the Cl of the $CaCl_2$ (orthorhombically distorted rutile) structure (van Bever, 1935; Haines *et al*., 2000). The structure is intrinsically enantiomorphic (space group $P2_12_12_1$) and has rather large channels || **y**, which are braced by hydrogen bonds between water molecules and TeO_3 groups, and into which point the lone pairs of Te atoms (Fig. 21). Chalcomenite, $Cu(SeO_3) \cdot 2H_2O$, is isomorphic (Pasero and Perchiazzi, 1989). Less obviously, the structural unit of $LiV^{5+}TeO_5 \equiv Li[(VO_2)(TeO_3)]$ (**#120**) is topologically the same as $[Cu(H_2O)_2(TeO_3)]$ of teineite, although change in axial ratios and atomic coordinates close the channels (which would be || **x** if they existed). Additional LiO_5 polyhedra share two oxygen ligands with (Te + V), two with (Li + V) and one with a single V atom only.

$[(Cu_6^{2+}Cl_4)(Mo_2^{6+}O_8)(TeO_3)_2] \cdot H_2O$ (**#121**) has a framework made out of two chemically dissimilar components. Square-planar CuX_4, CuO_4 and Cu_2O_3Cl, link corners and some edges to form thick layers || (001), which are braced by TeO_3 groups and additional long Cu···Cl bonds. There are no tetrahedral molybate complexes: instead, MoO_5 square pyramids share edges to form $[Mo_2O_8]^{4-}$ dimers in the interlayer region. These share the four non-apical oxygens with Cu of the layers on either side. Half-occupied H_2O sites complete a very distorted octahedron around Mo: these are at 2.50 Å from the cation, compared to 1.70 Å for the apical oxygen opposite (Fig. 21). $[Cu_7(TeO_3)_2(SO_4)(OH)_6]$ (**#122**) similarly has a framework in which relatively dense layers are connected through sparse bridges. There are five kinds of Cu^{2+}, all in square-planar coordination except that Cu5 has a fifth oxygen ligand if the threshold is set at 2.3 Å. Edge-sharing trimers Cu4 = Cu3 = Cu4 and Cu5 = Cu2 = Cu5 link corners to form complex chains || [101], with additional corners shared between Cu4 and bridging Cu1, which further condense the chains into layers || $(\bar{1}11)$. Layers are linked into a framework through TeO_3 and SO_4 groups, which show some orientational disorder as indicated by splitting of oxygen sites.

$[Ge(TeO_3)_2]$ (**#123**) has a framework in which GeO_6 octahedra and TeO_3 pyramids share corners. Interestingly, the $GeTe_2$ substructure is a slight monoclinic distortion of the rutile structure, with **x** as the pseudotetrad axis. The Ge–O bonds of argutite (rutile-type GeO_2; cf. Haines *et al*., 2000) are replaced by Ge–O–Te links in this compound.

$HLi_2[Ga_3(TeO_3)_6] \cdot 6H_2O$ (**#124**) has Ga–O–Te links between GaO_6 octahedra and TeO_3 pyramids, making a rhombohedral structure with alternating layers of 2 × Ga surrounded by Te in an approximate trigonal prism, and 1 × Ga surrounded octahedrally by Te. $LiO_3(H_2O)_3$ octahedra share faces with the former. There are three of each type of Ga layer per cell. $Na_3[Ga_3(TeO_3)_6] \cdot 7.2H_2O$ (**#125**) has a closely related structure which retains the alternation of sparser and denser Ga layers, but in which Ga is always surrounded by six Te in a trigonal prismatic fashion, and there are only two of each type of Ga layer per unit cell. $Na_3(H_2O)_5$ clusters with each Na bonded to four H_2O and two tellurite oxygen atoms also lie in the sparse Ga layers, and another water site in the denser layers is 36% occupied. $K[Ga(TeO_3)_2] \cdot 1.8H_2O$ (**#126**) has Ga of the sparse layers surrounded octahedrally by Te, as for **#124**. The layers are || (001), but the structure is triclinically distorted. K^+ ions in 7–8 coordination and H_2O molecules occupy interstices in the sparse Ga layers (Fig. 21). $Li_6[Ga_{8.67}(H_2O)_2(TeO_3)_{14}]$ (**#127**) also has alternating sparse and dense Ga layers, but these are quite different to those of **#124–126**. The GaO_6 octahedra of the sparse layer have a pseudo-diad axis || **z** rather than a true triad axis, and those of the denser layers occur in edge-sharing dimers Ga_2O_{10}, which link into a honeycomb-like layer through CN3 water molecules. Out of three types of Te, Te2 and Te3 link the two different types of Ga layer, along with CN5 Li^+, while Te1 sit on triad axes and connect Ga octahedra within the sparse layers.

One dimorph of $[Fe_2^{3+}(TeO_3)_3]$ (**#128**) has FeO_6 octahedra in an approximately face-centred orthorhombic array of face-sharing Fe_2O_9 dimers, all with Fe ≡ Fe vectors || **y**. TeO_3 groups connect an upper oxygen atom of one dimer, lower oxygen atom of a second dimer and middle oxygen atom of a third, to make a continuous framework. The other dimorph (**#129**) has the same *Pnma* space group but a topologically quite different structure in which FeO_6 octahedra share four corners to form Fe_2O_8 layers || (020). As the unshared ligands are *cis* to one

https://doi.org/10.1180/minmag.2016.080.093 Published online by Cambridge University Press

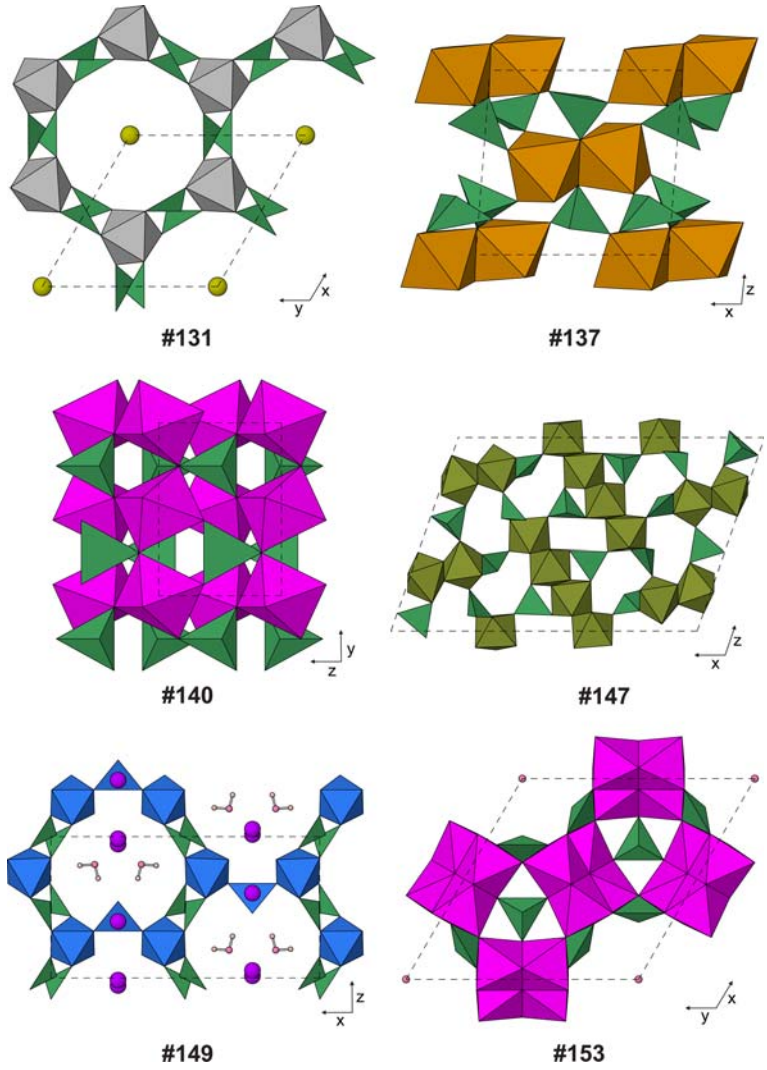

FIG. 22. Examples of structures with monomeric TeO_3 pyramids that are part of larger structural units that are frameworks (Table 12, deposited). Small spheres: H (pale pink) and O (dark pink), when not part of a polyhedron. Large spheres: K (purple) and Na (dark yellow). Polyhedra: Co (magenta), Fe (orange-brown), Sb (brown-green), Te (dark green), V (blue) and Zn (pale grey).

another, the layers are highly corrugated. One of two types of Te braces the Fe layer, with the lone pair pointing into the interlayer gap, while the other type of Te bridges two Fe layers to make a continuous framework, with its third ligand not bonded to Fe. $[In_2(TeO_3)_3]$ (**#130**) is isostructural, but was described in a different axial setting.

Structures **#131–136** all have the microporous zemannite framework, which has zeolitic ion-exchange properties. $Na_2[Zn_2(TeO_3)_3]$ (**#131**) has face-sharing octahedral dimers Zn_2O_9 which are cross-linked through TeO_3 in a fashion very similar to **#128**, except that the dimers are arranged in a very open hexagonal honeycomb pattern (Fig. 22). Thus, the resulting framework has hexagonal channels $\parallel$ **z** that are very large (~10 Å across). Sodium cations occur in the channels in **#131**, and are accompanied by water molecules in $NaH[Zn_2(TeO_3)_3] \cdot 2.67H_2O$ (**#132**) and $Na_2[Zn_2(TeO_3)_3] \cdot 2.97H_2O$ (**#133**). Cobalt

https://doi.org/10.1180/minmag.2016.080.093 Published online by Cambridge University Press

replaces Zn in **#134**. The negative charge on the framework can be modified by substituting trivalent cations for Zn^{2+}, and other channel cations may substitute for Na^{+}. The channel cation is Mg^{2+} in the mineral zemannite itself, $Mg_{0.45}[(Fe^{3+}_{1.12}Zn_{0.80}Mn_{0.08})(TeO_3)_3] \cdot 4.08H_2O$ (**#135**), which can be idealized as $Mg_{0.5}[(Zn^{2+}Fe^{3+})(TeO_3)_3] \cdot 4.5H_2O$, although the data of Miletich (1995*a*) show that the mean charge on *M* can vary over the range 2.33–2.56. The channel contents are arranged as chains $[Mg(H_2O)_6]^{2+}\cdots(H_2O)_3\cdots[Mg(H_2O)_6]^{2+}\cdots(H_2O)_3$ that have local trigonal symmetry, but are orientationally and translationally disordered. Kinichilite, ideally $Mg_{0.5}[(Mn^{2+}Fe^{3+})(TeO_3)_3] \cdot 4.5H_2O$, and keystoneite, $Mg_{0.5}[(Ni^{2+}Fe^{3+})(TeO_3)_3] \cdot 4.5H_2O$, have similar unit-cell parameters to zemannite, but have not had their structures refined (Miletich, 1995*a*). The new mineral ilirneyite, $Mg_{0.5}[(ZnMn^{3+})(TeO_3)_3] \cdot 4.5H_2O$, is also isostructural (Pekov *et al.*, 2015). The channels are completely empty and the framework electrostatically neutral in $[Ga_2(TeO_3)_3]$-β (**#136**), much less dense than the α polymorph with the eulytine structure described above (**#113**). Synthetic selenite analogues of zemannite, $K_2M_2[SeO_3]_3 \cdot 2H_2O$ (*M* = Co or Ni) are also known (Wildner, 1993).

Emmonsite, $[Fe^{3+}_2(H_2O)(TeO_3)_3]$ (**#137**) is triclinic but has pseudotetragonal symmetry down the **x** direction. FeX_6 octahedra occur in edge-sharing dimers $Fe_2O_8(H_2O)_2$, but these stack such that they can be derived from a continuous edge-sharing chain || **x** by deletion of every third Fe atom. The Fe dimers of neighbouring chains are connected through TeO_3 pyramids, which define the walls of nearly-square channels || **x**, which accommodate the Te lone pairs (Fig. 22). There is a marked resemblance to the tetragonal structure of minium, $Pb^{4+}Pb^{2+}_2O_4$ (Gavarri and Weigel, 1975) or schafarzikite, $Fe^{2+}Sb^{3+}_2O_4$ (Fischer and Pertlik, 1975). The atomic arrangement of emmonsite can in fact be regarded as a threefold superstructure of the schafarzikite type with ordered vacancies: $Fe^{2+}_3Sb^{3+}_6O_{12} = (Fe^{3+}_2\square)(Te^{4+}_3\square_3)(O_9(H_2O)_3)$. $Co^{2+}_6[Te^{6+}O_6][Te^{4+}O_3]_2Cl_2$ (**#678**, below) has a closely related structure. $[Ga_2(H_2O)_3(TeO_3)_3]$ (**#138**) has the Ga_2Te_3 substructure arranged approximately like the atoms of α-Ga_2O_3, which has the corundum structure (Marezio and Remeika, 1967). However, there are Te–O–Ga links from Te to only three out of the four nearest Ga. There are two types of Ga atom, one bonded to only tellurite oxygen atoms, while the other centres a $GaO_3(H_2O)_3$ octahedron. The structure is polar, as groups $Ga1(TeO_3)_3Ga2(H_2O)_3$ all point in the same sense along **z**. $[Nb_3O_3(TeO_3)_4]Cl$ (**#139**) has a quite different type of structure, in which linear chains || **y** of corner-sharing NbO_6 octahedra pack in a trellis-like arrangement, and are cross-linked through TeO_3. Lone pairs and Cl^- anions are accommodated in large square channels || **y**.

The $[M(TeO_3)]$ structures **#140–142** (*M* = Co, Ni or Cu) are all of perovskite type. MO_6 octahedra share all corners to form a framework, while Te^{4+} occupies the cubic cages thus defined. The octahedral tilt system is of $a^+b^-b^-$ type, as in $GdFeO_3$ (Glazer, 1972), producing a unit cell with space group *Pnma* and cell parameters $\sqrt{2} \times 2 \times \sqrt{2}$ of the aristotypical perovskite cube. Bending of Fe–O–Fe links and displacement of Gd in $GdFeO_3$ reduce the Gd coordination from 12 equidistant oxygen atoms to six at 2.26–2.39 Å, two at 2.82 Å and four effectively non-bonded oxygen atoms at >3.1 Å (Coppens and Eibschuetz, 1965). However, the displacement of Te in $Co(TeO_3)$ is much more extreme, giving three O at 1.90–1.92 Å, five at 2.70–2.98 Å and four at >3.4 Å. Thus, Te forms only three strong bonds, and acts as a brace on the MO_3 framework (Fig. 22). This form of Cu (TeO_3) (**#142**) is a high-pressure polymorph of **#117** and **#297**. Note that Te^{6+} in octahedral coordination can act as the smaller '*B*' cation in the perovskite structure: **#562–584** below, are examples. An unusual example of Te^{4+} in the '*B*' site of a defect perovskite is provided by **#195**, below.

$[Fe^{3+}F(TeO_3)]$ (**#143**) has zigzag *zweier* chains || **y** of edge-sharing FeO_4F_2 octahedra (the shared edges are alternately F_2 and O_2). TeO_3 groups link trios of neighbouring chains to make a framework. In one polymorph of $V^{5+}_2Te_2O_9 \equiv [V_2O_3(TeO_3)_2]$ (**#144**), alternating VO_5 and VO_6 polyhedra (V1 and V2 respectively) share corners to make a zigzag *vierer* chain V_2O_9, with V2 at the angles in the chain. The V1 polyhedron has a geometry that would be more typical for V^{4+} than V^{5+}: a square pyramid with four V–O distances 1.78–2.00 Å, and a very short distance of 1.58 Å corresponding to an apical V=O double bond. The V2 geometry is an extremely distorted octahedron with four distances 1.97–2.30 Å to oxygen atoms that are shared with V1, Te or both, and two much shorter *cis* distances 1.60–1.72 Å to unshared oxygen atoms. Thus, the structure appears to contain two types of vanadyl (V) complex, $[V{=}O]^{3+}$ and $[O{=}V{=}O]^{+}$. The V chains lie in layers || (100). One of two types of Te shares two oxygen atoms with V1 + 2 × V2 of one chain and the other oxygen atom with V2 of an adjacent chain. The other type of Te bridges between layers to complete the framework. A second polymorph containing Te_2O_5 dimers is described below (**#203**).

https://doi.org/10.1180/minmag.2016.080.093 Published online by Cambridge University Press

Sonoraite, $Fe^{3+}(TeO_3)(OH)\cdot H_2O \equiv [Fe_2^{3+}(OH)_2(H_2O)(TeO_3)_2]\cdot H_2O$ (**#145**), has edge-sharing octahedral dimers $Fe_2O_8(OH)_2$ and $Fe_2O_4(OH)_5(H_2O)$ alternating and linked through shared OH^- corners to make *vierer* chains || [101]. The chains are packed in an approximately hexagonal array, and TeO_3 groups link trios of neighbouring chains into a framework. The non-framework water molecule is loosely held in a structural cage between TeO_3 groups. $[Ta_2O_3(TeO_3)_2]$ (**#146**) has a similar stoichiometry for its structural unit, but a quite different structure in which TaO_6 octahedra share three corners to form a layer || (002) of 4- and 8-rings. The Te atoms are in the interlayer regions, and half of the TeO_3 groups share all three ligands while the other half share only two, in order to link the Ta layers into a framework. The structure of stoichiometrically analogous $[Sb_2^{5+}O_3(TeO_3)_2]$ (**#147**) is again quite different. Half of the SbO_6 octahedra share four corners and half share two corners to make $[Sb_2O_9]^{8-}$ ribbons of zigzagging 4-rings || **y**. These ribbons pack in a herringbone fashion, and are connected into a framework through four crystallographically distinct types of TeO_3 group (Fig. 22). The wide variety of structures possible for $M_2Te_nX_9$ structural units is demonstrated further by $Na_2[W_2O_6(TeO_3)]$ (**#148**), which has a structure in which eight types of WO_6 octahedron share two to three corners to form corrugated layers || (200), which have bands of 4-rings || **y** alternating with bands of 8-rings. Two of the four types of Te act as braces on particular W layers, while the other two types link the layers into a framework. Na^+ cations lie between the layers, in irregular 7–8 coordination. $K_3[(V^{4+}O)_4(V^{5+}O_4)(TeO_3)_4]\cdot 4H_2O$ (**#149**) has clusters of five VO_n polyhedra: four very distorted octahedra $V^{4+}O_6$ (V–O distances are 1 × 1.61, 4 × 1.96–2.07 and 1 × 2.26 Å) and a $V^{5+}O_4$ distorted tetrahedron (2 × 1.63 and 2 × 1.82 Å). The octahedra form two face-sharing dimers V_2O_9, which each share one of their bridging oxygen atoms with the tetrahedron to make a mixed-valence pentameric anion $[V_4^{4+}V^{5+}O_{20}]^{19-}$. All oxygens which are not part of the VO_4 tetrahedron or the $[V=O]^{2+}$ cation are shared with TeO_3 groups, which again connect trios of neighbouring vanadate units into an open framework which has large channels (7–8 Å diameter) running || **y** and **z**. Water molecules and CN 8–10 K^+ ions are in the channels (Fig. 22).

$[Ni_{11}(TeO_3)_{10}Cl_2]$ (**#150**) has five types of NiO_6 octahedra forming thick layers || (001), which are linked into a framework through edge-sharing pairs of NiO_5Cl octahedra. Five types of TeO_3 brace the structure, two of which show orientational disorder, evidenced by mutually exclusive split positions for oxygen atoms. $[Ni_7(TeO_3)_6Cl_2]$ (**#151**) has NiO_5Cl octahedra sharing edges in a very open honeycomb pattern, making very low-density layers || (003). The framework is formed by TeO_3 and additional NiO_6 between the layers and sharing edges with them. $Ni_3(TeO_3)_2(OH)_2$ (**#152**) is more informatively written $[Ni_6(TeO_3)_4(OH)_3](OH)$. It, and its Co analogue (**#153**), have an unusual structure in which face-sharing dimers of octahedral $M_2O_7(OH)_2$ share additional edges to form zigzag chains $M_4O_{10}(OH)_2$ || **z**. These chains in turn share corners to act as walls surrounding large channels (9 Å diameter) along the 6_3 screw axis of the structure, and small channels along the triad axes (Fig. 22). The overall composition of the resulting nanoporous framework is $M_{12}O_{24}(OH)_6$ per unit cell. Two Te occupy the small channels and another six brace the large channels, which contain two more very loosely bound OH^- anions to complete the unit-cell content, $M_{12}(TeO_3)_8(OH)_8$.

In $[Ga_2Mo^{6+}O_4(TeO_3)_2]$ (**#154**), edge-sharing chains || **y** of GaO_6 octahedra are linked through chains $[MoO_4(TeO_3)]$ of alternating TeO_3 and distorted MoO_6 octahedra (4 × 1.71–1.99 and 2 × 2.37 Å) to form undulating layers || (002). A second type of Te connects these layers into a framework. $K[Nb_3O_6(TeO_3)_2]$, its Ta analogue and the corresponding Rb compounds (**#155–158**) have octahedral MO_6 (M = Nb or Ta) sharing four corners to make corrugated layers of 4-rings, M_3O_{12} || (020). Interlayer TeO_3 shares all three corners to link these layers into a framework. CN12 K^+ ions are also in the interlayer gap.

The structure of $[Ni_3(MoO_4)(TeO_3)_2]$ (**#159**) bears some resemblance to those of **#152–153**. Four zigzag chains of edge-sharing NiO_6 and two of corner-sharing NiO_5, all chains having the composition Ni_2O_8, share additional corners to form walls around large pseudohexagonal and small pseudotrigonal channels || **x**, forming a nanoporous framework Ni_6O_{18}. The small channels are empty, but the large hexagonal channels are braced by four TeO_3 pyramids and two MoO_4 tetrahedra. Reduction of some Ni coordination numbers to 5 occurs because of elimination of a bond to an oxygen atom of a neighbouring Ni polyhedron, preventing overbonding of the latter oxygen, which is part of the MoO_4 group. $[Co_7(TeO_3)_4Br_6]$ (**#160**) has layers of *cis*-CoO_4Br_2 octahedra sharing edges to make layers with 7-rings, || (200). The layers are linked into a framework via *trans*-CoO_2Br_4 octahedra, which

https://doi.org/10.1180/minmag.2016.080.093 Published online by Cambridge University Press

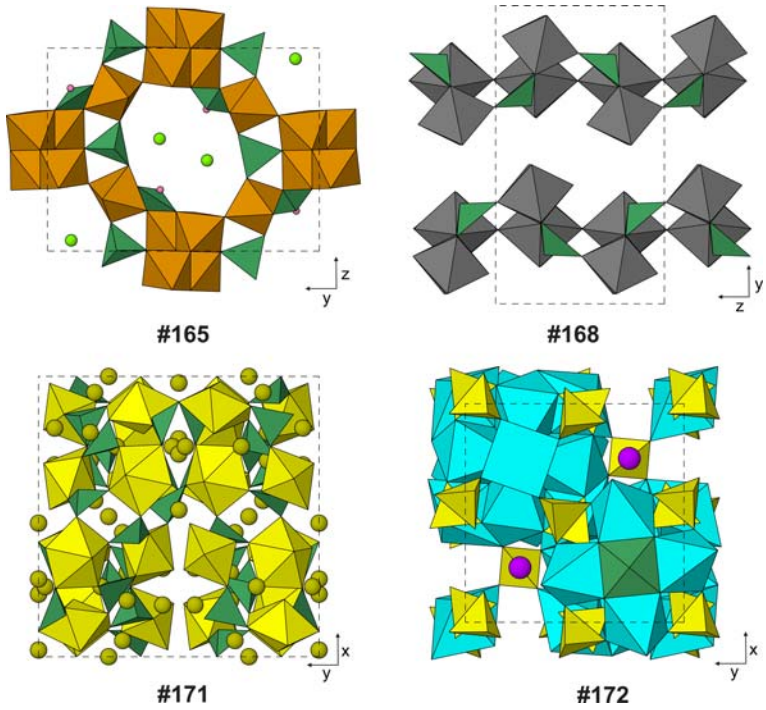

FIG. 23. Examples of structures with monomeric TeO_3 pyramids that are part of larger structural frameworks (Table 12) and nabokoite, in which a TeO_4 square pyramid is part of a structural layer (**#172**, Table 13, deposited). Small spheres: O (dark pink) when not part of a polyhedron. Large spheres: Cl (yellow-green), K (purple) and Na (dark yellow). Polyhedra: Cu (cyan), Fe (orange-brown), Mo (dark grey), S (yellow tetrahedra), Te (dark green) and U (yellow bipyramids).

share faces with octahedra in the layers above and below. Tellurium atoms brace the layers, rather than acting as interlayer bridges. $[Fe_2^{3+}(TeO_3)O_2]$ (**#161**) has corrugated layers of edge-sharing FeO_6 octahedra || (100), with Te bridging across the interlayers. $[Co_2(H_2O)(SO_4)(TeO_3)]$ and its Mn analogue (**#162–163**) have crankshaft chains || **z** of edge-sharing octahedra $MO_5(H_2O)$ (M = Co or Mn), which additionally link their H_2O corners to make undulating layers with 6-rings || (100). The layers are braced by TeO_3 but connected into a framework by SO_4 tetrahedra, which share two oxygen atoms with the layer on one side and one oxygen atom with the layer on the other. $[Zn_2(MoO_4)(TeO_3)]$ (**#164**) has alternating ZnO_6 and ZnO_4 polyhedra sharing corners to make layers of 6-rings || (001). TeO_3 groups span the 6-rings, acting as braces, while interlayer MoO_4 tetrahedra share two oxygen atoms with each adjacent Zn layer to make a framework. $[Fe_3^{3+}O(TeO_3)_3]Cl$ (**#165**) has FeO_6 octahedra sharing edges to make a helical *vierer* chain || **x** that is a thin fragment of a rocksalt-like structure. These chains are linked through two opposite ligands of additional FeO_6 octahedra to make a very open nanoporous framework with rhombic channels || **x** of diameter ~12 × 8 Å (Fig. 23). TeO_3 groups reinforce the cross-links, and have their lone pairs pointing into the large channels. While the non-tellurite O^{2-} ion is part of the structural unit, in the core of the Fe chain, Cl^- is only loosely bound, and sits in the channels.

$K_2[W_3O_9(TeO_3)]$ (**#166**) has WO_6 octahedra sharing four corners to form layers || (020) with the 3- and 6-rings of the kagome net. Tellurium atoms link these layers into a framework, forming additional 3-rings with two W atoms on one or other side of the interlayer gap. Potassium in the interlayer is 8-coordinated. $[Ni_6(Mo_4O_{16})(TeO_3)_2]$ (**#167**) has rhomb-shaped tetramolybdate anions $[Mo_4O_{16}]^{8-}$ which are held together by two CN3 and four CN2 bridging oxygen atoms. Layers of molybdate anions || (200) alternate with layers containing zigzag *sechser* chains of edge-sharing NiO_6 running || y. The molybdate groups link Ni

https://doi.org/10.1180/minmag.2016.080.093 Published online by Cambridge University Press

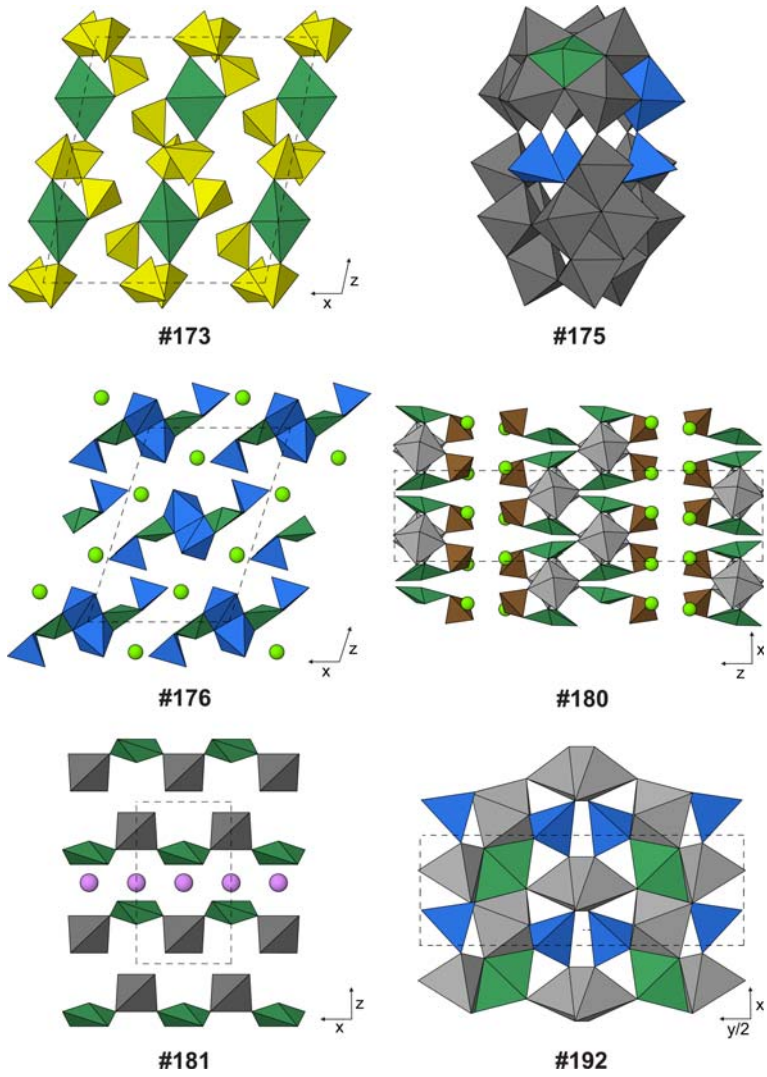

FIG. 24. Examples of structures with monomeric TeO_4 polyhedra that are part of larger structural units (Table 13, deposited). Large spheres: Ba (yellow-green) and Cd (pink). Polyhedra: Co (magenta), Mo (dark grey), Nb or Zn (pale grey), P (brown), S (yellow), Te (dark green) and V (blue). Only the heteropolyanion cluster is shown for **#175**.

chains of the same and successive layers to form a framework. Between the molybdate groups, there are channels || **z** containing the Te, which also cross-link the Ni layers. $[(Mo_2^{5+}Mo_3^{6+})O_{13}(TeO_3)]$ (**#168**) has five types of Mo in very distorted octahedral coordination. There is a very wide spread of Mo–O distances: all Mo atoms have one very short Mo–O of 1.69–1.71 Å, all except Mo1 have one very long (2.38–2.46 Å), while the rest are 1.78–2.13 Å. The bond-valence parameters of Brese and O'Keeffe (1991) give a correspondingly wide spread of individual bond valences (0.22–1.78 vu) but a narrow range of bond-valence sums of 5.82–6.12 vu for all Mo, implying that there is no ordering of Mo^{5+} and Mo^{6+}. MoO_6 polyhedra share four corners to form layers || (002). The layers are of a modified 'tungsten bronze' type, in which bands of 4-rings || **y** alternate with bands of 3- and 6-rings. Mo2–Mo5, in the 4-rings, share additional corners with octahedral in the layers above and below, connecting the layers into a $[Mo_2^{5+}Mo_3^{6+}O_{16}]^{4-}$ anionic framework. The charge-balancing Te^{4+} ion

https://doi.org/10.1180/minmag.2016.080.093 Published online by Cambridge University Press

sits in the 6-ring of the layer (Fig. 23). The TeO_3 group shares an edge with the Mo1 octahedron, where 3- and 6-rings meet, and its remaining ligand is one apical oxygen atom of the Mo1 octahedron of the layer either above or below. A high-temperature polymorph is described as **#281** below. $Ba_2[Nb_6O_{15}(TeO_3)_2]$ and its Ta analogue (**#169–170**) have octahedral MO_6 (M = Nb or Ta) sharing corners to make a three-cation wide layer that is a slice of ReO_3-type structure ‖ (221) of the cubic ReO_3 cell. The layers are connected into a framework by sparse shared edges, which separate the interlayer into channels ‖ **y** of the resulting monoclinic cell. The channels contain CN11 Ba^{2+}, while Te braces the layers but unusually has its lone pair directed in towards the centre of the layer rather than into the interlayer gap. $Na_4[(UO_2)_3(TeO_3)_5]$ (**#171**) has a large ($a \approx 17$ Å) unit cell in a low-symmetry cubic space group ($I2_13$). UO_7 and TeO_3 polyhedra form a framework in which every equatorial ligand of U links to one of three types of Te. The Te2 and Te3 sites lie on triad axes, and are arranged like $2 \times 2 \times 2$ unit cubes of the CsCl structure. Three Te1 and three U form a buckled hexagon around each Te2, and the equatorial oxygen atoms of UO_7 link to the central Te2, the nearest Te3, the two nearest Te1 of the same hexagon and one Te1 of a neighbouring hexagon (Fig. 23). Three types of Na^+ are weakly held in interstices, in irregular 3–6 coordination.

Structures with neso $Te^{4+}X_{4-5}$ as part of the structural unit

Table 13 (deposited) shows structures **#172–194**, in which TeX_4 or TeX_5 polyhedra do not link to other Te. However, it is interesting to note that unlike TeX_3, these polyhedra always link to some other relatively strongly bonded cation, and thus are always part of a larger structural unit. Nabokoite, $K[Cu_7(TeO_4)(SO_4)_5]Cl$ (**#172**) is the only example of a structure with neso square-pyramidal $[TeO_4]^{4-}$ anions (cf. Fig. 4*b*). Favreauite, $Pb[Cu_6(BiO_4)(SeO_3)_4(OH)](H_2O)$, is nearly isostructural according to Mills *et al.* (2014*b*), who noted that the lone-pair cations (Bi, Te) are partially surrounded by corner-sharing CuO_4 squares to make a thick layer ‖ (002), that can be regarded as a slice of the structure of murdochite, $Cu_6Pb^{4+}O_8$ (Dubler *et al.*, 1983). The resemblance is emphasized if the arrangement is considered of oxygen-centred tetrahedra OCu_3A (A = Te and Pb), according to the approach of Krivovichev *et al.* (2013). The layers are braced by SO_4 tetrahedra, while the interlayers contain Cl^-, which is a distant fifth ligand for one of the Cu^{2+} cations, and CN8 K^+ (Fig. 23). Atlasovite, $KCu_6Fe^{3+}BiO_4(SO_4)_5Cl$, is closely associated and appears to be isostructural with nabokoite (Popova *et al.*, 1987).

Four-coordinate Te^{4+} is rare in the square-pyramidal geometry, but occurs much more often in the 'trigonal bipyramid – 1' or 'folded rhombus/kite' geometry of Fig. 4*c*. An example is the pyrosulfate $[Te(S_2O_7)_2]$ (**#173**). The $(S_2O_7)^{2-}$ anions are bidentate ligands for the Te^{4+} cation, so neutral molecules are formed which consist of butterfly-like pairs of Te–S–S 3-rings. These are held together through long Te···O bonds (Fig. 24). In $In_2[Mo^{6+}O_3(TeO_4)](TeO_3)$, (**#174**), InO_6 and InO_8 polyhedra share corners and edges to form a stepped layer ‖ $(10\bar{1})$, which is not treated as a structural unit here, given the high coordination number of half of the In cations. The layers are braced by isolated (TeO_3) pyramids but also by MoO_4 tetrahedra and TeO_4 polyhedra, which share a corner to form the dimeric anion $[MoO_3(TeO_4)]^{3-}$. Layers are held together by long Te···O bonds. A much more complex finite cluster occurs in $(NH_4)_9K[V_4^{4+}V_8^{5+}Mo_{12}^{6+}O_{65}(TeO_4)(TeO_3)_2] \cdot 27H_2O$ (**#175**). The clusters are very similar to the expanded/modified Keggin/Dawson-type anions of **#54–62**, but are included here because it includes not only two TeO_3 groups centring its two dissimilar half-cages, but also a TeO_4 polyhedron as part of one half-cage (Fig. 24). There is considerable (V, Mo) disorder in the half-cuboctahedral cages. One Keggin half-cuboctahedron of composition $[(V_{4.25}Mo_{4.75})O_{30}(TeO_3)]$ shares edges and CN3 oxygens with the Mo octahedra of a ring of three MoO_6 octahedra alternating with three $V^{5+}O_4$ tetrahedra; the Mo and V polyhedra of this ring also share corners with the other half-cuboctahedron $[(V_{4.75}Mo_{4.25})O_{30}(TeO_3)]$, which has the CN4 Te sitting outside one of the square faces, and bonded to the oxygen atoms surrounding that face. The anions pack with their long axes approximately parallel to $[10\bar{2}]$, and are held together through weak bonds to K^+ and NH_4^+ ions and H_2O molecules.

$BaV_2^{5+}TeO_8 \equiv Ba_2[(VO_2)_4(TeO_4)_2]$ (**#176**) has VO_5 polyhedra forming edge-sharing dimers $[V_2O_8]^{6-}$ and isolated tetrahedra $[VO_4]^{3-}$. TeO_4 polyhedra share an edge with VO_5 and the remaining corners with two VO_4 groups to form a *zweier* double chain with 8-rings, $[(VO_2)_4(TeO_4)_2]^{4-}$ (Fig. 24). Expressing the V component as vanadyl $[VO_2]^+$ complexes is suggested by the bond distances: 2×1.65 and 2×1.78–1.83 Å for VO_4 and 2×1.64–1.65 and 3×1.89–1.99 Å for

https://doi.org/10.1180/minmag.2016.080.093 Published online by Cambridge University Press

VO_5. The chains run || **y**, and are flattened || (103); they are linked through CN10 Ba^{2+}. The Sr analogue (**#177**) has a much more complex structure in which eight kinds of VO_n polyhedron occur as corner-sharing dimers, either $O_3V–O–VO_3$ or $O_3V–O–VO_4$, and these are linked through TeO_3 and TeO_4 to make *sechser* double chains with 6- and 10-rings, $[V_8O_{18}(TeO_4)_2(TeO_3)_2]^{8-}$. The subchains are joined through TeO_4 and VO_5 sharing an edge. Two topologically similar but crystallographically distinct types of such chain run || $[1\bar{1}0]$, and are connected through CN8–10 Sr^{2+} ions. $(NH_4)_4[Mo_6O_{16}(TeO_4)] \cdot 2H_2O$ and its Rb equivalent (**#178–179**) have clusters $[Mo_6O_{22}]^{6-}$ in which the six Mo atoms are arranged as a pair of tetrahedra sharing an edge; they are held together through two CN4 oxygen atoms at the centres of the tetrahedra and eight CN2 oxygen atoms along edges. These clusters are linked through Te into continuous complex chains || **z**, held together through NH_4^+/Rb^+ and water molecules.

The structural unit of $Ba[NbO(PO_3)(TeO_4)]$ (**#180**) is a highly corrugated layer || (002). Corner-sharing NbO_6 octahedra form linear chains || **y**. Each pair of adjacent Nb polyhedra then share additional corners with a TeO_4 polyhedron and a PO_4 tetrahedron to form a tetrahedral Nb_2TeP cluster. The Te atom makes an additional link to Nb in the next chain, thus joining chains into layers. Note that TeO_4 and PO_4 share one oxygen atom: the formula above has been written to emphasize the Te coordination, but the structural unit could equally be written $[NbO(PO_4)(TeO_3)]^{2-}$. CN10 Ba^{2+} share edges with the phosphate groups, holding the layers together (Fig. 24). $CdMo^{6+}TeO_6 \equiv [Cd(MoO_2)(TeO_4)]$ (**#181**) has a layered structure that is a highly modified $1 \times 1 \times 2$ superstructure of the fluorite type with ordered cations and also cation and anion vacancies, $(CdMoTe\square)(O_6\square_2) \equiv Ca_4F_8$. The cations occupy ¾ of the sites in a *ccp* array, with a four-layer sequence along **z** in which layers repeat in the order Cd, (Mo+Te), □, (Mo+Te). Only long Te···O bonds hold the structure together across the layers of vacant cation sites. Cadmium is 8-coordinated by oxygen atoms, but half of the oxygen sites that are not adjacent to Cd are vacant. Displacements of the remaining oxygen atoms reduce the coordination number of Te and Mo from 6 to 4, although the geometries are different: respectively 'trigonal bipyramid – 1' and tetrahedral. The TeO_4 and MoO_4 polyhedra share corners to form chains $[MoTeO_6]^{2-}$ that run || [110] and $[1\bar{1}0]$ in alternate layers along **z** (Fig. 24). When smaller divalent cations replace Cd, a small lattice strain reduces the coordination number from 8 to 6, and the symmetry from tetragonal to orthorhombic, as seen for $[M(MoO_2)(TeO_4)]$, (M = Mg, Mn, Co and Zn) (**#182–185**). Given the close structural relationship and very strong layering, the Cd compound has been grouped with these as having a layer rather than chain structural unit, even though 8-coordination would normally exclude Cd^{2+} from the unit as too weakly bonded. In $BaMo_2^{6+}TeO_9 \equiv Ba[Mo_2O_5(TeO_4)]$ and its W analogue (**#186–187**), MO_6 octahedra (M = Mo or W) share three *fac* corners to form undulating layers || (001) of 6-rings that are in chair configuration. The layers are reinforced by TeO_4 sharing edges with two Mo polyhedra and a corner with a third octahedron, while the layers are held together by CN11 Ba^{2+} ions.

The compounds $A_2Mo_2^{6+}Te(PO_4)_2O_6 \equiv A_2[Mo_2P_2O_{10}(TeO_4)]$ (A = Rb, Cs and Tl; **#188–190**) alternating MoO_6 octahedra and PO_4 tetrahedra share corners to form layers $[(MoO_3)_2(PO_4)_2]^{6-}$ || (002) with a 3-connected net of 4- and 8-rings. Interlayer TeO_4 polyhedra link these layers into a framework, sharing corners to make Te–P–Mo 3-rings. The A^+ cations are in 9-coordination in the interlayer. Note that Tl^+ shows little sign of lone-pair stereoactivity (Tl–O = 2.77–3.17 Å, compared to 2.83–3.17 Å for Rb). $Mn^{2+}V_2^{4+}TeO_7 \equiv [Mn^{2+}V_2^{4+}O_3(TeO_4)]$ (**#191**) has double chains || [110] in which pairs of VO_5 alternate with pairs of VO_6, sharing edges and CN3 oxygen atoms in a manner similar to the Te chain of Fig. 10*a*. These chains are linked into double layers || (001) by markedly asymmetric TeO_{3+1} groups (Te–O = 3 × 1.86–1.94 and 1 × 2.34 Å; with no more until 2.87 Å), which share edges with two VO_6 of one chain and a corner with VO_5 of an adjacent chain. The layers are then linked into a framework through MnO_6 octahedra, which also share edges with VO_6 and TeO_4. For simplicity, the formula above does not indicate that each V atom has one very close (1.64–1.67 Å), approximately double-bonded oxygen ligand, as is typical for V^{4+}. The remaining non-tellurite oxygen atom is shared by one VO_6 and two VO_5 polyhedra.

In $Zn_3V_2^{5+}TeO_{10} \equiv [Zn_3(VO_3)_2(TeO_4)]$ (**#192**), two types of ZnO_5 and one of ZnO_6 polyhedra share edges and corners to make very thick, but looped and low-density layers || (020). The higher-valence cations are linked into bow-shaped anions $[O_3V–O–TeO_2–O–VO_3]^{6-}$, which are embedded in the Zn layers, but also cross-link them into a framework through one of the terminal vanadate groups (Fig. 24). $Co_6^{2+}Te_5O_{16} \equiv [Co_6(TeO_4)(TeO_3)_4]$ (**#193**) has blocks of edge-sharing tetramers of CoO_6 octahedra sharing corners with

https://doi.org/10.1180/minmag.2016.080.093 Published online by Cambridge University Press

edge-sharing dimers of CoO_5 to make a framework with large channels running || **y**. Four types of TeO_n groups cross-link across the channels and other interstices between the Co blocks. The only example of TeX_5 in a framework is $Co_3^{2+}Te_2(PO_4)_2O_2(OH)_4 \equiv [Co_3(PO_2)_2(TeO_3(OH)_2)_2]$ (**#194**), which has *trans* edge-sharing chains of CoO_6 octahedra running || **y**. These are linked into layers || (200) through corner-sharing chains of alternating PO_4 tetrahedra and $TeO_3(OH)_2$ square pyramids, $[TePO_5(OH)_2]^{3-}$, and then into a framework through interlayer $CoO_2(OH)_4$ polyhedra.

Dimeric Te^{4+} oxyanions $[Te_2X_n]$ (n = 5–9)

Compounds with dimeric sorotellurite groups are **#195–227**, shown in Table 14 (deposited). The simplest example of the $[Te_2O_5]^{2-}$ anion (Fig. 8*a*) is provided by $Cs_2[Te_2O_5]$ (**#195**). Interestingly, the structure can be regarded as a defect perovskite, with $^1/_6$ of the anions missing. The orthorhombic unit cell corresponds to a $2\sqrt{2} \times 2\sqrt{2} \times 2$ supercell of the aristotypical perovskite cube, with Cs^+ in the large-cation *A* positions and Te in *B* sites. The Te_2O_5 dimers are separated from one another by vacancies on the anion sites and asymmetrical Te–O···Te links, where the short distances are 1.83–1.97 Å and the long ones are 2.68–4.43 Å. The Te–Te vectors of anions point along [110] or $[1\bar{1}0]$ in a herringbone pattern (Fig. 25). The Cs^+ ions are in 9-coordination. $Ba_3[Te_2O_5](TeO_3)Br_2$ (**#196**) has edge-sharing BaO_8Br and BaO_5Br_3 polyhedra forming columns || **y**, which share edges sparsely to surround elongated micelles. These channels accommodate the Br^- anions and also the lone pairs of the Te dimers and monomers, which brace the micelle walls. In $Nd_2[Te_2O_5](TeO_3)(MoO_4)$ (**#197**), NdO_8 polyhedra share edges to form undulating honeycomb layers || (200). The layers are braced by molybdate and tellurite groups, and are held together only by long Te···O bonds.

$TiTeO_3F_2 \equiv [Ti_2OF_4(Te_2O_5)]$ (**#198**) has $TiO_2(O_{0.5}F_{0.5})_2F_2$ octahedra sharing corners to make *zweier* double chains of 4-rings, $[Ti_4O_8F_8]^{8-}$ running || **x**. Te_2O_5 groups share four oxygen atoms with a square of adjacent Ti atoms in the double chain to make Te_2Ti_4 triangular prisms. Long (2.73–2.77 Å) Te···O bonds link the resulting loop-branched double chains into double layers || (020), which are then held together through 2.56 Å Te···F bonds (Fig. 25). $V_2^{4+}Te_2O_7F_2 \equiv [(VO)_2F_2(Te_2O_5)]$ (**#199**) has *cis*-VO_4F_2 octahedra sharing alternately O_2 and F_2 edges to make zigzag *zweier* chains || **x**. Te_2O_5 groups cross-link the V chains into layers || (010) in such a way that Te < (V = V) > Te 'double triangle' clusters are formed. As is typical for V^{4+}, the distance to the non-tellurite oxygen ligand is very short (1.595 Å). The layers are held together via long Te···O and Te···F links. $Fe_8Cu_3Te_{12}O_{32}Cl_{10} \equiv [(Fe^{2+}Fe_7^{3+})(Te_2O_5)_4(TeO_3)_4](Cu_2^{1+}Cl_6)(Cu^{1+}Cl_2)Cl_2$ (**#200**) has zigzag chains of edge-sharing FeO_6 polyhedra || z, which share corners to make layers || (200). These layers are braced by the monomeric and dimeric Te anions. Between the layers lie three types of Cl^- anions. One of these makes long bonds to the Te of Te_2O_5 in the adjacent layers, while the other Cl^- anions form chains of edge-sharing tetrahedra || **z**. The tetrahedral interstices are half occupied by Cu^{1+}, which also occupies linear twofold coordinated sites in the tetrahedron edges that are || **y**. Thus, a chain is formed of alternating $[Cu_2Cl_6]^{4-}$ and $[CuCl_2]^-$ anions (Fig. 25).

The elegant framework structure of $[Cu_2(Te_2O_5)Cl_2]$ and its Br analogue (**#201–202**) has square pyramids CuO_4X (*X* = Cl or Br) that share edges in groups of four to make clusters with a Cu_4O_4 cube at the core and have $\bar{4}$ point symmetry. These clusters sit in columns || **z**, and are linked to their neighbours by corner-sharing with Te_2O_5 groups, which act as the walls of ~6 Å diameter square channels || **z**. The channels accommodate the X^- anions and Te lone pairs (Fig. 25). Our second polymorph of $V_2^{5+}Te_2O_9 \equiv [(VO_2)_2(Te_2O_5)]$ (**#203**) has corner-sharing *zweier* chains of VO_5 polyhedra that lie in layers || (400) and run || [011] or $[0\bar{1}1]$ in alternate layers. Te_2O_5 groups bridge two V chains of one layer and two chains of the next to make a framework. A polymorph with monomeric rather than dimeric TeO_3 groups was described above (**#144**). $Cr_2^{3+}Te_4O_{11} \equiv [Cr_2(Te_2O_5)(TeO_3)_2]$ (**#204**) has edge-sharing dimers of CrO_6 octahedra linked into a framework through Te; only the central oxygen of Te_2O_5 does not link to Cr. $Ni_{3.4}[Ni_{30}(Te_2O_5)_6(TeO_3)_{20}]Br_{14.8}$ (**#205**) and $Ni_{4.5}[Ni_{30}(Te_2O_5)_6(TeO_3)_{20}]Cl_{18.45}$ (**#206**) are isotypical compounds with large cubic unit cells ($Im\bar{3}$, $a \approx 17.5$ Å). The ordered part of the structure consists of NiO_6 and NiO_5 polyhedra which shared edges to form large icosahedral cages, braced by the Te anions, $[Ni_{30}^{2+}(Te_2O_5)_6(TeO_3)_{20}]^{8+}$. The rest of the structure shows substantial disorder. The large cages contain an icosahedral cluster of 12 Ni positions which cannot be >50% occupied due to short Ni···Ni distances. Partly occupied halide anion sites are at the core of these clusters, surrounding their exteriors so that the additional Ni^{2+} are in approximate 4-coordination by $(Br,Cl)^-$,

https://doi.org/10.1180/minmag.2016.080.093 Published online by Cambridge University Press

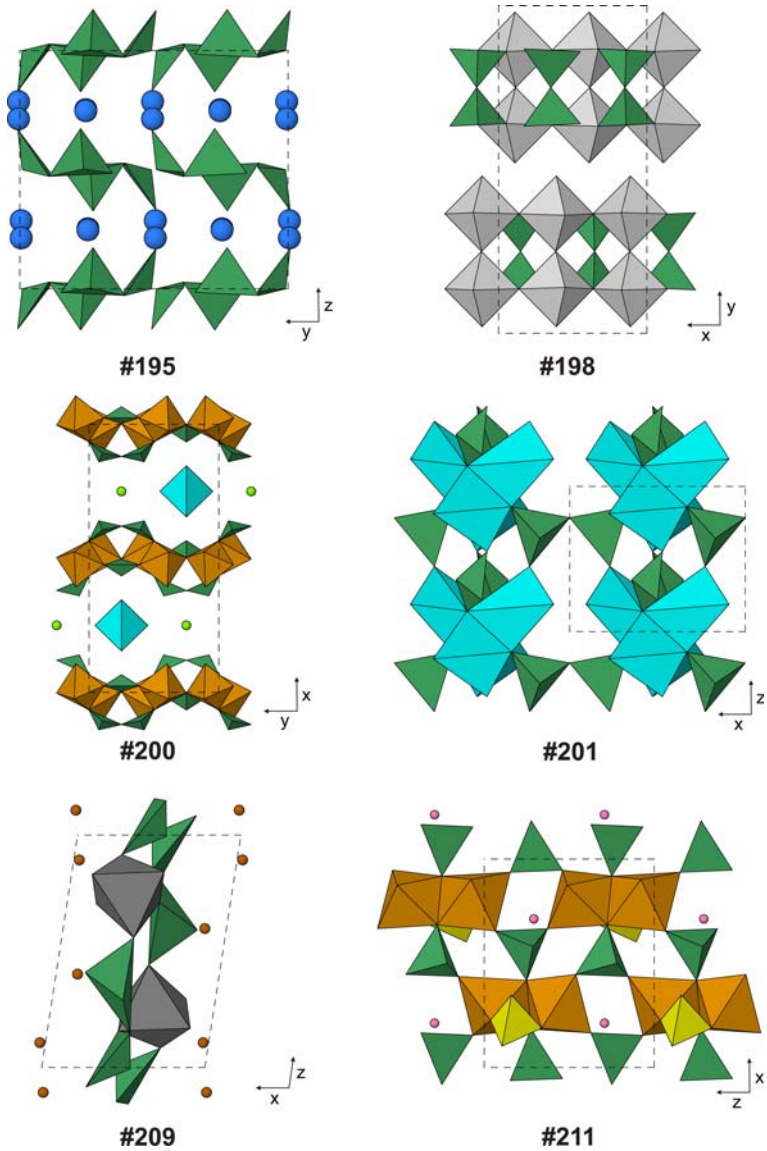

FIG. 25. Examples of structures with $Te_2^{4+}O_{5-6}$ dimers (Table 14, deposited). Small spheres: Cl (yellow-green), N (brown) and O (dark pink) when not part of a polyhedron. Large spheres: Cs (blue). Polyhedra: Cu (cyan), Fe (orange-brown), S (yellow), Te (dark green), Ti (pale grey) and W (dark grey).

and halfway between the Ni clusters in channels || <100>, making long Te···(Br,Cl) bonds.

$Ho_{11}[Te_2O_6]_2(TeO_3)_{12}Cl$ (**#207**) has layers || (012) of edge-sharing HoO_{6-8} polyhedra, sparsely connected into a framework with channels running || **x**. The walls of the channels are braced by six types of monomeric $(TeO_3)^{2-}$ and also a dimer in which TeO_3 shares a corner with TeO_4 to form the structural unit, $[Te_2O_6]^{4-}$ (Fig. 8*b*). The shortest Te–O distance is 2.18 Å; there are no others until 2.47 Å. The Cl^- ion is loosely bound in the centre of the channels, into which the Te lone pairs also point. Moctezumite, $Pb[(UO_2)(Te_2O_6)]$ (**#208**) has similar Te_2O_6 dimers, fringing zigzag chains of edge-sharing UO_7 polyhedra to form broad ribbons || **y**. The ribbons lie in layers || $(10\bar{2})$, which are held

https://doi.org/10.1180/minmag.2016.080.093 Published online by Cambridge University Press

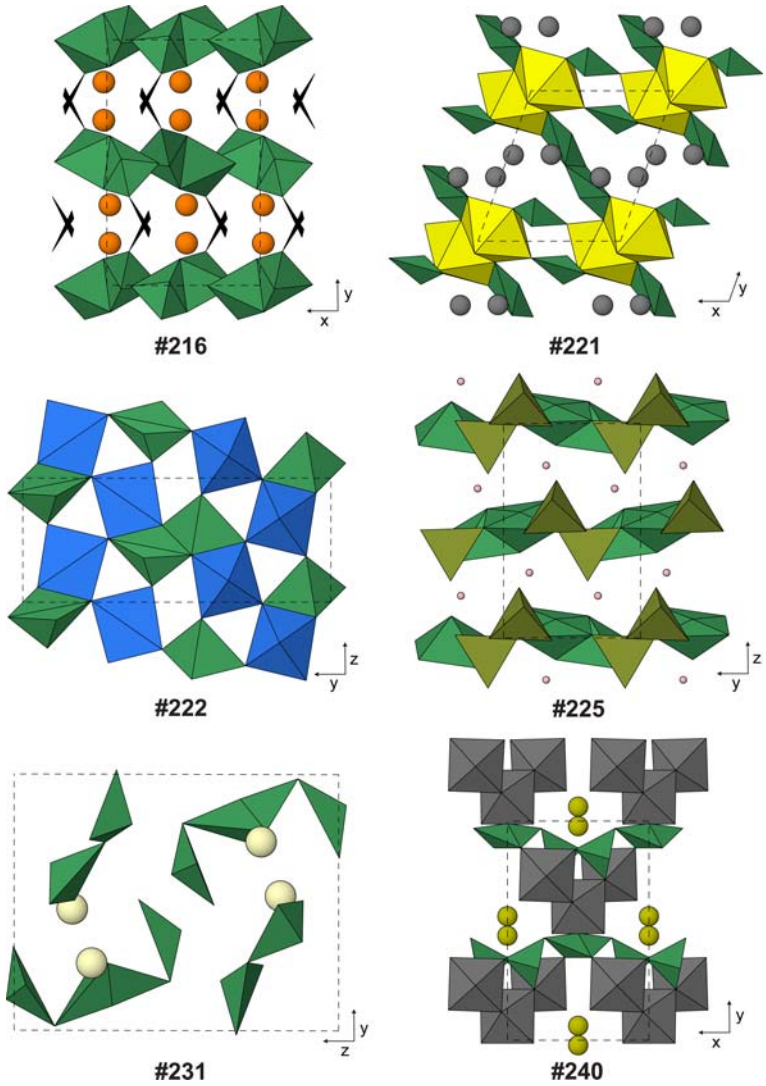

FIG. 26. Examples of structures with soro groups $Te_2^{4+}O_{6-8}$ or Te_3O_8 (Tables 14–15, deposited). Large spheres: Ca (orange), Dy (light yellow), Na (dark yellow) and Tl (grey). Black triangles in mroseite, **#216**: CO_3 groups. Polyhedra: As (brown-green), Mo (grey), Te (dark green), U (yellow) and V (blue).

together by PbO_{3+4} polyhedra. A high-pressure (5.09 GPa) structure of $(NH_4)_2WTe_2O_8 \equiv (NH_4)_2[WO_2(Te_2O_6)]$ (**#209**) has layers ∥ (100) in which WO_6 octahedra share four corners and each Te of Te_2O_6 shares two, to form a net of Te–W–Te–Te–W 5-rings which has the topology of the 'Cairo tiling' (Hyde and Andersson, 1989), seen in less crumpled form in the tetrahedral sheet of the melilite group of minerals, e.g. $(Ca,Na)_2[(Al,Si,Mg)_3O_7]$ (Smith, 1953). Layers are held together by NH_4^+ ions (Fig. 25). $InV^{5+}Te_2O_8 \equiv [In(VO_2)(Te_2O_6)]$ (**#210**) has zigzag corner-sharing chains of InO_6 octahedra ∥ **y**, sharing additional corners with VO_4 tetrahedra to make In–In–In–V 4-rings. Te_2O_6 groups link the resulting ribbons to their neighbours to form thick layers ∥ $(10\bar{1})$, held together only through long Te···O bonds. Showing the V as vanadyl is validated by the asymmetry in V–O distances (2×1.61–1.69 Å and 2×1.81–1.83 Å). Poughite, $Fe_2^{3+}Te_2O_6(SO_4) \cdot 3H_2O \equiv [Fe_2(H_2O)_2$

https://doi.org/10.1180/minmag.2016.080.093 Published online by Cambridge University Press

$(SO_4)(Te_2O_6)] \cdot H_2O$ (**#211**), has an edge-sharing dimer of $FeO_5(H_2O)$ octahedra sharing additional corners with an SO_4 tetrahedron to form a finite 3-ring cluster $[Fe_2O_6(H_2O)_2(SO_4)]^{8-}$. These are linked together in groups of four through Te_2O_6 to make layers || (020), with the remaining H_2O molecule in the interlayer (Fig. 25). $Sr[Cu_2Cl(Te_2O_6)]Cl$ and the isostructural Ba compound (**#212–213**) have Te_2O_6 sharing all six oxygen atoms with Cu_2O_6Cl dimers of CuO_4 and CuO_3Cl squares, to make a rather open framework, with channels || **x** and **y** which contain the remaining Cl^- and also $(Sr,Ba)^{2+}$ ions, coordinated by 6O + 2Cl.

$Pb_3Te_2O_6Cl_2 \equiv Pb_6[Te_2O_6](TeO_3)_2Cl_2$ and its Br analogue (**#214–215**) contain edge-sharing dimers of TeO_4 (Fig. 8*c*). They have edge-sharing layers || $(20\bar{1})$ of PbO_4X_4, PbO_5X_3 and PbO_8X polyhedra (X = Cl or Br). The layers are braced by Te_2O_6 and TeO_3 groups, and loosely held into a framework through Pb–X and Te···X bonds. The Te–O bonds out to 2.05 Å in mroseite (**#216**) define a neutral dimer $[Te_2O_4]^0$, made from an edge-sharing pair of TeO_3 pyramids, suggesting that the formula be written $Ca_2(Te_2O_4)[CO_3]_2$. However, each Te is only 2.31 Å from a carbonate oxygen atom, so it could also be expressed as $Ca[(CO_2)_2(Te_2O_6)]$. The S-shaped $[(CO_2)_2(Te_2O_6)]^{4-}$ heteropolyanions pack in a herringbone pattern to form strongly corrugated layers || (002), which are held together through CN8 Ca^{2+} ions (Fig. 26). $NaV^{5+}TeO_5 \equiv Na_2[(VO_2)_2(Te_2O_6)]$ is isotypical with its K^+ and Ag^+ analogues (**#217–219**). In these compounds, edge-sharing Te_2O_6 dimers share corners with VO_4 tetrahedra to make chains with 4-rings Te–V–Te–V, which extend || [101]. These pack, herringbone fashion, in layers || (020). Large cations between the layers are in 8-fold coordination, but while this is fairly regular for K^+ (K–O = 2.67–2.99 Å), it is less so for the smaller cations (Na–O and Ag–O both = 2.41–2.91 Å). $Ba_2V_2^{5+}Te_2O_{11} \equiv Ba_2[(VO_2)(VO_3)(Te_2O_6)]$ (**#220**) has Te_2O_6 groups alternating with VO_4 tetrahedra to make a *dreier* chain || **y**, which has a second type of VO_4 as an open branch on one of the central oxygen atoms of each Te_2O_6. The chains lie in layers || (200), which have BaO_{8-10} polyhedra between them. The α form of $Tl_2(UO_2)Te_2O_6 \equiv Tl_4[(UO_2)_2(Te_2O_6)(TeO_3)_2]$ (**#221**) has a β dimorph with monomeric TeO_3 in a heteropoly chain structure, **#70** above. The α structure has edge-sharing pairs of UO_7 polyhedra sharing further edges with Te_2O_6 to make ribbons || [110]. The U polyhedra are bridged by additional TeO_3 to link the ribbons into layers || $(1\bar{1}\bar{1})$ with 12-rings and U–Te–U–Te 4-rings. Between the layers are Tl1 showing little lone-pair stereoactivity (8 × O at 2.63–3.13 Å) and Tl2 with much less symmetrical coordination (3 × O at 2.49–2.69 Å and four more at 3.27–3.56 Å) (Fig. 26). The β phase of $V^{4+}TeO_4 \equiv [(VO)_2(Te_2O_6)]$, stable at high-temperature, has corner-sharing VO_5 making zigzag chains || (**#222**); the V polyhedra share edges with Te_2O_6 to make layers || (100) (Fig. 26). The vanadyl oxygen atom is at 1.61 Å from V, but also makes three weak bonds to Te of the next layer (2.96–3.25 Å). There is little resemblance to the raspite structure of the α dimorph (**#82**). $NiV_2^{5+}Te_2O_{10} \equiv [Ni(VO_2)_2(Te_2O_6)]$ (**#223**) has distorted VO_6 octahedra sharing edges to make zigzag chains $[V_2O_8]^{6-}$ || **x**. Te_2O_6 groups each bridge four such chains, while NiO_6 octahedra bridge two V chains and two Te_2O_6 groups, forming a quite dense framework with many Ni–V–V and Ni–V–Te 3-rings.

$BaMo_2Te_2O_{11} \cdot H_2O \equiv Ba[Mo_2O_4(Te_2O_7)] \cdot H_2O$ (**#224**) has *cis*-corner-sharing MoO_6 octahedra forming helical *vierer* chains || **y**. These are linked into thick layers || (002) via Te dimers which are corner-sharing $[Te_2O_7]^{6-}$ groups (Fig. 8*d*), if Te–O distances out to 2.43 Å are included. Water molecules and CN10 Ba^{2+} ions are between the layers. Polymorph I of $TeO(As^{5+}O_3OH) \equiv [(AsOH)_2(Te_2O_8)]$ (**#225**), like many compounds of Te with other high bond-valence cations, has Te^{4+} in 5-coordination. Here, two TeO_5 pyramids share edges to make a $[Te_2O_8]^{8-}$ dimer (Fig. 8*e*). These share corners with $[AsO_3OH]^{2-}$ tetrahedra to make As<(Te=Te)>As clusters which are yet another variant of the common 'double triangle' motif (Fig. 26). The remaining unprotonated oxygen atom on As is shared with Te of a neighbouring cluster, linking clusters to form double chains || **y**. Chains are held together through hydrogen bonds and long Te···O bonds. Tellurium polyhedra are condensed further in polymorph II (**#299**, below). The edge-sharing Te_2O_8 group also features in $Ba_2TeO(PO_4)_2 \equiv Ba_4[(PO_2)_2(PO_3)_2(Te_2O_8)]$ (**#226**), where such groups are bridged by pairs of corner-sharing PO_4 tetrahedra to form *dreier* chains with [–Te = Te–P–] backbones, not unlike the Te–V chains of **#220**. Again, a second type of tetrahedron forms open branches, but this time, the additional PO_4 groups attach to a single Te atom rather than to a bridging oxygen of the chain backbone. The resulting ribbons lie in layers || $(10\bar{1})$, with BaO_{9-11} between them. $Te_2O(PO_4)_2 \equiv [P_2(Te_2O_9)]$ (**#227**) again has CN5 Te^{4+} (cf. **# 225**), but this time in corner-sharing dimers $[Te_2O_9]^{10-}$ (Fig. 8*f*). The dimers are linked into a framework through

https://doi.org/10.1180/minmag.2016.080.093 Published online by Cambridge University Press

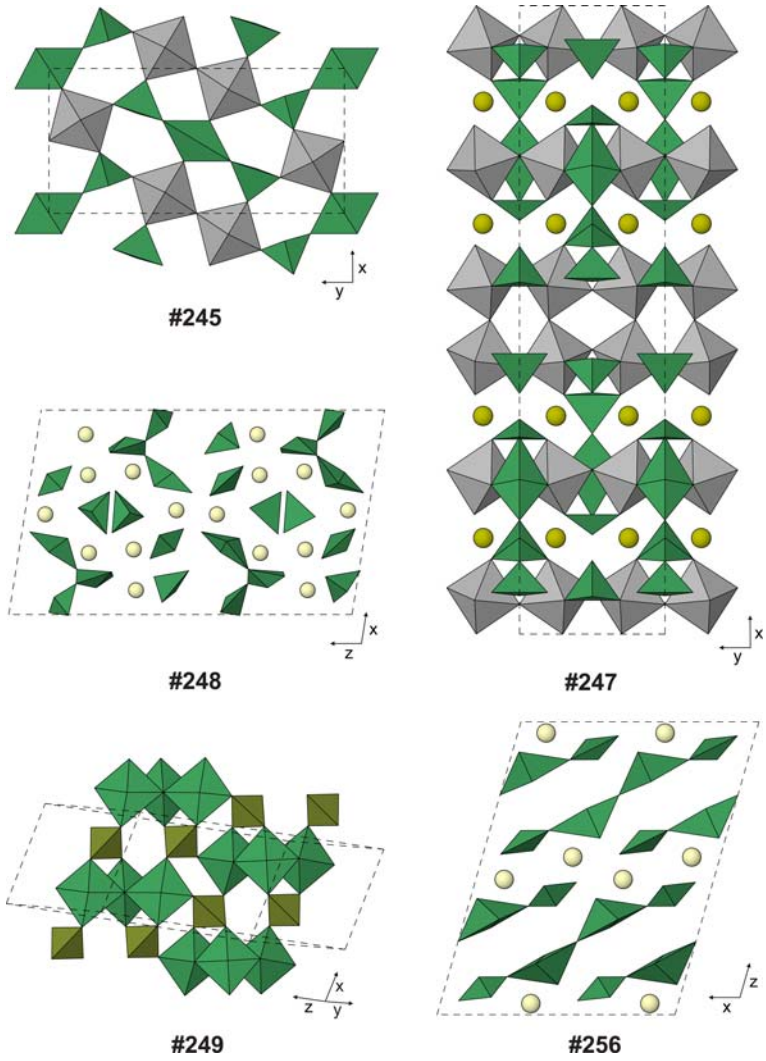

FIG. 27. Examples of structures with soro groups $Te_3^{4+}O_{8-11}$ or Te_4O_{11} (Table 15, deposited). Large spheres: rare-earth elements Dy or La (light yellow) and Na (dark yellow). Polyhedra: As (brown-green), Nb (grey) and Te (dark green).

two types of PO_4 tetrahedra: one type shares oxygen atoms with Te atoms of four different dimers, whereas the other type links only three dimers, but forms a Te–Te–P 3-ring with both Te atoms of one of them.

Trimeric Te^{4+} oxyanions $[Te_3X_n]$ (n = 8–11)

Trimeric sorotellurite groups occur in structures **#228**–**249** (Table 15, deposited). $Sr_3[Te_3O_8](TeO_3)$ (**#228**) has a triclinic structure in which 2-wide and 4-wide ribbons of edge-sharing SrO_{7-9} polyhedra run || **x** and are linked into a framework through a few additional shared edges. Two types of $[Te_3O_8]^{4-}$ (Fig. 8*g*) and two types of monomeric $[TeO_3]^{2-}$ line channels || **x** in the Sr–O matrix. $Ba_3[Te_3O_8](TeO_3)$ (**#229**) is nearly isostructural, although with **x** and **z** axes exchanged, as published. However, it retains a centre of inversion symmetry that is lost in the Sr compound, concomitant with which all Te_3O_8 groups are equivalent and Ba^{2+} has CN = 8–9. Both structures resemble the unexpectedly complex structures of

https://doi.org/10.1180/minmag.2016.080.093 Published online by Cambridge University Press

the (Ca,Sr)(TeO_3) phases (**#9–15**). $BaLa_2[Te_3O_8](TeO_3)_2$ (**#230**) is quite different, in that it has layers || (200) of edge-sharing BaO_{12} and LaO_8 polyhedra, which are braced by TeO_3 groups and bridged by Te_3O_8. The series $A_2[Te_3O_8](Te_2O_5)$ (A = Dy, Ho, Er, Tm, Yb, Lu and Y; **#231–237**) show even less polymerization of large-cation polyhedra. They have 4-wide ribbons of edge-sharing $AO_{7–8}$ polyhedra running || **x**. Interestingly, the Te_3O_8 groups do not link the ribbons, but only decorate their edges, while Te_2O_5 groups link the ribbons into thick double layers || (001) (Fig. 26). Long bonds to both types of tellurite anion hold the layers together. $Sr_4[Te_3O_8]Cl_4$ (**#238**) has SrO_8Cl, SrO_4Cl_5 and SrO_2Cl_7 polyhedra. These share O_2 edges to form 8-cation-wide ribbons of a fluorite-like structure || **y**, which connect through the longer Sr–Cl bonds into continuous layers || $(20\bar{1})$, and more sparsely into a three-dimensional framework. The Te_3O_8 groups brace the Sr–O ribbons. In $La_2[Te_3O_8](MoO_4)$ (**#239**), LaO_9 polyhedra share faces, edges and corners to form an open framework La_2O_{11} that has channels || **x** and **y**. Te_3O_8 groups run down the length of the **y** channels, sharing all oxygen atoms with La, while MoO_4 tetrahedra brace the **x** channels, sharing only three ligands with La.

$Na_2Mo_3Te_3O_{16} \equiv Na_2[Mo_3O_8(Te_3O_8)]$ and its Ag analogue (**#240–241**) have MoO_6 octahedra sharing edges to form V-shaped trimers [Mo2 = Mo1=Mo2], which are linked via Te_3O_8 groups [Te2–Te1–Te2] to form complex loop-branched *dreier* chains || **x**. The chain has two equivalent backbones –Te1–Te2–Mo2– and –Te1–Mo2–Te2–, which intersect at Te1 and are further braced through Mo1=Mo2 and a CN3 oxygen atom which bonds to Mo1, Mo2 and Te2. Chains are held together via CN6–8 $(Na, Ag)^+$ (Fig. 26). $Ca[Co_2Cl_2(Te_3O_8)]$ and its isostructural Sr–Co and Sr–Ni analogues (**#242–244**) have a structure in which MO_5Cl octahedra (M = Co or Ni) share edges to form helical *vierer* chains || **y** (cf. **#165** and **224**). Te_3O_8 groups bridge these chains to form double layers || (002), the long axes of the Te anions pointing || [110] on one side of the layer and || $[1\bar{1}0]$ on the other side. CN8 $(Ca,Sr)^{2+}$ ions sit in the cores of the double layers, which are held together through long Te···Cl interactions. $Nb_2Te_3O_{11} \equiv [Nb_2O_3(Te_3O_8)]$ (**#245**) has ladder-like *einer* double chains of 4-rings || **z** of corner-sharing NbO_6 octahedra, arranged in a herringbone pattern. Te_3O_8 groups share two corners with octahedra in each of the Nb chains in the ±**x** directions and one corner with each of the Nb chains in the ±**y** directions, forming a framework (Fig. 27). $NaNb_3Te_4O_{16} \equiv Na[Nb_3O_5(Te_3O_8)(TeO_3)]$ (**#246**) has broader *zweier* triple chains of 4-rings || **y** of NbO_6 octahedra, which are decorated by the TeO_3 monomer, making Nb–Nb–Te 3-rings. The Te_3O_8 groups link each Nb ribbon to three of its neighbours in a framework. The CN8 Na^+ ion lies between the TeO_3 monomers of neighbouring Nb chains. $Na_{1.4}Nb_3Te_{4.9}O_{18} \equiv Na_{1.4}[Nb_3O_4(Te_{2.9}O_8)(TeO_3)_2]$ (**#247**) has a very similar composition and two very similar unit-cell parameters, but the topology is quite different. The NbO_6 octahedra form single and double *zweier* chains || **y**, that alternate in the **x** direction. Te_3O_8 groups are slightly defective, in that the central Te is only 90% occupied. They link Nb single chains with each other and with neighbouring double chains, forming an open framework with numerous Nb–Nb–Te and Nb–Te–Te 3-rings, while two types of TeO_3 monomer form additional Nb–Nb–Te rings on the double chains. The CN8 Na^+ ions partially occupy sites that lie in channels || **y** (Fig. 27).

$Dy_2(TeO_3)_3 \equiv Dy_4[Te_3O_9](TeO_3)$ (**#248**) has a surprisingly complex structure with thick, loop-branched layers of edge-sharing $DyO_{7–8}$ polyhedra || (100). These are bridged by V-shaped corner-sharing trimers $[Te_3O_9]^{6-}$, including Te–O distances out to 2.44 Å (Fig. 8*h*), and three types of independent $(TeO_3)^{2-}$ ion (Fig. 27). The high As^{5+}–O bond valence (~1.25 vu) leads to Te adopting 5-coordination in $Te_3O_3(AsO_4)_2 \equiv [As_2(Te_3O_{11})]$ (**#249**). Three TeO_5 pyramids share a common CN3 oxygen atom and two CN2 oxygen atoms to form $[Te_3O_{11}]^{10-}$ trimers (Fig. 8*i*). AsO_4 tetrahedra share two corners with one such trimer and one each with two neighbouring trimers to form continuous layers || (010), with Te–Te–As 3-rings, Te–As–Te–As 4-rings and Te–Te–As–Te–Te–As 6-rings. Layers are held together only through long Te···O bonds (Fig. 27).

Finite Te^{4+} oxyanions $[Te_mX_n]$ with $m \geq 4$

$Na_2Te_2O_5 \cdot 2H_2O \equiv Na_4[Te_4O_{10}] \cdot 4H_2O$ (**#250**) has linear $[Te_4O_{10}]^{4-}$ tetramers with a central shared edge (Fig. 8*j*). These lie in layers || (001) with their long axes all || [110]. Water molecules and CN5–6 Na^+ ions lie between the layers. The analogous NH_4^+ compound (**#251**) has Te_4O_{10} groups lining up nose-to-tail to form rods || $[10\bar{1}]$, which pack in a hexagonal array, with NH_4^+ ions and H_2O molecules between them. $Sc_2Te_5O_{13} \equiv Sc_4[Te_4O_{10}](Te_3O_8)_2$ (**#252**) has ScO_6 and ScO_7 polyhedra sharing alternately corners and edges to form zigzag chains || **x**. Linear Te_4O_{11} groups

https://doi.org/10.1180/minmag.2016.080.093 Published online by Cambridge University Press

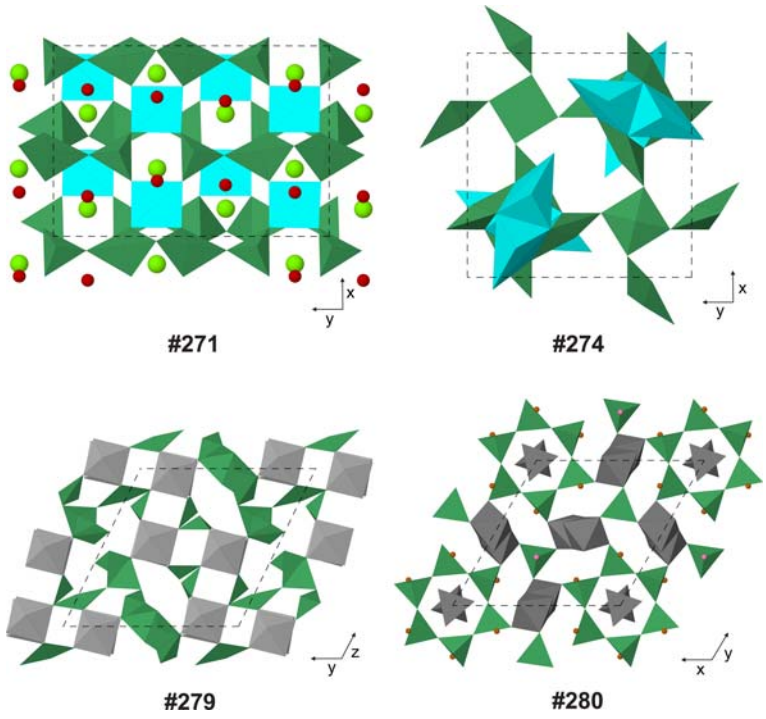

FIG. 28. Examples of structures with soro groups $Te_4^{4+}O_{11}$, Te_5O_{12}, $Te_{10}O_{26}$ or cyclo Te_6O_{12} (Table 15, deposited). Small spheres: N (brown) and O (dark pink) when not part of a polyhedron. Medium spheres: Br (red). Large spheres: Ba (yellow-green). Polyhedra: Cu (cyan), Mo (dark grey), Nb (pale grey) and Te (dark green).

pointing || [01$\bar{1}$] connect the Sc chains to make double layers || (001), while C-shaped Te_3O_8 groups wrap around individual Sc chains. The double layers contain slot-like micelles || **x** which accommodate most of the Te lone pairs; layers are held together through long Te···O bonds. $Ca_2[Cu(Te_4O_{10})]Cl_2$ (**#253**) has Te_4O_{10} groups pointing || [011], sharing corners with CuO_4 squares to make a continuous layer || (01$\bar{1}$). The Ca^{2+} ions form zigzag edge-sharing chains of CaO_7 polyhedra || **x** between the Cu–Te layers. Cl^- ions also lie in the interlayer gap, and complete a very elongated octahedron around Cu^{2+} (Cu–Cl = 2.74 Å). $Sm_2Mn^{2+}Te_5O_{13}Cl_2 \equiv Sm_4[Mn_2(Te_4O_{10})(Te_3O_8)_2]Cl_4$ and isostructural $Dy_4[Cu_2(Te_4O_{10})(Te_3O_8)_2]Br_4$ (**#254–255**) have Te anions pointing || [10$\bar{2}$] and arranged in layers || (201); each layer contains both Te_4O_{10} and Te_3O_8 groups. The anions are held together by (Mn,Cu)O_6 octahedra between the layers, which are considered part of the structural unit, and edge-sharing ribbons of (Sm,Dy)O_8 polyhedra, which are not. A very open framework results, in which there remain elongated channels || **y** which accommodate $(Cl,Br)^-$ anions, which are weakly bonded to Te. Unusually, the CuO_6 octahedron is not much less regular than MnO_6 (Cu–O = 1.99–2.32 Å, vs. Mn–O = 2.12–2.28 Å).

The compounds $A_2[Te_4O_{11}]$ (*A* = La–Nd, Sm–Lu and Y; **#256–270**) show the progressive, monotonic change in parameters and properties with atomic number that is characteristic of the lanthanide elements. In particular, the fourth-shortest Te2–O distance changes so much along the series, from 2.515 Å for the La compound to 2.354 Å for Lu, that the classification of the Te anion(s) changes if the usual 'strong bond' threshold of 2.40–2.45 Å is used. For such a threshold, the compounds of larger *A* cations such as La would be regarded as having dimeric $[Te_2O_5]$ + two monomeric TeO_3 groups. In order to keep this family of isostructural compounds together, a threshold of 2.53 Å is used for all of them, and they all classify as having corner-linked tetramers $[Te_4O_{11}]^{6-}$ (Fig. 8*k*), with the long Te–O bonds linking the terminal Te1 atoms to the core Te2–Te2 dimer. The third-shortest Te2–O distance increases slightly from 1.989 to 2.022 Å as the *A* cation decreases in size from La to Lu. The

https://doi.org/10.1180/minmag.2016.080.093 Published online by Cambridge University Press

structure is relatively simple, with layers || (002) of edge-sharing AO_8 polyhedra linked through linear Te_4O_{11} groups that all point || [20$\bar{1}$] (Fig. 27). $Ba_2[Cu_2(Te_4O_{11})]Br_2$ (**#271**) has layers in which Te_4O_{11} groups with long axes || **y** share corners with CuO_4 squares to make sheets with Cu–Te–Te 3-rings, Cu–Te–Cu–Te 4-rings and Cu–Te–Te–Cu–Te–Te 6-rings. The sheets are parallel to (001) but have a polarity in the **z** direction; a pair of such sheets occurs back-to-back in every *c* repeat. BaO_{10} polyhedra occur in the interlayer gaps that that are faced by Cu, while Br^- anions occur in the gap that is lined by Te atoms (Fig. 28). A very similar Cu–Te sheet occurs in $Ba_4[Cu_2^{2+}(Te_4O_{11})]_2(Cu_4^{1+}Cl_8)$ (**#272**). The sheets again occur in back-to-back pairs, but this time they are parallel to (010), with Te_4O_{11} groups trending || [10$\bar{1}$]. Again, the Cu^{2+} ions face an interlayer unit of BaO_{10} polyhedra. However, the Te side of the sheets faces a wide interlayer space that contains $[Cu_4^{1+}Cl_8]^{4-}$ clusters. These consist of a central pair of edge-sharing $CuCl_4$ tetrahedra, linked through corners to two $CuOCl_2$ triangles. The long axis of the cluster is || [101], approximately perpendicular to that of the Te_4O_{11} groups. The terminal Cu^{1+} atoms share the middle oxygen atoms of the Te–O anions, thus providing additional bridges between them, but are not counted as part of the structural unit due to the low valence of Cu. $[Co_5^{2+}(Te_4O_{11})Cl_4]$ (**#273**) has thick layers || (100) of corner- and edge-sharing CoO_4Cl pyramids, CoO_5Cl trigonal prisms and octahedra, and *cis*-CoO_4Cl_2 octahedra. The layers are braced by Te_4O_{11} groups with their long axes || [01$\bar{1}$], and are held together though long Te···O and Te···Cl bonds.

$[Cu_4(Te_5O_{12})Cl_4]$ (**#274**) has an elegant tetragonal structure in which the tellurite anion is the pinwheel-like Te_5O_{12} pentamer of Fig. 8*l*. CuO_4Cl square pyramids occur in clusters of four, where the oxygen atoms of the cube-shaped Cu_4O_4 cluster core are tetrahedrally coordinated by 3 Cu + 1 Te, thus linking Te and Cu polyhedra into an open framework. The Cl^- anions are in channels || **z**, and make additional long bonds to Cu and Te (Fig. 28). $Nd_5MoTe_7O_{23}Cl_3 \equiv Nd_5(MoO_4)[Te_5O_{13}](TeO_3)_2Cl_3$, its W analogue and the corresponding Pr analogues (**#275–278**) have edge-sharing columns of (Nd,Pr)O_{7-8} polyhedra || **x**, which share a few additional edges to make pillared double layers || (001) with very large channels (14 × 9 Å) running between the sublayers || **x**. These are further linked through $(Mo,W)O_4$ tetrahedra into a very open framework, leaving small interlayer channels containing monomeric TeO_3 groups, while the large channels are lined by V-shaped Te_5O_{13} pentamers (Fig. 8*m*). The Cl^- anions are held loosely, in the centres of large and small channels. $Nb_2Te_4O_{13} \equiv [Nb_8O_8(Te_{10}O_{26})(TeO_3)_6]$ (**#279**) has *zweier* chains of corner-sharing NbO_6 octahedra || **x**. The pseudo-monoclinic unit cell contains four distinct such chains, but despite the apparent simplicity of this arrangement, these are connected together through a remarkably complex arrangement of Te atoms. There are eight distinct Te sites. Sites Te2, Te3 and Te5 are in monomeric TeO_3 groups that share corners with Nb to make 4-cation-wide ribbons || **x** with Nb–Nb–Te 3-rings (alternately on each side of the Nb–O backbones, similar to the chain of Fig. 15*c*), Nb–Te–Nb–Te 4-rings and Nb–Nb–Te–Nb–Nb–Nb–Te 7-rings (Fig. 28). The ribbons lie in layers || (01$\bar{1}$), which are then bridged by the open-branched decameric anion $[Te_{10}O_{26}]^{12-}$ of Fig. 8*o*, in which a central edge-sharing pair of Te8 are linked through Te6 to Te1, which is then connected to both Te4 and Te7. The long axis of the anion Te7···Te8 = Te8···Te7 is approximately || [311] in the interlayer gap, while the Te4 branches complete the Nb–Te layers || (01$\bar{1}$). Note that this description is valid if the strong bonding threshold for Te is chosen in the range 2.36–2.44 Å; however, two slightly longer Te–O bonds (2.44–2.47 Å) connect the finite decamers into infinite open-branched *achter* chains, in which the additional bridging oxygens are CN3, shared by Te7 of two different decamers and Te2 as a new branch. $(NH_4)_6Mo_8Te_8O_{43} \cdot H_2O \equiv (NH_4)_6[(MoO_3)_6(Te_6O_{12})(TeO_3)_2](Mo_2O_7) \cdot H_2O$ (**#280**) has the only true cyclo Te^{4+} complex of the present study. Hexagonal rings $[Te_6O_{12}]^0$ (Fig. 8*n*) and monomeric $[TeO_3]^{2-}$ anions are linked into a layer || (001) through edge-sharing dimers of MoO_6 octahedra. Additional corner-sharing dimers of MoO_4 tetrahedra $[Mo_2O_7]^{2-}$, with point symmetry $\bar{3}$, lie in the centres of the hexagonal rings. The NH_4^+ cations and water molecules lie in the interlayer gap (Fig. 28).

Structures with Te^{4+} complexes that are infinite chains

Structures **#281–334** are inotellurites (Table 16, deposited). The various topological types of chain are summarized in Tables 2 (single chains) and 3 (multiple chains), and depicted in Fig. 9. Our first example is the structure of a high-temperature phase of $Mo_5TeO_{16} \equiv [(Mo_2^{5+}Mo_3^{6+})O_{13}(TeO_3)]$ (**#281**). As in the polymorph **#168**, MoO_6 octahedra share four corners to form layers of 3-, 4- and 6-rings || (010), which then link through the

https://doi.org/10.1180/minmag.2016.080.093 Published online by Cambridge University Press

remaining octahedral vertices to form a framework, and there is no ordering of Mo^{5+} and Mo^{6+}. As before, Te is in the centre of the hexagonal ring, but this time it is 4-coordinated, and shares oxygen atoms with Te of layers above and below to form a corner-sharing chain || **y**. In the long-range average crystal structure the chain is *einer*, but the bridging oxygen is on a twofold split site, which implies that the Te–O–Te configuration is nonlinear and the true local periodicity of a chain is at least *zweier*. $AgTeO_2(NO_3) \equiv Ag_2[Te_2O_4](NO_3)_2$ (**#282**) has TeO_4 polyhedra of the type shown in Fig. 4*c*, sharing edges to make an electrostatically neutral zigzag chain $[Te_2O_4]^0$ || **z** (Fig. 9*a*). These lie in layers || (020), with interstitial NO_3^- and CN6 Ag^+ ions, which themselves form a weakly bonded layer in which Ag^+ and NO_3^- are arranged respectively like the Pb^{2+} and O^{2-} in the litharge form of PbO (Boher *et al*., 1985). Telluroperite, $Pb_3TeO_4Cl_2$, is more precisely written as $Pb_2[(Pb_{0.5}Te_{0.5})_2O_4]Cl_2$ (**#283**). The Te–O complex is a chain topologically similar to Fig. 9*a*, but with square-pyramidal polyhedra (Fig. 4*b*) and a net negative charge due to random substitution of 50% of the Te^{4+} by Pb^{2+}. The (Pb,Te)–O chains and the remaining Pb^{2+} cations form litharge-type layers || (002), with Cl^- anions between the layers (Fig. 29). The resulting structure is isostructural with perite, $Pb_2[Bi_2^{3+}O_4]Cl_2$, and its Sb^{3+} analogue nadorite (Kampf *et al*., 2010*f*). Rajite, $[Cu(Te_2O_5)]$, has the corner-sharing chain of alternating CN3 and CN4 Te^{4+} seen in Fig. 9*b* (**#284**). The chains run || **x**, and are made from finite dimers by the rather long fourth bond to Te2 (2.30 Å). Chains are cross-linked into a framework through CuO_4 squares, which do not link to each other unless a fifth Cu–O distance (also 2.30 Å) is included, in which case the resulting CuO_5 pyramids form edge-sharing dimers. Nd $[Te_2O_5]Br$ (**#285**) has layers || (002) of edge-sharing NdO_{8-12} polyhedra, braced above and below by $[Te_2O_5]^{2-}$ chains || **y** which are topologically similar to those of rajite, but have an unusual planar T-shaped geometry for the CN3 polyhedron. This may be due to the presence of four interlayer Br^- ions at a relatively short distance from the Te cation (3.35–3.47 Å). The structures of the Cl analogue (**#336**) and the Ho analogue of that compound (**#307**) are different (see below). $Nd_2[Te_2O_5](Te_2O_5)(MoO_4)$ and its Pr analogue (**#286–287**) have edge-sharing zigzag double chains of $(Nd,Pr)O_{8-9}$ || **x**, which are bridged via MoO_4 tetrahedra to form looped layers || (001). Dimeric $[Te_2O_5]^{2-}$ ions (Fig. 8*a*) brace the layers, while *zweier* chains of the same composition (Fig. 9*b*) run || **x**, and hold the layers together. The chains are the structural unit, for the purposes of this classification. In $[Ga_2(Te_2O_5)(Te_2O_6)]$ (**#288**), the Te_2O_5 chains are || $[1\bar{1}0]$. These, and dimeric groups $[Te_2O_6]^{4-}$, which consist of two TeO_3 units linked by a long (2.35 Å) fourth bond to Te4, cross-link otherwise isolated GaO_5 and GaO_4-polyhedra into a framework. $[InF(Te_2O_5)]$ (**#289**) has *trans*-InO_4F_2 octahedra sharing F atoms to form a helical *vierer* chain || **z**. These are cross-linked into a framework by Te_2O_5 chains, which occur in four layers per unit cell along the **z** direction, and run || [110] and || $[1\bar{1}0]$ in alternate layers.

$La_4Ta_2Te_6O_{23} \equiv La_4[Ta_2O_6(Te_2O_{5.4})(TeO_3)_2][Te_2O_{5.6}]$ (**#290**) has a somewhat disordered structure with three fundamentally distinct types of Te. One type (Te3) approximates a chain of the *zweier* CN4 type $[Te_2O_6]^{4-}$ (Fig. 9*c*) running || **z**. However, the bridging oxygen atoms are only 77–80% occupied. Another type (Te1+Te2) ostensibly forms a similar chain, but the Te atoms are actually on a twofold split site and again the bridging oxygen sites are only partly occupied (71%), implying that the Te atoms are locally in a very strongly asymmetrical 3+1 coordination environment, and that the 'chain' is actually a sequence of Te_2O_5 dimers (58%) and orientationally disordered TeO_3 monomers (42%). The Te atoms of the second chain share corners with a parallel *zweier* chain of corner-sharing TaO_6 octahedra, which are decorated by additional TeO_3 groups (Te4) to form a second one-dimensional structural unit. All the Te lone pairs point in towards the centres of large rhomb-shaped channels || **z** of a trellis-like matrix of edge-sharing LaO_9 polyhedra (Fig. 29). $K[(UO_2)(Te_2O_5(OH))]$ (**#291**) has chains || **x** of Fig. 9*c* type, which share corners with UO_6 octahedra to form pleated layers || (020). The layers have Te–Te–U 3-rings and Te–Te–U–Te–Te–U 6-rings. The layers are held together by CN10 K^+ ions, which sit at the centres of the hexagonal rings.There are two types of bridging oxygen atom in the Te chain, with different Te–O distances of 2.07 and 2.28 Å; the latter oxygen atom probably accommodates the H^+. Schmitterite, $UO_2TeO_3 \equiv [(UO_2)_2(Te_2O_6)]$ (**#292**), also has its TeO_3 groups linked into a $[Te_2O_6]^{4-}$ chain (|| **z**), and these are linked through U into a pleated sheet || (010). However, the U^{6+} forms edge-sharing chains of UO_7 polyhedra, all Te–U links are through CN3 oxygen atoms bonding to either 2Te + U or to Te + 2U, and layers are held together only through long Te···O bonds (Fig. 29). $Tl_3[(UO_2)_2(Te_2O_5(OH))(Te_2O_6)] \cdot 2H_2O$ (**#293**) has two symmetrically

https://doi.org/10.1180/minmag.2016.080.093 Published online by Cambridge University Press

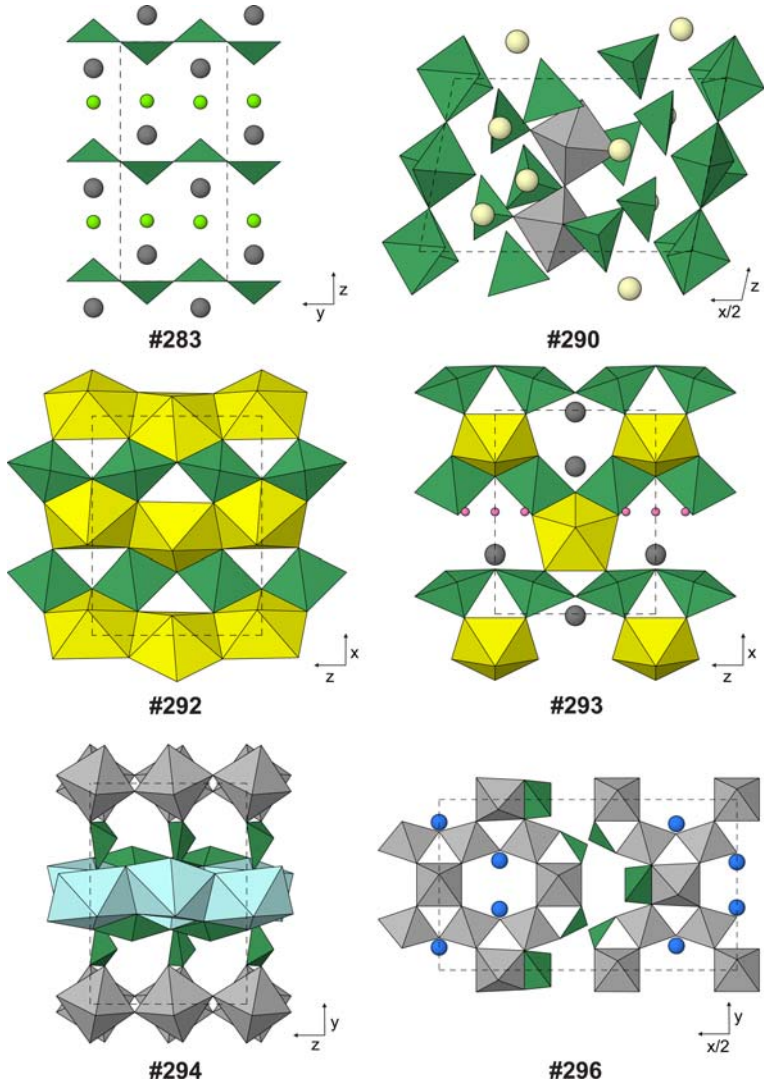

FIG. 29. Examples of structures with *zweier* chains of Te^{4+} polyhedra (Table 16, deposited). Small spheres: O (dark pink) when not part of a polyhedron. Medium spheres: Cl (yellow-green). Large spheres: Cs (blue), La (light yellow) and Pb or Tl (grey). Polyhedra: In (pale blue), Nb (grey), Te (dark green) and U (yellow).

distinct Te_2X_6 chains running || z; as in **#291**, the hydrogen atom can be located by noting the unusually long Te2–O7 distance: 2.21 Å as opposed to 2.04–2.07 Å for the other bridging oxygen atoms. Isolated UO_7 polyhedra link the Te chains into corrugated layers || (040), held together through three kinds of Tl^+ ion (CN = 5–9) and water molecules in the interlayers (Fig. 29).

$InNbTe_2O_8 \equiv In_2[NbO_2(TeO_3)]_2[Te_2O_6]$ (**#294**) has NbO_6 octahedra sharing four corners to form a square-net layer || (010), resembling the $(Nb, Ta)_nO_{4n}$ layers of **#155–158**. Half of the Te are in monomeric TeO_3 groups that share additional corners to form Nb–Nb–Te 3-rings that are alternately above and below the Nb layer along the *x* direction, while the other half of the Te form *zweier* chains Te_2O_6 || **z** that do not connect directly to Nb, but brace a layer of edge-sharing InO_7 polyhedra that holds together the Nb–Te layers. Thus, there are two separate structural units, a

https://doi.org/10.1180/minmag.2016.080.093 Published online by Cambridge University Press

Te chain and a Nb–Te heteropoly layer (Fig. 29). The related compound $BiNbTe_2O_8 \equiv Bi_2[NbO_2(TeO_3)]_2[Te_2O_6]$ (**#295**) also has corner-sharing Nb_nO_{4n} sheets, but while the unshared corners are *trans* in **#294** so that the sheets are planar, in the Bi compound the unshared corners are *cis*, and the sheets ∥ (002) are strongly pleated. Again, half of the TeO_3 link to the Nb sheets, completing Nb–Nb–Nb–Te 4-rings rather than 3-rings, this time, while the rest of the Te form Te_2O_6 chains between the layers, running ∥ **y**. The BiO_{4+3} polyhedra share edges to form a corrugated layer that is braced by the Te chains and also links to the Te of the Nb–Te units. $Cs_3[Nb_9O_{20}(Te_2O_6)(TeO_3)_2]$ (**#296**) has very thick layers of NbO_6 octahedra ∥ (200) that are slices of a pyrochlore framework. Kagome layers of 3- and 6-rings ∥ (011) and $(0\bar{1}1)$ are very prominent in projection down **z**. The pyrochlore framework is displaced by $\frac{1}{2}c$ on planes ∥ (200), which breaks otherwise infinite chains of octahedra running ∥ **x** after only four Nb atoms. These chains are terminated by half of the Te rather than Nb, and the offset of the pyrochlore framework allows Te to retain 3-fold rather than 6-fold coordination. Thus, the layers are not condensed any further by strong bonds. The other half of the Te atoms form $[Te_2O_6]$ chains which run ∥ **z** in notches in the sides of the thick layers. The Cs^+ ions are in 6–8 coordination in large interstices within the layers, which are held together only through long-distance Te···O interactions (Fig. 29). $CuTeO_3 \equiv [Cu_2(Te_2O_6)]$ (**#297**) is a polymorph of balyakinite (**#117**) and the high-pressure phase **#142**. In this structure, CuO_4 squares form edge-sharing dimers, condensed into chains ∥ **x** through a fifth Cu–O bond at 2.43 Å. The Cu chains lie in layers ∥ (020), which are cross-linked into a framework by Te_2O_6 chains running ∥ [101]. Like Cu, Te has a very irregular coordination environment, with three Te–O distances of 1.87–1.92 and the fourth at 2.43 Å; it has no other oxygen atoms within 2.8 Å. $TlV^{5+}TeO_5 \equiv Tl_2[(VO_2)_2(Te_2O_6)]$ (**#298**) has *trans* corner sharing chains of distorted VO_6 octahedra in a centred-rectangular array, running ∥ **x**. These are cross-linked by Te_2O_6 chains running ∥ **z** into a framework with large channels ∥ **x** and **z**. The resulting three-dimensional net has intersecting layers of kagome topology ∥ (011) and $(0\bar{1}1)$, like the weberite structure (Knop *et al*., 1982, Fig. 14*g*, **#672** below). In fact, the framework can be derived from that of weberite by $\frac{1}{2}a$ displacement of slices ∥ (002), thus condensing into chains what would otherwise be isolated Te polyhedra, and adjusting the Te–O–V bonding pattern slightly. In **#298**, oxygen atoms are removed so that Te has CN = 4 rather than 6, while the environment of V is changed from Q^{0600} to Q^{1411}, with V making a bond to a CN3 bridging oxygen of the Te chain rather than to the missing anion. The V–O–V bridges are very asymmetrical, one distance being 2.24 Å while the other is 1.66 Å, almost identical to the distance between V and the CN1 ligand. Thus, nonlinear $[VO_2]^+$ complexes can be recognized in the structure. The Tl^+ ions are in very one-sided 7-coordination in the channels.

Polymorph II of $TeO(As^{5+}O_3OH) \equiv [(AsOH)_2(Te_2O_8)]$ (**#299**), like polymorph I (**#225** above), has Te in 5-fold coordination, but the TeO_5 polyhedra now form corner-sharing *zweier* chains Te_2O_8 ∥ **y** (Fig. 9*d*) rather than edge-sharing dimers. $[AsO_3OH]^{2-}$ tetrahedra share the three unprotonated ligands with the Te chains to form a corrugated layer ∥ (002) with Te–Te–As 3-rings and Te–Te–As–Te–As 5-rings. Hydrogen bonds brace individual layers, which are held together through long Te···O bonds. The triclinic polymorph of $TeO(Se^{4+}O_3) \equiv [Se_2(Te_2O_8)]$ (**#300**) has CN5 Te in similar *zweier* Te_2O_8 chains ∥ **x**. The chain backbones have the asymmetrical crankshaft geometry of the Pb–O chains in massicot (Hill, 1985). SeO_3 pyramids share all corners with the Te chains to make a framework with hexagonal channels ∥ **y**, which accommodate the lone pairs of both Se and Te. The monoclinic (pseudo-orthorhombic) polymorph **#301** is topologically very similar, but slight displacements of atoms mean that the two Te atoms of the chain repeat are now related to each other through a glide plane, rather than being symmetrically independent.

Chekhovichite, $Bi_2Te_4O_{11} \equiv Bi_4[Te_4O_{10}](TeO_3)_4$ (**#302**) has the zigzagging *vierer* Te chain of Fig. 9*e*, with CN3 Te at the sharp bends. The chains trend ∥ **y**, and zigzag in layers ∥ (002). BiO_{7-8} polyhedra share edges to form corrugated sheets with a honeycomb net, between the Te chains, and the monomeric TeO_3 groups brace the Bi sheets. $Na_2MoTe_4O_{12} \equiv Na_2[MoO_2(Te_4O_{10})]$, its W analogue and the corresponding Ag–Mo compound (**#303–305**) have topologically similar but more contorted *vierer* Te chains, which are cross-linked in pairs through otherwise isolated $(Mo,W)O_6$ octahedra to make looped heteropoly chains ∥ **z**. These chains lie in layers ∥ (200), which are loosely held together through CN7 $(Na,Ag)^+$ ions. The Te bond threshold for these structures has been set at 2.38 Å. If an additional bond at 2.39–2.48 Å is included, then Te2 atoms of neighbouring chains share edges to join the chain structural units into a continuous layer with 10-rings ∥ (200). The

https://doi.org/10.1180/minmag.2016.080.093 Published online by Cambridge University Press

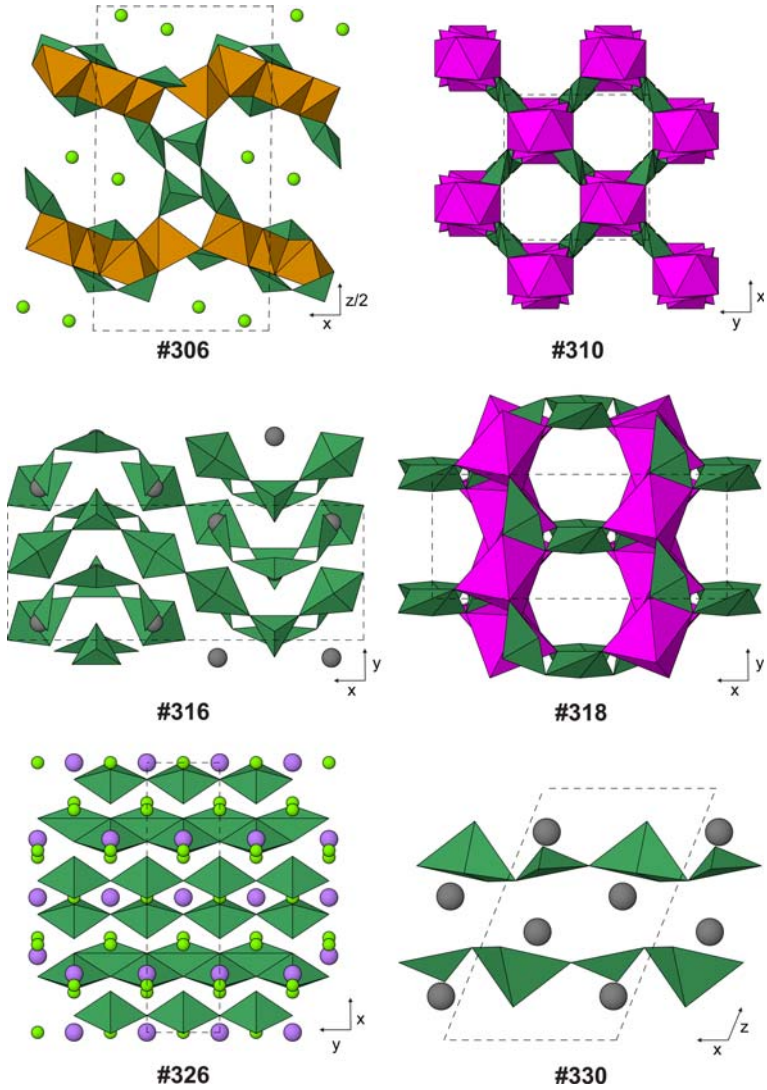

FIG. 30. Examples of structures with *vierer* or *sechser* single chains or with double chains of Te^{4+} polyhedra (Table 16, deposited). Medium spheres: Cl (yellow-green). Large spheres: Bi (violet) and Pb or Tl (grey). Polyhedra: Fe (orange-brown), Mn (magenta) and Te (dark green).

compound $Fe_8Te_{12}O_{32}Cl_3Br_3 \equiv [(Fe_2^{2+}Fe_6^{3+})(Te_4O_{10})(Te_2O_5)_2(TeO_3)_4]Cl_3Br_3$ (**#306**) has four types of Fe atom in 5 or 6 coordination, which link in a honeycomb net to form layers || (004). The different linkage patterns for Fe1–Fe4 polyhedra are described concisely by Q states as Q^{0603}, Q^{1502}, Q^{1501} and Q^{2300}, respectively. Bond-valence sums indicate that Fe^{2+} is ordered at Fe3. Two types of interlayer gap alternate between Fe layers. One gap type contains two-thirds of the loosely bound, partly-disordered $(Cl, Br)^-$ ions, and is lined by Te_2O_5 groups which brace the Fe layers. Monomeric TeO_3 groups decorate the other side of the Fe layers, facing the other type of gap, but on this side, the layers also link to Te_4O_{10} chains running || **y**, which join the Fe layers in pairs and thus complete the extremely complex pillared double layer structural unit (Fig. 30). The remaining $(Cl, Br)^-$ are in channels || **y** between the Te chains. The chains still have alternation of

https://doi.org/10.1180/minmag.2016.080.093 Published online by Cambridge University Press

CN3 and CN4 Te, but are quite different in conformation from those of **#302–305**: they are helically coiled, with the sharpest bending at the CN4 Te atoms rather than CN3.

In $HoTe_2O_5Cl \equiv Ho_2[Te_4O_{10}]Cl_2$ (**#307**), nearly-cubic HoO_8 polyhedra share edges to make square-net layers ∥ (001); half of the Ho atoms have interlayer Cl as a more distant neighbour. The Ho layers are braced by *vierer* Te chains which are a topological isomer of those in **#302–306**, with a different sequence of CN3 and CN4 Te atoms (Table 2, Fig. 9*f*). The chains trend ∥ [1$\bar{1}$0]. Layers are held together only through weak Te···Cl interactions. The compositionally similar Nd compounds **#285** and **#336** have quite different structures. $Na_2Te_2O_5 \equiv Na_4[Te_4O_{10}]$ (**#308**) has yet another isomer of Te_4O_{10} chain, with all Te 4-coordinated, but an alternation of corner- and edge-sharing (Fig. 9*g*). Chains trend ∥ [101], and are held together by CN6–7 Na^+ ions. The arrangement of (Na,Te) and O atoms can be described as slightly distorted slabs ∥ (100) of rocksalt type, alternating with fluorite-like slabs, with there being two of each slab type per unit cell. $K_2Te_2O_5 \cdot 3H_2O \equiv K_4[Te_4O_{10}] \cdot 6H_2O$ (**#309**) has similar *vierer* chains which lie in layers ∥ (002). The chains run in [110] and [1$\bar{1}$0] directions in alternate layers. Water molecules and CN7–8 K^+ ions lie between the layers. The edge-sharing Te_4O_{10} chains of Fig. 9*g* are also found in the denningite structure of $Mn^{2+}Te_2O_5 \equiv Mn^{2+}[Mn^{2+}(Te_4O_{10})]$ (**#310**). This nanoporous tetragonal structure has two different types of Mn site, with coordination numbers 8 and 6 respectively, which alternate in edge-sharing chains ∥ **z**. The Mn chains are linked to their neighbours by Te chains which also run ∥ z, so delineate square channels with a minimum diameter of ~5 Å (Fig. 30). Note that the CN6 Mn are considered to be part of the overall framework structural unit, while CN8 Mn is not. The CN6 Mn^{2+} may be substituted by Cu^{2+} to produce solid solutions and ultimately the end-member $Mn^{2+}[Cu^{2+}(Te_4O_{10})]$ (**#311**). Although Mn-dominant synthetic compositions have been called 'denningite', it seems likely that the mineral denningite itself has Ca replacing Mn in the 8-coordinated cation site. The type material has composition $(Ca_{0.60}Mn_{0.40})[(Mn_{0.72}Zn_{0.24}Mg_{0.04})(Te_4O_{10})]$ (Mandarino *et al*., 1963), and the ideal composition is given as $CaMn^{2+}Te_4^{4+}O_{10}$ in the IMA list of minerals (http://ima-cnmnc.nrm.se/IMA_Master_List_2015-05.pdf). Although the refinements of Walitizi (1964, 1965) constrained occupancies to be the same on CN8 and CN6 sites, Ca would be expected to partition strongly into the larger 8-coordinated site, but the structure needs to be reinvestigated to confirm this. A different polymorph of $Mn[Te_2O_5]$ is described as **#347**.

Despite the apparently simple formula, $K_2Te_2O_5$ (**#312**) has an open-branched *zweier* Te_4O_{10} chain (Fig. 9*h*). The chains have a V-shaped cross-section, run ∥ **x** and pack in a herringbone fashion. They are cross-linked by undulating layers ∥ (001) of $KO_{7–8}$ polyhedra. $Ba_2V^{5+}Te_4O_{12}(OH) \equiv Ba_2[VO_3(Te_4O_9(OH))]$ (**#313**) contains yet another Te_4X_{10} isomer, the open-branched *dreier* tellurite chain of Fig. 9*i*. The hydroxide group is located on the CN4 Te atom that does not have the branch (Te4), while a VO_4 tetrahedron shares an oxygen atom with the branch Te atom (Te1). Chains run ∥ **y** and lie in double layers ∥ (10$\bar{1}$), with the branches directed into the interiors of the double layers. $BaO_{8–9}$ polyhedra lie between the double layers. $(NH_4)_2WTe_2O_8 \equiv (NH_4)_4[(WO_2)_2(Te_4O_{12})]$ (**#314**) has *zweier* Te chains with branches attached to CN3 bridging oxygen atoms (Fig. 9*j*). The chains run ∥ y, and are cross-linked by individual WO_6 octahedra, which share four corners to form layers ∥ (100) with Te–Te–W 3-rings and Te–Te–W–Te–W 5-rings. NH_4^+ ions are between the layers. $NiTe_2O_5 \equiv [Ni_4(Te_6O_{14})(TeO_3)_2]$ (**#315**) has loop-branched *vierer* chains Te_6X_{14}, with CN5 Te at the nodes and CN3 Te in the loops (Fig. 9*k*). The chains run ∥ **x**, and alternate with monomeric TeO_3 groups in layers ∥ (002). The tellurite anions are cross-linked into a framework through chains of *trans* edge-sharing NiO_6 octahedra which run ∥ **y**; micelles between these chains accommodate the Te lone pairs.

$Pb_2Te_3O_8 \equiv Pb_8[Te_6O_{16}](Te_3O_8)_2$ (**#316**) has both zigzag *sechser* chains Te_6O_{16} of the type shown in Fig. 9*l*, and the soro Te_3O_8 groups of Fig. 8*g*. Note that the chains contain both CN3 and CN4 Te, with the sharp bends at the CN3 Te atoms. The chains and tritellurite long axes all point ∥ **x**. Chains lie in double layers with Te_3O_8 groups between the layers, and the resulting thick sheets repeat ∥ (002). Tellurite anions within the thick sheets are held together by Pb^{2+} ions that lie on the outsides of the sheets, and sheets are held together via long Pb···O bonds. Lead is in distorted 7–8 coordination with three short bonds to oxygen atoms (Fig. 30). The compounds $M_2^{2+}Te_3O_8 \equiv [M_4(Te_6O_{16})]$ with M = Mg, Mn, Co, Ni, Cu or Zn (**#317–322**) have the spiroffite structure. No structure refinement exists for an Fe compound with this stoichiometry, while those with M = Mn and Zn are the minerals spiroffite and

https://doi.org/10.1180/minmag.2016.080.093 Published online by Cambridge University Press

zincospiroffite, respectively. The MO_6 octahedra share edges and corners to make honeycomb layers || (200), and are linked into a framework by a different Te_6X_{16} *sechser* chain in which all Te are CN4, but edge-sharing pairs alternate with a polyhedron that shares only corners, at which the chain bends (Fig. 9*m*). The chains run || $[10\bar{1}]$ and lie in layers || (202). The trellis-like intersection pattern of *M* and Te layers results in 5 Å diameter channels running || **y** and **z**, which accommodate the Te lone pairs (Fig. 30).

$Fe_3Te_4O_{12} \equiv [Fe^{2+}_2Fe^{3+}_4(Te_6O_{18})(TeO_3)_2]$ (**#323**) has edge-sharing dimers of $Fe^{3+}O_6$ octahedra (Fe1 = Fe3, Fe–O = 1.94–2.15 Å) and edge-sharing dimers of $Fe^{2+}O_6$ octahedra (Fe2 = Fe2, Fe–O = 2.05–2.48 Å), which share CN3 oxygen atoms to make layers || (100). The layers are braced by TeO_3 monomers and linked into a framework through open-branched *vierer* chains Te_6O_{18} (Fig. 9*n*). The chains run || **y**, but zigzag || [101], obliquely to the Fe layers. $Te_3O_3(PO_4)_2 \equiv [P_4(Te_6O_{22})]$ (**#324**) also has an open-branched *vierer* chain, but with CN4 and CN5 Te atoms (Fig. 9*o*). The chains run || **z**, with branches extended in the **y** direction, and lie in layers || (200). Two types of PO_4 tetrahedra share all corners with the Te chains to make a framework which, unusually, has no 3-rings, but does have Te–Te–Te–P and Te–P–Te–P 4-rings and Te–Te–P–Te–P 5-rings. $Ca_4Te_5O_{14} \equiv Ca_8[Te_8O_{22}](TeO_3)_2$ (**#325**) has open-branched *sechser* chains (Fig. 9*p*) running || **y** and zigzagging in the **x** direction, and lying with TeO_3 monomers in layers || (004). The chains wind through a trellis-like framework of CaO_7 polyhedra, which has 7 Å channels || **z** accommodating the chain branches.

The next few structures have multiple chains (Table 3). Interestingly, two of them are compounds with Fe^{3+}, and two are complex compounds with Cd and Cl. $Bi_3Te_4O_{10}Cl_5 \equiv Bi_3[Te_2O_4](TeO_3)_2Cl_5$ (**#326**) has the simple *einer* $[Te_2O_4]^0$ ribbon of Fig. 10*a*, in which Q^{1032} Te atoms are linked through CN3 oxygen atoms. These run || **y**, and with TeO_3 monomers and BiO_4Cl_2 and BiO_4Cl_5 polyhedra, define layers || (201), with the Cl^- ions in the interlayers. Although the Te double chain is nominally neutral, in reality, Te1 makes weak bonds to Cl^-, and the non-bridging oxygen is shared with Bi1. $Cd_7Te_7O_{17}Cl_8 \equiv Cd_7[Te_5O_{12}](Te_2O_5)Cl_8$ (**#327**) has a commensurately modulated structure in which seven types of Cd polyhedra (variously CdO_3Cl_3, CdO_4Cl_3 or CdO_3Cl_4) form edge-sharing ribbons, flattened in the *yz* plane and running || **y**. These ribbons are braced on one side by the rather complex *zweier* double chain Te_5O_{12} of Fig. 10*b* and also by the relatively simple Te_2O_5 single chain of Fig. 9*b*. The Cd–Te compound layers repeat || (200), with Cl^- ions in the interlayer and long Te···Cl bonds holding layers together. However, the facing direction of the pair alternates back and forth along the 28 Å *c* repeat (Fig. 30).

$Fe^{3+}Te_3O_7Cl \equiv [Fe_2(Te_6O_{14})]Cl_2$ (**#328**) and the Br analogue (**#329**) have *dreier* double chains Te_6O_{14} made out of 5-rings (Fig. 10*c*), flattened on $(10\bar{1})$ and running || **y**. The chains are linked through edge-sharing dimers of FeO_5 polyhedra to make very thick double layers || (100), which contain channels || **z**. Halide ions lie in the interlayer spaces, and the layers are held together only through weak Te···(Cl, Br) and Te···O interactions. Te2 in this structure has coordination that is strongly 3+1: the third- and fourth-nearest oxygen atoms are at ~1.95 and 2.42 Å. If the fourth ligand is not included, the double chain becomes a serpentine *sechser* single chain. $Tl_2Te_3O_7 \equiv Tl_4[Te_6O_{14}]$ (**#330**) has a very different Te_6O_{14} double chain which is only *zweier* but has the subchains linked through edge-sharing Te dimers (Fig. 10*d*). Thus, the subchains are open-branched but are linked via the branches so that the double chain as a whole is not. The resulting ribbons are flattened on approximately $(01\bar{1})$ and run || **x**. The Te chains interpenetrate with and cross-link layers || (010) of edge-sharing TlO_5 polyhedra (Fig. 30). $Fe^{3+}_2Te_4O_{11} \equiv [Fe_4(Te_6O_{16})(Te_2O_6)]$ (**#331**) has a Te_6O_{16} chain whose description is again dependent on the Te–O bonding threshold. Here, we include a fourth Te2–O link at 2.496 Å, which makes a rather simple *zweier* double chain of 6-rings (Fig. 10*e*). Without that link to close the rings, the chain is an open-branched *vierer* single chain. The chains are flattened on (102) and run || **y**. The chain is topologically the same as a slice of the alumino-silicate sheet of prehnite, $Ca_2[Al(AlSi_3O_{10})(OH)_2]$, which has a similar alternation of Q^2 and Q^4 polyhedra in its 6-rings (Papike and Zoltai, 1967). FeO_6 and FeO_5 polyhedra share a corner to form Fe_2O_{10} dimers, which cross-link the Te chains, leaving channels || **y** which accommodate additional Te in edge-sharing dimers Te_2O_6 (Fig. 8*c*). $Na_2Te_4O_9 \equiv Na_4[Te_8O_{18}]$ (**#332**) has a very complex *zweier* double chain in which the two subchain backbones are linked through the familiar 'double-triangle' tetrameric clusters (Fig. 10*f*). These chains run || **y**, and their parallelogram-shaped cross-section defines the geometry of the unit cell. The chains are held together through layers || (100) of NaO_{5-6} polyhedra. The K and NH_4 analogues have a quite different layer structure (**#354–355**).

https://doi.org/10.1180/minmag.2016.080.093 Published online by Cambridge University Press

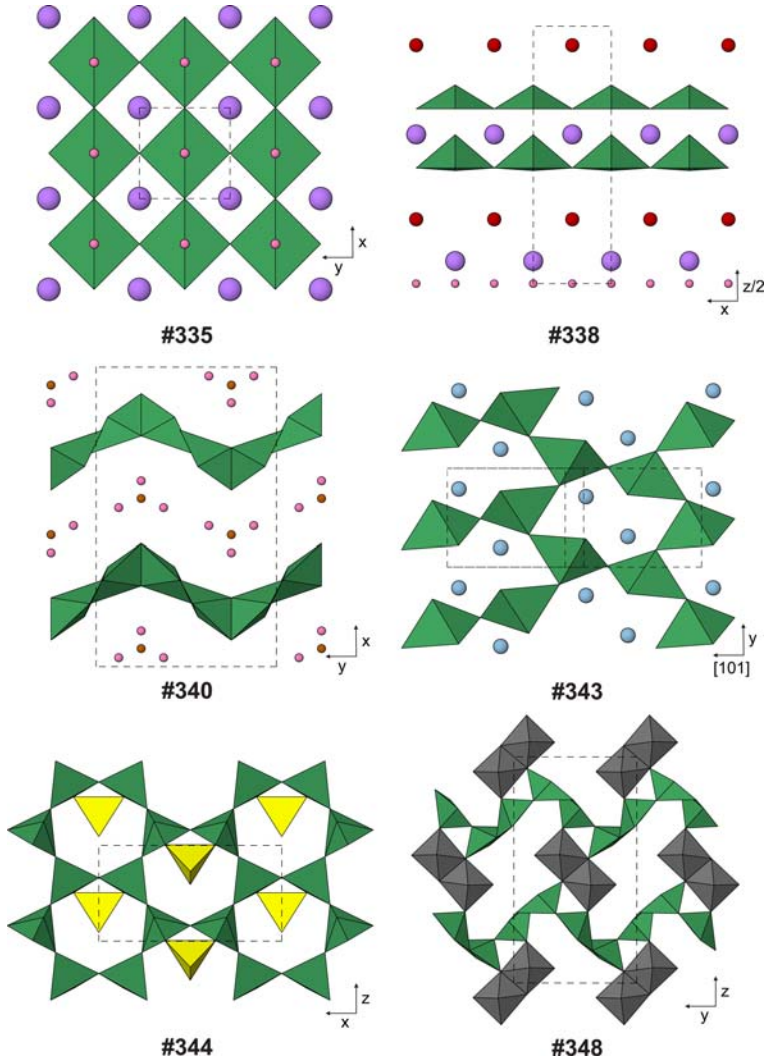

FIG. 31. Examples of structures with layers of Te^{4+} polyhedra (Table 17, deposited). Small spheres: N (brown) and O (dark pink) when not part of a polyhedron. N and O constitute interlayer NO_3 groups in **#340**. Medium spheres: Br (red). Large spheres: Bi (violet) and Li (pale blue). Polyhedra: Mo (dark grey), S (yellow) and Te (dark green).

We have two instances of chains with multiplicity greater than two. $Te_4O_5(PO_4)_2 \equiv [P_2(PO)_2(Te_8O_{24})]$ (**#333**) has the open-branched *zweier* triple chain shown in Fig. 10*g*. As noted earlier, the central ribbon of 6-rings resembles that of 'biopyribole' silicate minerals such as jimthompsonite, $(Mg,Fe)_5(Si_6O_{16})(OH)_2$ (Veblen and Burnham, 1978), except for the increased coordination number of the Q^{2300} polyhedra. The Te ribbons are run || **y**, and are connected to form strongly pleated layers || (201) by PO_4 tetrahedra, half of which share all four corners and half of which share only three. $Cd_4Te_6O_{13}Cl_6 \equiv Cd_2[Te_6O_{13}](Cd_2Cl_6)$ (**#334**) contains the extraordinary quadruple chains of Fig. 10*h*. The outer two backbones are *zweier*, and contain edge-sharing Te trimers surrounding a CN3 oxygen atom, similar to those of Fig. 8*i*. Conversely, the central backbones are *dreier*, and are linked through shared 'double-triangle' clusters. The resulting ribbons are flattened on (012) and run || **x**. They stack *en échelon*, and are connected into layers || (001) through edge-sharing ribbons of

https://doi.org/10.1180/minmag.2016.080.093 Published online by Cambridge University Press

CdO_7 and CdO_8 polyhedra. Between these layers, $CdCl_6$ octahedra form edge-sharing ribbons, and the structure is held together by weak Te···Cl bonds.

Structures with Te^{4+} complexes that are infinite sheets

Table 17 (deposited) lists phyllotellurites **#335–363**, whose various types of Te–O sheet are summarized in Table 4 and shown in Fig. 11 (single layers) or Table 5 and Fig. 12 (double layers). $Bi_{10}Te_2O_{17}Br_4 \equiv Bi_{10}[TeO_2]_2O_{13}Br_4$ (**#335**) has the simple, electrostatically neutral TeO_2 layer of Fig. 11*a*, with square-pyramidal TeO_4. It is a pseudotetragonal with $a \approx b \approx 4$ Å. The Te pyramids share edges with BiO_8 cubes which have BiO_4 pyramids on the other side. The composite Bi_2TeO_4 layers || (001) that are thus formed can be regarded as slices of a fluorite-like structure. These layers alternate along **z** with topologically similar but Te-free Bi_3O_4 layers. In both cases, an additional 'interstitial' anion site, in an 'octahedral' interstice of the cubic close-packed cation slab, is 25% occupied by O^{2-} to give a 'stuffed fluorite slab' stoichiometry $(Bi,Te)_3O_4(O_{0.25})$. These interstitial oxygen atoms are weakly bonded to Bi and Te, but are too far from Te (2.51 Å) to be included in the Te–O complex of our classification. It should be noted that short O···O distances of 2.38 Å suggest that accommodation of the additional oxygen requires adjustment to other parts of the structure. Br^- anions lie between the layers, which are held together through weak Bi···Br and Te···Br interactions (Fig. 31). $NdTe_2O_5Cl \equiv Nd[TeO_2]_2OCl$ (**#336**) is structurally very similar, although it is truly tetragonal, has all stuffed-fluorite $NdTe_2O_4(O)$ layers equivalent, and thus has a halved *c* repeat. The similarity between these compounds is best seen if the formulae are written as $[(Bi_2Te)O_4(O_{0.25})][Bi_3O_4(O_{0.25})]Br_2$ and $[(NdTe_2)O_4(O)][(NdTe_2)O_4(O)]Cl_2$. The fully-occupied interstitial oxygen site has 8 × O at 2.58 Å, 4 × Nd atoms at 2.86 Å and 2 × Te atoms at 2.42 Å. If these oxygen atoms were included as Te ligands, then the Te coordination would increase from square-pyramidal CN4 to CN5 (Fig. 4*b*,*e*), and the Te–O complex would be not the single $[TeO_2]^0$ layer of Fig. 11*a*, but a double layer $[Te_2O_5]^{2-}$, in which sublayers of the type shown in Fig. 11*c* are linked by corner-sharing of the additional oxygen atoms. Note the very different chain structures exhibited by the Ho analogue (**#307**) and the Br analogue (**#285**). Compound **#337** approximates $Bi[Te_2O_5]Cl$, but is more accurately written $Bi_{0.87}[Te_2O_{4.9}]Cl_{0.87}$. Again, it has a strongly layered structure in which Bi atoms are at the core of the layers, Te on the outsides, and weak Te···Cl bonds are holding the layers together. However, layers have trigonal rather than (pseudo) tetragonal symmetry, and there is very extensive long-range disorder. Tellurium has one apical ligand O1 at 2.02 Å, but other oxygen sites at 3 × 2.14 Å (O3), 3 × 2.37 Å (O3) and 3 × 2.41 Å (O2). The O2 and O3 sites are only 73% and 24% occupied, respectively, and short O···O distances imply that there must be considerable short-range order. The O3 sites occur in triangles with O3···O3 = 1.27 Å, so only one position out of each triplet can be occupied, and each O2 site has three O3 at 1.70 Å, so either O2 or one of those O3 positions can be occupied. The simplest and most symmetrical occupancy pattern which satisfies these constraints and approximates the refined occupies of the average structure is shown in Fig. 11*b*. Each Te atom has ligands which are 1 × O1 plus either 3 × O2 (¾ of the time) or 2 × O2 and 2 × O3 (¼ of the time). The resulting layer has 3-rings of Q^{1030} and Q^{1220} Te polyhedra with the geometry of Fig. 4*d* and a distorted variant of Fig. 4*e* respectively, an ideal stoichiometry Te_2O_5, and a within-layer repeat that is a 2 × 2 superstructure of the crystallographic unit cell. The long-range disorder reflects at least stacking disorder of that ordering pattern, possibly with an admixture of other short-range ordering schemes. Compound **#338** is another Bi tellurite halide with an ostensibly simple stoichiometry concealing structural complexity (Fig. 31). It approximates $BiTeO_3Br$, is more accurately represented by the structural formula $Bi_2[TeO_3][TeO_2]OBr_2$, which if partial occupancies are indicated becomes in turn $Bi_{1.93}[TeO_3][TeO_2]OBr_{1.8}$. Like **#336**, it is a tetragonal structure with $a \approx 4$ Å. There is a stuffed-fluorite compound layer $(BiTe_2)O_4(O)$ similar to the $(NdTe_2)O_4(O)$ layers of that structure or $(BiTe_2)O_4(O_{0.25})$ of **#335**. Again, there is a fully-occupied 'interstitial' oxygen site, but this is now at 2.87 Å from 4 × Bi, 2.59 Å from one Te and only 1.88 Å from the other Te atom. Thus, individual layers are polar, the Te–O complex on one side being the neutral layer $[TeO_2]^0$ with CN4 Te (Fig. 11*a*), while that on the other side is anionic $[TeO_3]^{2-}$ with CN5 Te (Fig. 11*c*). The full stacking sequence includes two such fluorite-like Te1–Bi–Te2 slabs of opposing polarity, and also a separate Bi_2O_2 layer which is thinner, with a geometry more obviously similar to the litharge form of PbO

https://doi.org/10.1180/minmag.2016.080.093 Published online by Cambridge University Press

(Boher *et al*., 1985). Indeed, the overall structure has the same *P*4/*nmm* space group as litharge. Bromium forms double layers between the two fluorite-like slabs and also single layers between fluorite and litharge slabs; the structure is held together through weak Te···Br and Bi···Br bonds.

$(Cu^{1+}Cl_2)[Sb^{3+}TeO_3]$ (**#339**) has a disordered 50 : 50 mix of Sb^{3+} and Te^{4+} cations, which are 4-coordinated and form $(Te,Sb)_2O_3$ layers of the type seen in Fig. 11*d*, which can be generated by condensing the double chains of Fig. 10*a* through additional corner-sharing. Note that in this compound, the layers are cationic, $[SbTeO_3]^+$. The layers are ‖ $(20\bar{1})$, and between them are intercalated 3-wide ribbons running ‖ **y** of $CuCl_n$ polyhedra. The outer two Cu positions form well-ordered chains of corner-linked $CuCl_4$ tetrahedra, while the central Cu atom is delocalized across triangular 3-fold and linear 2-fold coordinated positions. $[Te_2O_3OH](NO_3)$ (**#340**) has corrugated layers ‖ (200) of the topology shown in Fig. 11*e*, in which Q^{0401} polyhedra form a 3-connected net of 6-rings despite having CN4, by virtue of sharing one edge. The Te atoms and O1, which does not participate in the shared edge, form corner-linked chains of massicot-like asymmetrical crankshaft geometry running ‖ **z** (cf. Hill, 1985). Te–O distances for O1 (1.89 + 2.05 Å), O2 (2 × 1.93 Å) and O3 (2 × 2.17 Å) indicate unambiguously that the H atom is attached to O3. The resulting layers are again cationic, $[Te_2O_3OH]^+$, and are held together through their electrostatic attraction to interlayer NO_3^- anions (Fig. 31). A layer of the Fig. 11*e* topology also occurs in the mineral tellurite, an orthorhomic polymorph of TeO_2 (**#341**), where very tightly corrugated layers of this type are ‖ (200). These layers are electrostatically neutral, and are held together only by long Te···O bonds. It should be noted that the structure is isopuntal with the brookite polymorph of TiO_2, but whereas the Ti atoms of brookite have six oxygen neighbours at 1.863–2.052 Å (Meagher and Lager, 1979), the lone-pair stereoactivity of Te^{4+} distorts the coordination octahedron to give only four neighbours in the range 1.88–2.20 Å, an additional neighbour within the layer at 2.64 Å, and a weak Te–O bond across the interlayer gap at 3.07 Å. A variant of the structure with additional anion-anion bonding occurs for the pararammelsbergite form of $NiAs_2$ (Fleet, 1972) and intermetallic compounds such as $AuSn_2$ (Rodewald *et al*., 2006). Two other polymorphs of TeO_2 are discussed as **#364–365** below. At present, there do not appear to be examples of more complex structures that contain uncharged Te^{4+}–O sheets, although analogues are known for other *p*-block elements. The mineral lucabindiite, ideally $K[As_4O_6]Cl$ (Garavelli *et al*., 2013), has planar As_4O_6 sheets which direct their lone pairs towards interlayers of Cl^-, while the oxygens face interlayers of K^+.

$Bi_4Te_2O_9Br_2 \equiv Bi_4[Te_2O_5]O_4Br_2$ (**#342**) is another Bi tellurite containing fluorite-like Bi–Te–O slabs ‖ (001), like **#335** and **#338**. In this case, *a* and $b \approx \sqrt{2} \times 4$ Å ≈ 5.6 Å, as the Te–O component layer contains alternating CN4 and CN5 Te atoms (Fig. 11*f*), and is in effect an ordered intermediate between the layers of Figs 11*a* and 11*c*. It should be noted that the CN4 Te atom is in almost square-planar coordination, which is unusual, and suggests that some atomic coordinates may be incorrect. The $(Bi_4Te_2)O_8(O)$ stuffed-fluorite slabs are polar, with Te on only one side. Single layers of Br^- ions lie between slabs, which are linked through weak Te···Br and Bi···Br bonds.

In one form of $Li_2[Te_2O_5]$ (**#343**; the other polymorph is **#351**), Q^{1300} Te polyhedra link to form layers of 6-rings, topologically equivalent to the silicate sheets of the 'micas' (Fig. 11*g*). Resemblance to micas is further enhanced by the fact that such sheets occur in pairs, and their apical oxygen atoms are directed inwards, towards a 'sandwich filling' layer of electropositive cations. In this compound, however, the core of the layer is composed of tetrahedrally coordinated Li^+ cations, rather than higher-valence species in octahedral coordination. The compound mica-like layers are ‖ $(10\bar{1})$, with Te lone pairs directed into the interlayer gap and only weak Te···O bonds connecting layers (Fig. 31). $(Te_2O_3)(SO_4) \equiv [(SO_2)(Te_2O_5)]$ (**#344**) also has phyllotellurite sheets ‖ (010) with the topology of Fig. 11*g*, but the non-bridging oxygen atoms are not all on one side of the sheet. Hexagonal rings are bent in a boat configuration, and pairs of apical oxygen atoms point alternately up and down along **y**. All 'up' or 'down' pairs have Te–Te ‖ **x**, and individual 6-rings have either four 'up' polyhedra and two 'down' or *vice versa* (Fig. 31). This is an analogue of the silicate sheet found in sanbornite, $Ba[Si_2O_5]$ (Hesse and Liebau, 1980), rather than the mica structure type. Each pair of apical oxygen atoms is shared with a SO_4 tetrahedron, thus completing the heteropoly layer structural unit. Layers are held together through long bonds between the Te of one layer and the non-bridging sulfate oxygen atoms of the next. Tilt of the SO_4 groups and asymmetry of the Te–O–Te angles make the structure polar ‖ **z**. The layer ‖ (010) of $(Te_2O_3)(PO_3OH) \equiv (POOH)[Te_2O_5]$

https://doi.org/10.1180/minmag.2016.080.093 Published online by Cambridge University Press

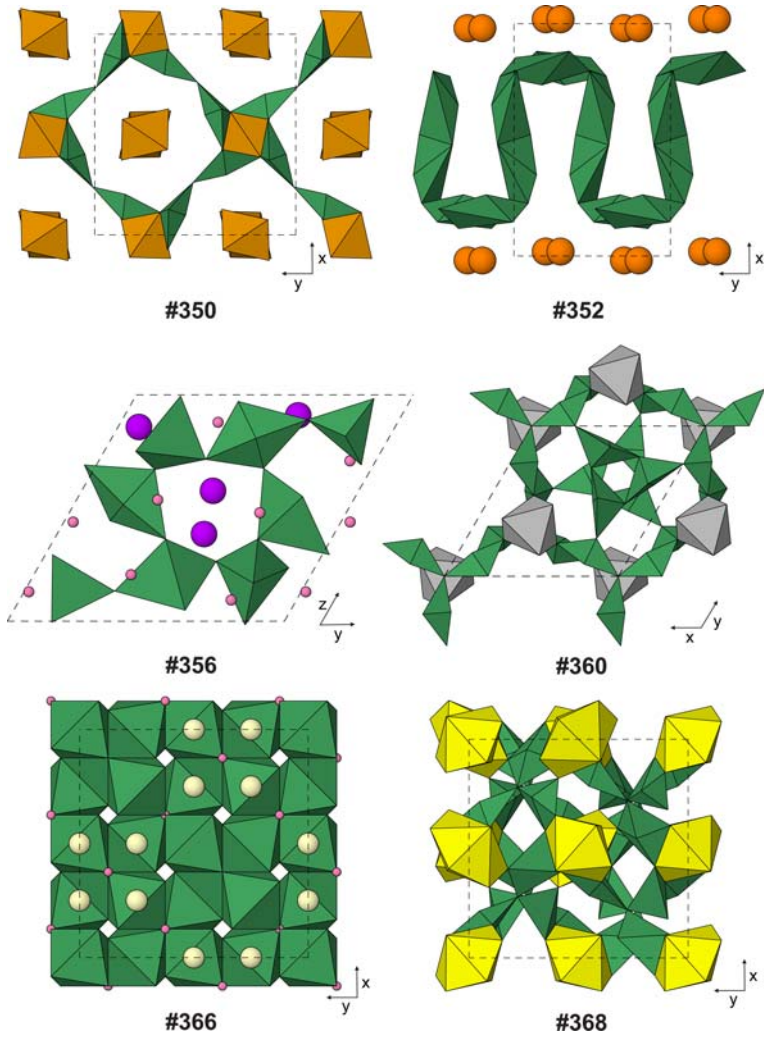

FIG. 32. Examples of structures with layers or frameworks of Te^{4+} polyhedra (Tables 17–18, deposited). Small spheres: O (dark pink) when not part of a polyhedron. Large spheres: Ca (orange), K (purple) and Pr (pale yellow). Polyhedra: Fe (orange-brown), Te (dark green), U (yellow) and Zn (pale grey).

(**#345**) also has pairs of 'up' or 'down' Te polyhedra, but each 6-ring has three of each, and the 'up' (or 'down') pairs are arranged in a herringbone pattern. The PO_3OH tetrahedra again share two corners with adjacent Te polyhedra of a layer. Interatomic distances indicate that the H atom is attached to the non-bridging phosphate oxygen atom O7, and forms hydrogen bonds that brace the layer, rather than connecting between layers. Layers are connected by weak bonds between Te and the other non-bridging phosphate ligand O5, and the overall structure is polar || **z** for the same reasons as **#344**. The *b* parameters of these two structures are very similar, reflecting the similarity of layers and their stacking.

$[Mg(Te_2O_5)]$ and the β polymorph of $[Mn(Te_2O_5)]$ (**#346–347**) have layers || (020) with 6-rings of the 'four up/two down' type, like **#344**, but the 6-rings are distorted so that 'up' Te–Te pairs point along [102] while 'down' pairs point || $[10\bar{2}]$. Layers are cross-linked into a framework through zigzag edge-sharing chains of MO_6 octahedra (M = Mg or Mn). The octahedral chains run || **z**, with small channels between them that can accommodate the Te lone pairs. The 'denningite' polymorph

https://doi.org/10.1180/minmag.2016.080.093 Published online by Cambridge University Press

of the Mn compound was discussed above (**#310**). $MoTe_2O_7 \equiv [(MoO_2)(Te_2O_5)]$ (**#348**) also has 'four up/two down' layers, this time || (002), but the layers are strongly pleated so that the Te–Te pairs point obliquely to the overall trend of the layer, || $[23\bar{2}]$ ('down' pairs relative to +**z**) or $[2\bar{3}\bar{2}]$ ('up'). Layers contain very obvious massicot-like Te–O–Te–O chains || **x**. Tellurium layers are linked into a framework through MoO_6 octahedra chains, which occur as edge-sharing Mo_2O_{10} dimers which then share four additional corners to make ladder-like double chains || **x** (Fig. 31).

$La_2[Te_3O_7]_2(WO_4)$ (**#349**) has the unique layers of 3- and 6-rings shown in Fig. 11*h*; note that the node where three 6-rings join is a CN3 oxygen atom. These layers are || (002), and the non-bridging oxygen atoms of the Q^{1210} Te polyhedra all point inwards from two such layers towards a central sheet of LaO_{10} polyhedra. Between the 6-rings of the two Te sheets are large interstices which contain WO_4 tetrahedra, disordered between 'up' and 'down' orientations. Mackayite, $Fe^{3+}(Te_2O_5)(OH)$ (**#350**) has layers that should be written Te_4O_{10} to reflect the translational periodicity. These have 4- and 8-rings similar to the 'apophyllite' type, as seen in Fig. 11*i*. In the mackayite layer, individual 'upward' and 'downward' pointing polyhedra alternate, unlike apophyllite, where whole 4-rings of 'up' and 'down' tetrahedra alternate (Colville *et al*., 1971). The layers lie || (004), repeated by a screw tetrad axis. The layers are held together by edge-sharing dimers of Fe octahedra, $Fe_2O_8(OH)_2$ (Fig. 32). Our second polymorph of $Li_2Te_2O_5 \equiv Li_4[Te_4O_{10}]$ (**#351**) like its dimorph **#343** has Te layers || (020) in which all Te are CN4; however, the polyhedra form 10-rings, and some of them are only 2-connected, occurring as edge-sharing Q^{1301} pairs rather than the Q^{1300} polyhedra typical of silicate-like sheets (Fig. 11*j*). The edge-sharing dimers act as bridges between bands where the other Te tetrahedra point downards and bands where they point upwards. The pointing direction reverses every $\frac{1}{2}c$. Tellurium sheets are held together through the non-bridging oxygen atoms, which link to LiO_4 tetrahedra, which occur as pairs of *vierer* corner-sharing helices (cf. $Li_2[TeO_3]$, **#1**) running || **x** between Te layers. The regular inversion of pointing direction in the Te layers, and breakup of the Li component into discrete ribbons, gives this structure a resemblance to commensurately modulated phyllosilicates such as sepiolite, $Mg_4[Si_6O_{15}](OH)_2 \cdot 6H_2O$ (Post *et al*., 2007). The Te_4O_{10} layer of $Ca[Te_2O_5]$ (**#352**) also has 10-rings and edge-sharing dimers of Te polyhedra; however, the latter are now 3-connected Q^{0401} type, as seen in Fig. 11*k*. The layers are crumpled and rather thick, with the edge-sharing Te=Te vectors almost normal to the overall layer plane (100). Layers are linked through sheets of CaO_7 polyhedra (Fig. 32). Note that this description requires a slightly longer than usual strong-bonding distance threshold; if a Te–O distance of 2.450 Å is not included, the layer breaks up into finite Te_4O_{10} tetramers of the type seen in Fig. 8*j*, **#250–255**. A similar topology of layer, less tightly corrugated, occurs || (10$\bar{1}$) in $Tl_2[Te_2O_5]$ (**#353**). Layers are linked through very irregular TlO_{5-7} polyhedra. $K_2[Te_4O_9]$ (**#354**) and its NH_4^+ analogue **#355** are isopuntal, but giving them a common description again requires a careful choice of Te–O bonding threshold, which is 2.43 Å here. This excludes additional neighbours at 2.433 and 2.489 Å to respectively Te1 and Te2 of the K compound, which are at 2.713 and 2.615 Å and hence clearly not strongly bonded in **#355**. The convoluted Te_8O_{18} layers || (100) in these structures have the topology of Fig. 11*l*, with 6- and very elongated 14-rings containing both CN3 and CN4 Te polyhedra. The layers are held together by large cations, 7–8 coordinated by oxygen in the case of K^+. This structure is very different from the double-chain type of the Na analogue (**#332**, Fig. 10*f*). Although $K_2[Te_4O_9] \cdot 3.2H_2O$ (**#356**) is triclinic, it is strongly pseudohexagonal ($b \approx c$, $\alpha \approx 60°$) and has rather symmetrical Te_8O_{18} layers || (100) containing two types of 6-ring (Fig. 11*m*). One quarter of the rings are regular hexagons containing only CN4 Te, with non-bridging ligands pointing alternately 'up' and 'down'. The rest of the rings are elliptical, and three of these meet at a CN3 Te atom. Between the Te layers are a central plane of water molecules and K^+ ions in 7–8 coordination (Fig. 32). $(NH_4)Rb[Te_4O_9] \cdot 2H_2O$ and the corresponding compound with Cs replacing Rb (**#357–358**) have a rather complex $Te_{16}O_{36}$ layer (Fig. 11*n*). The layers are || (002), and can be regarded as formed by condensation of Te_8O_{20} clusters. The clusters, in turn, consist of a central edge-sharing pair of Q^{0501} Te atoms, common to two 4-rings which are each completed by a pair of Q^{1300} Te atoms, each 4-ring in turn sharing one side with a 3-ring formed by links to a Q^{0300} Te atom. The remaining corners of the 4-rings and the CN3 Te atom of the 3-rings then link to other clusters to make a continuous layer, which has very elongate 12-rings. Large cations and water molecules are between the layers.

Our final single-layer structure, $Ba_6[Te_{10}O_{25}]Br_2$ (**#359**), also has an extraordinarily complex layer

https://doi.org/10.1180/minmag.2016.080.093 Published online by Cambridge University Press

with a translational repeat $Te_{40}O_{100}$ and ten symmetrically distinct types of Te (Fig. 11*o*). The layers are || (002) and are rather thick but looped rather than double, with tubular cavities running || **x** which contain the Br^- ions. Ba^{2+} cations between the layers link to 8–9 O atoms of the tellurite layer and 0–1 Br. Again, the layer is most simply described if an unusually long bonding threshold of 2.52 Å is used. This includes all the moderately strong Te–O bonds: seven out of the ten Te sites have oxygen neighbours in the 2.41–2.52 Å range, while none have any other neighbours within 2.98 Å. With the Te–O bond network thus defined, Te are CN4 (Te1 Te2, Te4 = Q^{0400}, Te9 = Q^{1300} and Te5–Te8 = Q^{2200}) except Te3 (Q^{0300}). Two types of tube alternate, both with flattened elliptical cross-sections. The denser type contains a ribbon of 4-rings (Te2–Te9–Te2–Te9) and 8-rings (Te2–Te3–Te1–Te9–Te2–Te3–Te1–Te9), with arches of three additional Te atoms completing 7-rings (Te4–Te8–Te7–Te3–Te2–Te9–Te1). These tubes are linked into a layer through Te10 and bridges –Te5–Te6– but the second type of tube defined by those is much more sparsely connected, its smallest rings having 9 and 10 members.

The compounds $[M^{2+}(Te_6O_{13})]$ (M = Zn, Fe and Mg; **#360–362**) have Te_6O_{13} double layers (Fig. 12*a*). These stack || (003) and are linked through corner-sharing with MO_6 octahedra. The individual sublayers contain triplets of Q^{0311} Te1 sharing a common CN3 oxygen atom, connecting to 3-rings of Q^{1300} Te2 so as to form crumpled 12-rings of Te1 and Te2, which surround the M cations. Two such sublayers are linked by their Te1 atoms sharing an edge (Fig. 32). $(Te_3O_5)(Se^{4+}O_3) \equiv [(SeO)_2(Te_6O_{14})]$ (**#363**) has a double layer || (001) with three types of Te polyhedron: Q^{0300}, Q^{1300} and Q^{1400} (Fig. 12*b*). Each sublayer has a net of 3-connected 8-rings, with CN4 and CN5 Te atoms at the nodes and CN3 Te making two links within the sublayer. These links result in smaller 4- and 6-rings that are shared by the sublayers. Two such sublayers are held together by links between CN3 Te of one and CN5 Te of the other. The SeO_3 pyramids are on the outside of the double layer, sharing one oxygen atom with CN5 Te and one with CN4 Te. Layers are held together by weak Te···O and Se···O bonds.

Structures with Te^{4+} complexes that are infinite frameworks

Tectotellurite structures **#364–375** are listed in Table 18 (deposited), summarized in Table 5 and have their Te–O frameworks depicted in Fig. 12. The structure of the paratellurite polymorph of TeO_2 (**#364**, Fig. 12*c*) is derived from that of the rutile form of TiO_2 (cf. Meagher and Lager, 1979) in a way analogous to the derivation of the tellurite structure from brookite (**#341** above). The lone-pair stereoactivity of the Te^{4+} changes the coordination environment from the relatively regular octahedron of rutile to a strongly distorted 4 + 2 pattern with 2 × O at 1.88 Å, 2 × O at 2.12 Å and 2 × O at 2.87 Å. However, unlike tellurite, the lengthening and weakening of two bonds per Te atom does not disrupt the framework of the TiO_2 aristotype. However, the tetragonal c repeat is doubled, and the 4_2 screw axis of rutile becomes a 4_3 (or 4_1) axis in paratellurite. Paratellurite is ~4.5% denser than tellurite. Interestingly, not only is the structure a distortion of the rutile structure, but it is isopuntal and topologically equivalent to the metastable low-temperature α-cristobalite form of SiO_2 (cf. Downs and Palmer, 1994). This suggests that the paratellurite geometry provides a pathway for diffusionless structural transformation of the type discussed by Christy (1993), between the relatively low-density cristobalite structure type (stable at relatively high temperature and low pressure in the SiO_2 system, for instance) and the high-density rutile type (stable at very high pressure for SiO_2, as stishovite). At high pressure (~0.95 GPa), paratellurite undergoes a continuous, displacive phase transition to a topologically similar but orthorhombic variant TeO_2-γ, whose structure has been refined at 1.98 GPa (**#365**). Paratellurite and the high-pressure phase are isostructural with, respectively, the β and γ phases of SnF_2, as noted by Denes *et al.* (1980), who also discuss transformations involving the cristobalite and rutile structures.

$Pr_2[Te_2O_6]O$ (**#366**) has a structure of the well-known pyrochlore type, which can be derived from a 2 × 2 × 2 block of face-centred cubes of the fluorite structure by slight displacement of ¾ of the anions so that half of the cations are in octahedral coordination by them, forming a continuous framework (Fig. 12*d*) and omission of half of the remaining anions. The overall stoichiometry is $A_2[B_2X_6]Y$, where the larger cation type A is coordinated by $6X + 2Y$ while B bonds to $6X$ only. In this case, B is Te^{4+}, which unsually is in rather regular octahedral coordination by oxygen, with no lone-pair stereoactivity (Fig. 32). The next few structures are also fluorite derivatives. $K[Ga(Te_6O_{14})]$ (**#367**) has a similar-sized $a \approx 11$ Å cubic unit cell to **#366**, but $^1/_8$ of the cations are 8-coordinated K^+, $^1/_8$ are 6-coordinated Ga^{3+}, and the rest are 4-coordinated Te^{4+}. The K, six Te and Ga are arranged in the $LiCa_6Ge$

https://doi.org/10.1180/minmag.2016.080.093 Published online by Cambridge University Press

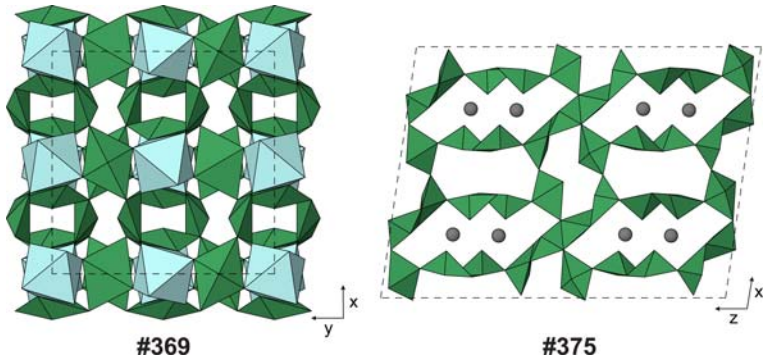

FIG. 33. Examples of structures with frameworks of Te^{4+} polyhedra (Table 18, deposited). Large spheres: Pb (dark grey). Polyhedra: Sn (pale blue) and Te (dark green).

pattern (Pavlyuk *et al*., 1993), a superstructure of the common Cu_3Au type (Kear and Wilsdorf, 1962). Relative to fluorite, $^1/_8$ of the anions are missing, as for pyrochlore. The remaining anions are of three types, bonded respectively to 2Te + K, Te + Ga and 3Te + K. If we consider only the Te–O substructure, it has Te_6O_{14} stoichiometry and Q^{1210} Te polyhedra forming the complex network shown in Fig. 12*e*. The Ga octahedra reinforce this framework. Cliffordite, $[(UO_2)(Te_3O_7)]$ (**#368**), has Te^{4+} and U^{6+} in a 3 : 1 ratio, ordered in the Cu_3Au arrangement like Te and (K+Ga) of **#367** (Fig. 32). As for that structure, the Te–O framework has Q^{1210} Te polyhedra and Te_6O_{14} stoichiometry, but the topology is different (Fig. 12*f*), and whereas TeO_4 polyhedra share corners with GaO_6 octahedra in **#367**, they share edges with UO_8 bipyramids in cliffordite. Note that the total anion content is higher than that of fluorite: while the uranyl oxygen positions and those of the oxygen atoms that link U to Te can all be derived by small displacements from their counterparts in the fluorite aristotype, this is not true for O5 of cliffordite, which joins 3 Te. Very closely related is the winstanleyite structure type of compounds $[A^{4+}(Te_3O_8)]$ (**#369–373**), where A = Ti in the mineral winstanleyite (**#372**), ($Fe^{3+}_{0.67}$ $Te^{6+}_{0.33}$) in walfordite (**#373**), and Sn, Zr or Hf in synthetic analogues (Fig. 33). Again, Te and A atoms are in the Cu_3Au pattern. The oxygen atoms of the fluorite aristotype are all present, but are displaced so as to form quite regular octahedra around the A cations and the common 'folded rhombus' arrangement of Fig. 4*c* aound Te. The Te polyhedra are Q^{2020}, and form a framework (Fig. 12*g*) where the non-bridging ligands share corners with A octahedra. Note that for taxonomic purposes, the minority Te^{6+} content of the A sites of walfordite is ignored. $Cs_2[Te_4O_9]$ (**#374**) has a tetragonal unit cell with the a parameter similar to that of **#366–373** but c about twice as large. The Cs and Te atoms form two cubes of the $MgCu_2$ Friauf-Laves structure arrangement (Friauf, 1927; Hyde and Andersson, 1989). That is, they are geometrically equivalent to, respectively, the D and T cubic lattice complexes of Fischer and Koch (2006). This is also the pattern of Mg and Al atoms in normal spinel, $MgAl_2O_4$, and of YB_2 atoms in the $A_2B_2X_6Y$ pyrochlore structure. However, whereas the B cations of the pyrochlore framework are linked through X to six B neighbours (cf. **#366** above), the Te atoms of **#374** are bonded to only a subset of these: half of them are CN4 (Q^{0400}) and the other half are CN3 (Q^{1300}). There are no 3- or 6-rings, as in the pyrochlore framework: every CN3 Te atom is a member of one 4-ring, while the CN4 atoms join two such rings, and the next-smallest rings have 8 members (Fig. 12*h*). Vacant sites which would be occupied by oxygen atoms in a pyrochlore allow a more open framework, with rather large interstices to accommodate Cs^+ ions in 9–10 coordination. $Pb[Te_5O_{11}]$ has a very complex, open framework with five symmetrically different types of Te atom (**#375**). If Te–O distances out to 2.45 Å are included as bonds, then the topology is as seen in Fig. 12*i*. Te1, Te2 and Te3 (respectively Q^{0312}, Q^{1210} and Q^{0401}) form complex double chains that run || $[1\bar{1}0]$ at $z = 0$ and || [110] at $z = ½$. These are in turn made from Te3=Te1=Te1=Te3 tetramers which are joined by Te2, which shares a CN3 oxygen with 2Te1 and a CN2 oxygen with Te3 (Fig. 33). Between these double chains, Te4 and Te5 (both Q^{1300}) form massicot-like single chains (cf. Hill, 1985) which run || **y** at $z = ¼$ and ¾. The component chains are joined in three dimensions byTe4 linking to Te3 on one side of these chains, while Te5 links to Te2 on

https://doi.org/10.1180/minmag.2016.080.093 Published online by Cambridge University Press

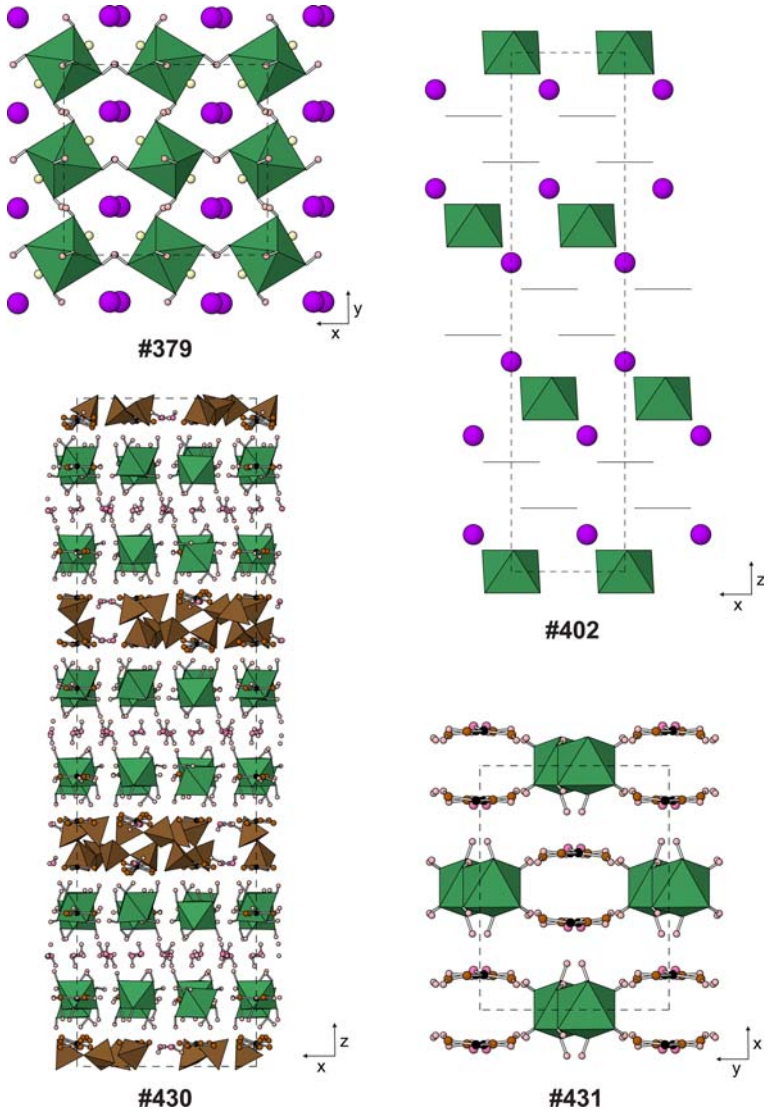

FIG. 34. Examples of structures of $Te^{6+}(OH)_6$ adducts (Table 19, deposited). Small spheres: C (black), H (pale pink), N (brown) and O (dark pink) when not part of a polyhedron. Large spheres: K (purple). Horizontal lines in **#402** indicate planes of oxygen triangles of pyramidal $I^{5+}O_3^-$ anions; I atoms are not shown. Polyhedra: P (brown) and Te (dark green).

the other. Lead atoms are in 8-coordination between the massicot-like chains.

$Te^{6+}(OH)_6$ and its adducts

Our first examples of Te^{6+} compounds are polymorphs and derivatives of orthotelluric acid, $Te^{6+}(OH)_6$. The large valence (~1 vu) of bonds to O from both Te and H means that any additioanl bonding must be weak, so the compound $Te(OH)_6$ has discrete octahedral molecules which are held together only through hydrogen bonds. Unsurprisingly, it is hygroscopic, extremely water-soluble, and unknown in minerals. As the molecule has six oxygen atoms, each of which carries one donor H atom and is able to accept low-valence bonds from other electron donors outside the molecule, $Te(OH)_6$ is able to co-crystallize with

https://doi.org/10.1180/minmag.2016.080.093 Published online by Cambridge University Press

a wide range of other compounds to form adducts. The other components may be polar organic molecules, simple salts of large cations such as alkali halides, or salts with larger and more complex anions such as polyphosphate species. These adducts are physically and crystal-chemically distinctive enough that they are considered separately from other Te^{6+} compounds. In many cases, small tilts of Te octahedra or changes to the H-bonding pattern may result in very similar molecular arrangements occurring in a range of different space groups and unit-cell shapes. The TeO_6 octahedron (Fig. 4*h*) is always rather regular, with Te–O = 1.90–2.07 Å, corresponding to bond valences of 1.04–0.77 vu using the parameters of Mills and Christy (2013). The individual structures **#376–431** are listed in Table 19 (deposited).

The cubic polymorph of $[Te(OH)_6]$ itself has the molecules packed in a *fcc* array, but with the octahedra tilted and hydrogen bonded so that the cell repeat is doubled to 15.71 Å, and the space group is $Fd\bar{3}c$ (**#376**). There is also a monoclinic polymorph (**#377**), where Te···Te distances shorter than 6.3 Å define 12 nearest neighbours in a monoclinically sheared face-centred cube, with pseudocube edges || [100], [101] and [010] of the $P2_1/n$ cell. $(NaF) \cdot [Te(OH)_6]$ (**#378**) retains a *fcc* arrangement of $Te(OH)_6$ molecules, albeit with rhombohedral distortion. Na^+–F^- ion pairs occur in the octahedral interstices between them, so that (NaF) units and $Te(OH)_6$ molecules form a rocksalt arrangement. Similarly, $(KF)_2 \cdot [Te(OH)_6]$ (**#379**) has K^+–F^- ion pairs in the tetrahedral interstices of an orthrohombically distorted *fcc* array of $Te(OH)_6$ molecules, so that (KF) and $Te(OH)_6$ are arranged like F and Ca of the fluorite structure (Fig. 34). Such ion pairs are almost unknown in mineral structures, although the Ca^{2+}–CO_3^{2-} pair occurs in a matrix of H-bonded water molecules in ikaite, $CaCO_3 \cdot 6H_2O$ (Swainson and Hammond, 2003) and hsianghualite, $(LiF)_2Ca_3[Be_3Si_3O_{12}]$, can be regarded geometrically as having ion pairs Li^+–F^- replacing the Cs^+ of pollucite, $Cs_2\square_3[Al_2Si_4O_{12}]$, or water of analcime, $(H_2O)_2(Na_2\square)[Al_2Si_4O_{12}]$ (Rastsvetaeva *et al*., 1991). However, the bond distances and the parameters of Brese and O'Keeffe (1991) indicate that the Li–F bond is not unusually strong, bond valences being ~0.25 vu for all bonds from Li to F + 3 O and to F from Li + 3 Ca.

Alkali halide adducts with larger ions do not have ion pairs intercalated into a matrix of *fcc* Te $(OH)_6$. $(CsCl)_2 \cdot [Te(OH)_6]$ (**#380**) has Te and Cl forming an array of monoclinically distorted $CaCl_2$ (or collapsed rutile) type, with Cs located in tetrahedra of four Cl. $(RbCl)_3 \cdot [Te(OH)_6]$ (**#381**) has a quite different rhombohedral structure in which $Te(OH)_6$ octahedra alternate with Cl_3 triangles to form rods || **z** which are linked through Rb, with each Rb having five Cl neighbours and *vice versa*.

$Na_2(SO_4) \cdot [Te(OH)_6]$ (**#382**) has a unique structure in which $Te(OH)_6$ octahedra form a primitive hexagonal array, and alternate trigonal prisms of such molcules contain either two Na or SO_4 tetrahedra. The pseudohexagonal layers of Te are || (002), with layers of Na and SO_4 groups between them. One type of Na bonds to only two SO_4 while the other type bonds to three SO_4, and their arrangement makes the structure polar in the (010) plane. There are a very large number of adducts of the type $A_2(TO_4) \cdot [Te(OH)_6]$, with larger cations A = (K, Rb, Cs, Tl and NH_4) and T = (S or Se) (**#383–398**). Despite the apparent diversity of symmetries and cell parameters, all of these are again based on a *fcc* array of $Te(OH)_6$ molecules, with the tetrahedral anion occupying octahedral interstices and the A cations occupying tetrahedral interstices. The edges of the pseudocubic cell have different indices depending on the axial setting chosen by authors, as follows. $K_2(SO_4) \cdot [Te(OH)_6]$ (**#383**) has space group $P\bar{1}$, with pseudocube edge vectors are $\frac{1}{2}[1\bar{1}\bar{1}]$, $\frac{1}{2}[311]$ and $\frac{1}{2}[13\bar{1}]$. The monoclinic structures with space group $C2/c$, Cc, $P2_1/a$, $P2_1/c$, $P2_1/n$ or Pn all have pseudocube edges $\frac{1}{2}[10\bar{1}]$, $\frac{1}{2}[121]$ and $\frac{1}{2}[1\bar{2}1]$ (**#384–390** and **392–397**) except for $(NH_4)_{1.16}K_{0.84}(SO_4) \cdot [Te(OH)_6]$ (**#391**), which was published in a different axial setting where the pseudocube edges are $\frac{1}{2}[102]$, $\frac{1}{2}[120]$ and $\frac{1}{2}[1\bar{2}0]$. Note that these structures include centrosymmetric and acentric polymorphs of $K_2(SeO_4) \cdot [Te(OH)_6]$ (**#384** and **385**), structures in which two A species occur in solid solution and others in which they are ordered, such as $CsK(SO_4) \cdot [Te(OH)_6]$ (**#397**), and that there may be one or two symmetrically distinct types of $Te(OH)_6$ octahedron per unit cell. $Cs_2(SO_4) \cdot [Te(OH)_6]$ (**#398**) has a rhombohedrally distorted structure, in which the pseudocube edges are $\frac{1}{3}[2\bar{2}1]$, $\frac{1}{3}[42\bar{1}]$ and $\frac{1}{3}[241]$. Hydrogen ions may be quite mobile in these compounds; Dammak *et al*. (2005) investigated the protonic conductivity behaviour of $Cs_{0.86}(NH_4)_{1.14}(SO_4) \cdot [Te(OH)_6]$, which has the $P2_1/c$ variant of the structure but has been excluded from this study because of some unrealistically short Te–O distances in the refinement.

$K_2(NO_3)_2(H_2O)_2 \cdot [Te(OH)_6]$ (**#399**) has a layered structure || (001) not unlike that of **#382**, in which Te octahedra form a monoclinically

https://doi.org/10.1180/minmag.2016.080.093 Published online by Cambridge University Press

sheared primitive-hexagonal array with trigonal prisms containing the other components. Conversely, $(Cs_{3.5}Rb_{0.5})(SeO_3)_{1.7}(SO_3)_{0.3} \cdot [Te(OH)_6]_3$ (**#400**) has the familiar *fcc* array of Te, although this time, large cations occupy only ⅔ of the tetrahedral interstices, pyramidal anions are in the other ⅓ of the tetrahedral voids, and the octahedral positions are empty. The pseudocubic edge vectors are [010], ⅙[203] and ⅙[20$\bar{3}$] of the orthorhombic cell. The iodate adducts all have layered structures. $K(IO_3) \cdot [Te(OH)_6]$ (**#401**) has K+Te and I layers alternating || (001), while $K_2(IO_3)_2 \cdot [Te(OH)_6]$ (**#402**) has thicker layers I–K–Te–K–I || (003), with the lone pairs of I^{5+} cations directed into the interlayer gap (Fig. 34). $(NH_4)(IO_3)(H_2O) \cdot [Te(OH)_6]$ (**#403**) has layers of Te + I alternating with $NH_4 + H_2O$ || (200).

A very large number of adducts have been made that contain phosphate anions, along with large cations Na, K, Rb, Ag, Tl or NH_4. The phosphate groups range from tetrahedral monomers $[PO_3OH]^{2-}$ or $[PO_2(OH)_2]^-$ (**#404–412**) through diphosphates $[P_2O_6OH]^{3-}$ or $[P_2O_5(OH)_2]^{2-}$ (**#413–415**), cyclo triphosphates $[P_3O_9]^{3-}$ (**#416–422**), $[P_4O_{12}]^{4-}$ (**#423–424**), $[P_6O_{18}]^{6-}$ (**#425–427**), $[P_8O_{24}]^{8-}$ (**#428–429**) and even $[P_{12}O_{36}]^{12-}$ (**#430**). Most of these compounds have layered structures with large unit cells, mainly of low symmetry, and will not be discussed in detail here. However, we note that $K_3Na_3(P_3O_9)_2 \cdot [Te(OH)_6]$ has monoclinic and rhombohedral dimorphs (**#420–421**), with alternation of (pseudo)hexagonal layers of Te + P and Na + K || (200) and (003), respectively. Most of the phosphate adducts are crystal-chemically unique: there are few examples of more than one compound sharing the same stoichiometry, and even when they do, the structures are different. Thus, despite the apparent chemical similarity, $(NH_4)_4(P_4O_{12})(H_2O)_2 \cdot [Te(OH)_6]$ and its K analogue (**#423–424**) are not isostructural, and the same is true for $(NH_4)_8(P_8O_{24})(H_2O)_2 \cdot [Te(OH)_6]$ and the corresponding K compound (**#428–429**). The most complex phosphate adduct, $(C(NH_2)_3)_{12}(P_{12}O_{36})(H_2O)_{24} \cdot [Te(OH)_6]_{12}$ (**#430**), has as a counterion not an alkali metal cation but guanidinium, $[C(NH_2)_3]^+$. This compound has six Te layers and three polyphosphate layers in its rhombohedral cell with $c \approx 51$ Å. The threefold rotational symmetry is inherited from the Te octahedra, triangular planar guanidinium complexes and cyclophosphate rings (Fig. 34). The final adduct described here also has a small organic molecular component, the neutral urea molecule in $(CO(NH_2)_2)_2 \cdot [Te(OH)_6]$ (**#431**). This compound has a rather simple structure in which each Te octahedron has four neighbours at 5.1–6.6 Å, in a monoclinically distorted version of the diamond arrangement. Each Te octahedron also has four nearby urea molecules (Te···C = 4.2–4.5 Å), and with them defines dense layers in the structure || (20$\bar{2}$). Hydrogen bonds link molecules both within and between these layers (Fig. 34).

A few additional compounds containing Te $(OH)_6$ molecules as hydrogen-bonded adducts along with other Te in other environments are included below at **#498–502**, **504** and **631**.

Monomeric $Te^{6+}X_n$ anions (n = 4–6)

$Te^{6+}X_4$ and $Te^{6+}X_5$

Te^{6+} almost always occurs in octahedral coordination with oxygen, as noted above and by Mills and Christy (2013). However, we have a very small group of compounds in which the coordination number is 4 or 5. Ligands distribute themselves symmetrically around the closed-shell Te^{6+} cation, unlike the situation with Te^{4+}, which usually has a strongly stereoactive lone pair of electrons. The coordination polyhedron for CN4 Te^{6+} is a tetrahedron (Fig. 4*f*), while that for CN5 Te^{6+} is a trigonal bipyramid (Fig. 4*g*). $Cs_2[TeO_4]$ (**#432**) has the K_2SO_4-β structure, in which Te and Cs form the same arrangement as Pb and Cl in cotunnite, $PbCl_2$ (O'Keeffe and Hyde, 1985) (Fig. 35). $Cs_2K_2[TeO_5]$ (**#433**) has a tetragonal structure in which TeO_5 polyhedra are linked through CN6 K^+ and CN6–8 Cs^+. $Rb_6[TeO_5][TeO_4]$ (**#434**) contains both types of Te polyhedron. In this compound, Rb and Te together form an approximately cubic close-packed array with pseudocube edge vectors [½00], [0½0] and [¼0½] of the monoclinic cell. Rubidium atoms are in 6–8 coordination by oxygen (Fig. 35). Note that in all these structures, the counterions are large, weakly-bonding alkali metal species. Details for these structures are summarized in Table 20 (deposited).

Monomeric $Te^{6+}X_6$ that are not part of a larger structural unit.

Although Te^{6+} occurs almost exclusively in one type of coordination polyhedron, and the range of Te–O polymers that it forms is very restricted compared with Te^{4+}, the monomeric tellurate octahedron TeX_6 is the single most prolific structure-forming Te–O complex in the present study: there are 172 compounds with such octahedral anions (**#435–616** below), in addition

https://doi.org/10.1180/minmag.2016.080.093 Published online by Cambridge University Press

to the 56 adducts of neutral molecular $Te(OH)_6$ that were briefly described above. Nesotellurates up to **#456**, with no larger structural unit including strongly-bonding non-Te cations, are listed in Table 20 and described here.

$(NH_4)_2[TeO_2(OH)_4]$ (**#435**) has a simple structure in which Te octahedra form a centred regular net in layers || (001), with layers of NH_4 cations between them. The Te–O distances show that the unprotonated oxygens (O1) are ordered in *trans* positions in the octahedron, with O–Te–O vectors || [201]. $K_3Na_2Li[TeO_6]$ (**#436**) has layers of K alternating with layers of Na+Li+Te || (020). Within the latter layers, TeO_6 octahedra and LiO_4 tetrahedra form edge-sharing chains || [101], alternating with chains of NaO_{5-6} polyhedra. The three types of K atom are in 6–8 coordination. $K_3Li_3[TeO_6]$ (**#437**), somewhat similarly, has alternation of K and Te+Li layers || (200). Within the Te+Li layers, chains || **y** of corner-linked LiO_4 tetrahedra alternate with chains of edge-sharing TeO_6 octahedra and unusual square-planar LiO_4 groups. The Li–O distances in the distorted tetrahedra are 1.94–2.05 Å; those in the squares are similar, at 2.01–2.11 Å, with no additional O neighbours until two at 3.27–3.29 Å, which complete a very elongated octahedron around Li. Potassium is 8–9 coordinated. $K_4Na_2[TeO_6]$ (**#438**) has K layers alternating with Te+Na || (001). The Te form a face-centred rectangular net, and NaO_6 octahedra share two opposite faces with neighbouring TeO_6 octahedra to complete the layer. Potassium coordination is 6–8.

The structure of $KNa_5[TeO_6]$ (**#439**) is best described as having cations in a *hcp* array, with layers of composition KNa_3 and $Te(Na_{0.67}\square_{0.33})_3$ alternating along **z**, and two of each layer type per cell. Oxygen atoms are all equivalent and in octahedral interstices in the cation array, coordinated by Te + K + 2Na + 2($Na_{0.67}$). The coordination environments for all alkali cations are slightly unusual: trigonal prismatic for K (K–O = 2.79 Å), square planar for partially occupied Na1 and square pyramidal for fully occupied Na2 (Na–O = 2.35 Å in both cases), while Te is in very regular octahedral coordination with Te–O = 1.94 Å (Fig. 35). $K[TeO(OH)_5] \cdot H_2O$ (**#440**) has KO_9 polyhedra sharing edges and faces to make a sheet with a honeycomb net || (100). The TeX_6 octahedra are bound to this sheet to make a compound layer, with H_2O molecules in the interlayer gaps. The layers are held together only by hydrogen bonds.

$Na[TeO(OH)_5]$ (**#441**) is very different from the above structures. It has a 2 × 2 × 2 cubic superstructure of the ReO_3 type with alternation of Na+ and Te^{6+} in octahedral coordination and no long-range order of O^{2-} and OH^-, and is thus isotypical with wickmanite, $Mn^{2+}[Sn^{4+}(OH)_6]$ and a family of related hydroxostannates, germanates and antimonates, including several mineral species (Basciano *et al*., 1998). Because of nonlinear *M*–O–*M*′ links and orientational order of O–H groups, these compounds do not have $Fm\bar{3}m$ symmetry but either $Pn\bar{3}m$ (Strunz and Contag, 1960), $Pn\bar{3}$ (Morgenstern Badarau and Michel, 1976; Cohen-Addad, 1977; Basciano *et al*., 1998) or $P4_2/n$ (Mikhaylov *et al*., 2011; Kleppe *et al*., 2012; Lafuente *et al*., 2015). $Na[TeO(OH)_5]$ may either be orientationally disordered, or may actually crystallize in one of these lower symmetry space groups. The ReO_3 and wickmanite structure types are derivatives of the ABX_3 perovskite type in which large cations *A* are absent, leaving only octahedrally coordinated species *B*. Many other perovskite-related tellurates are described below (**#562–584**), while here, we include two unusual examples which have large cations in both *A* and *B* positions. These are $Sr_3[TeO_6]$ and $Ba_3[TeO_6]$ **(#442–443)** whose unit cells are very large superstructures of the basic perovskite cube (the cells reported are respectively 4 × 4 × 4 and $\sqrt{20} \times \sqrt{20} \times 8$ of the ~4 Å cube), with rather low symmetry: the triclinic structure of **#442** has eight distinct Te sites, four '*B*-type' Sr sites and eight '*A*-type' Sr, while for **#443**, which is tetragonal, the corresponding numbers of distinct sites are five, five and 13. Substantial rotations of TeO_6 octahedra allow some '*B*-type' (Sr,Ba) to increase their coordination number from 6 to 7 (Sr) or even 8 (Ba).

Rhombohedral $Li_6[TeO_6]$ and $Tl_6[TeO_6]$ (**#444–445**) are isopuntal, even though the great difference in size and stereochemistry between Li^+ and Tl^+ means that their coordination environments are rather different. These compounds have defect superstructures of rocksalt, in which (Li,Tl) and Te are ordered on a *ccp* array. In **#444**, oxygen atoms occupy $^7/_8$ of the octahedral interstices. Tellurium has six oxygen neighbours at 1.93 Å, Li has four at 1.94–2.08 Å and one at 2.37 Å, and oxygen is surrounded by Te + 5Li. In the Tl compound, the inter-cation distances and cell parameters are much larger, and the oxygen atoms are in one of the triangular faces shared by an octahedral and a tetrahedral interstice of the *ccp* array. While the TeO_6 octahedron itself is little changed (Te–O = 1.95 Å), Tl is very irregularly coordinated by six oxygen neighbours at 2.11, 2.46, 2.86, 3.60, 3.88 and 3.90 Å. There is a remarkable relationship between the structure of $Tl_6^{1+}[TeO_6]$ and that of $[Tl_6^{3+}(TeO_6)O_6]$ (**#616**, below), which can be

https://doi.org/10.1180/minmag.2016.080.093 Published online by Cambridge University Press

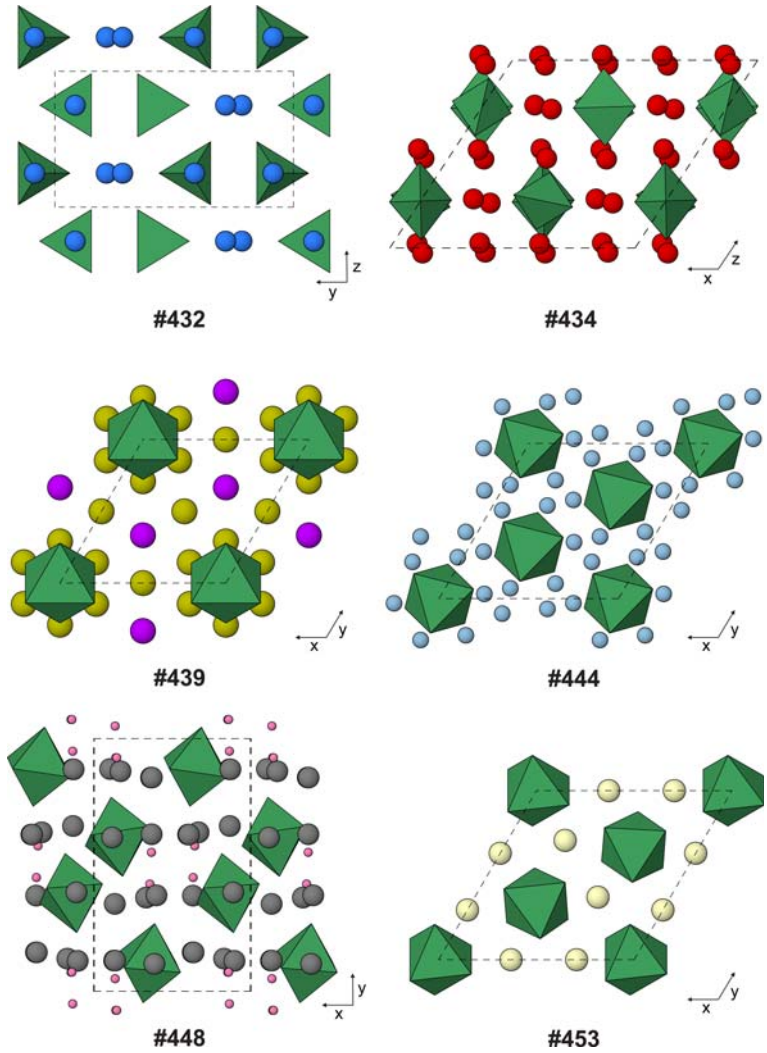

FIG. 35. Examples of structures with monomeric $Te^{6+}O_{4-6}$ anions that are not part of a larger structural unit (Table 20, deposited). Small spheres: O (dark pink) when not part of a polyhedron. Large spheres: Cs (deep blue), K (purple), Li (pale blue), Na (dark yellow), Pb (grey), Rb (red) and Sc (pale yellow). Polyhedra: Te (dark green).

derived from it by stuffing with additional oxygen atoms (Fig. 35). $Li_4Zn[TeO_6]$ (**#446**) also has a defect rocksalt superstructure, but this time, there are no vacancies. Edge vectors of a face-centred pseudocube are [½0 $\bar{1}$/2], [½⅓½] and [½ $\bar{1}$/3½] of the true monoclinic cell. Lithium and Zn are partially ordered on three types of octahedral site, although Li is dominant in all cases.

$Ag_2[TeO_2(OH)_4]$ (**#447**) has TeX_6 octahedra arranged on the *D* lattice complex (Fischer and Koch, 2006) of its *Fdd*2 space group. The unprotonated oxygen atoms (O1) are ordered in a *cis* fashion, and their orientation defines the polarity of the structure along the **z** direction. The Te octahedra are linked by Ag^+ ions in irregular tetrahedral coordination (Ag–O = 2.23–2.58 Å). Silver and the hydroxide oxygen O2 form massicot-like chains (cf. Hill, 1985) which lie in layers || (400) between the Te octahedra, and run || [011] or [0$\bar{1}$1] in alternate layers. $Pb_5[TeO_6]O_2$ (**#448**) has an unusual, very dense arrangement of Pb and Te atoms. Cations lie in rods || **x** that are in a

https://doi.org/10.1180/minmag.2016.080.093 Published online by Cambridge University Press

pseudohexagonal array ($\sqrt{\frac{3b}{c}} = 1.95 \approx 2$), but the x coordinates are such that the cation substructure is not conventionally close-packed. Layers of cations ∥ (040) form nets in which cations form squares and triangles, such that the connectivity is 3^6, 3^34^2, 3^34^2 and then repeats along the **z** direction (Fig. 35). The arrangement can be generated from thinned and faulted 2×3 blocks of hexagonal close-packing. Each cation has from 11 to 13 cation next-nearest neighbours at 3.6–4.6 Å, while the oxygen coordination number of Pb^{2+} is 5–8. Oxygen atoms are in interstices such that layers ∥ (040) of tetrahedrally coordinated oxygen alternate with layers where CN = 5–6. $Pb_6Cd[TeO_6]O_4$ (**#449**) has an approximately *ccp* array of Pb, Cd and Te atoms, the unit cell containing a $2 \times 2 \times 2$ array of distorted face-centred cubes, with irregular $PbO_{4–6}$ polyhedra, CdO_6 trigonal prisms and TeO_6 octahedra.

The compounds $A_2^{3+}[TeO_6]$ (A = Y, La and Gd; **#450–452**) have the enantiomorphic ($P2_12_12_1$) structure of the orthorhombic form of Nd_2WO_6 (Efremov *et al.*, 1984). The TeA_2 substructure is in the cotunnite ($PbCl_2$) arrangement (Léger *et al.*, 1996, and cf. **#432** above), with oxygen atoms coordinated by Te + 2A or Te + 3A so as to form two different types of AO_7 polyhedron. Conversely, $A_2^{3+}[TeO_6]$ with A = Sc, Yb, In or Tl^{3+} adopt a different, trigonal structure (**#453–456**). These compounds have either smaller A–O bonded distances than those above or A cations with relatively large non-bonded radii in the sense of O'Keeffe and Hyde (1981), so all oxygen atoms are 3-coordinate. The structure adopted is shared with malladrite, $Na_2[SiF_6]$ (Babel, 1967). The oxygen atoms are approximately *hcp*, with (A, Te) cations filling variously $^4/_9$ or $^5/_9$ of the octahedral interstices between alternate oxygen layers, and the smaller minority cation (Te ≡ Si) forming a substructure with the AlB_2 arrangement (Hofmann and Jäniche, 1935). Every occupied cation site alternates with vacancies along **z**, so as to avoid face-sharing of octahedra (Fig. 35). Note that **#453–456** could be considered as examples of $[A_2^{3+}(TeO_6)]$ frameworks, given the relatively low CN and high bond valence for the A cations, but they are included here because of the chemical similarity to **#450–452** and the isostructurality with malladrite, in which the A cation Na^+ is much more weakly bound.

Monomeric $Te^{6+}X_6$ as part of a larger structural unit that is a finite cluster

Table 21 (deposited) lists compounds **#457–502**, in which monomeric TeX_6 anions are strongly bound to non-Te cations as part of a larger structural unit. The first of these compounds is unusual, in that the structural unit is in part organic: it is *tris*(tetramethyldisilyl) tellurate, $[(CH_3)_2Si–Si(CH_3)_2]_3(TeO_6)$ (**#457**). The three tetramethyldisilyl groups each bond to two oxygens of the tellurate octahedron, to form a propellor-shaped neutral molecule. The monoclinic cell contains four such molecules, two of opposite rotational senses with their local pseudotriad axes pointing ∥ ±[011], and two with their pseudotriad axes ∥ ±[0$\bar{1}$1] (Fig. 36).

Compounds **#458–461** have stoichiometry of the form $Na_5[M^{3+}(TeO_4(OH)_2)_2] \cdot 16H_2O$, where M = Cu, Ag and Au, except that **#459** is a variant of **#458** with 13% of the Na^+ replaced by H^+. All are isostructural. Two TeX_6 octahedra share *trans* edges of a MO_4 square in these compounds, the square-planar coordination being typical for M^{3+} in a low-spin d^8 electronic configuration. The hydrogen atoms were located in the refinement of **#461**, where they are located on the Te ligands that lie out of the principal plane of the cluster. The corresponding Te–O distances are long, 1.98–1.99 Å, compared to 1.97 Å for the Au=Te bridging oxygens and 1.85–1.86 Å for the unprotonated non-bridging Te ligands opposite the Te=M shared edge. The lath-shaped [Te=M=Te] clusters all have their long axes ∥ [111] of the triclinic cell, and their principal plane approximately ∥ (2$\bar{1}\bar{1}$). These structural units cross-link layers ∥ (10$\bar{1}$) of NaX_6 polyhedra, which contain the additional H_2O molecules (Fig. 36).

The next three compounds **#462–464** feature similar trimeric [Te=M=Te] heteropoly clusters containing a high-valence noble metal cation, but the central polyhedron is an MX_6 octahedron rather than an MX_4 square. The three structures are all different. $K_6Na_2[Pt^{4+}(OH)_2(TeO_5OH)_2] \cdot 12H_2O$ (**#462**) has all [Te=Pt=Te] clusters parallel, with long axes ∥ [10$\bar{1}$] and equatorial planes of octahedra ∥ (101). The clusters are held together through separate $Na(H_2O)_6$ octahedra and K^+ ions in 6–8 coordination. In $Rb_2Na_4[Os^{6+}O_2(TeO_4(OH)_2)_2] \cdot 16H_2O$ (**#463**), the [Te=Os=Te] complexes have their long axes ∥ [010] and equatorial planes ∥ (102). They share the two $O^{2–}$ ligands of one Te (Te2) with similarly oriented edge-sharing tetramers of NaX_6 octahedra, $Na_4O_2(H_2O)_{16}$, to form long structural rods ∥ **y**, which are held together by 8-coordinated Rb^+. Despite the similar stoichiometry, $Na_6[Ru^{6+}O_2(TeO_4(OH)_2)_2] \cdot 16H_2O$ (**#464**) has a very different triclinic structure with trimer long axes ∥ [2$\bar{2}\bar{3}$] and equatorial planes ∥ (302). These structural units act as bridges between

https://doi.org/10.1180/minmag.2016.080.093 Published online by Cambridge University Press

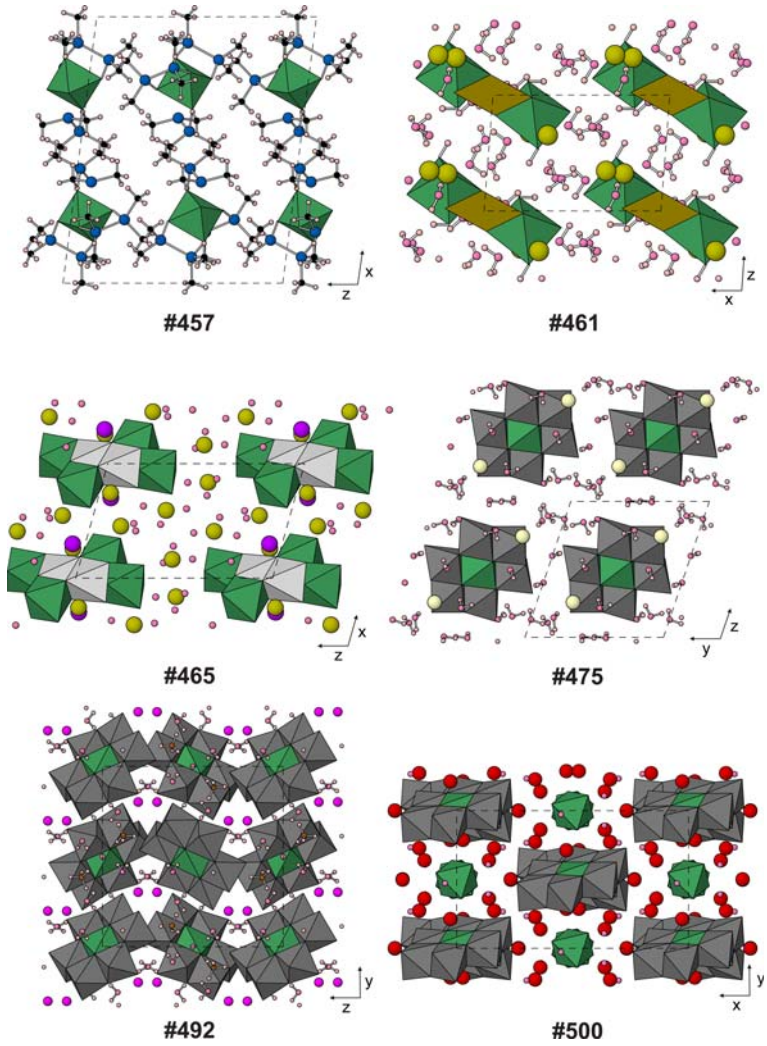

FIG. 36. Examples of structures with monomeric $Te^{6+}O_{4-6}$ anions that are part of a larger structural cluster (Table 21, deposited). Small spheres: C (black), H (pale pink) and O (dark pink) when not part of a polyhedron. Medium spheres: Mn (magenta) and Si (blue). Large spheres: Ce (pale yellow), K (purple), Na (dark yellow) and Rb (red). Polyhedra: Au (yellow-brown), Mo (dark grey), Pd (pale grey) and Te (dark green).

layers || (100) in which NaX_6 octahedra share corners, edges and faces with each other. The H atoms were located in this refinement, and are again confirmed to be located on the oxygen atoms away from the principal plane of the cluster (Te–O = 1.98–2.01 Å), rather than the terminal oxygen ligands in that plane (Te–O = 1.85–1.86 Å). $K_2Na_8[Pd_2^{4+}Te_4O_{18}(OH)_6] \cdot 20H_2O$ (**#465**) has a heteropoly hexameric cluster with a central core of two edge-sharing PdX_6 octahedra. Each shares its *trans* edge with a Te1 cation, while the two Te2 octahedra share the remaining Pd ligands to form 3-rings with both Pd atoms, and in addition make a third bond to the oxygen atoms of the Pd = Pd edge. The hydroxide H atoms are not located in the structure. They are most probably located on the non-bridging oxygen atoms of TeX_6 (of which there are 14 per cluster), but only two of these have long Te–O distances (Te1–O4 = 1.99 Å) as opposed to the typical 1.80–1.83 Å. The rhombus-shaped clusters have long axes || [011] and are flattened || $(1\bar{1}1)$. They lie in layers parallel to that plane with

https://doi.org/10.1180/minmag.2016.080.093 Published online by Cambridge University Press

NaX_6 octahedra, while additional NaX_6 and KX_7 lie between the layers (Fig. 36).

A large group of structures feature the $[M_6^{6+}Te^{6+}O_{24}]^{6-}$ Anderson–Evans heteropolyanion, where M = (Mo or W), and six MO_6 octahedra form a hexagonal ring around a central TeO_6 octahedron (Anderson, 1937; Evans, 1948, 1974). The shape and size of the unit cell is controlled largely by the stacking of these large, tabular structural units, which are held together principally by hydrogen bonds to hydrated alkali cations or NH_4^+ (**#466–470**), hydrated lanthanide cations (**#471–487**) or both (**#488–490**), hydrated transition elements (**#491–497**) or alkalis plus additional molecular $Te(OH)_6$ (**#498–502**).

Although the alkali tellurohexamolybdates and tungstates are all triclinic with very similar cell dimensions, they differ in detail. $Li_6[Mo_6TeO_{24}] \cdot 18H_2O$ (**#466**) has the planes of the Mo–Te hexagons || $(2\bar{3}\bar{3})$, with LiX_6 octahedra between them, sharing edges to form rods of rocksalt-like structure || $[01\bar{1}]$. $Na_6[Mo_6TeO_{24}] \cdot 22H_2O$ and its W analogue (**#467–468**) have layers of NaX_6 polyhedra || $(1\bar{1}0)$, between M–Te hexagons that lie parallel to approximately $(6\bar{4}3)$. $Rb_6[Mo_6TeO_{24}] \cdot 10H_2O$ (**#469**) has hexagons || $(1\bar{1}1)$, sitting in voids in a three-dimensional framework of RbX_{7-9} polyhedra. $(NH_4)_2Na_4[Mo_6TeO_{24}] \cdot 16H_2O$ (**#470**) has layers || (001) of NH_4^+ and Mo–Te ions, alternating with layers of monomeric NaX_6 octahedra and Na_2X_{10} dimers.

$(Ce(H_2O)_4)_2[Mo_6TeO_{24}] \cdot 3H_2O$ and the Nd analogue (**#471–472**) have Mo–Te hexagons that lie in layers || (020), and are canted slightly relative to that plane in opposite senses in alternate layers. Layers are cross-linked by AX_9 polyhedra (A = Ce or Nd), while additional H_2O molecules lie in the Mo–Te layers. The next several compounds are all triclinic with similar unit-cell dimensions, with only a single orientation of Mo–Te hexagon. Again, these lie in layers with some of the water molecules, while AX_n polyhedra lie between the layers and bridge them. The coordination number, n, is usually 9, although it is reduced to 8 for the smaller Eu^{3+}, Ho^{3+} and Yb^{3+} cations in **#485–487**. The layers are usually || (100), although they are || (110) for $(Sm(H_2O)_5)_2[Mo_6TeO_{24}] \cdot 6H_2O$ (**#482**), which has a different axial setting. The orientation of the Mo–Te hexagons varies depending on the hydration state and cation size. For $(La(H_2O)_7)_2[Mo_6TeO_{24}] \cdot 6H_2O$ (**#473**), the hexagons are || $(10\bar{1})$, while for the less hydrated $(La(H_2O)_6)_2[Mo_6TeO_{24}] \cdot 6H_2O$ (**#474**) and its Ce analogue (**#475**), they lie flatter, approximately || (411) (Fig. 36). The hexagons also lie flatter for the Nd compounds: || (411) in $(Nd(H_2O)_6)_2[Mo_6TeO_{24}] \cdot 6H_2O$ (**#479**), || (611) in $(Nd(H_2O)_7)_2[Mo_6TeO_{24}] \cdot 5H_2O$ (**#480**) and || $(41\bar{1})$ in $(Nd(H_2O)_7)_2[Mo_6TeO_{24}] \cdot 5H_2O$ (**#481**), although they are strongly canted || $(20\bar{1})$ in the Pr analogue of the latter compound (**#478**). In $K_6(Eu(H_2O)_7)_2[Mo_6TeO_{24}]_2 \cdot 16H_2O$ (**#488**), layers of two differently oriented and symmetrically independent Mo-Te hexagons alternate along the **z** axis; one type has $EuO_2(H_2O)_7$ polyhedra connecting them into columns || **y**, while the other type does not. A matrix of CN9–10 hydrated K^+ ions holds the layers together. The Gd analogue (**#489**) is nearly isostructural, but is in a different axial setting, with the layers of hexagons || (010) not (001), and the Gd–Mo–Te columns || **x**, not **y**. Also, slight atomic rearrangements lead to doubling of the c parameter relative to the corresponding a parameter of **#488**.

$(Co(H_2O)_6)_3[Mo_6TeO_{24}]$ and its Ni analogue (**#490–491**) have a simple, highly symmetrical rhombohedral structure in which $[Mo_6TeO_{24}]^{6-}$ hexagons alternate with triangles of $[M(H_2O)_6]^{2+}$ octahedra (M = Co or Ni) to make columns running along the threefold rotation axes. $(NH_4)_2(M^{2+}(H_2O)_3)_2[Mo_6TeO_{24}] \cdot H_2O$ (M = Mn, Co, Ni, Cu and Zn; **#492–496**) (Fig. 36) and the Ni–W analogue (**#497**) are also highly symmetrical (cubic, space group $Pa\bar{3}$, $a \approx 14$ Å). The TeM_2 part of the structure forms a distorted fluorite array of the type found as predicted for SiO_2 at very high pressure by Park *et al*. (1988) and found experimentally for SnO_2 above 21 GPa by Haines and Léger (1997). Because of the distortion, M^{2+} bonds to only three of its four nearest Mo–Te hexagons, as well as to three water molecules. The other components in the structure, NH_4^+ ions and the remaining H_2O molecule (O6) form hydrogen-bonded dumbells (N···O = 2.84 Å) which, together with the Te atoms, are arranged similarly to the covalent $[S_2]^{2-}$ dumbells and Fe in pyrite, FeS_2.

The remaining compounds of this section are alkali tellurohexamolybdates which also contain $Te(OH)_6$ molecules as adducts. $Li_6[Mo_6TeO_{24}](H_2O)_{18} \cdot [Te(OH)_6]$ (**#498**) has sinuous chains of LiX_{4-6} polyhedra and $Te(OH)_6$ || **y**, which cross-link Mo–Te hexagons that are oriented || (103). $Cs_6[Mo_6TeO_{24}](H_2O)_2 \cdot [Te(OH)_6]_2$ (**#499**) has one Mo–Te anion per unit cell oriented || $(1\bar{1}2)$, embedded in a trellis-like open framework of CsX_{7-10} and $Te(OH)_6$ polyhedra. $Rb_6[Mo_6TeO_{24}](H_2O)_6 \cdot [Te(OH)_6]_2$ (**#500**) has a C-centred monoclinic cell with strong $\frac{1}{2}c$ pseudosymmetry, and thus four Mo–Te hexagons per cell. These are all oriented || (010) and alternate with $Te(OH)_6$ molecules along the **y**

https://doi.org/10.1180/minmag.2016.080.093 Published online by Cambridge University Press

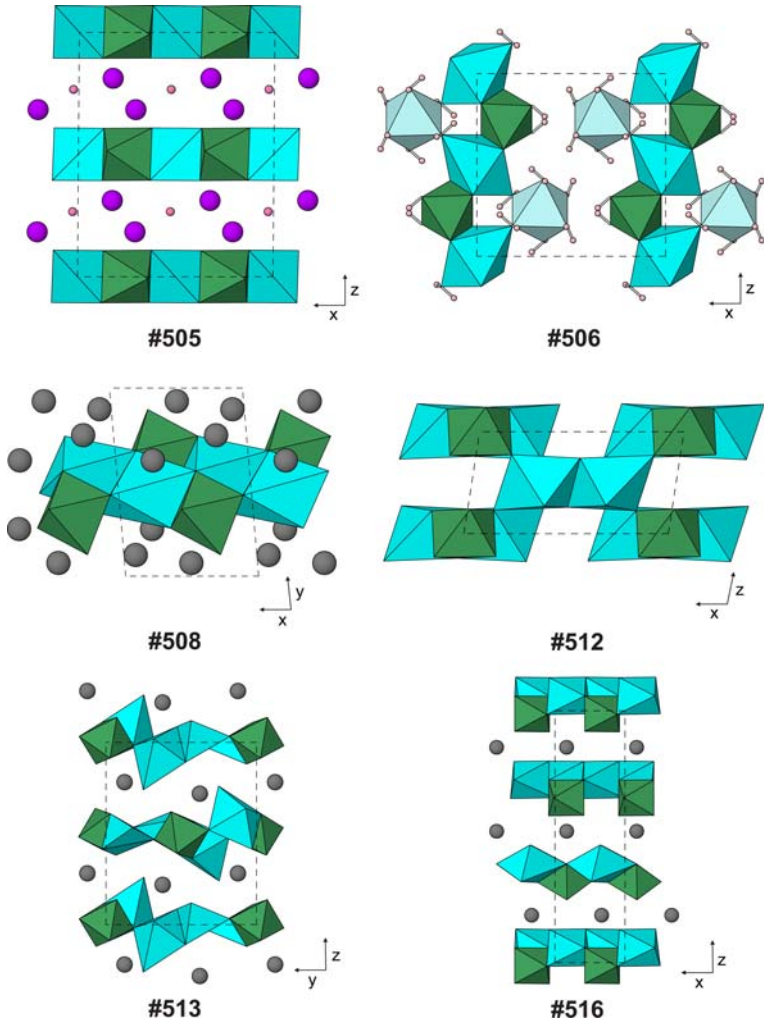

FIG. 37. Examples of structures with monomeric $Te^{6+}O_6$ anions that are part of a larger structural chain or layer (Table 22, deposited). Small spheres: H (pale pink) and O (dark pink), when not part of a polyhedron. Large spheres: K (purple) and Pb or Tl (grey). Polyhedra: Cu (cyan), Mg (pale blue) and Te (dark green). Additional long Cu–O bonds complete octahedra in frankhawthorneite (**#512**) and link layers into a framework.

direction, forming Te-rich rods in a matrix of Rb$X_{7–9}$ polyhedra (Fig. 36). The ordered K–NH_4 compound **#501** is nearly isostructural, as is the more highly hydrated NH_4 compound **#502** (although this is in an *A*-centred axial setting).

Monomeric $Te^{6+}X_6$ as part of a larger structural unit that is an infinite chain

The next few structures have TeX_6 anions that are strongly bound with other cations into one-dimensional structural units. They are listed in Table 22 (deposited). $[Hg^{2+}(TeO_2(OH)_4)]$ (**#503**) has TeX_6 octahedra linked via their *cis* unprotonated ligands through linear 2-coordinated Hg^{2+} into chains || **y**, which pack in a hexagonal array. Chains are connected only through hydrogen bonds and long, weak Hg···O bonds (within-chain Hg–O distances are 2.02–2.05 Å, while the two next nearest oxygen atoms to Hg are at 2.67 and 2.75 Å). In $[(Hg_2^{2+})(TeO_2(OH)_4)] \cdot [Te(OH)_6] \cdot 2H_2O$ (**#504**), TeX_6 octahedra linked through *trans* unprotonated ligands to linear $[Hg–Hg]^{2+}$ dimers,

https://doi.org/10.1180/minmag.2016.080.093 Published online by Cambridge University Press

forming infinite chains || [101]. These lie in layers || (010), which alternate with layers containing Te$(OH)_6$ and H_2O molecules. Mercury is even more strongly 2-coordinate than in the previous compound, with one O neighbour at 2.11 Å, one Hg at 2.50 Å. and the next O neighbours not until 2.91 and 2.93 Å. $K_2[Cu(TeO_4(OH)_2)] \cdot H_2O$ (**#505**) has TeX_6 octahedra sharing opposite edges with CuO_4 squares to form straight chains, which lie in layers || (002). Chains of alternate layers run || to [110] or to [1$\bar{1}$0]. Water molecules and CN8–9 K^+ ions lie between the layers (Fig. 37). Copper has no additional ligands within 3 Å. Very slight tilts and displacements reduce the symmetry from orthorhombic and centrosymmetric (space group *Cccm*) to monoclinic and acentric (*Cc*). The mineral raisaite, $(Mg(H_2O)_6)[Cu(TeO_4(OH)_2)]$ (**#506**) has TeX_6 octahedra sharing edges which are not opposite with CuO_4 squares (Cu–O = 1.94–1.98 Å), to form zigzag chains || **z**. These form a centred-rectangular array, which have $[Mg(H_2O)_6]^{2+}$ octahedra lying betwen them. The structure is held together through hydrogen bonds, and also weak Cu···O bonds: Cu has two O atoms of water molecules at 2.78 Å, completing an elongated octahedron of ligands (Fig. 37). $Ag_4[Cu(TeO_6)]$ (**#507**) has TeO_6 octahedra sharing an edge with one CuO_4 square and corners with two others to make a double chain running || **z** that zigzags in the (100) plane. The double chain consists of Cu=Te–Cu=Te 4-rings, united by the shared edges. Two additional O ligands are much closer to Cu than in **#506** above (Cu–O = 2 × 1.98, 2 × 2.00 and 2 × 2.49 Å). If these are included to complete a CuO_{4+2} octahedron, the chains become ribbons of edge-sharing Cu and Te octahedra in which Cu atoms form a central zigzag backbone while Te sit on the outside of the ribbon. The chains form a centred-rectangular array, and are held together by three types of Ag^+ ions in distorted octahedral coordination (Ag–O = 2.27–2.83 Å). The oxygen atoms approximate *ccp*, with pseudocube edge vectors || [¼0¾], [$\bar{¼}$⅓¼] and [$\bar{¼}\bar{⅓}$¼]. If the structure is considered as a packing of (Ag, Cu, Te) octahedra, then it is a superstructure of the rocksalt type. $Tl_4[Cu(TeO_6)]$ (**#508**) has Cu–Te chains with the same topology as those of **#507** and also forming an approximately centred-rectangular array, but this time running || **x** and zigzagging in the (01$\bar{1}$) plane of the triclinic cell. The oxygens do not form a continuous close-packed array as in **#507**, but discrete close-packed ribbons which surround large channels || **x**. Four types of Tl^+ ions in irregular 5–7 coordination hold the chains together, with their lone pairs pointing into the channels (Fig. 37). $(NH_4)_2V_2^{5+}TeO_8(OH)_2 \equiv (NH_4)_2[(VO_2)_2(TeO_4(OH)_2)]$ (**#509**) has TeX_6 octahedra sharing non-opposed edges with edge-sharing dimers V_2O_8 of VO_5 square pyramids. One of the bridging oxygens links to 1 Te + 1 V, while the other connects to 1 Te + 2 V atoms. Small atomic displacements break the potential 2/*a* symmetry of the chain, so that there are two distinct Te atoms and four distinct V atoms per repeat unit. These chains run || **x** and lie in layers || (002), with NH_4^+ ions between the layers.

Monomeric $Te^{6+}X_6$ as part of a larger structural unit that is an infinite layer

Table 22 also includes structures **#510–547**, where monomeric TeX_6 octahedra are linked with non-Te cations to form two-dimensional strucural units. $Na_2[Cu_2(TeO_6)]$ (**#510**) has a Cu–Te layer || (001) that can be regarded as an ordered version of a brucite-like trioctahedral sheet, but with strong Jahn-Teller distortion of the CuO_6 octahedra, giving Cu a square of four O neighbours at 1.98–2.00 Å and two more distant ligands at 2.53 Å. If all six neighbours are considered, then the structural unit has the same bond topology as those of **#538–541** below. However, unlike those structures, the oxygen atoms of **#510** are approximately *ccp* in three dimensions, and Na atoms are ordered in ⅔ of the octahedral sites between $[Cu_2(TeO_6)]^{2-}$ layers. The structure can be regarded as an ordered defect derivative of the rocksalt type. $NaTl_3^{1+}[Cu_4^{2+}(TeO_6)_2]$ (**#511**) has similarly distorted Cu–Te layers || (200), alternating with layers that contain an ordered array of Na^+ in octahedral coordination and Tl^+ in very irregular 6-fold coordination. The three-dimensional arrangement of oxygen atoms can again be considered a derivative of cubic close-packing, except that the coordination requirements of Tl cause the Cu–Te–O layers to undulate, and lead to the Tl atoms being far from the centres of octahedral interstices.

Frankhawthorneite, $[Cu_2(TeO_4(OH)_2)]$, (**#512**), has oxygen atoms forming a slightly distorted *hcp* array, with close-packed layers || (002). Copper and Te atoms occupy octahedral interstices to form ribbons in which one Te atom alternates with two Cu along the **y** direction. Ribbons form a centred rectangular array, and share corners with their neighbours. However, Jahn-Teller distortion of the Cu coordination polyhedron is of a similar degree to that in **#507–508** above (Cu–O = 4 × 1.98–2.06 Å and 2 × 2.46–2.52 Å), so only the four shortest bonds are counted when defining the structural unit, which is hence not a framework but a layer || (10$\bar{1}$). In frankhawthorneite, the component

https://doi.org/10.1180/minmag.2016.080.093 Published online by Cambridge University Press

ribbons of the layer have each Te octahedron sharing two opposite edges with CuO_4 squares, and ribbons are linked through CN3 oxygen atoms in a stepped pattern. The Jahn-Teller distortion also reduces the symmetry to monoclinic $P2_1/n$ from orthorhombic *Pmnn*, and allows ordering of the H atom on O2, as shown by long Te–O bonds (1.99 rather than 1.91–1.92 Å). Layers are held together by long Cu···O bonds and hydrogen bonds (Fig. 37). A similar arrangement of more regular octahedra is found in kotoite, $Mg_3(BO_3)_2$, which has similar unit-cell dimensions but the orthorhombic space group, and has additional B atoms in triangular coordination, providing strong links between ribbons (Berger, 1988). The octahedral arrangement in the average structure of one form of $(H,Li)_2[Ti(TeO_6)]$ is also very similar (**#585**, below). Paratimroseite, $Pb[Cu_2(TeO_6)] \cdot H_2O$ (**#513**) has stepped layers || (002) composed by condensation of ribbons || **x**, in exactly the same topology as frankhawthorneite (**#512**), but the layers are separated widely and also alternate between two orientations related by a screw diad axis, so their anions form disconnected oblique slices of *hcp* structure rather than constituting a three-dimensionally continuous close-packed substructure. Water molecules and Pb^{2+} cations in irregular 9-coordination lie between the layers, and the Pb coordination geometry causes shift of the layers in the **x** direction such that any reflection symmetries are eliminated, and the space group is $P2_12_12_1$ rather than the *Pbca* or *Pbcm* of hypothetical aristotypes. An elongated coordination octahedron around Cu is completed by an interlayer water molecule at 2.42 Å and an additional tellurate oxygen atom at 2.54 Å (Fig. 37). The structure of timroseite is closely related (**#555**, below). $Sr_2[Cu_2(TeO_6)]Br_2$ (**#514**) has edge-sharing ribbons of CuO_{4+1} square pyramids (Cu–O = 4 × 1.93–2.02 Å and 1 × 2.36 Å) and TeO_6 octahedra running || **y**, which share corners with each other so as to form a continuous layer || (100) in which the oxygen atoms again form the stepped, *hcp* slice of **#512–513**. Interlayer SrO_4Br_3 polyhedra hold the structure together. The Br^- anion is also a very distant sixth ligand for Cu^{2+} (2.97 Å). In bairdite, $Pb_2[Cu_4(TeO_5OH)_2](SO_4) \cdot H_2O$ (**#515**), two stepped Cu–Te layers || (100) stack adjacent to each other, related by a screw diad axis, and are linked through long Cu···O bonds so as to form a double layer (Cu2–O4 = 2.36 Å, as opposed to 1.94–2.04 Å for the four shortest Cu2–O bonds, and 2.57 Å for an additional within-layer distance that completes the octahedron). O4 also has another Cu2 at 2.00 Å and an unusually long distance of 2.03 Å to Te, and is where the H is located. Between Cu–Te double layers are Pb atoms which show some positional disorder, and SO_4 tetrahedra. Cu1 has a square of O atoms at 1.91–2.00 Å and one at 2.41 Å within the Cu–Te layer, and a sulfate oxygen atom at 2.46 Å. A differently oriented oblique slice through an *hcp* anion array is an element of the 'tri-harmunite' structure of **#598**, below.

The polytypes of khinite (-3*T* and -4*O*), $Pb[Cu_3(OH)_2(TeO_6)]$ (**#516–517**) share a more complex layer type, in which rows of edge-sharing CuO_4 squares =Cu1=Cu2= alternate with rows of CuO_4 squares and TeO_6 octahedra, =Cu3=Te=. The coordination octahedron of the Te is completed by sharing bridging oxygen atoms of the all-Cu chain, thus making a layer containing 5-rings [–Te=Cu3=Te–Cu1=Cu2–]. In projection normal to the layer, the cations form a hexagonal net, but the all-Cu chain is at a different height from the Cu–Te chain, so the layer has an overall polarity (Fig. 37). In the 3*T* polytype (originally known as 'parakhinite'), the subchains of layers point along **x**, **y** or –[110], successive layers rotating by 120°, consistent with a screw triad axis. There are three layers || (003) per $P3_2/P3_1$ unit cell. In the 4*O* polytype, layers are || (004), alternate layers have subchains || [110] or $[1\bar{1}0]$, and the layers are related by the *d* glides of the space group *Fdd*2. Note that $a_{4O} \approx a_{3T}$, and that a pseudohexagonal metric is retained, as $b_{4O} \approx \sqrt{3}a_{4O}$. In both cases, Pb^{2+} lies between the layers, in 8-fold coordination. Agaite, $Pb_3[Cu(TeO_5OH)](CO_3)(OH)$ (**#518**) has layers || (020) in which alternating TeX_6 and CuX_5 polyhedra form a 6^3 honeycomb net. These polyhedra share non-opposing edges to form zigzag chains trending || **x**, which are joined in the **z** direction by sharing of a fifth corner. Between the Cu–Te layers lie triple layers of CN8 Pb^{2+} ions, additional OH^- ions (bound to 3 Pb) and a central plane of CO_3^{2-} ions (each oxygen atom bound to 3 Pb as well as to C). The orientation of Cu=Te zigzags in the structural unit and the pointing direction of CO_3 triangles both define a polarity in the **z** direction (Fig. 38).

$Na_{1.8}[(Sn^{4+}_{0.9}Te^{6+}_{0.1})(TeO_6)]$ and $Na_2[Ge(TeO_6)]$ (**#519–520**) both have a trigonal structure in which oxygen atoms approximate *hcp* (cf. **#512**). It is a superstructure of one of the $TlSbO_3$ polytypes (Bouchama and Tournoux, 1975). The other such polytype has the structure of ilmenite ($Fe^{2+}Ti^{4+}O_3$) in that ⅔ of the octahedral interstices between each pair of oxygen layers are occupied by cations, and

https://doi.org/10.1180/minmag.2016.080.093 Published online by Cambridge University Press

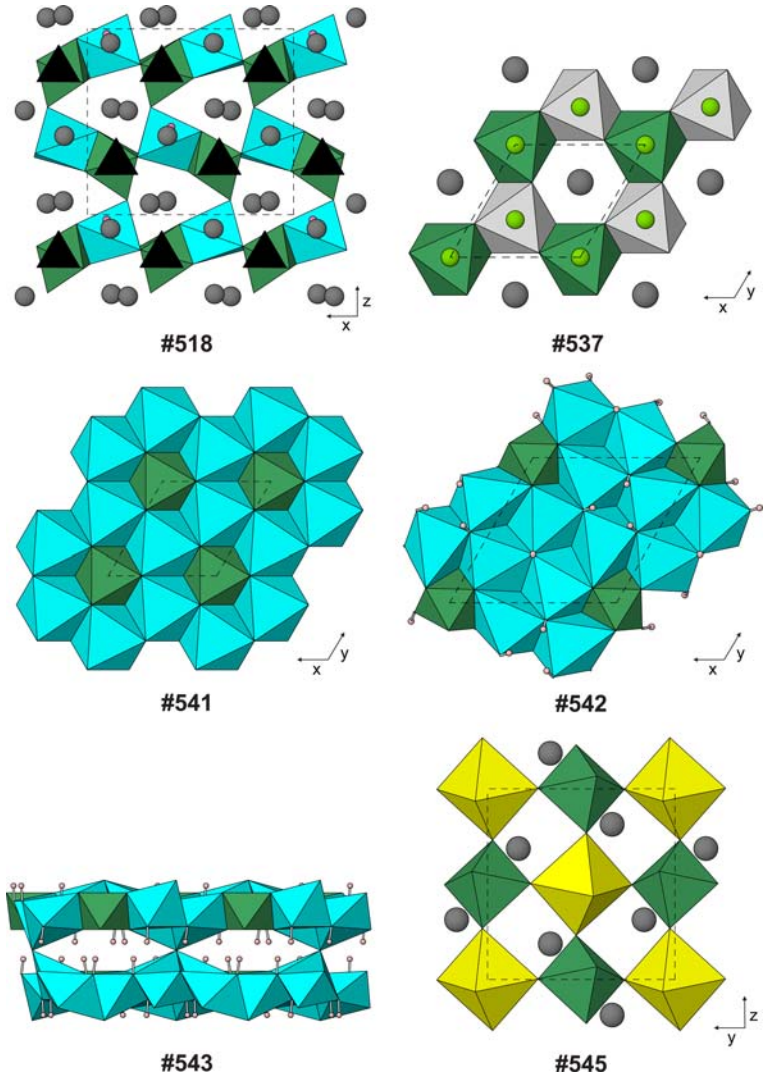

FIG. 38. Examples of structures with monomeric $Te^{6+}O_6$ anions that are part of a larger structural layer (Table 20, deposited). Small spheres: H (pale pink) and O (dark pink) when not part of a polyhedron. Large spheres: Cl (green-yellow) and Pb (grey). Black triangles in **#518**: CO_3 groups. Polyhedra: Al (pale grey), Cu (cyan), Te (dark green) and U (yellow).

that two types of cation occupy alternate cation layers. However, whereas the vacant octahedral sites in the ilmenite polytype are offset in a sequence *ABCABC* so as to produce a 6-layer rhombohedral cell (space group $R\bar{3}$), the vacant sites in the current structures are arranged in a pattern *ABAC*, giving a 4-layer trigonal cell with space group $P\bar{3}1c$. In these tellurate compounds, layers of Na cations alternate with layers of (M^{4+} + Te^{6+}), where M = (Sn or Ge). NaO_6 octahedra share faces with TeO_6 octahedra above and below along the **z** direction, while $M^{4+}O_6$ octahedra have vacant sites above and below. Note that such face-sharing relationships would not be achievable in an ilmenite-like polytype, where every occupied octahedron shares one face with another that is occupied. Sr[Ge(TeO_6)] (**#521**) also has *hcp* oxygen atoms, and a primitive trigonal cell that

https://doi.org/10.1180/minmag.2016.080.093 Published online by Cambridge University Press

has the same ~5 Å *a* parameter but half the *c* parameter of **#519–520**. (Ge+Te) atoms occupy ⅔ of the octahedral sites every other octahedral cation layer, forming a honeycomb pattern with Ge and Te alternating, while Sr atoms are in the intervening layers, above and below the vacant sites in the (Ge+Te) layer). This is the *P*312 structure of $NaNi^{4+}I^{7+}O_6$ (Brown, 1969), which is a cation-ordered superstructure of the $P\bar{3}1m$ type of Li_2ZrF_6 (Brunton, 1973) or rosiaite, $Pb^{2+}Sb_2^{5+}O_6$ (Basso *et al*., 1996). The compounds $A^{3+}[Cr^{3+}(Te^{6+}O_6)]$ (*A* = La, Pr, Nd, Sm–Yb and Y; **#522–534**) and La[Fe(TeO_6)] (**#535**) have a polytypical relative of the Sr[Ge(TeO_6)] structure in which the *c* repeat is doubled from 5.4 Å to ~10 Å and the space group changes to $P\bar{3}$, because the relative positions of (Cr, Fe) and Te are reversed in alternate Cr–Fe–Te layers. This structure is also that of colquiriite, CaLi[AlF_6] (Yin and Keszler, 1992). Compound **#535** shows some Fe–Te disorder which may imply short-range mixing of the two cations, but given the large difference in charge, more probably implies displacement of layers by stacking faults, while retaining two-dimensional order within layers. Thus, it may have a nanoscale intergrowth of rosiaite and colquiriite structure types.

Ba[Ge(TeO_6)] (**#536**), despite the chemical similarity to its Sr analogue **#521**, has a different structure with the same *P*312 space group. Oxygen atoms are double-hexagonal close-packed (*AABB* stacking), and layers of (Ge+Te) in octahedral coordination alternate with layers of BaO_6 trigonal prisms. Backite, Pb_2[Al(TeO_6)]Cl (**#537**) has dioctahedral $AlTeO_6$ layers resembling the $MTeO_6$ unit in structures **#519–536** (Fig. 38). However, these layers are now widely spaced, and the oxygen atoms are not three-dimensionally close-packed. Instead, the unit cell contains one such layer, separated from the next by layers of Pb, Cl and Pb such that each Pb atom lies above a vacant octahedral site of the Al–Te layer and is coordinated by 3O + 6Cl. The compounds $Na_{2-x}[M_2(TeO_6)]$ (*M* = Ni, Zn and Co, *x* = 0–0.05; **#538–540**) are based upon a *AABB* stacking of oxygen atoms, like **#536**. *M* and Te cations are in octahedral coordination, and form a structural unit that is an ordered brucite-like trioctahedral layer, with Na cations partially occupying the trigonal prismatic sites between the *M*–Te layers. The Na^+ ions are highly mobile, leading to fast-ion conduction in these compounds (Evstigneeva *et al*., 2011). Small atomic displacements result in the Zn and Co compounds being acentric ($P6_322$), while the Ni compound has space group $P6_3/mcm$. The Cu analogue of these compounds was discussed above (**#510**).

Leisingite, $(Mg(H_2O)_6)[Cu_2(TeO_6)]$ (**#541**) has a layered $[Cu_2(TeO_6)]^{2-}$ structural unit || (001) which resembles the trioctahedral layers of **#538–540**, with no evident Jahn-Teller distortion of CuO_6 octahedra (Cu–O = 6 × 2.11 Å), unlike the layers of **#510–511**. Isolated $[Mg(H_2O)_6]^{2+}$ octahedra lie between these layers, and connect them through hydrogen bonding. Apart from a 30° rotation of the Mg octahedron and the locations of H atoms, this mineral is isotypical with zincalstibite (Bonaccorsi e*t al*., 2007), a member of the cualstibite group of the hydrotalcite supergroup of Mills *et al*. (2012). The correspondence can be shown as $[Cu_2(TeO_6)][Mg(H_2O)_6]$ (leisingite) ≡ $[Zn_2Al(OH)_6][Sb(OH)_6]$ (zincalstibite). Zincalstibite has a lower-symmetry space group ($P\bar{3}$ as opposed to $P\bar{3}1\,m$), but very similar unit-cell parameters *a* = 5.321(1) Å and *c* = 9.786(2) Å (Fig. 38).

Mojaveite, $[Cu_6(TeO_4(OH)_2)(OH)_7]Cl$ (**#542**), has brucite-like octahedral sheets in which $^1/_7$ of the cations are Te and $^6/_7$ are Cu, while $^1/_{14}$ of the anions are Cl, and thus are not counted as part of the structural unit. The degree of Jahn-Teller distortion is relatively small, half the Cu are regarded as coordinated by five (O,OH) ligands (+1 Cl) while the other half have six O neighbours. The ordering pattern of cations and anions forces the structure to adopt the relative low-symmetry polar space group *R*3. The layers are held together by hydrogen bonds (Fig. 38). The mineral is isostructural with bluebellite, $Cu_6[I^{5+}O_3(OH)_3](OH)_7Cl$, which is unusual in that Te^{6+} does not have a lone pair of electrons while I^{5+} does so (Mills *et al*., 2014*a*). The substitution is presumably facilitated by the polar symmetry of the Te/I site, which frees the coordination environment to distort. Fuettererite, $Pb_3Cu_6(TeO_6)(OH)_7Cl_5$ ≡ $(Pb_3(OH)Cl_3)_2[Cu_6(TeO_6)(OH)_6]_2Cl_4$ (**#543**), has Cu–Te layers very similar to those of mojaveite, although all Cu atoms now have one Cl as a sixth ligand, rather than just half of them. There are Cl atoms on both sides of the layer, and the structure retains a centre of inversion symmetry. Pairs of Cu–Te–O layers are linked through a shared Cl atom, and these layers are stacked with the other components between them in the sequence $[Cu_6(TeO_6)(OH)_6]\cdots Cl\cdots[Cu_6(TeO_6)(OH)_6]\cdots Cl\cdots(Pb_3(OH)Cl_3)\cdots Cl\cdots(Pb_3(OH)Cl_3)\cdots Cl$ (Fig. 38).

Markcooperite and its synthetic analogue, ideally $Pb_2^{2+}[(U^{6+}O_2)(TeO_6)]$, have a quite different type of layer (**#544–545**). TeO_6 and UO_6 octahedra

https://doi.org/10.1180/minmag.2016.080.093 Published online by Cambridge University Press

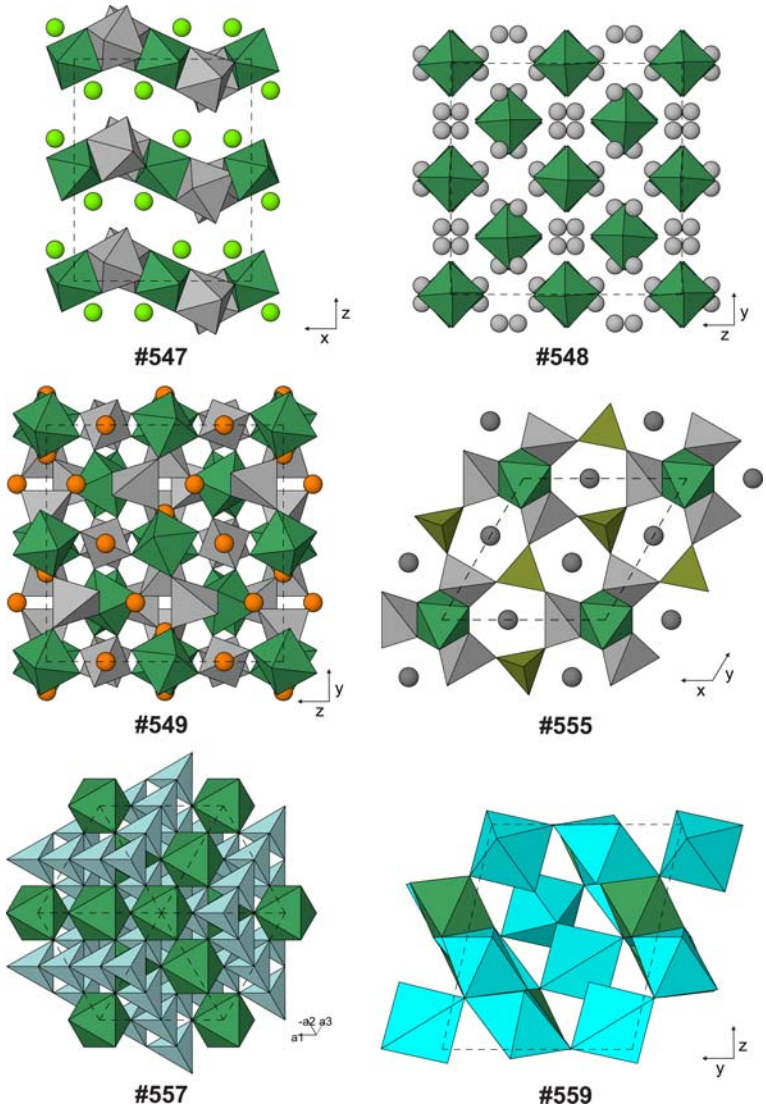

FIG. 39. Examples of structures with monomeric $Te^{6+}O_6$ anions that are part of a larger structural layer or framework (Tables 22–23, deposited). Large spheres: Ba (yellow-green), Ca (orange), Hg (pale grey) and Pb (dark grey). Polyhedra: As (brown-green), Be (pale blue), Cu (cyan), Nb (grey octahedra), Te (dark green) and Zn (grey tetrahedra). In **#548**, the two Hg–O bonds per Hg atoms are omitted for clarity.

both share four corners to form a layer with 4-rings, similar to that of Fig. 14*c* but with alternation of Te and U atoms. These layers lie || (100) and have CN7 Pb^{2+} ions between them. In the end-member synthetic compound (**#545**), the Te octahedron is relatively regular (Te–O = 2 × 1.91, 2 × 1.94 and 2 × 1.95 Å) while the U octahedron is strongly compressed (U–O = 2 × 1.84, 2 × 2.24 and 2 × 2.29 Å), consistent with the presence of linear $[O=U=O]^{2+}$ groups (Fig. 38). The natural mineral shows 25% substitution of Te on the U site, but the pattern of bond-length variation remains similar. The substitution makes the structure transitional towards those with continuous layers of corner-sharing TeO_6 octahedra (Fig. 14*c*), such as **#688–670** below.

https://doi.org/10.1180/minmag.2016.080.093 Published online by Cambridge University Press

$ThV_2^{5+}TeO_{10} \cdot 2H_2O \equiv Th[(VO_2)_2(TeO_6)] \cdot 2H_2O$ (**#546**) has layers || (200) consisting of TeO_6 octahedra, VO_5 (V1) trigonal bipyranids and VO_4 tetrahedra (V2). V1 polyhedra share an edge with Te on one side and a corner with Te on the other side in the **z** direction, while V2 tetrahedra share a corner with Te on each side in the **y** direction, so the layer has square-shaped 8-rings of alternating Te and V in which Te is 4-connected while V is always only 2-connected. Each V atom has two non-bridging ligands with short V–O distances (1.63–1.67 as opposed to 1.77–2.04 Å), validating their description as vanadyl groups $[VO_2]^+$. Th^{4+} ions are in 9-coordination between the layers. $Ba_2Nb_2TeO_{10} \equiv Ba_2[Nb_2O_4(TeO_6)]$ (**#547**) has corrugated layers || (020) containing *zweier* chains of corner-sharing NbO_6 octahedra which run || **x**. The TeO_6 octahedron shares one edge and one corner with a pair of Nb octahedra in the chain on one side, making an [–Nb–Te=Nb–] 3-ring, and the same with the next chain on the other side, so that the layer has 3- and 6-rings with the topology of the kagome net. Ba^{2+} ions between the layers are 9-coordinated. Although the layer contains four non-tellurate oxygen atoms per formula unit, only two of these are non-bridging oxygen atoms with short Nb–O distances (1.78 Å; compare 1.90–2.26 Å for all other Nb–O) (Fig. 39).

Monomeric $Te^{6+}X_6$ as part of a larger structural unit that is a framework

A large group of compounds have TeX_6 octahedra strongly bound to non-Te cations to form a three-dimensional framework. These are listed as **#548–618** in Table 23 (deposited). $[Hg_3^{2+}(TeO_6)]$ (**#548**) has a highly symmetrical structure with a large cubic unit cell ($Ia\bar{3}$, $a \approx 13$ Å). Two types of Te atom are arranged as a $2 \times 2 \times 2$ block of CsCl unit cubes, while the Hg atoms are positioned so as to form, in combination with Te, a slightly perturbed $2 \times 2 \times 2$ array of cubes with the Cr_3Si arrangement (Boren, 1933; Andersson, 1978), analogous to the cations of the garnet structure (O'Keeffe and Andersson, 1977; Grew *et al*., 2013; **#549–553** below), which has the same space group and similar unit-cell parameter. However, Hg^{2+} has linear two-fold coordination, unlike the CN4/CN8 cations of garnet: two Hg–O distances are 2.06 Å, while the next neighbours are not until 2.57, 2.59, 2.76 and 2.83 Å. Links Te–O–Hg–O–Te connect each Te atom to six out of the eight neighbouring Te of the other type (Fig. 39).

The important garnet structure is an ordered and anion-stuffed superstructure of the Cr_3Si type (Geller, 1967; O'Keeffe and Hyde, 1985). The $Ia\bar{3}d$ cubic cell of typical garnets $A_3B_2C_3X_{12}$ has a $2 \times 2 \times 2$ array of body-centred cubes of *B* atoms corresponding to Si of Cr_3Si, and non-intersecting rods || <100> directions of alternating *A* and *C* atoms corresponding to Cr. Anions *X* occupy distorted tetrahedral interstices, so that each anion is bonded to $2A + B + C$, while coordination numbers of *A*, *B* and *C* are, respectively, 8, 6 and 4. The numerous mineralogical examples of garnets were reviewed by Grew *et al*. (2013). The $B_2C_3X_{12}$ substructure forms a framework in which each *X* links to one cation of each type. Depending on the relative bond valences, it may be reasonable to identify within this framework either BX_6 or CX_4 as a principal anionic complex. An example of the former would be cryolithionite, $Na_3Al_2Li_3F_{12} \equiv Na_3Al_2[LiF_4]_3$ more appropriately than $Na_3Li_3[AlF_6]_2$, while silicate garnets are examples where the strongest-bound cation is in the tetrahedron: grossular, $Ca_3Al_2Si_3O_{12} = Ca_3Al_2[SiO_4]_3$. Several tellurate garnets are known, in which the *B* cation is Te^{6+}; these compounds are of the first type, because of the high Te–O bond valence. These include the mineral yafsoanite (Fig. 39), $Ca_3[Zn_3(TeO_6)_2]$ (**#549**) and also synthetic $Na_3[M_3^{3+}(TeO_6)_2]$ ($M = Fe_{0.5}Al_{0.5}$ or Ga, **#550–551**). $Nd_3Li_{3.05}$ $[(Te_{0.975}Sb_{0.025})O_6]_2$ (**#552**) and $Nd_3Li_4[(Te_{0.5}\ Sb_{0.5})O_6]_2$ (**#553**) are included here because they still have the garnet structure, albeit slightly modified. However, the *C* cation Li is now so low in charge that it no longer forms a structural unit with the octahedral cations: the Nd–O bond valence (0.375) is larger than that of Li–O (0.25). Furthermore, both these compounds have considerably higher Li contents than the 2 atoms per formula unit expected for a normal garnet, due to stuffing of additional Li into normally vacant interstices, and the Li are very mobile in the structure, making the compounds fast-ion conductors (O'Callaghan *et al*., 2008).

$LaV_3^{5+}TeO_{12} \cdot 3H_2O \equiv La[(VO_2)_3(TeO_6)] \cdot 3H_2O$ (**#554**) has a framework in which an approximately primitive cubic array of TeO_6 octahedra are linked to all six of their neighbours through 2-connected VO_4 tetrahedra. La^{3+} ions are near the centre of each cube. Thus, the $LaTeV_3$ substructure corresponds to the atomic arrangement of an ABX_3 perovskite. The La atom is coordinated by six oxygen atoms of the framework but also by three water molecules which all lie on one side of La, reducing the symmetry to polar rhombohedral *R*3*c*. Relative to a cubic metric, the structure is slightly stretched along the rhombohedral triad axis

https://doi.org/10.1180/minmag.2016.080.093 Published online by Cambridge University Press

($c/a = 2.48 = \sqrt{6.15}$, rather than $\sqrt{6}$). As is typical for vanadyl tellurates, V–O distances are much shorter (1.63–1.64 Å) for the V–O–La oxygens than for the V–O–Te oxygens (1.80–1.84 Å).

The minerals of the dugganite group include dugganite itself, $Pb_3[Zn_3(TeO_6)(AsO_4)_2]$ (**#555**), its phosphate analogue kuksite (**#556**) and also cheremnykhite (the vanadate analogue), $Pb_3[Zn_3(TeO_6)(VO_4)_2]$ (Kim *et al*., 1990), whose structure has not been refined, and joëlbruggerite, ideally $Pb_3[Zn_3(Sb^{5+}O_6)(AsO_{3.5}(OH)_{0.5})_2]$ (Mills *et al*., 2009*c*), which has only minor Te substituting for Sb. The dugganite structure has layers ∥ (001) in which 3-connected AsO_4 on triad axes and 2-connected ZnO_4 tetrahedra share corners to form a net of trefoil-shaped 12-rings in which Zn and As alternate. One third of the triad axes does not have an As tetrahedron, but instead have Te octahedra between two Zn–As layers and linking the layers. Each TeO_6 octahedron links to three Zn tetrahedra below and to three more above. Thus, the three-dimensional framework that results contains [Zn–Te–Zn–Te] 4-rings and [Zn–As–Zn–Te–Zn–As] 6-rings (Fig. 39).

$[Be_4O(TeO_6)]$ (**#557**) has a simple face-centred cubic structure in which Be_4O_6 tetrahedra, with Be atoms at the corners and O1 oxygen atoms along the edges, and additional oxygen atoms (O2) are arranged in the 'zincblende' arrangement. Thus, there is a rather open $[Be_4O_7]^{6-}$ framework in which O2 is at the centre of an anion-centred tetrahedron, where four BeO_4 tetrahedra meet. Oxygen atoms occupy $^7/_8$ of the positions of *ccp*, with the eighth position vacant, and the sixth O1 oxygen atom defines an octahedral interstice that contains Te (Fig. 39). The structure may be compared with that of swedenborgite, $Na[Be_4O(Sb^{5+}O_6)]$, which has a similar stoichiometry. In swedenborgite (Huminicki and Hawthorne, 2001), the oxygen atoms again occupy $^7/_8$ of the positions of *ccp*, but the stacking of close-packed layers is now *ABAC* rather than *ABC*, and the eighth position contains CN12 Na^+ ions. There is also a unique octahedral interstice, which contains Sb, and a Be_4O_7 framework in which Be_4O_6 tetrahedra can be identified. However, the additional oxygen atom that connects the tetrahedra is no longer bonded to four Be, but instead to two Be + Sb, while the oxygen that centres an OBe_4 tetrahedron is now part of the Be_4O_6 tetrahedron. Apart from **#557** and swedenborgite, isolated OBe_4 tetrahedra have also been reported from two polymorphs of $(Be_4O)(NO_3)_6$ (Haley *et al*., 1997; Troyanov *et al*., 2000; Krivovichev *et al*., 2013).

$Pb[Cu_3O(TeO_6)]$ (**#558**) has Cu–Te–O rods running ∥ **y** in which the oxygen atoms approximate small blocks of cubic close-packed structure. Relatively regular TeO_6 octahedra alternate with pairs of Cu1 atoms in elongated CuO_{4+2} polyhedra, while $Cu2O_4$ squares brace the sides of the rods, as well as sharing corners with Te and Cu1 atoms of neighbouring rods to form a framework with large channels ∥ **y**, which contain CN7 Pb^{2+} ions. Jensenite, $Cu_3TeO_6 \cdot 2H_2O \equiv [Cu_3(H_2O)_2(TeO_6)]$ (**#559**), has brucite-like Cu_2TeO_6 layers ∥ $(10\bar{1})$ in which Cu and Te are ordered in a honeycomb pattern. While the Te octahedral are quite regular (Te–O = 1.89–1.98 Å), the Cu polyhedra show the usual Jahn-Teller distortion, with Cu–O = 4 × 1.94–2.06 Å and 2 × 2.32–2.45 Å. The layers are bridged into a framework by an additional Cu cation in the interlayer gap that is in strict square-planar coordination. This Cu atom (Cu1) has as ligands two interlayer water molecules, plus a tellurate oxygen atom in each layer (Fig. 39).

Timroseite, $Pb_2[Cu_5(TeO_6)_2](OH)_2$ (**#560**) has stepped *hcp* layers ∥ (002) of the type previously seen in frankhawthorneite, paratimroseite, $Sr_2[Cu_2(TeO_6)]Br_2$ and bairdite (**#512–515**, above). As in paratimroseite, the layers are in two different orientations which alternate, but in timroseite, they are connected into a three-dimensional framework through additional CuO_4 squares (Fig. 40). Large channels remain ∥ **x**, which contain OH^- anions and Pb^{2+} in 8–10 coordination. All Cu are in square-planar coordination if a bonding cutoff of <2.27 Å is used, but all Cu atoms also have one channel OH^- anion at 2.27–2.64 Å, and Cu1 and Cu2 within the *hcp* layers, also have an additional tellurate oxygen at 2.47–2.71 Å. Quetzalcoatlite, $[Zn_6Cu_3(TeO_6)_2(OH)_6] \cdot (Ag_xPb_yCl_{x+2y})$ (**#561**), has a more explicitly nanoporous structure in which hexagonal rings of six corner-sharing $ZnO_2(OH)_2$ tetrahedra alternate along **z** with layers ∥ (001) in which TeO_6 octahedra share edges with CuO_4 squares to form a honeycomb net with walls Te=Cu=Te surrounding large hexagonal voids. The hexagonal channels contain rods of alternating, partially occupied (Ag^+, Pb^{2+}) and Cl^- sites (Fig. 40).

A large group of tellurate compounds have a superstructure of the perovskite type (**#562–584**). An aristotypical ABO_3 perovskite has a unit cube with $Z = 1$, $a \approx 4$ Å and space group $Pm\bar{3}m$. The compounds described here all have two types of octahedrally coordinated *B* atom, one of which is Te^{6+}. Other perovskite variants have been described earlier, including $M^{2+}Te^{4+}O_3$ (M = Co, Ni and Cu)

https://doi.org/10.1180/minmag.2016.080.093 Published online by Cambridge University Press

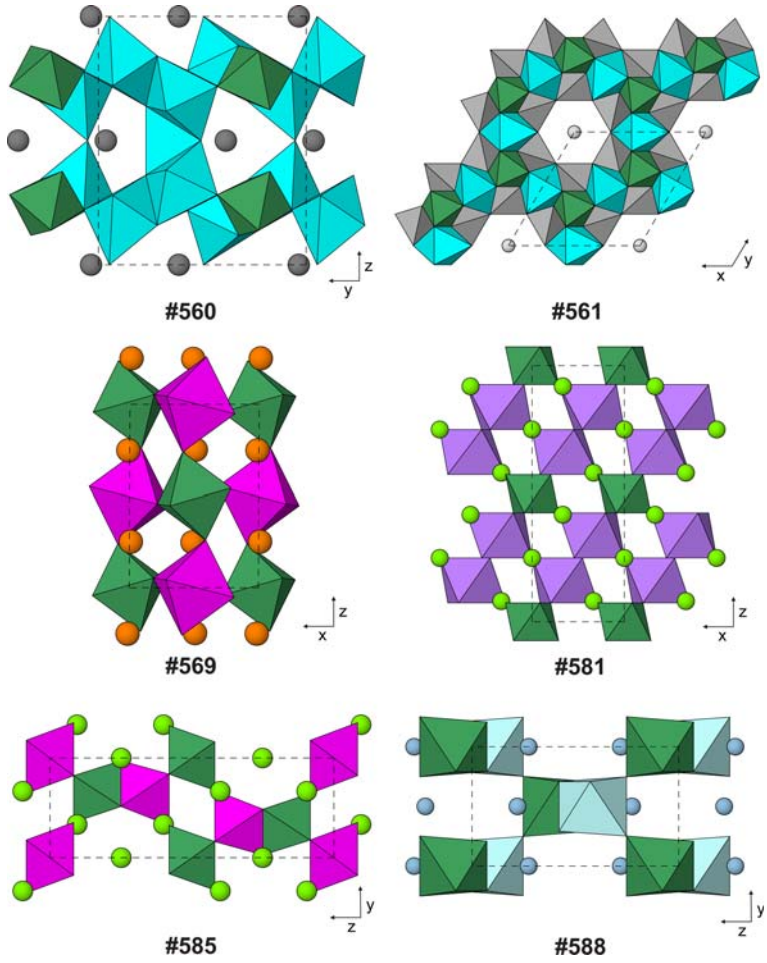

FIG. 40. Examples of structures with monomeric $Te^{6+}O_6$ anions that are part of a larger structural framework (Table 23, deposited). Large spheres: Ag (pale grey), Ba (yellow-green), Ca (orange), Li (pale blue) and Pb (dark grey). Polyhedra: Bi (violet), Co (magenta), Cu (cyan), Sn (pale blue), Te (dark green) and Zn (pale grey).

with Te^{4+} as the *A* cation (**#140–142**), $Cs_2[Te^{4+}_2O_5]$ with Te^{4+} as the *B* cation and some ordered oxygen vacancies (**#195**), the wickmanite-like $Na[Te^{6+}O(OH)_5]$, with a vacant *A* site (**#441**), and the complex superstructures of $M_3[Te^{6+}O_6]$ (M = Sr and Ba; **#442–443**). One form of $Pb_2[Co^{2+}(TeO_6)]$ (**#562**) has Te alternating with Co in the *B* sites, a $\sqrt{2} \times \sqrt{2} \times 2$ superstructure of the basic perovskite type, and tetragonal space group *I*4/*mmm*, consistent with slight tetragonal distortion but no octahedral tilt. Howard *et al*. (2003), in their analysis of possible octahedral tilt systems (Glazer, 1972) and symmetries of ordered perovskites, expressed scepticism about the existence of such structures in the absence of strong Jahn-Teller or other distortion (as occurs in '$CsAuCl_3$' = $Cs_2[Au^{1+}Cl_2][Au^{3+}Cl_4]$; Tindemans-van Eijndhoven and Verschoor, 1974). It is possible that the oxygen positions in this structure need reinvestigation. A rhombohedral polymorph occurs at high and at low temperature (**#582**, below). $A_2[Cu^{2+}(TeO_6)]$ (*A* = Sr and Ba; **#563–564**) have similar cell dimensions to **#562** but the tetragonal space group *I*4/*m* is obtained by octahedra tilt according to the $a^0a^0c^-$ pattern in these compounds, independent of the Jahn-Teller distortion of the CuO_{4+2} octahedra (Howard *et al*., 2003; Howard and Carpenter, 2010). The ICSD gives as the archetype of this

https://doi.org/10.1180/minmag.2016.080.093 Published online by Cambridge University Press

perovskite structure Sr_2NiWO_6 (Köhl, 1973). $Ba_2[Cu(TeO_6)]$ (**#564**) has another polymorph whose structural topology is polytypically related to that of normal perovskites (**#587**, below).

$NaLa[Mg(TeO_6)]$ (**#565**) has similar cell dimensions again but in addition to two types of *B* cation ordered in a 'rocksalt' fashion, there are two types of *A* cation ordered layerwise along the **z** direction, and the symmetry is monoclinic, $P2_1/m$. However, most of the perovskites with $\sqrt{2} \times \sqrt{2} \times 2$ superstructure have the $P2_1/n$ space group exhibited by cryolite, $Na_3AlF_6 = Na_2[Na(AlF_6)]$ (Hawthorne and Ferguson, 1975). These include compounds $A_2[B(TeO_6)]$ with A = Ca or Sr and B = Ca or Co (**#566**, **569–571**) (Fig. 40), $Cd_2[Cd(TeO_6)]$ (**#567**), $Na_2[Sn^{4+}(TeO_6)]$ (**#568**) and A = disordered ($Ca_{0.5}Pr^{3+}_{0.5}$), ($Sr_{0.5}Pr^{3+}_{0.5}$) or ($Sr_{0.5}Eu^{3+}_{0.5}$), B = Li (**#572–574**).

$Sr_2[Ni(TeO_6)]$ has a larger $2 \times 2 \times 2$ superstructure than the perovskites above, and $C2/m$ symmetry (**#575**), although it is nearly cubic, with all three cell parameters within 0.3% of their mean value, and $\beta \approx 90.4°$. The next five compounds have the truly cubic 'double perovskite' structure of elpasolite ($K_2Na[AlF_6]$: Sabelli, 1987), with a $2 \times 2 \times 2$ supercell but $Fm\bar{3}m$ symmetry. In all these compounds, Te alternates in the *B* sites in a 'rocksalt' fashion with Ni (**#575**), Ca (**#576**), Li (**#577–578**), Mg (**#579**) or partially occupied Bi (**#580**), while in **#577** and **578**, the alkaline earth cation Ba^{2+} and lanthanides $(La,Pr)^{3+}$ are disordered in the *A* site, analogous to the situation in **#572–574** above.

Our final group of perovskites have trigonal cells with $a \approx \sqrt{2}$ and $c \approx 2\sqrt{3}$ times the edge of the fundamental perovskite cube. This is an alternative axial setting for a structure produced by compression or extension of a $2 \times 2 \times 2$ cube along one [111] direction. The lattice type for such a perovskite is *R* in most cases, but in $Ba_3[Bi_2O_3(TeO_6)]$ (**#581**), the unusual ordering pattern, with Te in only ⅓ of the *B* sites, reduces the symmetry to $P\bar{3}c1$ (Fig. 40). The space group is $R\bar{3}$ or $R\bar{3}m$ for the other structures **#582–584**, which have the standard 'double perovskite' cation arrangement, and include the rhombohedral polymorph of $Pb_2[Co(TeO_6)]$ (cf. **#562** above). Three additional compounds in the present study could be regarded as aberrant examples of rhombohedral double perovskites, but are more usefully considered as superstructures of the corundum type. These are $[Ni_3(TeO_6)]$ and its relatives, **#599–601** below.

In the ABX_3 cubic perovskite structure, the large cations *A* and anions *X* together form a cubic close-packed array, with X_3A ordered in the Cu_3Au pattern. The structure can thus be described as an *ABC* stacking of AX_3 layers, with *B* cations filling the X_6 octahedral interstices. Other 'perovskite polytypes' can be produced by stacking AX_3 differently (Mitchell, 2002). These structures require some BX_6 octahedra to share faces, implying short $B\cdots B$ distances and the possibility that they may require some $B\cdots B$ bonding interaction to be stable. Most mineralogical perovskites are derived from only the 3*C* polytype, although some examples with face-sharing octahedra are known for antiperovskite polytypes, with anions O^{2-}, F^- or Cl^- in the *B* sites (Krivovichev, 2008). The synthetic compound $Ba_2[Co(TeO_6)]$ (**#585**) has very similar unit-cell parameters to **#584** but a different space group and structural topology. Unlike its analogues with Ca, Sr and Mn in *B* sites (**#576**, **583** and **584** above), it is based on a 6*H* *ABACBC* stacking of BaO_3 layers: the *hkk* sequence, where '*h*' = '*hcp*-like (layers above and below superimposed)' and '*k*' = '*ccp*-like (layers above and below not superimposed)'. A very different 6*H* perovskite is described as **#620**, below. Because layers of Co^{2+} and Te^{6+} cations alternate along **z** in **#585**, there are 12 oxygen layers altogether in the unit cell, which has space group $P\bar{3}m1$, and two crystallographic types each of Co and Te. Co2 and Te2 octahedra each share one face with each other, while Co1 and Te1 share only corners (Fig. 40). In contrast, $Ba_2[Ni(TeO_6)]$ (**#586**) has a 12*R* (*hhkk*) layer sequence (space group $R\bar{3}m$), in which corner-sharing octahedra $(Te1)O_6$ alternate along **z** with columns of three face-sharing octahedra, $Ni \equiv (Te2) \equiv Ni$. $Ba_2[Cu(TeO_6)]$ (**#587**) has the same topology, but distortion of the CuO_6 octahedra reduces the symmetry to triclinic $P\bar{1}$. The distortion is not the usual symmetrical elongation, but gives Cu^{2+} five oxygen neighbours at 1.98–2.11 Å and the sixth at 2.26 Å. The triclinic (001) plane corresponds to (003) of the pseudorhombohedral cell, while the pseudotriad axis is [113] in the triclinic axial setting. A tetragonally distorted 3*C* perovskite polymorph of this compound was discussed at **#564**, above.

The next four closely-related compounds have structures derived from the $LiSbO_3$ type (Genkina, 1992). This structure has a *hcp* oxygen substructure, as for the corundum superstructures of $LiNbO_3$ and $NaSbO_3$, but a quite different arrangement of cations. $LiSbO_3$ has an orthorhombic structure with space group *Pncn*, which is permuted into the *Pnna* axial setting here. Then,

https://doi.org/10.1180/minmag.2016.080.093 Published online by Cambridge University Press

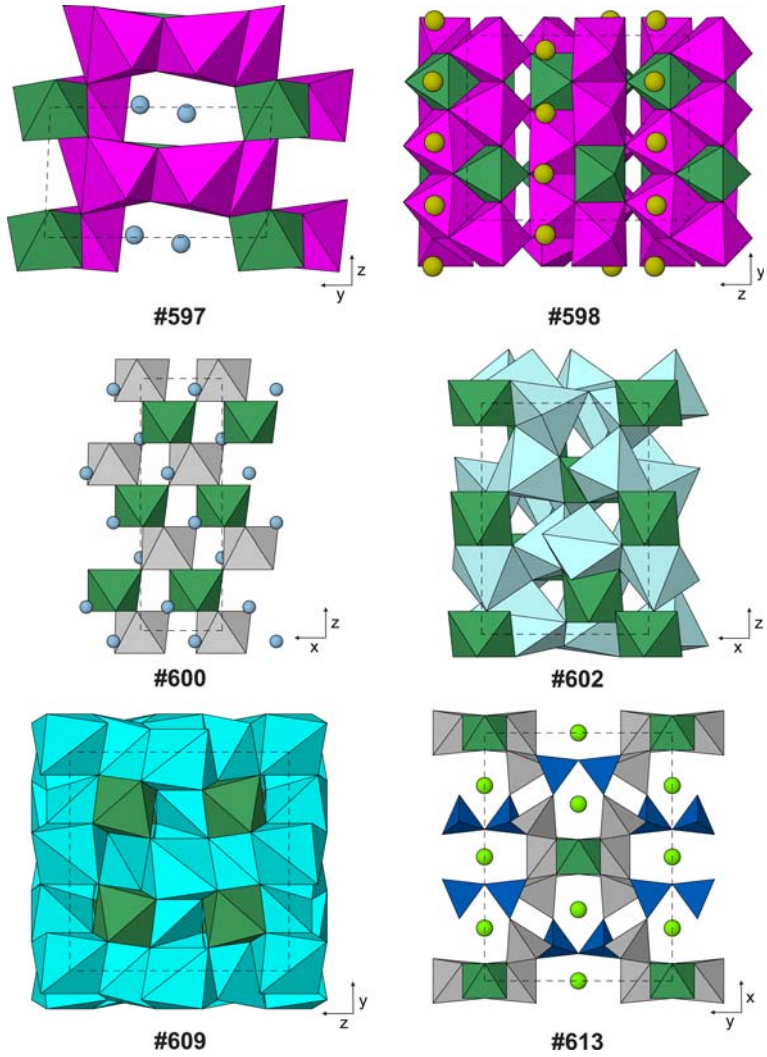

FIG. 41. Examples of structures with monomeric $Te^{6+}O_6$ anions as part of a larger structural framework (Table 23, deposited). Large spheres: Ba (yellow-green), Li (pale blue) and Na (dark yellow). Polyhedra: Cu (cyan), Mg (pale blue), Mn (magenta), Si (dark blue), Te (dark green), Zn (grey tetrahedra) and Zr (pale grey octahedra).

cell parameters a, b, $c \approx \sqrt{3}$, $\sqrt{(8/3)}$ and 3, measured in units of the mean 'close-packed' O···O distance. There are two close-packed anion layers per cell (as opposed to six for corundum/ilmenite) || (020), and between each layer pair, Li and Sb each occupy ⅓ of the octahedral interstices. SbO_6 octahedra form edge-sharing chains || **x**, and these share corners with the chains above and below to form a framework. The vacant octahedral sites of each cation layer lie above and below Sb, so that SbO_6 octahedra do not share faces. LiO_6 octahedra do not form edge-sharing chains, but do form face-sharing columns || **y**. Even in the idealized structure, a and b are only ~6% different, so the structure is metrically pseudotetragonal with pseudotetrad axis || **z**, and the two types of cation are arranged similarly to Ca and W of the scheelite structure (Hazen *et al.*, 1985), although the disposition of oxygen atoms is quite different. The compounds $Li_2[M^{4+}(TeO_6)]$ (M = Sn or Ti; **#588–589**) have this structure, but with M and Te alternating in the zigzag chains, which reduces the

https://doi.org/10.1180/minmag.2016.080.093 Published online by Cambridge University Press

symmetry to *Pnn*2 (Fig. 40). Partial leaching of Li^+ from the Ti compound and replacement with H^+ indicated no structural change for small degrees of leaching (Crosnier *et al*., 1992), but $(H_{1.68}Li_{0.32})[Ti(TeO_6)]$ showed considerable redistribution of non-Te cations, while preserving the (Te + O) substructure. A significant proportion of Ti occupied former Li or vacant sites (**#590**), giving an arrangement with the space group *Pnnm*, which is in effect a tri-$CaCl_2$ (orthorhombically collapsed trirutile) structure. The structure of frankhawthorneite, $[Cu_2(TeO_4(OH)_2)]$, is closely related (**#512** above). Annealing of this compound re-ordered the octahedral site occupancies to give a tetragonal but acentric trirutile structure with space group $P4_2nm$ (**#591**). More conventional $P4_2/mnm$ trirutile structures are covered below (#**594–596**).

$Pb_6[Co_9(TeO_6)_5]$ and its Ni analogue (**#592–593**) have an unusual structure containing defect brucite-like layers with $^1/_6$ of the cations missing, $(M_7^{2+}Te_3\square_2)O_{24}$ (M = Co or Ni). These are connected into a framework through additional $M \equiv$ Te face-sharing dimers, which share corners with the layers above and below to form a pillared-layer structure with very large interlayer channels, which contain the Pb atoms (Fig. 41). $[M_2^{3+}(TeO_6)]$ with M = Cr, Fe or Ga (**#594–596**) have the well-known trirutile structure also known for minerals such as the byströmite and tapiolite groups, $M^{2+}Sb_2^{5+}O_6$ (M = Mg or Zn) and $M^{2+}Ta_2^{5+}O_6$ (M = Fe or Mn) (Byström *et al*., 1942). The space group is the same as rutile, $P4_2/mnm$, while the c repeat is tripled due to cation ordering. An unusual acentric trirutile phase with $M1$–$M2$–□ ordering along its pseudo-tetrad direction was discussed above (**#586**). $Li[Mn^{2+}Mn^{3+}(TeO_6)]$ (**#597**) again has slightly distorted *hcp* of oxygen atoms, a pseudotetragonal unit-cell metric, and cell dimensions very similar to **#583–586** and **#594–596** above. However, a greater proportion of the octahedral sites are occupied, although it should be noted that irregularity of the octahedra and off-centring of cations mean that the coordination number is unambiguously 6 only for Te1, Te2 and Mn1–3, while Mn4 and Li2 are CN7 and Li3 is CN8, if all cation–oxygen distances within 3 Å are included. Bond-valence sums using the parameters of Brese and O'Keeffe (1991) indicate that Mn1 and Mn3 are Mn^{2+}, while Mn2 and Mn4 are Mn^{3+}. The approximate close-packed oxygen layers are || (002), with the pseudotetrad direction || **y**. Cations are arranged such that two out of every three sites are occupied along the **y** direction. Two types of cation layer alternate. In one of these, Te1 and Mn2 share edges to form a zigzag chain || **x**, with an adjacent zigzag of Li2 and Li3 on one side. In the other layer, zigzag chains || **x** are formed by Te2 and Mn4 and by Mn1 and Mn4. The vacancies of the second layer share faces with Te1 and Mn2, while the vacancies of the first layer share faces with Mn1 and Mn3. The refinement indicates some mixing (17%) of Li on Mn4 and of Mn on Li3, but if this is ignored, all 'Li' sites excluded from the structural unit and all 'Mn' sites included, then we define a framework in which layers of 2-wide and 4-wide octahedral ribbons share edges, with channels between them || **x** which accommodate Li^+ ions. $Na_3[(Mn_3^{2+}Mn^{3+})(TeO_6)_2]$ (**#598**) has a 'tri-harmunite' structure which can be derived from the *Pnma* structure of harmunite, $CaFe_2^{3+}O_4$ (Gaulskina *et al*., 2014), one of three closely related structures known to high-pressure researchers as 'post-spinel' phases, as they have the same cation: oxygen ratio as spinel but larger coordination numbers, making them potential high-pressure polymorphs (cf. Yamanaka *et al*., 2013). These structures all have frameworks made by corner sharing between 2-wide edge-sharing ribbons of octahedra, with channels which contain CN8 cations (Fig. 41). In **#598**, the octahedral ribbons run || **y**, but ordering of Te and mixed-valence Mn triples the unit cell repeat in this direction. Na occupies the CN8 site. Note that the octahedral ribbons define oblique, stepped slices of cations in an *hcp* anion array, repeated by twinning on (020), as noted by Hyde and Andersson (1989). The hexagonal close-packed planes are || (210) or $(2\bar{1}0)$ in alternate twin lamellae. The oblique *hcp* slices differ from those of frankhawthorneite etc (**#512–515**) in that the ribbon direction is parallel to an octahedral edge, rather than perpendicular.

$[Ni_3(TeO_6)]$ (**#599**) has a *hcp* array of oxygen atoms in which ⅔ of the octahedral interstices are filled in the same pattern as corundum, Al_2O_3. However, alternate cation layers along the **z** direction are either all Ni or are Ni+Te, ordered so as to reduce the symmetry to the polar space group $R3$. The resulting structure is a superstructure not just of the corundum type ($R\bar{3}c$), but also of its two *zellengleich* 1 : 1 superstructures: ilmenite ($FeTiO_3$: $R\bar{3}$) and $LiNbO_3$ ($R3c$). Ilmenite-structure compounds in which there is alternation of cation layers with Na and with disordered ($M^{4+} + Te^{6+}$) are discussed below at **#664–665**. The compounds $Li_2[M^{4+}(TeO_6)]$ (M = Zr or Ge; **#600–601**) are placed here because they are isopuntal, although cation layers of (Li1 + M) and (Li2 + Te) now alternate along **z**. Lithium octahedra share faces with M or Te octahedra, and the Li cations are

https://doi.org/10.1180/minmag.2016.080.093 Published online by Cambridge University Press

displaced strongly away from these neighbours along **z**, in accord with the polar symmetry of the structure (Fig. 41). If the low-valence Li atoms are excluded from the structural unit, the remaining MTeO$_6$ framework has a rhombohedrally stretched version of the 'double perovskite' type. The c/a ratio is 17% larger in **#601** than the value of $\sqrt{12}$ which would correspond to a primitive cubic arrangement of cations. As Li can be regarded as an off-centre 'A' cation in the $A_2BB'X_6$ double perovskite topology, these compounds could in fact be classified with the rhombohedral double perovskites **#582–584** above, which have similar cell dimensions. Thus, the range of cation valences in these compounds, and the resulting choice of whether or not to include cations in the structural unit, highlight a relationship between perovskite and corundum structure families which is not otherwise obvious.

[$Mg_3(TeO_6)$] (**#602**) is an archetype for several isostructural tellurates of Mn, Mn+Cu or Cd+Mn (**#603–605**). The rather dense structure is not conventionally close-packed, but the key to comprehending it is to note that the rhombohedral cell parameters for Mg are $a_{rh} = 6.047$ Å and $\alpha_{rh} = 90.86°$, with Te atoms forming an almost perfect body-centred cubic array (more precisely a CsCl-type array, as there are two nonequivalent Te atoms per cell) (Fig. 41). Like [$Hg_3(TeO_6)$] (**#548**) and the tellurate garnets (**#549–553**) above, these compounds have an oxygen-stuffed Cr_3Si structure, with oxygen atoms occupying a different set of tetrahedral interstices than those that they do in garnets, such that each oxygen bonds to 3 Mg (≡Cr) and 1 Te (≡Si), while Mg and Te are all in octahedral coordination. There is no long-range order of Cd and Mn in [$(Cd_2Mn)(TeO_6)$] (**#605**). The Co and Zn analogues have monoclinically distorted superstructures (**#606–607**). The Co and Zn compounds have space group $C2/c$, with $a_{mon} \sim \sqrt{3}a_{trig}$, $b_{mon} \approx b_{trig}$, $c_{mon} \approx c_{trig}$, $\beta = 92–95°$. There are still two distinct Te sites per cell, but the single octahedrally-coordinated M^{2+} site of the rhombohedral phases splits into five distinct sites with a wider range of coordination numbers: CN = 6, 6, 5, 6 and 4 for [$Co_3(TeO_6)$] (**#606**) and CN = 4, 4, 5, 5 and 6 for [$Zn_3(TeO_6)$] (**#607**). The ordered Cu–Zn compound [$Cu_5Zn_4(TeO_6)_3$] (**#608**) has similar cell parameters, but additional displacements of atoms which reduce the symmetry further to $C2$. There are three Te sites, six Cu sites and four Zn sites. While Te is in fairly regular octahedral coordination, the Cu atoms are in Jahn-Teller distorted 4+2 coordination if the threshold between strong and weak bonding is set at Cu–O = 2.2 Å, except for Cu2, which is 4+3 coordinated, with three oxygen ligands in the range 2.5–2.8 Å. Two Zn atoms are 4-coordinated and two are 5-coordinated.

The mineral mcalpineite has been recently redefined as anhydrous [$Cu_3(TeO_6)$] (Carbone *et al*., 2013). It is interesting to note that its structure (**#609**) is the explicitly ternary variant of the 'C-sesquioxide' structure of heavy rare-earth oxides and the bixbyite group of minerals $M_2^{3+}O_3$, where M = Mn, Tl, Y and Sc, in respectively, bixbyite (Zachariasen, 1928), avicennite (Radtke *et al*., 1978), yttriaite-(Y) (Mills *et al*., 2011) and kangite (Ma *et al*., 2013) (Fig. 41). This is another structure like the pyrochlore type (cf. **#366**, **700**) which can be regarded as a defect fluorite. Again, the overall cation array is cubic close-packed and there is a cubic unit cell with $a \approx 10$ Å, corresponding to 2 × 2 × 2 fluorite unit cubes, but this time, ¼ of the anions are missing, which correspond to O2 in the winstanleyite structure (**#369–373**), which has similar cell dimensions and the same $Ia\bar{3}$ space group. As in winstanleyite, the cations are split into two distinct types in a 3:1 ratio. All cations are 6-coordinate in mcalpineite, but one type (Te^{6+}, here) has a coordination polyhedron that is close to regular octahedral geometry, while the other (Cu^{2+}) has a less regular geometry that is best described as twisted trigonal prismatic. Up to half the Cu may be substituted by Co or Zn, with no further ordering (**#610–612**). Some Te-free synthetic isotypes are also rich in Cu, such as the phases $Cu^{2+}_{2-x}Fe^{3+}_{2x}Ti^{4+}_{2-x}O_6$ (Mouron *et al*., 1985) and $Cu_2^{2+}M^{3+}Sb^{5+}O_6$ (M = Mn, Fe and Ga; Bazuev *et al*., 1994).

$Ba_3[Zn_6(Si_2O_7)_2(TeO_6)]$ (**#613**) has a unique zincotellurosilicate framework, with 9- and 12-coordinate Ba^{2+} ions in large cages. Paired ZnO_6 and single TeO_6 octahedra share edges to form ribbons running ∥ **z** that resemble the Cu_2Te octahedral ribbons of frankhawthorneite and related compounds (**#512–515**). These ribbons are linked into a framework by sharing corners with corrugated layers ∥ (200) of ZnO_4 tetrahedra and Si_2O_7 tetrahedral dimers. The tetrahedral layers contain [Zn–Si–Zn–Si] 4-rings and [Zn–Si–Si–Zn–Si–Si] 6-rings (Fig. 41).

[$M_6^{3+}(TeO_6)O_6$] (M = Y, In and Tl: **#614–616**) again have a defect fluorite structure like the bixbyite isotypes **#609–612** above, but the rhombohedral structure is more complex, with approximately cubic close-packed cations ordered into two types in a 6 : 1 ratio, $^1/_7$ of the anions missing, and the rest split into two types, coordinated either by 2 M + 1 Te or by 4 M. All cations are 6-coordinate.

https://doi.org/10.1180/minmag.2016.080.093 Published online by Cambridge University Press

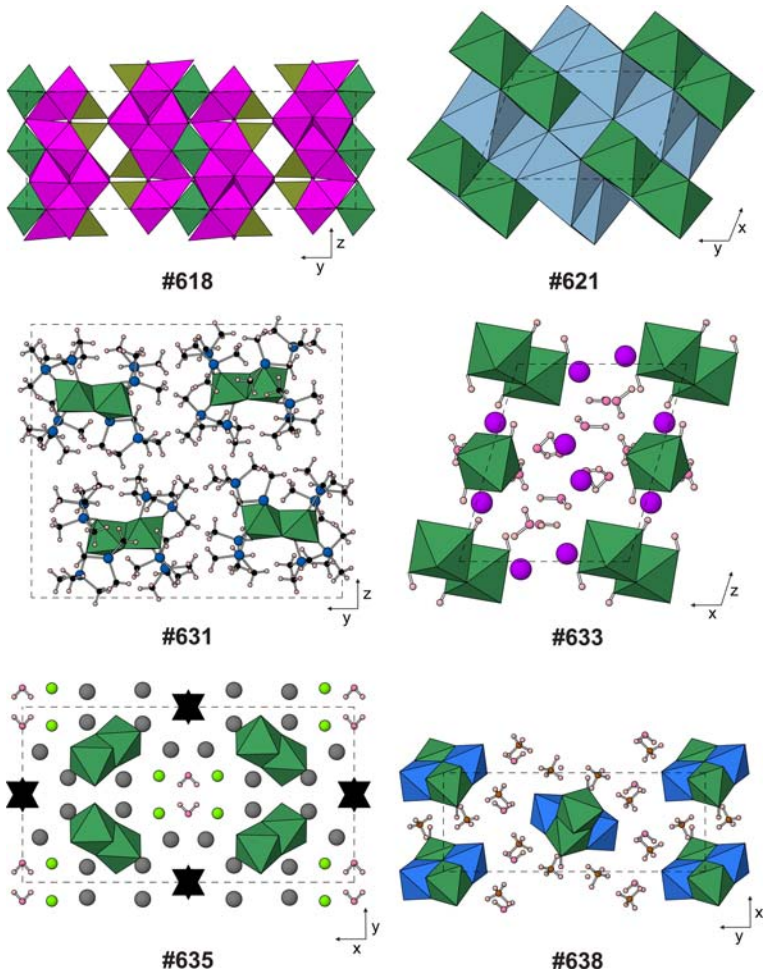

FIG. 42. Examples of structures with monomeric $Te^{6+}O_6$ as part of a larger structural framework (**#618**, Table 23, deposited) and with soro dimers of TeO_6 octahedra (Table 24). Small spheres: C (black), H (pale pink), N (brown) and O (dark pink) when not part of a polyhedron. Medium spheres: Si (blue) and Cl (yellow-green). Large spheres: K (purple) and Pb (grey). Black triangles in **#635**: CO_3 groups. Polyhedra: As (brown-green), Co (magenta), Li (grey-blue) and V (bright blue).

This structure is also known for compounds such as $Y_6(U^{6+}O_6)O_6$ (Bartram, 1966), the meteoritic mineral allendeite, $Sc_4Zr_3O_{12} \equiv [(Sc_4Zr_2)(ZrO_6)O_6]$ (Thornber *et al*., 1968; Ma *et al*., 2014) and $Pr_7O_{12} \equiv [(Pr_4^{3+}Pr_2^{4+})(Pr^{4+}O_6)O_6]$ (von Dreele *et al*., 1975). Remarkably, $Tl_6^{1+}[TeO_6]$ (**#445**, above) has the same space group and cation substructure, and very nearly the same cell parameters as $Tl_6^{3+}(TeO_6)$ (**#616**). However, all the non-tellurate oxygen atoms are missing in **#445**, and the Tl–O bonds to the remaining oxygen atoms are longer and less regular.

This section concludes with two Co-rich frameworks. $Na_5Co_{15.5}^{2+}(TeO_6)_6 \equiv Na_{2.5}(Na_{2.5}Co_{1.5})[Co_{14}(TeO_6)_6]$ (**#617**) has a nanoporous hexagonal structure in which Co1 and Te octahedra share edges to form 2-wide ribbons running || **z**. These ribbons link at corners to delineate relatively large hexagonal tunnels (diameter ≈ 6.5 Å) and smaller ditrigonal tunnels, which are internally braced by Co2 atoms in trigonal prismatic coordination, to complete a framework $[(Co1)_{12}(Co2)_2(TeO_6)_6]^{8-}$. An additional site in the small channels is occupied by mixed Na + Co, while the remaining Na^+ ions

https://doi.org/10.1180/minmag.2016.080.093 Published online by Cambridge University Press

are in the large channels. $[Co_8^{2+}(TeO_6)(AsO_4)_2O_2]$ (**#618**) has four types of Co^{2+} ion (CN = 4, 6, 6 and 6) sharing edges and corners to make thick double layers || (020). TeO_6 octahedra act as internal braces in the middle of the double layers, while AsO_4 tetrahedra cross-link the layers into a three-dimensional framework (Fig. 42).

Soro or cyclo finite polymers $Te_m^{6+}X_n$

Structures **#619–645** contain $Te^{6+}O_6$ octahedra that are linked into finite polymers Te_mX_n ($m = 2$–6); these are listed in Table 24 (deposited). Our first two examples are closely related to each other. $Ba_3[Te_2O_9]$ (**#619**) has a simple hexagonal structure containing the face-sharing dimer of Fig. 13*a*. These groups lie with ⅓ of the Ba^{2+} ions in layers || (002), which alternate with layers containing the other ⅔ of the Ba^{2+} ions. $Ba_3[Fe^{3+}((Fe^{3+}Te^{6+})O_9)]$ (**#620**) has the same $P6_3/mmc$ space group and nearly identical unit-cell parameters. It contains the same dimeric anion, except that 50% of the Te^{6+} is now randomly substituted by Fe^{3+}, and charge balance is maintained by insertion of additional Fe^{3+} ions into octahedral interstices which were vacant in #**619**. The additional Fe octahedra in **#620** join corners with the face-sharing dimers to form a three-dimensional framework which is a 6*H* perovskite polytype, with *hkk* stacking of (BaO_3) close-packed layers. It is thus very closely related to $Ba_2[Co(TeO_6)]$ (**#585**), where the different cation-ordering pattern results in lower symmetry. The relationship to these phases shows that **#619** can be considered a defect 6*H* perovskite with ordered *B*-site vacancies.

$Li_4TeO_5 \equiv Li_8[Te_2O_{10}]$ and its Na analogue (**#621–622**) has the edge-sharing dimeric anion of Fig. 13*b*. All atoms are 6-coordinated, with each oxygen atom linked to 5 Na + 1 Te or to 4 Na + 2 Te. The cation array is *ccp* and the structure is actually a superstructure of the rocksalt type, with the pseudocube edge vectors parallel to [0½½] and approximately $\left[\frac{5}{12}\ \frac{\bar{1}}{12}\ \frac{3}{4}\right]$ and $\left[\frac{5}{6}\ \frac{1}{3}\ \frac{\bar{1}}{12}\right]$ of the triclinic cell in **#622**. The Te = Te dimer axes are oriented || [331] (Fig. 42). The Ag analogue (**#623**) has a monoclinic structure in which layers of close-packed cations stack || (004) in an *ABAC* sequence (alternating *h* and *k* layers). All cations and anions again occupy 6-coordinated interstices of the opposite substructure, so while Ag^+ and Te^{6+} of the *k* cation layers are in octahedral coordination, the Ag^+ ions of *h* layers are in trigonal prisms. Within the *k* layers, edge-sharing Te=Te dimers alternate with Ag=Ag=Ag triplets along rows || **x**.

$K_4[Te_2O_6(OH)_4] \cdot 5H_2O$ (**#624**) has a simple but incompletely determined structure in which dimers with Te=Te axes || **x** are linked into layers || (020) through K^+ ions. Water molecules were not located, but are presumably in the interlayer gap and complete the coordination polyhedra of the K^+ ions. The structure of $K_4[Te_2O_6(OH)_4] \cdot 8H_2O$ (**#625**) is more completely determined, with all O and H atoms located, and bears little resemblance to that of its lower hydrate. Again, all Te=Te dimers are parallel (|| [01$\bar{1}$]), and lie in layers || (200), which alternate with layers of KO_{8-9} polyhedra. $Rb_4[Te_2O_6(OH)_4] \cdot 10H_2O$ (**#626**) is somewhat similar, but in this triclinic cell, the layering is || (110), Te=Te axes are || [2$\bar{1}\bar{4}$], and the Rb atoms are 8–10 coordinated and lie in less convoluted layers. $Cs_3[Te_2O_5(OH)_5] \cdot 4H_2O$ (**#627**) has one Te=Te group per triclinic cell, aligned || [3$\bar{2}$2], in a matrix of water molecules and CN10 Cs^+ ions, while $Cs_4[Te_2O_4(OH)_4] \cdot 8H_2O$ (**#628**) has a more obviously layered structure in which Te=Te groups pointing || [2$\bar{1}\bar{2}$] and CsX_{9-10} polyhedra form sheets || (10$\bar{1}$), which are linked only through hydrogen bonds. $K_4Na_2[Te_2O_8(OH)_2] \cdot 14H_2O$ (**#629**) has a body-centred array of Te=Te dimers pointing || **z**, which bridge layers || (10$\bar{1}$) of water molecules, CN8 K^+ and CN6 Na^+ ions. $K_7Na[Te_2O_6(OH)_4]_2 \cdot 12H_2O$ (**#630**) has Te=Te dimers || **x**, lying in undulating layers || (020) that are connected weakly through CN6–10 K^+ and CN6 Na^+ ions.

The next two compounds are ditellurates of organic complexes. $((CH_3)_3Si)_8[Te_2O_{10}]$ (**#631**) has a trimethylsilyl group strongly bonded (1 vu) to each of the eight non-bridging oxygen atoms of the Te=Te anion, to form a large neutral molecule that has only point symmetry 1, with two distinct Te and eight distinct Si atoms. Four such molecules in slightly different orientations pack together per unit cell (Fig. 42). $(C(NH_2)_3)_4[Te_2O_6(OH)_4]$ (**#632**) is not molecular, having well-defined guanidinium cations $[C(NH_2)_3]^+$ and tellurate anions $[Te_2O_6(OH)_4]^{4-}$. However, the structure is surprisingly complex, with four distinct C atoms and two types of Te=Te anion per unit cell. Te1 dimers pointing || [221] form layers || (100), which alternate with layers that contain both Te2 dimers pointing || [2$\bar{1}\bar{1}$] and one type of guanidinium group. The other three types of guanidinium lie between the Te layers.

Two structures have edge-sharing Te_2X_{10} (Fig. 13*b*) in combination with monomeric TeX_6 octahedra. $K_6[Te_2O_6(OH)_4](TeO_2(OH)_4) \cdot 12H_2O$ (**#633**) has Te=Te dimers (Te2) aligned || [110], alternating along **z** with monomeric octahedra

https://doi.org/10.1180/minmag.2016.080.093 Published online by Cambridge University Press

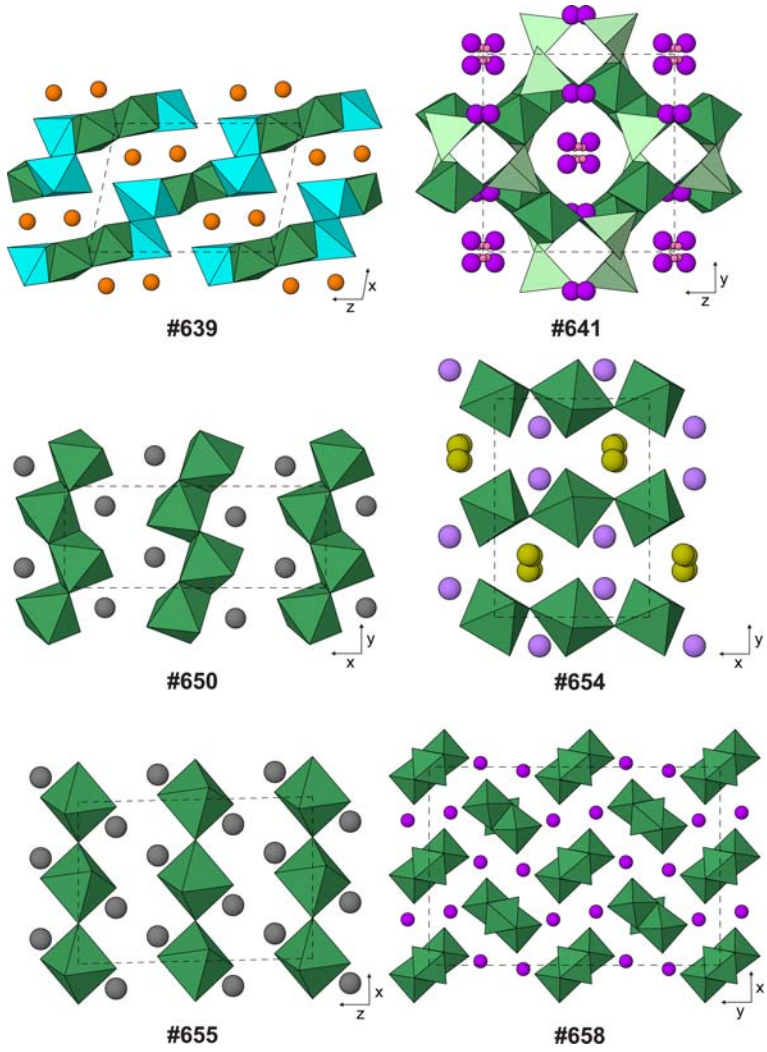

FIG. 43. Examples of structures with Te_2O_{10} octahedral dimers as part of a larger structural layer or framework (Table 24, deposited) and of infinite chains of TeO_6 octahedra (Table 25). Small spheres: O (dark pink) when not part of a polyhedron. Large spheres: Bi (violet), Ca (orange), K (purple), Na (dark yellow) and Pb (grey). Polyhedra: Cu (cyan), Ga (pale green) and Te (dark green).

(Te1). The rows of Te anions lie between layers || $(1\bar{1}0)$ of CN8–10 K^+ ions (Fig. 42). $Cs_2[Te_2O_4(OH)_6] \cdot (Te(OH)_6)$ (**#634**) has Te=Te pointing || $[2\bar{1}\bar{1}]$ and lying in layers || (001), which alternate with layers of CN9 Cs^+ ions and neutral $Te(OH)_6$ molecules. Note that this is a special case of an orthotelluric acid adduct, more conventional examples of which are described as **#376–431** above.

Thorneite, $Pb_6[Te_2O_{10}](CO_3)Cl_2 \cdot H_2O$ (**#635**, see front cover image), has Te=Te dimers pointing || $[12\bar{4}]$ or $[1\bar{2}\bar{4}]$, lying in sheets || (200). The Te sheets have on each side of them PbO_7Cl, PbO_6Cl_2 and PbO_5Cl_2 polyhedra which complete thick layers, and carbonate groups and water molecules lie between the layers (Fig. 42). $K_3[Ga(Te_2O_8(OH)_2)] \cdot H_2O$ (**#636**) has Te=Te dimers alternating with GaO_4 tetrahedra to form loop-branched *vierer* chains || **z**. The Te and Ga polyhedra between them form 'double-triangle' clusters; for a topologically similar chain made only of Te octahedra, see $K_2[Te_3O_8(OH)_4]$ below (**#658**;

https://doi.org/10.1180/minmag.2016.080.093 Published online by Cambridge University Press

Fig. 13*i*). The chains form an approximately hexagonal rod packing, and are held together through CN7–8 K^+ ions and water molecules. $Tl_6^{1+}[Cu^{2+}(Te_2O_{10})]$ (**#637**) has chains that are very similar in topology, but the non-Te component is a CuO_4 square rather than GaO_4 tetrahedron. The four shortest Cu–O distances are 1.96–1.98 Å, but a fifth neighbour to Cu at 2.52 Å provides an additional brace along the chain. The chains run || **x** and are arranged in a chequerboard fashion, leaving large square channels. Tl^+ ions line the sides of these channels, and are in one-sided 5–8 coordination. $(NH_4)_2V^{5+}TeO_6(OH) \cdot H_2O \equiv (NH_4)_4[(V^{5+}O_2)_2(Te_2O_8(OH)_2)] \cdot 2H_2O$ (**#638**) has a loop-branched *dreier* chain made from regular Te octahedra and very distorted V octahedra. Edge-sharing Te=Te and V=V pairs alternate along the chain || **z**. Every Te atom shares an oxygen ligand with each V of its adjacent dimer, and also a CN3 oxygen atom with both of them. V–O distances are 1.65–1.66 Å (non-bridging oxygen), 1.95–1.96 Å (CN2 bridging oxygen) and 2.16 and 2.47 Å (CN3 bridging oxygen), consistent with its description as the core of a $[VO_2]^+$ cation. The chains pack in a centred-rectangular array, with NH_4^+ ions and H_2O molecules between them (Fig. 42).

Eckhardite, $Ca_2[Cu_2(Te_2O_{10})] \cdot 2H_2O$ (**#639**) has TeO_6 and CuO_{4+2} polyhedra sharing edges to form layers || (101). The Cu ligands form a slightly twisted square at 1.96–2.02 Å, plus two more completing an elongated octahedron at 2.51 and 2.67 Å (Fig. 43). The oxygen atoms associated with all these polyhedra form a stepped, oblique slice through a *hcp* array, somewhat similar to the layer seen in the frankhawthorneite-related structures **#512–515** above. However, while the frankhawthorneite layer 'steps' are edge-sharing ribbons which alternate between two octahedra in width (Cu=Cu) and one (Te), the eckhardite ribbons alternate between three octahedra (Cu=□=Cu) and two (Te=Te) in width. These run || **y**. Between the layers lie CN7 Ca^{2+} ions. $Ag[(UO_2)(Te_2O_8(OH)_2)]$ (**#640**) has edge-sharing ribbons of UO_7 pentagonal bipyramids running || **x**, which share CN3 oxygen atoms with Te_2O_{10} dimers to form layers || (020). The layer topology contains 'double-triangle' clusters U < (Te=Te) > U. The Ag^+ ions are in irregular 5-fold coordination between the layers. In $K_2[Ga_2(Te_2O_{10})] \cdot 2H_2O$ (**#641**), GaO_4 tetrahedra and Te_2O_{10} octahedral pairs share corners to form a three-dimensional framework. Two ligands of each Ga connect it to a neighbouring Te = Te dimer as part of a 'double triangle' Ga < (Te = Te) > Ga, while the other two ligands link Ga to two other dimers, as part of a [Ga–Te–Ga–Te] 4-ring. The double triangles and 4-rings alternate, forming crankshaft ribbons || **z**, which are arranged in a centred-rectangular array and are connected into a framework via the remaining Ga–O–Te links. The framework is very open, with 6–8 Å diameter channels || **x** and **z**, which contain water molecules and CN9–11 K^+ ions, and has very strong pseudotetragonal symmetry in projection down **x** (Fig. 43).

Schieffelinite, $Pb_{10}[Te_2O_8(OH)_3]_2(TeO_2(OH)_4)_2(SO_4) \cdot 5H_2O$, and its chromate analogue chromschieffelinite (**#642–643**), have as their structural unit the corner-sharing Te_2X_{11} dimer of Fig. 13*c*. The Te–Te dimers lie in undulating layers || (020), with CN8–10 Pb^{2+} ions on either side. Water molecules, additional TeX_6 monomers and orientationally disordered SO_4^{2-} or CrO_4^{2-} tetrahedra lie between the layers.

We have two examples of cyclo anions made from Te^{6+} octahedra. $K_2[Te_4O_8(OH)_{10}]$ (**#644**) has an edge-sharing pair of octahedra joining the two halves of a Te_4X_{18} 'double triangle' tetramer (Fig. 13*d*). These isolated clusters are arranged in a herringbone pattern in layers || (100), with CN10 K^+ ions between the layers. $K_{8.5}(H_3O)_{0.5}[Te_6O_{18}(OH)_9] \cdot 17H_2O$ (**#645**) has ditrigonal rings Te_6X_{27} in which Te octahedra alternately share corners and edges with their neighbours (Fig. 13*e*). Rings are in two different orientations with the ring plane always normal to **z**, and form pseudohexagonal columns running || **z**, which are arranged in a hexagonal rod packing, with hydronium and CN6–11 K^+ ions between them. Successive layers of the rods || (200) are shifted by $\frac{1}{4}c$, which reduces the symmetry to monoclinic.

Infinite polymers $Te_m^{6+}X_n$

Inotellurates

In structures **#646–677** Te^{6+} octahedra are linked to form infinite polymers (Table 25, deposited). Our first examples of ino tellurates have edge-sharing *zweier* chains Te_2X_8. In all cases, the shared edges of an octahedra are not *cis* to one another, so the chain zigzags (Fig. 13*f*). The database includes two polymorphs of $Na_2TeO_4 \equiv Na_4[Te_2O_8]$. The *Pbcn* polymorph (**#646**) has Te chains || **z**, arranged in a centred-rectangular array. The chains are flanked by edge-sharing ribbons of NaO_6 polyhedra which hold the structure together. Overall, the oxygen arrangement approximates *hcp*, with close-packed planes || (200) and (Na+Te) occupying ¾ of the octahedral interstices between each pair of

https://doi.org/10.1180/minmag.2016.080.093 Published online by Cambridge University Press

layers. The $P2_1/c$ polymorph (**#647**) has a slightly sheared version of the same structure, with $\mathbf{x}_{mon} = \left[\frac{3}{2}, \frac{1}{2}, 0\right]_{orth}$ and $\mathbf{z}_{mon} = [1\bar{1}0]_{orth}$. The isostructural pair of compounds $CaTeO_4$ and $SrTeO_4$ (**#648–649**) have the same space group as **#646** (*Pbcn*, although strongly pseudo-*Cmnm*), very similar cell parameters, and the same type of Te chain. However, only half of the Na sites of **#646** are occupied by alkaline earth cations. $(Ca,Sr)O_6$ and TeO_6 octahedra together form open-branched *zweier* chains of edge-sharing octhedra running || **z** between each pair of close-packed anion layers, thus avoiding shared faces between (Ca,Sr) octahedra. This structure is shared with the pucherite polymorph of $BiVO_4$ (Qurashi and Barnes, 1953) and alumotantite, $AlTaO_4$ (Ercit *et al*., 1992) as well as synthetic MUO_4 (M = Cr, Fe and Ni; Hoekstra and Marshall, 1967). A Te-rich variety of raspite, $Pb[(W_{0.56}Te_{0.44})O_4]$ (**#650**) is included in this review, as the W:Te ratio is close to 1:1. Raspite is ideally $PbWO_4$ (Fujita *et al*., 1977), and was discussed earlier, as one of the forms of $Te^{4+}V^{4+}O_4$ is isostructural (**#82**, above). While Te^{4+} may occupy large, irregularly-coordinated sites like Pb^{2+}, also a cation with a stereoactive lone pair, Te^{6+} readily enters octahedral sites, and so behaves analogously to W in raspite or V in $TeVO_4$. The raspite structure is a monoclinically sheared derivative of the pucherite type, in which the anion arrangement is strongly perturbed away from hexagonal close-packing and the larger cation is irregularly 7-coordinated. The $P2_1/a$ axial setting can be related back to the *Pbcn* setting of pucherite through the relations $\mathbf{x}_{puch} = \mathbf{z}_{rasp}$, $\mathbf{y}_{puch} = [101]_{rasp}$ and $\mathbf{z}_{puch} = \mathbf{y}_{rasp}$; a pucherite-like cell for raspite would have space group $P112_1/n$, $a = 5.59$ Å, $b = 13.03$ Å, $c = 5.02$ Å and $\beta = 96.1°$ (Fig. 43). $KTeO_3(OH) \equiv K_2[Te_2O_6(OH)_2]$ (**#651**) has similar cell parameters to **#646–649** and a very similar arrangement of Te chains, although chains in successive layers || (020) are translated by $\frac{1}{2}a$ relative to their positions in the pucherite structure, the K atoms are near positions that are vacant octahedra of $(Ca,Sr)TeO_4$ and are in 7- rather than 6-coordination, and the symmetry is monoclinic $P2_1/a$, but this time not as a subgroup of pucherite symmetry. $(NH_4)TeO_3(OH)$ (**#652**) has a triclinic distortion of this structure with $\mathbf{x}_{orth} = [011]_{tcl}$ and $\mathbf{y}_{orth} = [01\bar{1}]_{tcl}$.

The corner sharing *zweier* chains Te_2X_{10} of the present study all have their bridging oxygen atoms *trans* to each other across a Te octahedron, but zigzag nevertheless due to having non-linear Te–O–Te links (Fig. 13*g*). $KTeO_2(OH)_3 \equiv K_2[Te_2O_4(OH)_6]$ (**#653**) has such chains running || **z** of the tetragonal structure, with bridging oxygen atoms disordered on a quadruply split site. Large square channels between the chains accommodate K^+ ions in 8-fold coordination. $NaBiTeO_5 \equiv Na_2Bi_2[Te_2O_{10}]$ (**#654**) has *zweier* Te_2O_{10} chains running || **x**, which form a pseudohexagonal array. Sodium and Bi atoms occupy trigonal prismatic interstices between Te atoms; both form zigzag chains || **z**, and are ordered in a chequerboard fashion. The Te(NaBi) cation array is similar but not identical to the ordered form of the $CeCu_2$ type (Larson and Cromer, 1961), apart from the strong monoclinic shear ($\beta = 106.8°$) of the structure in **#654**. The oxygen coordination number of both Na and Bi is 7 (Fig. 43). The mineral ottoite, $Pb_2TeO_5 \equiv Pb_4[Te_2O_{10}]$ (**#655**) has a very similar structure but with monoclinic shear much smaller ($\beta = 91.3°$) and in a different direction (**y** and **z** are reversed relative to **#654**) and Na and Bi positions merged into a single Pb site (Fig. 43). The Pb is in irregular 7-coordination (Pb–O = 2.37, 2.37, 2.53, 2.59, 2.71, 2.88 and 3.04 Å; no others at <3.4 Å). Hg_2TeO_5 (**#656**) has cell parameters quite close to those of ottoite, and the structure looks very similar in projection down **x**. However, the symmetry is now orthorhombic ($Pna2_1$). The Te chains are displaced along **x** so that the Te substructure has elongate octahedral and tetrahedral interstices rather than trigonal prismatic ones, and Hg atoms are split into two distinct types, both of which lie at the centres of Te triangles. Both Hg atoms have 7 oxygen neighbours within 3.1 Å, but the bond-length variation is such that Hg1 coordination is best regarded as plane-triangular (Hg–O at 2.13, 2.21 and 2.31 Å; no more until 2.49 Å) and Hg2 as linear 2-coordinate (Hg–O at 2.07 and 2.08 Å, with no more until 2.53 Å). Because of the large bond valence of the short Hg–O bonds, this structure is regarded as having a Hg–Te heteropolyhedral framework.

$Ag_3TeO_4I \equiv Ag_9[Te_3O_{12}]I_3$ (**#657**) has an edge-sharing *dreier* chain Te_3X_{12} in which again the shared edges are not *trans* (Fig. 13*h*). The chains spiral helically || **y**, and are surrounded by nine types of Ag^+ ion so as to form thick layers || (200), with I^- anions in the interlayer gaps. Ag atoms are irregularly coordinated by 3 O + I, 2 O + 2 I, O + 3 I or 2 O + I. $K_2[Te_3O_8(OH)_4]$ and its NH_4 analogue (**#658–659**) have a quite different Te_3X_{12} chain, with a Q^{2400} octahedron alternating with a pair of Q^{2401} octahedra to make a loop-branched *zweier* type as seen in Fig. 13*i*. This chain represents a condensation of the 'double triangle' cluster that is

https://doi.org/10.1180/minmag.2016.080.093 Published online by Cambridge University Press

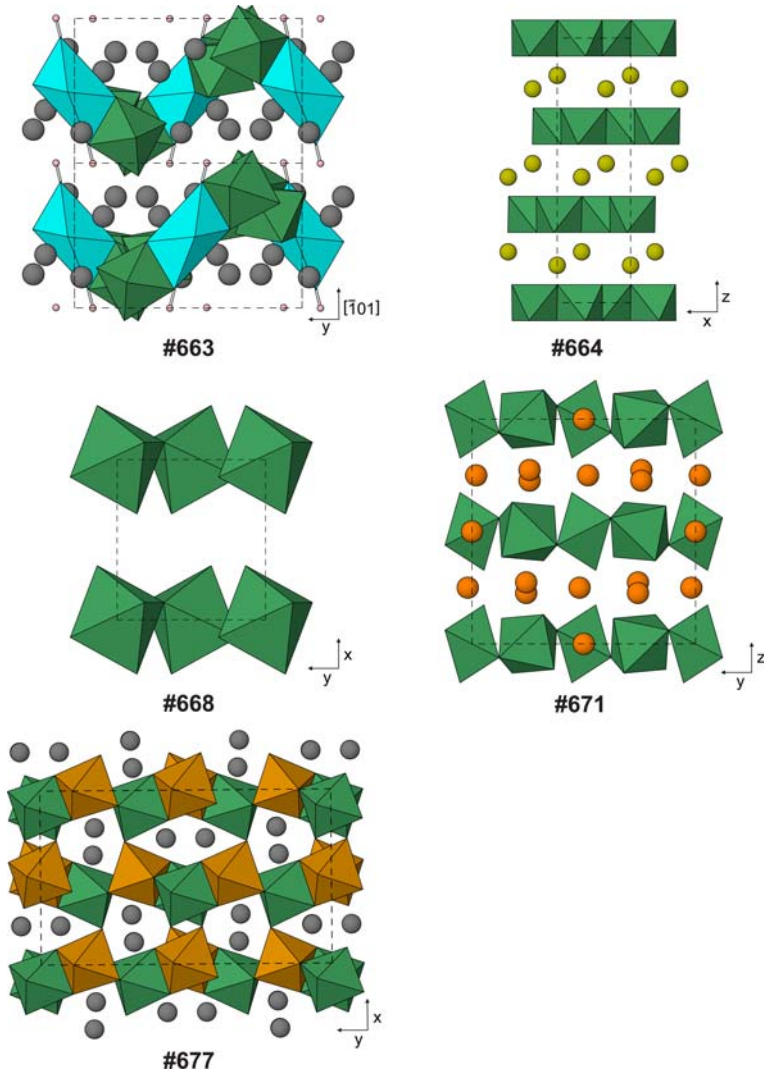

FIG. 44. Examples of structures with TeO_6 linked to form infinite layers or frameworks (Table 25, deposited). Small spheres: H (pale pink). Large spheres: Ca (orange), Li (pale blue), Na (dark yellow) and Pb (grey). Polyhedra: Cu (cyan), Fe (orange-brown) and Te (dark green). There is substantial Fe–Te disorder in **#677**.

seen in isolation in $K_2[Te_4O_8(OH)_{10}]$ (**#644**, Fig. 13*d*). Eight such chains per unit cell run || **z** and pack in a herringbone arrangement, held together by large cations in 8-coordination (Fig. 43). Similar chains of double triangles occur in $Ag_2TeO_4 \equiv Ag_6[Te_3O_{12}]$ (**#660**) and $Ag_2[Hg_2(Te_3O_{12})]$ (**#661**). In the first of these compounds, the pseudotetragonal cell has chains that lie in layers || (002), and chains run || [110] or [1$\bar{1}$0] in alternate layers. Silver atoms lie between the layers in 2–4 coordination. In **#661**, the Te chains all are || **x**, and linear 2-coordinated Hg^{2+} link the chains to form layers || (002). Ag atoms lie between the layers in irregular 6-coordination.

$Li_2TeO_4 \equiv Li_8[Te_4O_{12}]$ (**#662**) has a chain that is the *vierer* analogue of the *dreier* chain in **#657**. This time, the nonlinear Te=Te=Te links result in a helical chain with periodicity four (Fig. 13*j*), which spirals around a screw tetrad axis in the structure, winding through a matrix of LiO_4 tetrahedra. Our final inotellurate is the mineral housleyite, $Pb_6[Cu(Te_4O_{18}(OH)_2)]$ (**#663**), in which the *vierer* chain is

https://doi.org/10.1180/minmag.2016.080.093 Published online by Cambridge University Press

entirely corner-sharing, but differs from the *zweier* chain of ottoite (**#655**) in that there is alternation of Te octahedra with *trans* bridging oxygen atoms and octahedra with *cis* bridging oxygen atoms (Fig. 13*k*). Tellurium chains run || [101], and are linked through CuO_{4+2} polyhedra to form corrugated layers || (10$\bar{1}$). Copper shares corners with two adjacent Te octahedra in the chains on each side, to make a pair of [Cu–Te–Te] 3-rings (Fig. 44). The four shortest Cu–O distances are 1.96–1.97 Å; two more neighbours at 2.65 Å complete an elongated octahedron, and further brace the structural layer. Pb atoms in irregular 7–8 coordination decorate the outsides of the layers and link them. Fortuitously, the structure has a pseudotetragonal aspect in projection down **x**, with the Te atoms appearing to form an apophyllite-like net of 4- and 8-rings, but the component Te chains are linked only through Cu atoms, so this pattern has little structural significance.

Phyllotellurates

The simplest layer tellurates have an edge-sharing dioctahedral sheet MX_3 of the topology seen in gibbsite and other polymorphs of $Al(OH)_3$ (Fig. 14*a*). Note that a $Te^{6+}O_3$ sheet would be electrostatically neutral and that a protonated sheet would be charged positively. In all the cases described here, some of the *M* cations are a different element of lower valence than Te, thus achieving a negative charge on the sheet. What is unusual is that even though the two elements are present in a 50:50 ratio in all cases, there is no evidence for long-range three-dimensional order of the cations. It is quite feasible that two-dimensional order occurs within the layers, but the *M* cations are treated as disordered here in the absence of experimental evidence to the contrary. The isostructural pair $Na_2[(GeTe)O_6]$ (**#664**) and $Na_2[(TiTe)O_6]$ (**#665**) have the ilmenite ($FeTiO_3$) structure, which is in turn a superstructure of the corundum type. Oxygen atoms are *hcp*, and between each pair of layers, ⅔ of the octahedral interstices are occupied either by Na or by disordered ($M^{4+} + Te^{6+}$). Discrete layers || (003) can be identified as structural units because of the weakly bonded Na layers that lie between them (Fig. 44). Brizziite, $NaSb^{5+}O_3$, is compositionally close and shares the same structure (Olmi and Sabelli, 1994). A superstructure of the ilmenite type, in which additional cation ordering results in isolated TeO_6 octahedra, occurs for $Ni_3(TeO_6)$ and its relatives, discussed as **#599–601** above. Burckhardtite, $Pb_2[(Fe^{3+}Te^{6+})O_6][AlSi_3O_8]$ (**#666**) has $[(Fe^{3+}Te^{6+})O_6]^{3-}$ layers of the same type, alternating with aluminosilicate double layers $[AlSi_3O_8]^-$ of the topology seen in minerals such as cymrite, $Ba[Al_2Si_2O_8] \cdot H_2O$ (Drits *et al.*, 1975).

$Sr[(Mn^{4+}Te^{6+})O_6]$ (**#667**) has a hexagonal cell with a parameter similar to those of **#664–666**, and a *c* parameter suggesting that it might be isotypical with rosiaite-type compounds such as $Sr[Ge(TeO_6)]$ (**#521** above), in which layers of Sr octahedra alternate with layers of (M^{4+} + Te). However, the structural refinement reveals that Mn and Te are disordered in trigonal prisms (Fig. 14*b*) rather than in octahedra, which is reflected in the different space group, $P\bar{6}2m$ as opposed to $P\bar{3}1m$ for disordered rosiaite (e.g. $Pb[Sb_2O_6]$) or $P312$ for ordered rosiaite (**#521**).

$[TeO_2(OH)_2]$ (**#668**) has TeX_6 octahedra sharing four corners with neighbours to form a slightly crumpled square net (Fig. 14*c*). The layers are || (100), and are held together only by hydrogen bonds (Fig. 44). $(Bi_2O_2)[TeO_4]$ (**#669**) has topologically similar but geometrically more regular square layers || (020), which intercalate with cationic sheets $[Bi_2O_2]^{2+}$ which have the litharge structure (Boher *et al.*, 1985). The two types of unit are held together by long Bi···O bonds. $[Cu(TeO_4)]$ (**#670**) also has square $[TeO_4]^{2-}$ layers || (020), but corner-sharing chains of CuO_4 squares run || [101] that share edges with TeO_6 octahedra above or below to link the whole structure into a strongly-bonded framework. The four shortest Cu–O are in the range 1.90–2.12 Å, but the Jahn-Teller elongation of the CuO_{4+2} octahedron is unusually small, as the next neighbours are at only 2.22–2.26 Å. Alternation of Te^{6+} with U^{6+} in a square-net layer such as those of **#668–670** produces the heteropoly structural layer of markcooperite (**#544–545** above).

$Ca_5[Te_3O_{14}]$ (**#671**) has more complex corner-sharing layers of the type shown in Fig. 14*d*, with Q^{2400} and Q^{4200} octahedra. It is isotypical with chiolite, $Na_5[Al_3F_{14}]$ (Jacoboni *et al.*, 1981), although with a slight orthorhombic distortion (chiolite is tetragonal, $P4/mnc$). This compound thus represents another valence-doubled structural analogy between tellurates and hexafluoroaluminates, along with examples such as the perovskite-superstructure phases Ca_3TeO_6 (**#561**) and cryolite, Na_3AlF_6 (Hawthorne and Ferguson, 1975), Ba_2CaAlF_6 (**#571**) and elpasolite, K_2NaAlF_6 (Sabelli, 1987), and the garnet-structure minerals yafsoanite, $Ca_3Zn_2(TeO_6)_2$ (**#587**) and cryolithionite, $Na_3Li_2(AlF_6)_2$ (Geller, 1971). In **#671**, tellurate

https://doi.org/10.1180/minmag.2016.080.093 Published online by Cambridge University Press

layers are || (002), with CN7–8 Ca^{2+} ions lying between them (Fig. 44). Other fluoride-tellurate analogies were noted in the discussion of Fig. 14*f–g*, above.

Tectotellurates

$[(Co^{2+}Te^{6+})O_4]$ and its Ni analogue (**#672–673**) have long-range disorder of the divalent cation and Te in octahedral sites, similar to the situation in the phyllotellurates **#664–667** above. However, in these compounds, the octahedra share two *trans* edges and all corners to form a framework with the same topology as the rutile form of TiO_2, but a strong monoclinic distortion (Fig. 14*e*). Thus, they are isostructural with tugarinovite, $Mo^{4+}O_2$ (Brandt and Skapski, 1967). The pseudotetrad direction is **x**, while vectors [010] and [½01] correspond to the **x** and **y** lattice vectors of the tetragonal rutile cell. $[TeO_3]$ (**#674**) has the rhombohedral FeF_3 type of structure (Hepworth *et al*., 1957) in which an octahedron shares each corner with a different neighbour (Fig. 14*f*). Topologically, the structure is the same as that of the cubic defect perovskite ReO_3, but the Te–O–Te angles are reduced from 180° so as to collapse the structure and achieve approximate hexagonal packing of oxygen atoms. These and other related structures are discussed by Hyde and Andersson (1989), and an analogous relationship between stuffed variants of these structures, namely the ilmenite/corundum structure and ABX_3 perovskite, was discussed in connection with Ni_3TeO_6 and its isotypes, **#599–601** above. $Na_2[Te_2O_7]$ and its Ag analogue (**#675–676**) have the same framework as weberite, $Na_2(MgAlF_7)$ (Knop *et al*., 1982), depicted in Fig. 14*g*. The extra-framework cations are in similar environments, Na having eight oxygen neighbours at 2.26–2.79 Å while Ag–O distances are in the range 2.39–2.81 Å. $Pb_3[Fe_2^{3+}Te_2O_{12}]$ (**#677**) has partial ordering of Fe and Te on four distinct octahedral sites. Te1 and Te2 are $(Te_{0.75}Fe_{0.25})$, while 'Te3' and 'Te4' are actually $(Fe_{0.75}Te_{0.25})$. Tellurium- and Fe-rich octahedra are related via a pseudo-*a*-glide reflection || (002). Here, all are considered as of equal status in the structural unit. Te-dominant and Fe-dominant octahedra alternate in the unique framework of Fig. 14*h*, which is strongly layered || (200). Within a layer, zigzag *zweier* chains of Te2 and Te4 alternate, both running || **z**. The Te1 atoms share corners to make 3-ring loops on the Te4 chains, while Te3 do the same for the Te2 chains. The Te1 of one chain and Te3 of an adjacent chain then share edges, so as to make 8-rings and complete the layer, and the layers are bridged further to link them in three dimensions through additional Te1–Te3 and Te2–Te4 links, which create 4- and 6-rings. The Pb atoms in 7–8 lie between the dense layers coordination (Fig. 44).

Mixed-valence Te^{4+} and Te^{6+}

Table 26 (deposited) lists structures **#678–703**, which feature Te in both +4 and +6 valence states. The first of these compounds, $[Co_6^{2+}(Te^{6+}O_6)(Te^{4+}O_3)_2Cl_2]$ (**#678**) is a somewhat trivial example in that it contains isolated $[Te^{6+}O_6]^{6-}$octahedra and $[Te^{4+}O_3]^{2-}$ trigonal pyramids. However, the structure is related closely to the interesting schafarzikite–apuanite–versiliaite polysomatic series of minerals. Schafarzikite, $Fe^{2+}Sb_2^{3+}O_4$, is isostructural with minium, $Pb^{4+}Pb_2^{2+}O_4$ (Fischer and Pertlik, 1975; Gavarri and Weigel, 1975) and has rutile-like edge-sharing chains of octahedra containing Fe^{2+} running || **z**, connected through chains of corner-sharing lone-pair cations, $[Sb_2O_4]^{2-}$. The overall structure has the same tetragonal space group $P4_2/mbc$ as **#678**, $a = 8.59$ Å and $c = 5.91$ Å. A series of additional phases is produced if some pairs of Sb^{3+} ions and their lone pairs (Sb^{3+}-: :-Sb^{3+}) are replaced by (Fe^{3+}–S–Fe^{3+}) bridges, with oxidation of some octahedral Fe^{2+} to Fe^{3+} in order to maintain electroneutrality (Mellini and Merlino, 1981). Chemically, the maximally substituted end-member, with all Fe oxidized, would be $(Fe_2^{3+})(Sb_2Fe_2^{3+})O_8(\square S)$. Versiliaite, with a *c* parameter doubled relative to schafarzikite and with orthorhombic symmetry, represents 50% substitution, $(Fe_2^{2+}Fe_2^{3+})(Sb_6Fe_2^{3+})O_{16}(\square_3 S)$, while apuanite, with a tripled *c* parameter and $P4_2/mbc$ symmetry, has the 67% substituted composition, $(Fe_2^{2+}Fe_2^{3+})(Sb_4Fe_2^{3+})O_{12}(\square_2 S)$. Compound **#678** has very similar cell parameters to apuanite (for which $a = 8.37$ and $c = 17.97$ Å) and is nearly isotypical with it, as evident if its formula is written $(Te^{6+}Co_2^{2+})(Co_4^{2+}Te_2^{4+})O_{12}(Cl_2\square)$. It thus represents an intermediate member of a series between two hypothetical end-members, with the interesting complication that it is not possible to write a formula that both makes crystal-chemical sense and is electrostatically neutral. The extreme compositions that correspond to those of the schafarzikite family are $[Te^{6+}Co_2^{2+}O_4Cl]^{1+}$ and $[Co_2^{2+}(Co_2^{2+}Te_2^{4+})O_{12}(Cl\square)]^{1-}$. The ordering of Co and Te is consistent with these, such that octahedral Co^{2+} is closely associated with pyramidal Te^{4+}, while octahedral Te^{6+} is close to tetrahedral Co^{2+}. The

https://doi.org/10.1180/minmag.2016.080.093 Published online by Cambridge University Press

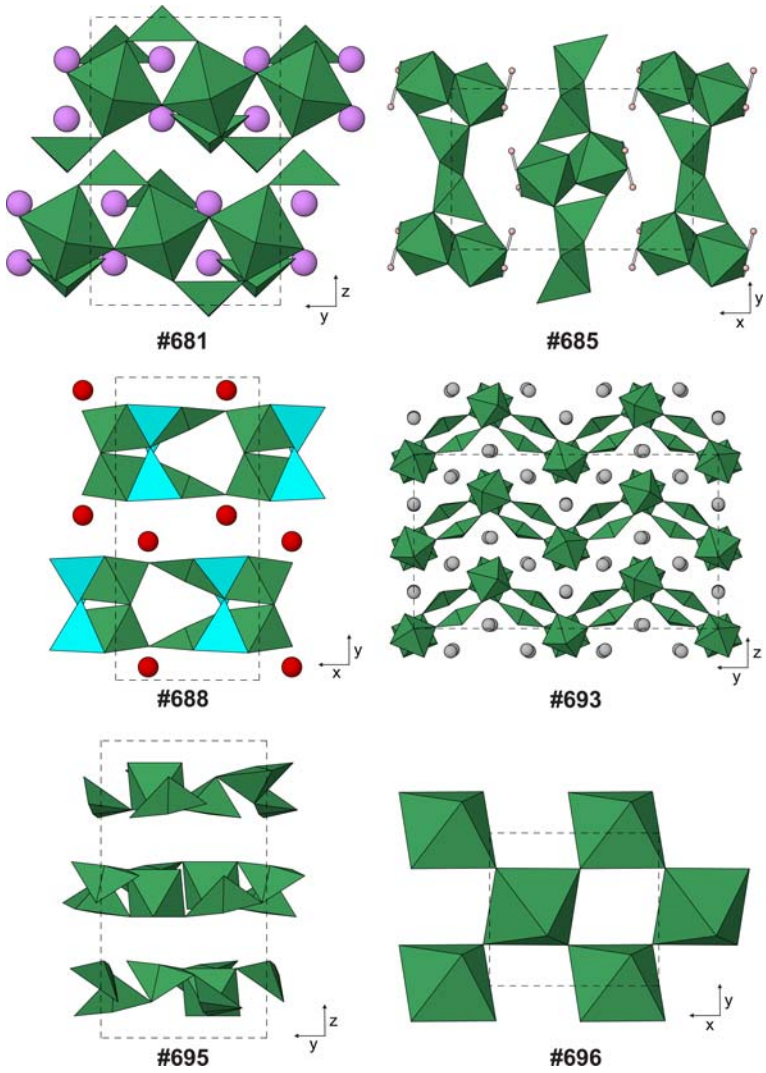

FIG. 45. Examples of structures containing both Te^{4+} and Te^{6+} (Table 26, deposited). Small spheres: H (pale pink). Large spheres: Cd (purple-pink), Hg (pale grey) and Sr (red). Polyhedra: Cu (cyan) and Te (dark green). The Te layers of **#693** are further linked into a framework through linear O–Hg–O links, which are not shown for clarity. The Te^{6+} cations are in nearly regular octahedra; the Te^{4+} cations are not.

structure of emmonsite, $[Fe_2^{3+}(H_2O)(Te^{4+}O_3)_3]$ (**#137**, above) is closely related.

It is noteworthy that there are no structures in which Te^{4+} and Te^{6+} polyhedra are linked together into a finite Te–O complex. The simplest Te–O polymers that contain both valence states are infinite chains. In $Bi[(Bi^{3+}Te^{4+})Te^{6+}O_8]$, **#679**, half of the Bi atoms occupy 8-coordinated sites (Bi1), while the other half (Bi2) randomly share a split site with Te2. The Bi atoms are displaced by ~0.38 Å from the Te position, so as to acquire an additional oxygen neighbour. The lone-pair cations and Te^{6+} link to form as a structural unit the loop-branched *zweier* chain of Fig. 15*a*. Note that this is a mixed-valence version of the chain that occurs in $K_2[Te_3^{6+}O_8(OH)_4]$ (**#658**, Fig. 13*i*), and that both are built from the very frequently occurring 'double-triangle' clusters. In **#679**, chains lie in layers ∥ (002), and chains of alternate layers run either ∥ [110] or ∥ [1$\bar{1}$0]. The Bi1 cations lie

https://doi.org/10.1180/minmag.2016.080.093 Published online by Cambridge University Press

between the chains and link them. Interestingly, Bi1 and octahedral Te1 also lie in layers, this time || (200), and form a square net in which TeO_6 octahedra share two *trans* edges with Bi atoms, and the remaining corners with another two Bi atoms. Layers of (Bi2, Te2) alternate with those of (Bi1 + Te1). The structure can be regarded as an extreme derivative of the fluorite type, given the 1:2 cation:oxygen ratio, and the fact that cations lie in an approximate *ccp* array with pseudocube edge vectors [00½], [010] and [¼0½] of the monoclinic cell, with lengths respectively 5.14, 5.56 and 5.82 Å.

$Cd_2Te^{4+}Te^{6+}O_7 \equiv Cd_4[Te^{4+}Te_2^{6+}O_{11}](Te^{4+}O_3)$ (**#680**) has two types of Te^{4+} (Te1 and Te3) and of Te^{6+} (Te2 and Te4). The Te^{6+} octahedra form the backbones of *zweier* chains || **x**, with Te3 attached to them to form 3-ring loops (Fig. 15*b*). The independent Te1 atom forms pyramidal $[TeO_3]^{2-}$ anions that lie between the loops. Te–O anions are embedded in a matrix of edge-sharing CdO_{6-8} polyhedra. $Cd_2Te_2^{4+}Te^{6+}O_9 \equiv Cd_4[Te_2^{4+}Te_2^{6+}O_{12}](Te^{4+}O_3)_2$ (**#681**) is rather similar, although the *zweier* tellurate chain is || **y**, has twice as many 3-ring loops (Fig. 15*c*) and twice as many associated but separate tellurite pyramids. The chains lie *en échelon* in well-defined layers || (100), which alternate with layers of edge-sharing CdO_7 polyhedra (Fig. 45). The tendency of Cd^{2+} ions to form rather complex structures was noted previously (**#327** and **334**, above).

$(NH_4)[Te^{4+}Te^{6+}O_5(OH)]$ (**#682**) has infinite Te–O layers || (002) in which $Te^{6+}O_6$ octahedra share corners to form *zweier* chains || **x**, and CN5 Te^{4+} share corners with two octahedra from each of a pair of chains to form a net with 3- and 4-rings (Fig. 15*d*). Thus, the layer contains looped chain elements similar to the anions of **#680–681**. Te^{6+} octahedra are Q^{0600}, while Te^{4+} polyhedra are Q^{1400} in connection pattern. NH_4^+ cations lie between the layers. The OH^- group was not located, but is presumably the unique non-bridging anion attached to Te^{4+}. $Ba[Te^{4+}Te^{6+}O_6]$ (**#683**) has a topologically identical Te–O layer || (020), with Te^{6+} chains running || **z**. The Ba^{2+} ions between the layers are in 10-coordination. The third structure with this layer topology is polymorph II of $Ag_2[Te^{4+}Te^{6+}O_6]$ (**#684**). In this monoclinic structure, the Te–O layers are || (001) with Te^{6+} chains || **y**, and layers are connected through sheets of Ag^+ ions in irregular 6-fold coordination. Two other polymorphs are described below (**#686–687**). $[Te^{4+}Te^{6+}O_4(OH)_2]$ (**#685**) has layers || (200) which again contain *zweier* chains of Te^{6+} octahedra (Te1), || **z** this time, and have Te^{4+} (Te2) polyhedra making 3-rings with adjacent pairs of octahedra. However, the layer is completed by Te^{4+} polyhedra linking to each other, to form (Te1–Te2–Te2–Te2–Te1) 5-rings (Fig. 15*e*) (Fig. 45). The polymerization state of Te1 is Q^{2400} while that of Te2 is Q^{0400}; the hydrogen atoms are located on the non-bridging ligands of Te1, with layers held together via both hydrogen bonds and long Te2···O interactions. The polarity of the structure along **z** is due to the orientation of both O–H groups and Te^{4+} lone pairs. Polymorphs I and III of $Ag_2[Te^{4+}Te^{6+}O_6]$ (**#686–687**) have layer topologies that are quite distinct from each other and from that of polymorph II (**#684**). In polymorph I, layers are || $(10\bar{1})$ and contain 'double-triangle' clusters of Q^{1501} Te^{6+} and Q^{1300} Te^{4+}, which link to form a net which has 8-rings as well as 3-rings (Fig. 15*f*). Note that the positions of Te^{4+} and Te^{6+} in the double triangle are reversed relative to their locations in the chain of $Bi[(Bi^{3+}Te^{4+})Te^{6+}O_8]$ (**#679**, Fig. 15*a*). Sheets of edge- and face-sharing AgO_{6-7} polyhedra lie between the Te–O layers. The Te–O layer of polymorph III is very similar, but is oriented || (100) in its structure, and an additional short Te^{4+}–O distance of 2.41 Å renders all oxygen ligands as 'bridging' and breaks the 8-rings into pairs of 4-rings (Fig. 15*g*). The Ag^+ ions between the layers are in irregular 5–6 coordination.

There are a number of polytypical compounds with the formula $A^{2+}[M^{2+}(Te^{4+}Te^{6+}O_7)]$, where A = Sr, Pb or Ba and M = Cu (**#688–690**), Mg (**#691**) or Zn (**#692**). All structures have similar-sized unit cells. The symmetries are primitive but centrosymmetric *Pbcm* for one polytype (**#688–689**) or centred but without inversion symmetry for the other (**#688–689**); the *Ama*2 space group used for the latter subgroup has **x** and **z** directions reversed relative to the *P* subgroup, and would be written *C*2*cm* in the same axial setting. In **#688**, Q^{2400} Te^{6+} octahedra (Te1) share *cis* corners to form zigzag *zweier* chains || **z**. Each octahedron also shares another pair of *trans* corners with Q^{2200} Te^{4+} (Te2) to make zigzag chains || **x**, thus forming strongly corrugated layers || (020) with four 6-rings meeting at each Te^{6+} cation (Fig. 15*h*). The *M* cations, Cu in this case, are in square-pyramidal 5-fold coordination above or below the Te sheet, and share corners with three Te1 atoms of one chain and two adjacent Te2 atoms, producing a structural unit that is a rather dense double layer (Fig. 45). The positioning of the Cu atoms is the main topological factor that gives the layer a polarity along the **x** direction. The Sr^{2+} ions lie between the layers in 10-coordination. In this

https://doi.org/10.1180/minmag.2016.080.093 Published online by Cambridge University Press

polytype, layers stack along **y** so that Te1 chains of successive layers superpose, but the polarity along **x** reverses from layer to layer. In the *C*2*cm* polytype, there is a displacement of $\frac{1}{2}a$ between adjacent layers, but the polarity is the same for all of them. The β and α polymorphs of $[Hg_2^{2+}(Te^{4+}Te^{6+}O_7)]$ (**#693–694**) also have Te–O layers with the topology of Fig. 15*h*. The layer in the β phase is corrugated very similarly to that of **#688–692**, while that of the α phase is much flatter, as the Te^{6+} octahedra are connected through *trans* corners. The β phase (**#693**) has layers ∥ (002), with chains of Te^{6+} running ∥ **x**. There are five types of Hg atoms between the layers, linking them into a framework. All Hg atoms have two close oxygen neighbours at 2.03–2.31 Å. However, while there is a distinct gap in distances before next-nearest neighbours for Hg1, Hg2 and Hg4, this is not true for Hg3 or Hg5, which have six neighbours in the ranges 2.24–2.38 and 2.30–2.36 Å, respectively (Fig. 45). This wide range of stereochemistries for Hg in the same compound is not unusual. Mercury and Te atoms form approximately close-packed layers ∥ (080), which form two repeats of the four-layer *ABCB* sequence along **y**. Within each layer, Te and Hg alternate in the **z** direction, while Te^{4+} and Te^{6+} alternate along **y** in the corrugated Te layers. In the α phase (**#694**), layers are ∥ $(20\bar{2})$ with Te^{6+} chains ∥ **y**. Mercury atoms between the layers are of four different types, each with two close oxygen neighbours at 2.05–2.28 Å and no more until 2.40–2.73 Å. Mercury and Te atoms lie on a *ccp* array, ordered layer-wise in a CuAu-type fashion. Cubic pseudocell edge vectors are [¼½¼] and [¼ $\bar{1}$/2¼] (5.20 Å long) and [¼0 $\bar{1}$/4] (5.43 Å), with layers of Hg and Te alternating ∥ $(20\bar{2})$ and Te^{4+} and Te^{6+} alternating along [101] within the Te layers.

$[Te_3^{4+}Te^{6+}O_9]$ (**#695**) has a rhombohedral structure with layers ∥ (003) of the form shown in Fig. 15*i*. Rings of six Q^{0400} Te^{4+} polyhedra surround ⅓ of the triad axes, which are linked through Q^{0600} Te^{6+} octahedra which are located on the remaining triads. The resulting net has 3-, 4- and 6-rings, such that the ring pattern around Te^{4+} is 6.3.4.3, while that around Te^{6+} is 3.4.3.4.3.4. Layers are held together only through long $Te^{4+}\cdots O$ bonds (Fig. 45).

$[Te^{4+}Te^{6+}O_5]$ (**#696**), like **#695**, has CN4 Te^{4+} and CN6 Te^{6+} sharing all vertices of their coordination polyhedra, but for this compound, the resulting structure is a three-dimensional framework (Fig. 16*a*). The Te^{6+} octahedra (Te1) share four vertices with other Te^{6+} cations to form sheets of 4-rings ∥ (001), as found in **#668–670**. Half of the Te–O–Te links in these sheets are decorated by Te^{4+} (Te2) so as to form (Te1–Te1–Te2) 3-rings, which define loop-branched *zweier* chains (cf. **#681**) running ∥ **y**. The Te2 cations associated with adjacent Te1 sheets then share remaining ligands with each other to link the sheets together; thus, the Te2 polyhedra in isolation form corner-sharing chains with a massicot-like geometry (Hill, 1985) (Fig. 45).

Carlfriesite, $Ca[Te_2^{4+}Te^{6+}O_8]$ (**#697**) has a nanoporous framework that contains loop-branched *vierer* chains of 4-rings, with Q^{2400} Te^{6+} at the nodes linked through Te^{4+} on the loops, that run ∥ **z** and are flattened ∥ (010). A centred-rectangular array of such chains is linked by Te^{4+} of neighbouring chains sharing edges to form a framework with ~6 Å wide channels ∥ **z**, which contain CN8 Ca^{2+} ions (Fig. 16*b*) (Fig. 46). The Sr analogue, $Sr[Te_2^{4+}Te^{6+}O_8]$ (**#698**) has a quite different tetragonal structure which contains chains of 'double-triangle' clusters similar to those in **#679** above (Fig. 15*a*). These chains run ∥ **z** and share corners to produce a framework with narrow (~4 Å) channels, which contain CN8 Sr^{2+} ions (Fig. 16*c*).

The remaining structures all feature Te polyhedra that share corners to form the hexagonal tungsten bronze or kagome net of hexagons and triangles, and all have at least one ~7.3 Å unit-cell parameter which corresponds to the repeat unit of that net. $Ag_2[Te_2^{4+}Te_2^{6+}O_{11}]$ (**#699**) has a strongly pseudo-hexagonal but intrinsically triclinic structure. Te1 and Te2 (CN6 Te^{6+}) and Te3 (CN5 Te^{4+}) form two layers of kagome type ∥ (001), which share corners but are offset relative to each other. These double layers are then linked into a framework via edge-sharing Te4 = Te4 dimers of CN5 Te^{4+}, which form additional 3-rings with Te1 and Te3 above and below (Fig. 16*d*). The Ag^+ ions, in irregular 6–8 coordination, lie in the hexagonal rings of the kagome layers, and between rows of Te4 atoms (Fig. 46). $Cs_2[Te^{4+}Te_3^{6+}O_{12}]$ (**#700**) has a rhombohedrally distorted pyrochlore framework (Fig. 16*e*). Both valence states of Te are in nearly regular octahedral coordination, which is extremely unusual for Te^{4+}, although it is also found in the pyrochlore $Pr_2[Te_2^{4+}O_6]O$ (**#366** above). Note that the lone pair of electrons is not stereochemically active in these compounds. When it occurs, stereoactivity usually causes strong distortion of the $Te^{4+}O_6$ polyhedra (cf. Christy and Mills, 2013). Ordering of Te^{4+} and Te^{6+} in the octahedral sites is the cause of the symmetry reduction from cubic. As is typical for 'inverse pyrochlores', the very large

https://doi.org/10.1180/minmag.2016.080.093 Published online by Cambridge University Press

TABLE 27. Unit-cell data and references for additional minerals, where no structure refinement is available.

Compound (Mineral name)	SG	*a*/Å	*b*/Å	*c*/Å	α, β, γ/°	Reference
$Mg_{0.5}[(Mn^{2+}\ Fe^{3+})(Te^{4+}O_3)_3] \cdot 4.5H_2O$ (Kinichilite)	$P6_3/m$	9.451(7)	9.451(7)	7.687(9)	90, 90, 120	Miletich (1995*a*)
$Mg_{0.5}[(Ni^{2+}\ Fe^{3+})(Te^{4+}O_3)_3] \cdot 4.5H_2O$ (Keystoneite)	$P6_3/m$ or $P6_3$	9.344(2)	9.344(2)	7.607(3)	90, 90, 120	Miletich (1995*a*)
$Mg_{0.5}[(Zn^{2+}\ Mn^{3+})(Te^{4+}O_3)_3] \cdot 4.5H_2O$ (Ilirneyite)	$P6_3/m$	9.40(2)	9.40(2)	7.657(17)	90, 90, 120	Pekov *et al.* (2015)
$Cu(Te^{4+}O_3) \cdot 2H_2O$ (Millsite)	$P2_1/c$	7.4049(2)	7.7873(2)	8.5217(2)	90, 110.203(3), 90	Rumsey *et al.* (2016)
$[Fe_2^{3+}(H_2O)_3(Te^{4+}O_3)_3] \cdot 3H_2O$ (Telluromandarinoite)	$P2_1/c$	16.9356(5)	7.8955(3)	10.1678(3)	90, 98.006(1), 90	Back *et al.* (2011)
$(K_{1.5}\square_{0.5})[(Te_{1.25}^{4+}W_{0.25}^{6+}\square_{0.5})W_5^{6+}O_{19}]$ (Tewite)	*Pban*	7.2585(4)	25.8099(15)	3.8177(2)	90, 90, 90	Li *et al.* (2014)
$PbMn^{4+}(Te^{6+}O_6)$ (Kuranakhite)	orth. *C?*	5.11(1)	8.91(1)	5.32(1)	90, 90, 90	Yablokova *et al.* (1975)
$Ca_2Mn_2^{4+}\ (Te^{6+}O_6)_2 \cdot H_2O$ (Xocolatlite)	*P*2/*m*, *P*2, or *Pm*	10.757(3)	4.928(3)	8.492(2)	90, 102.39(3), 90	Grundler *et al.* (2008)
$Pb_3[Zn_3(TeO_6)(VO_4)_2]$ (Cheremnykhite)	orth. *C?*	8.58(3)	14.86(5)	5.18(3)	90, 90, 90	Kim *et al.* (1990)
$Pb_2[Cu_2(Te_2^{6+}O_{10})] \cdot 2H_2O$ (Andychristyite)	$P\bar{1}$	5.322(3)	7.098(4)	7.511(4)	83.486(7), 76.279(5), 70.742(5)	Kampf *et al.* (2016)

Cs^+ cation occupies the *Y* site of the $A_2B_2X_2Y$ pyrochlore pattern, while the CN8 *A* sites are vacant. The K analogue of **#700**, $K_2[Te^{4+}Te^{6+}_3O_{12}]$ (**#701**) has a variant of the same structure that is monoclinically sheared. The monoclinic cell axes correspond to the hexagonal axes of **#700** as follows: $\mathbf{a}_{mon} = [1\bar{1}0]_{hex}$, $\mathbf{b}_{mon} = \mathbf{b}_{hex}$, $\mathbf{c}_{mon} = [⅓\bar{⅓}⅔]_{hex}$. The distortion reduces the coordination number of Te^{4+} from 6 to 5 (Fig. 16*f*), which allows the lone pair to become stereoactive, and the coordination number of K^+ decreases from 12 to 10. The compound $(Na_{1.6}Ag_{0.4})[Te^{4+}_2Te^{6+}_3O_{14}]$ (**#702**) has kagome layers of Te^{6+} octahedra ∥ (100), which are linked through corner-sharing dimers of CN4 Te^{4+} polyhedra (Fig. 16*g*) in a manner reminiscent of the linkage via edge-sharing CN5 dimers in **#699** above. Again, the Te^{4+} dimers form 3-rings with pairs of Te^{6+} octahedra in the kagome layers above and below, and weakly bound 8-coordinated cations (Na,Ag) lie in the hexagonal holes of the kagome net and between the Te^{4+} dimers. The ordered distribution of the interlayer (Na,Ag) and an associated undulation of the kagome layers results in the very long (~25 Å) *b* repeat (Fig. 46). $Rb_4[Te^{4+}_3Te^{6+}_5O_{23}]$ (**#703**) has a defect pyrochlore superstructure. Intact kagome layers of mixed Te^{4+} and Te^{6+} polyhedra occur ∥ (220) and (2$\bar{2}$0) of the orthorhombic cell. However, there are also modified kagome layers ∥ (201) and (20$\bar{1}$), with some oxygen atoms missing so as to allow reduction of the Te^{4+} coordination number from 6 to 5, and to provide space for accommodation of the stereoactive lone pairs (Fig. 16*h*). CN8–10 Rb^+ ions occupy the large interstices in the framework.

Additional tellurium oxyminerals

In the section above on zemannite and related compounds (**#131–136**), we mentioned the minerals kinichilite, keystoneite and ilirneyite as isostructural with zemannite itself, although their crystal structures have not been published. For completeness, the available data on these species are included in Table 27, along with several other minerals for which refinements are not yet available, but for which some structural details can be deduced. Such species could not be included in the classification above, as quantitative bond-distance data are not available.

Millsite, $Cu(Te^{4+}O_3) \cdot 2H_2O$ (Rumsey *et al*., 2016), is a new dimorph of teineite (**#119**) with a unique structure in which TeO_3^{2-} pyramids cross-link $Cu_2O_2(H_2O)_4$ dimers to form a two-dimensional layer. Telluromandarinoite $Fe^{3+}_2(Te^{4+}O_3)_3 \cdot 6H_2O$ (Back *et al*., 2011), is the Te analogue of the selenite mineral mandarinoite, and has similar symmetry and unit-cell dimensions. If the two minerals are isostructural, then two symmetrically distinct $[TeO_3]^{2-}$ pyramids share corners with FeX_6 octahedra to form layers ∥ (100) with 8-rings of alternating Fe and Te, which are bridged by a third type of TeO_3 group to form a very open $[M_2Y_3(TeX_3)_3]$ framework with additional water molecules in large cavities (cf. Hawthorne, 1984). Such a structure would follow $Sb^{5+}_2O_3(TeO_3)_2$ (**#147**) in our tables. The full description has not yet been published for the mineral tewite, $(K_{1.5}□_{0.5})[(Te^{4+}_{1.25}W^{6+}_{0.25}□_{0.5})W^{6+}_5O_{19}]$, but the W-rich composition suggests that it is a tungsten bronze-like phase containing layers of corner-sharing WO_6 octahedra, with layers oriented normal to the very short (3.8 Å) *c* repeat, along which W–O–W links connect them into a framework. There may be some modification of the kagome net due to replacement of some W by Te^{4+} with stereoactive lone-pair electrons, as in structures **#699–703** above. Note in particular that $a \approx 7.3$ Å and $b \approx 25.8$ Å are very similar to $a \approx 7.3$ Å and $b \approx 24.7$ Å for $(Na_{1.6}Ag_{0.4})[Te^{4+}_2Te^{6+}_3O_{14}]$ (**#702**). However, tewite contains only Te^{4+}. It cannot be placed more precisely in our classification without knowledge of the coordination environment of the Te atoms.

Kuranakhite, $PbMn^{4+}(Te^{6+}O_6)$, is a long-known mineral (Yablokova *et al*., 1975) whose structure has never been fully determined. However, its unit cell parameters suggest that it is structurally related to the $Li_2[M^{4+}(TeO_6)]$ phases **#583–585**, based upon a *hcp* array of oxygen atoms, but with one Pb^{2+} replacing two Li^+ ions. Grundler *et al*. (2008) suggested that the hydrated Ca analogue xocolatlite was structurally related to kuranakhite, which seems feasible. Cheremnykhite, $Pb_3[Zn_3(TeO_6)(VO_4)_2]$, was noted earlier as probably isotypical with dugganite and kuksite (**#550–551**), on the basis of its stoichiometry and unit-cell dimensions. However, although it has a strongly pseudo-hexagonal unit-cell metric with $b = \sqrt{3}a$, note that its symmetry is reported as orthorhombic, *Cmmm*, *Cmm*2, *Cm*2*m* or *C*222. None of these can be correct if the symmetry is a subgroup of the *P*321 space group exhibited by **#550–551**. Such a relationship would imply that cheremnykhite is actually monoclinic *C*211, with $\alpha \approx 90°$. Andychristyite, $Pb_2[Cu_2(Te^{6+}_2O_{10})] \cdot 2H_2O$ (Kampf *et al*., 2016), is a new mineral that is chemically the Pb analogue of eckhardite (**#639**). However, although the structures of the two minerals are related, they are not the same. Both contain

https://doi.org/10.1180/minmag.2016.080.093 Published online by Cambridge University Press

edge-sharing $[Te_2O_{10}]^{8-}$ dimers, and both have structure units based upon stepped oblique slices through a *hcp* anion array (cf. **#512–515**), but the component ribbons of the slices and disposition of the Te=Te dimers are different.

There remain several Te minerals for which structures have never been determined, and even the true valence state of Te remains unknown. This is the case even for apparently simple species such as cesbronite, $Cu_5(Te^{4+}O_3)_2(OH)_6 \cdot 2H_2O$ (Williams, 1974) and xocometatlite, $Cu_3Te^{6+}O_4(OH)_4$ (Williams, 1975). As these minerals become better characterized and additional natural and synthetic Te oxycompounds are discovered, the diversity of known structures is likely to increase. However, the dataset and classification of the present study are sufficiently large to provide a robust framework into which new structural architectures can be fitted.

Acknowledgements

We thank Mark Welch and Sergey Krivovichev for their helpful comments on the manuscript and Helen Kerbey for all her help with setting up the article for publication. This study has been funded by The Ian Potter Foundation grant "tracking tellurium" to SJM which is gratefully acknowledged.

References

Abdelhedi, M., Dammak, M., Cousson, A. and Kolsi, A. W. (2005) Structural, calorimetric and conductivity study of the new mixed solution $Rb_2(SO_4)_{0.5}(SeO_4)_{0.5}Te(OH)_6$. *Journal of Alloys and Compounds*, **398**, 55–61.

Ahmed, M.A., Fjellvåg, H. and Kjekshus, A. (2000) Synthesis, structure and thermal stability of tellurium oxides and oxide sulfate formed from reactions in refluxing sulfuric acid. *Dalton Transactions*, **24**, 4542–4549.

Ajaz, H., Deiseroth, H.J., Schlosser, M. and Rabbani, F. (2009) Synthesis and crystal structure of indium tellurium trioxide bromide. *Synthesis and Reactivity in Inorganic, Metal-Organic, and Nano-Metal Chemistry*, **39**, 209–210.

Al Ansari, S.V., Al Ansari, Ya.F., Chumakov, V.M., Albov, D.V., Savinkina, E.V., Davydova, M.N. and Tsivadze, A.Y. (2007) Synthesis and structure of the stoichiometric sodium bis(dihydrotellurato)cuprate(III) $Na_5[Cu(H_2TeO_6)_2] \cdot 16(H_2O)$. *Kristallografiya*, **52**, 256–258.

Alcock, N.W. and Harrison, W.D. (1982) Refinement of the structure of tellurium phosphate $Te_2O_3 \cdot HPO_4$. *Acta Crystallographica*, **B38**, 1809–1811.

Allmann, R. (1976) $Te(OH)_6 \cdot NaF$, eine Struktur mit kurzen OH···F-Wasserstoffbrücken. *Acta Crystallographica*, **B32**, 1025–1028.

Allmann, R. and Haase, W. (1976) Crystal structure of an adduct of telluric acid with potassium fluoride, $Te(OH)_6 \cdot 2KF$. A compound with short oxygen-hydrogen···fluorine hydrogen bonds. *Inorganic Chemistry*, **15**, 804–807.

Almond, P.M. and Albrecht Schmitt, T.E. (2002) Expanding the remarkable structural diversity of uranyl tellurites: hydrothermal preparation and structures of $K(UO_2Te_2O_5(OH))$, $Tl_3((UO_2)_2(Te_2O_5(OH))(Te_2O_6)) \cdot 2(H_2O)$, β-$Tl_2(UO_2(TeO_3)_2)$ and $Sr_3(UO_2(TeO_3)_2)(TeO_3)_2$. *Inorganic Chemistry*, **41**, 5495–5501.

Almond, P.M., McKee, M.L. and Albrecht Schmitt, T.E. (2002) Unusual uranyl tellurites containing $(Te_2O_6)^{4-}$ ions and three-dimensional networks. *Angewandte Chemie, International Edition*, **41**, 3426–3429.

Alonso, J.A., Castro, A., Enjalbert, R., Galy, J. and Rasines, I. (1992) The quadruple chains of SbO_6 octahedra in $Sb_2Te_2O_9$: an example of low extent of aggregation of pentavalent antimony polyhedra. *Dalton Transactions*, **17**, 2551–2557.

An, Y., Mosbah, A., Le Gal La Salle, A., Guyomard, D., Verbaere, A. and Piffard, Y. (2001) $K_2[Te_4O_8(OH)_{10}]$: synthesis, crystal structure and thermal behavior. *Solid State Sciences*, **3**, 93–101.

Anders, E. and Ebihara, M. (1982) Solar system abundances of the elements. *Geochimica et Cosmochimica Acta*, **46**, 2363–2380.

Andersen, L. and Moret, J. (1983) Dipotassium ditellurium (IV) pentaoxide trihydrate, $K_2Te_2O_5 \cdot 3H_2O$. *Acta Crystallographica*, **C39**, 143–145.

Andersen, L., Lindqvist, O. and Moret, J. (1984) The structures of magnesium tellurate (IV) hexahydrate, $MgTeO_3 \cdot 6H_2O$, and magnesium selenate (IV) hexahydrate, $MgSeO_3 \cdot 6H_2O$. *Acta Crystallographica*, **C40**, 586–589.

Andersen, L., Langer, V., Stromberg, A. and Stromberg, D. (1989) The structure of K_2TeO_3 – an experimental and theoretical study. *Acta Crystallographica*, **B45**, 344–348.

Anderson, J.B., Rapposch, M.H., Anderson, C.P. and Kostiner, E. (1980) Crystal structure refinement of basic tellurium nitrate: A reformulation as $(Te_2O_4H)^+(NO_3)^-$. *Monatshefte für Chemie/Chemical Monthly*, **111**, 789–796.

Anderson, J.S. (1937) Constitution of the poly-acids. *Nature*, **140**, 850.

Andersson, S. (1978) Structures related to the β-tungsten or Cr_3Si structure type. *Journal of Solid State Chemistry*, **23**, 191–204.

Andrade, M.B., Yang, H., Downs, R.T., Jenkins, R.A. and Fay, I. (2014) Te-rich raspite, $Pb(W_{0.56}Te_{0.44})O_4$, from Tombstone, Arizona, U.S.A: the first natural

https://doi.org/10.1180/minmag.2016.080.093 Published online by Cambridge University Press

example of Te^{6+} substitution for W^{6+}. *American Mineralogist*, **99**, 1507–1510.

Andreae, M.O. (1984) Determination of inorganic tellurium species in natural waters. *Analytical Chemistry*, **56**, 2064–2066.

Arnaud, Y., Averbuch-Pouchot, M.T., Durif, A. and Guidot, J. (1976) Structure cristalline de l'oxyde mixte de molybdène-tellure: $MoTe_2O_7$. *Acta Crystallographica*, **B32**, 1417–1420.

Artner, C. and Weil, M. (2012) $Pb_6Co_9(TeO_6)_5$. *Acta Crystallographica*, **E68**, i71–i71.

Artner, C. and Weil, M. (2013) Re-examination of Pb_3TeO_6: Determination of its correct composition as Pb_5TeO_8. *Journal of Solid State Chemistry*, **199**, 240–247.

Astier, R., Philippot, E., Moret, J. and Maurin, M. (1979) Evolution de la coordination des atomes de tellure IV et de fer III dans les composés du système Fe_2O_3–TeO_2. *Revue de Chimie Minerale*, **13**, 359–372.

Augsburger, M.S., Viola, M.C., Pedregosa, J.C., Munoz, A., Alonso, J.A. and Carbonio, R.E. (2005) Preparation, crystal and magnetic structures of two new double perovskites: Ca_2CoTeO_6 and Sr_2CoTeO_6. *Journal of Materials Chemistry*, **15**, 993–1001.

Averbuch-Pouchot, M.T. (1980) Structure d'un phosphate tellurate de sodium: $Te(OH)_6 \cdot Na_2HPO_4 \cdot NaH_2PO_4$. *Acta Crystallographica*, **B36**, 2405–2406.

Averbuch-Pouchot, M.T. (1983) Crystal chemistry of some addition compounds of alkali iodates with telluric acid. *Journal of Solid State Chemistry*, **49**, 368–378.

Averbuch-Pouchot, M.T. (1984) Crystal structure of $Te(OH)_6 \cdot 2KNO_3 \cdot 2H_2O$: an addition compound of telluric acid. *Zeitschrift für Kristallographie*, **167**, 247–252.

Averbuch-Pouchot, M.T. (1988*a*) Structure of a new adduct between telluric acid and a condensed phosphate: $Cs_3P_3O_9 \cdot Te(OH)_6 \cdot H_2O$. *Acta Crystallographica*, **C44**, 1166–1168.

Averbuch-Pouchot, M.T. (1988*b*) Crystal structure of a new telluric acid adduct: $Te(OH)_6 \cdot 2CsCl$. *Zeitschrift für Kristallographie*, **182**, 291–295.

Averbuch-Pouchot, M.T. and Durif, A. (1981) Crystal data for two new phosphate-tellurates: $Te(OH)_6(Tl(H_2PO_4))_2(Tl_2(HPO_4))$ and $Te(OH)_6(Tl(H_2PO_4))_2$. *Materials Research Bulletin*, **16**, 71–76.

Averbuch-Pouchot, M.T. and Durif, A. (1983) Structure of a potassium diphosphate tellurate hydrate, $K_3HP_2O_7 \cdot Te(OH)_6 \cdot H_2O$. *Acta Crystallographica*, **C39**, 27–28.

Averbuch-Pouchot, M.T. and Durif, A. (1987*a*) Structure of a new adduct between telluric acid and a condensed phosphate: $K_4P_4O_{12} \cdot Te(OH)_6 \cdot 2H_2O$. *Acta Crystallographica*, **C43**, 1245–1247.

Averbuch-Pouchot, M.T. and Durif, A. (1987*b*) Crystal structure of a new adduct between telluric acid and alkali cyclo-triphosphates: $Te(OH)_6 \cdot Na_3P_3O_9 \cdot K_3P_3O_9$. *Acta Crystallographica*, **C43**, 1653–1655.

Averbuch-Pouchot, M.T. and Durif, A. (1989) Determination des liaisons hydrogène dans le compose d'addition urée-acide tellurique: $Te(OH)_6(CO(NH_2)_2)_2$. *Comptes Rendus Hebdomadaires des Séances de l'Academie des Sciences, Serie C*, **309**, 25–28.

Averbuch-Pouchot, M.T. and Durif, A. (1990) Crystal chemistry of cyclo-hexaphosphates. VI. Structure of ammonium cyclo-hexaphosphate tellurate dihydrate. *Acta Crystallographica*, **C46**, 179–181.

Averbuch-Pouchot, M.T. and Durif, A. (1991) Crystal chemistry of cyclo-hexaphosphates. XVI. Structures of potassium cyclo-hexaphosphate ditellurate trihydrate and rubidium cyclo-hexaphosphate tritellurate tetrahydrate. *Acta Crystallographica*, **C47**, 1576–1579.

Averbuch-Pouchot, M.T. and Durif, A. (1992) Structure of an adduct between diammonium dihydrogendiphoshate and telluric acid: $(NH_4)_2H_2P_2O_7 \cdot Te(OH)_6$. *Acta Crystallographica*, **C48**, 973–975.

Averbuch-Pouchot, M.T. and Durif, A. (1993*a*) Ammonium cyclo-octaphosphate-telluric acid dihydrate adduct. *Acta Crystallographica*, **C49**, 361–363.

Averbuch-Pouchot, M.T. and Durif, A. (1993*b*) $Cs_2H_2P_2O_7 \cdot Te(OH)_6$, a new adduct between a diphosphate and telluric acid. *European Journal of Solid State Inorganic Chemistry*, **30**, 1153–1162.

Averbuch-Pouchot, M.T. and Schuelke, U. (1996) Preparation and crystal structure of guanidinium cyclododecaphosphate telluric acid hydrate: $(C(NH_2)_2)_{12}P_{12}O_{36} \cdot 12Te(OH)_6 \cdot 24H_2O$. *Zeitschrift für anorganische und allgemeine Chemie*, **622**, 1997–2002.

Averbuch-Pouchot, M.T., Durif, A. and Guitel, J.C. (1979) Structure cristalline d'un phospho-tellurate de rubidium: $Te(OH)_6Rb_2(HPO_4)Rb(H_2PO_4)$. *Materials Research Bulletin*, **14**, 1219–1223.

Averbuch-Pouchot, M.T., Durif, A. and Guitel, J.C. (1980) Crystal structures of two cesium phosphate-tellurates: $(Te(OH)_6)(Cs_2HPO_4)$ and $(Te(OH)_6)(Cs_2HPO_4)(CsH_2PO_4)_2$. *Materials Research Bulletin*, **15**, 387–395.

Ayed, B. and Haddad, A. (2013) The crystal structure of potassium ammonium hexamolybdotellurate with telluric acid $K_5NH_4(TeMo_6O_{24}) \cdot Te(OH)_6 \cdot 6H_2O$. *Comptes Rendus Chimie*, **16**, 114–121.

Babel, D. (1967) Structural chemistry of octahedral fluorocomplexes of the transition elements. *Structure and Bonding*, **3**, 1–87.

Back, M.E., Grice, J.D., Gault, R.A., Criddle, A.J. and Mandarino, J.A. (1999) Walfordite, a new tellurite species from the Wendy open pit, El Indio-Tambo mining property, Chile. *The Canadian Mineralogist*, **37**, 1261–1268.

Back, M.E., Grice, J.D., Sturman, B.D., Cooper, M.A., Gault, R.A. and Walford, P.C. (2011) Telluromandarinoite, IMA 2011-013. CNMNC Newsletter No. 10, October 2011, page 2551. *Mineralogical Magazine*, **75**, 2549–2561.

Baker, L.C.W. and Figgis, J.S. (1970) A new fundamental type of inorganic complex: hybrid between the

https://doi.org/10.1180/minmag.2016.080.093 Published online by Cambridge University Press

heteropoly and conventional coordination complexes. Possibilities for geometrical isomerism in 11-, 12-, 17- and 18-heteropoly derivatives. *Journal of the American Chemical Society*, **92**, 3794–3797.

Baldinozzi, G., Grebille, D., Sciau, P., Kiat, J.M., Moret, J. and Berar, J.F. (1998) Rietveld refinement of the incommensurate structure of the elpasolite (ordered perovskite) Pb_2MgTeO_6. *Journal of Physics: Condensed Matter*, **10**, 6461–6472.

Balraj, V. and Vidyasagar, K. (1998) Low-temperature syntheses and characterization of novel layered tellurites, $A_2Mo_3TeO_{12}$ ($A = NH_4$, Cs), and "zero-dimensional" tellurites, $A_4Mo_6Te_2O_{24} \cdot 6H_2O$ (A = Rb, K). *Inorganic chemistry*, **37**, 4764–4774.

Balraj, V. and Vidyasagar, K. (1999*a*) Hydrothermal synthesis and characterization of novel one-dimensional tellurites of molybdenum (VI), $A_4Mo_6TeO_{22} \cdot 2H_2O$ ($A = NH_4$, Rb). *Inorganic Chemistry*, **38**, 1394–1400.

Balraj, V. and Vidyasagar, K. (1999*b*) Hydrothermal synthesis and characterization of a novel two-dimensional tellurite of molybdenum (VI), $(NH_4)_6Mo_8Te_8O_{43}(H_2O)$. *Inorganic Chemistry*, **38**, 3458–3462.

Balraj, V. and Vidyasagar, K. (1999*c*) Syntheses and characterization of novel three-dimensional tellurites, $Na_2MTe_4O_{12}$ (M = W, Mo), with intersecting tunnels. *Inorganic Chemistry*, **38**, 5809–5813.

Bartram, S.F. (1966) Crystal structure of the rhombohedral $MO_3 \cdot 3R_2O_3$ compounds (M = U, W or Mo) and their relation to ordered R_7O_{12} phases. *Inorganic Chemistry*, **5**, 749–754.

Basciano, L.C., Peterson, R.T., Roeder, P.L. and Swainson, I. (1998) Description of schoenfliesite, $MgSn(OH)_6$, and roxbyite, $Cu_{1.72}S$, from a 1375 BC shipwreck, and Rietveld neutron-diffraction refinement of synthetic schoenfliesite, wickmanite $MnSn(OH)_6$ and burtite, $CaSn(OH)_6$. *The Canadian Mineralogist*, **36**, 1203–1210.

Basso, R., Lucchetti, G., Zefiro, L. and Palenzona, A. (1996) Rosiaite, $PbSb_2O_6$, a new mineral from the Cetine mine, Siena, Italy. *European Journal of Mineralogy*, **8**, 487–492.

Bats, J.W. (1978) A refinement of potassium chlorate. *Acta Crystallographica*, **B34**, 1679–1681.

Bazuev, G.V., Golovkin, G.V., Zubkov, V.G. and Tyutyunnik, A.S. (1994) Synthesis, crystal structure, and magnetic properties of complex oxides Cu_2BSbO_6 (B = Mn,Fe,Ga) with a bixbyite structure. *Journal of Solid State Chemistry*, **113**, 132–137.

Becker, R. and Berger, H. (2006*a*) Reinvestigation of Ni_3TeO_6. *Acta Crystallographica*, **E62**, i222–i223.

Becker, R. and Berger, H. (2006*b*) Cu_2CoTeO_6. *Acta Crystallographica*, **E62**, i261–i262.

Becker, R. and Johnsson, M. (2004) Crystal structure of the new compound $Co_6(TeO_3)_2(TeO_6)Cl_2$. *Solid State Sciences*, **6**, 519–522.

Becker, R. and Johnsson, M. (2007) Three new tellurite halides with unusual Te^{4+} coordinations and iron honeycomb lattice variants. *Journal of Solid State Chemistry*, **180**, 1750–1758.

Becker, R. and Mats, J. (2005) Crystal structure of $Cu_3Bi(TeO_3)_2O_2Cl$: a Kagome lattice type compound. *Solid State Sciences*, **7**, 375–380.

Becker, C.R., Tagg, S.L., Huffman, J.C. and Zwanziger, J. W. (1997) Crystal structures of potassium tetratellurite, $K_2Te_4O_9$, and potassium ditellurite, $K_2Te_2O_5$, and structural trends in solid alkali tellurites. *Inorganic Chemistry*, **36**, 5559–5564.

Becker, R., Johnsson, M., Kremer, R. and Lemmens, P. (2003) Crystal structure, magnetic properties and conductivity of $CuSbTeO_3Cl_2$. *Solid State Sciences*, **5**, 1411–1416.

Becker, R., Johnsson, M., Kremer, R. and Lemmens, P. (2005) Crystal structure and magnetic properties of $Cu_3(TeO_3)_2Br_2$ – a layered compound with a new Cu (II) coordination polyhedron. *Journal of Solid State Chemistry*, **178**, 2024–2029.

Becker, R., Berger, H., Johnsson, M., Prester, M., Morohnic, Z., Miljak, M. and Herak, R. (2006*a*) Crystal structure and magnetic properties of $Co_2TeO_3Cl_2$ and $Co_2TeO_3Br_2$. *Journal of Solid State Chemistry*, **179**, 836–842.

Becker, R., Johnsson, M., Berger, H., Prester, M., Zivkovic, I., Drobac, D., Miljak, M. and Herak, R. (2006*b*) Crystal structure and magnetic properties of $Co_7(TeO_3)_4Br_6$ – a new cobalt tellurite bromide. *Solid State Sciences*, **8**, 836–842.

Becker, R., Prester, M., Berger, H., Johnsson, M., Drobac, D. and Zivkovic, I. (2007*a*) Crystal structure and magnetic properties of the new cobalt tellurite halide $Co_5(TeO_3)_4X_2$ (X = Cl, Br). *Solid State Sciences*, **9**, 223–230.

Becker, R., Johnsson, M. and Berger, H. (2007*b*) Crystal structure of the new cobalt tellurite chloride $Co_5Te_4O_{11}Cl_4$. *Zeitschrift für anorganische und allgemeine Chemie*, **633**, 422–424.

Benmiloud, L., Moret, J., Maurin, M. and Philippot, E. (1980) Structure d'un tellurate d'ammonium: $NH_4TeO_3(OH)$. *Acta Crystallographica*, **B36**, 139–141.

Benmiloud, L., Maurin, M., Moret, J. and Philippot, E. (1981) Étude cristallographique d'un tellurite d'ammonium: $(NH_4)_2Te_4O_9$. *Revue de Chimie Minerale*, **18**, 190–198.

Berand, N. and Range, K.J. (1994) Single-crystal structure refinement of the trirutile-type compound Ga_2TeO_6. *Journal of Alloys and Compounds*, **205**, 3–5.

Berdonosov, P.S., Dolgikh, V.A. and Lightfoot, P. (2007) The crystal structure of a new bismuth tellurium oyxchloride $Bi_{0.87}Te_2O_{4.9}Cl_{0.87}$ from neutron powder diffraction data. *Journal of Solid State Chemistry*, **180**, 1533–1537.

https://doi.org/10.1180/minmag.2016.080.093 Published online by Cambridge University Press

Berger, S.V. (1988) The crystal structure of the isomorphous orthoborates of cobalt and magnesium. *Acta Chemica Scandinavica*, **3**, 660–675.

Beyer, H. (1967) Verfeinerung der Kristallstruktur von Tellurit, dem rhombischen TeO_2. *Zeitschrift für Kristallographie*, **124**, 228–237.

Bhuvanesh, N.S.P. and Halasyamani, P.S. (2001) Synthesis and characterization of $NaGaTe_2O_6 \cdot 2.4(H_2O)$: a new open-framework tellurite related to zemannite. *Inorganic Chemistry*, **40**, 1404–1405.

Bindi, L. and Cipriani, C. (2003) The crystal structure of winstanleyite, $TiTe_3O_8$, from the Grand Central Mine, Tombstone, Arizona. *The Canadian Mineralogist*, **41**, 1469–1473.

Bindi, L. and Pratesi, G. (2007) Centric or acentric crystal structure for natural schmitterite, $UTeO_5$? New evidence from a crystal from the type locality. *Mineralogy and Petrology*, **91**, 129–138.

Blanchandin, S., Champarnaud-Mesjard, J.C., Thomas, P. and Frit, B. (2000*a*) Crystal structure of $BiNbTe_2O_8$. *Solid State Sciences*, **2**, 223–228.

Blanchandin, S., Champarnaud-Mesjard, J.C., Thomas, P. and Frit, B. (2000*b*) Crystal structure of $Nb_2Te_4O_{13}$. *Journal of Alloys and Compounds*, **306**, 175–185.

Boher, P., Garnier, P., Gavarri, J.R. and Hewat, A.W. (1985) Monoxyde quadratique PbOα(I): description de la transition structurale ferroélastique. *Journal of Solid State Chemistry*, **57**, 343–350.

Bonaccorsi, E., Merlino, S. and Orlandi, P. (2007) Zincalstibite, a new mineral, and cualstibite: crystal chemical and structural relationships. *American Mineralogist*, **92**, 198–203.

Boren, B. (1933) X-ray investigation of alloys of silicon with chromium, manganese, cobalt and nickel. *Arkiv för Kemi, Mineralogi och Geologi*, **11A**, 2–10.

Bouchama, M. and Tournoux, M. (1975) Polytypisme de $TlSbO_3$. *Revue de Chimie Minérale*, **12**, 80–92.

Boudjada, N. and Durif, A. (1982) Structure d'un trimetaphosphate-tellurate de rubidium monohydrate: $Te(OH)_6 \cdot Rb_3P_3O_9 \cdot H_2O$. *Acta Crystallographica*, **B38**, 595–597.

Boudjada, N., Averbuch-Pouchot, M.T. and Durif, A. (1981*a*) Structure du trimetaphosphate-tellurate de sodium hexahydrate $Te(OH)_6 \cdot (Na_3P_3O_9)_2 \cdot (H_2O)_6$. *Acta Crystallographica*, **B37**, 645–647.

Boudjada, N., Averbuch-Pouchot, M.T. and Durif, A. (1981*b*) Structure d'un trimetaphosphate-tellurate de potassium dihydrate $Te(OH)_6 \cdot K_3P_3O_9 \cdot 2H_2O$. *Acta Crystallographica*, **B37**, 647–649.

Boujada, N., Boujada, A. and Guitel, J.C. (1983) Hexaammonium cyclo-triphosphate telluric acid. *Acta Crystallographica*, **C39**, 656–658.

Boukharrata, N.J., Thomas, P. and Laval, J.P. (2009) $GeTe_2O_6$, a germanium tellurate(IV) with an open framework. *Acta Crystallographica*, **C65**, i23–i26.

Boukharrata, N.J., Duclère, J.-R, Laval, J.P. and Thomas, P. (2013) A new oxyfluorotellurate(IV), $InTe_2O_5F$. *Acta Crystallographica*, **C69**, 460–462.

Bragg, W.L. (1930) The structure of silicates. *Zeitschrift fur Kristallographie*, **74**, 237–305.

Brandstätter, F. (1981) Synthesis and crystal structure determination, of $Pb_2[UO_2][TeO_3]_3$. *Zeitschrift für Kristallographie*, **155**, 193–200.

Brandt, B.G. and Skapski, A.C. (1967) A refinemnt of the crystal structure of molybdenum dioxide. *Acta Chemica Scandinavica*, **21**, 661–672.

Brese, N.E. and O'Keeffe, M. (1991) Bond-valence parameters for solids. *Acta Crystallographica*, **B47**, 192–197.

Brown, I.D. (1969) Crystal structures of $NaNiIO_6$, $NaMnIO_6$, and $KMnIO_6$. *Canadian Journal of Chemistry*, **47**, 3779–3782.

Brown, I.D. (2002) *The Chemical Bond in Inorganic Chemistry: The Bond Valence Model.* Oxford University Press, UK, 278 pp.

Brown, I.D. and Altermatt (1985) Bond-valence parameters obtained from a systematic analysis of the Inorganic Crystal Structure Database. *Acta Crystallographica*, **B41**, 244–247.

Brunton, G. (1973) Li_2ZrF_6. *Acta Crystallographica*, **B29**, 2294–2296.

Burckhardt, H.G., Platte, C. and Trömel, M. (1982) Cadmiumorthotellurat (VI) Cd_3TeO_6: ein pseudo-orthorhombischer Kryolith im Vergleich mit Ca_3TeO_6. *Acta Crystallographica*, **B38**, 2450–2452.

Burdett, J.K. and McLarnan, T.J. (1984) An orbital interpretation of Pauling's rules. *American Mineralogist*, **69**, 601–621.

Burns, P.C., Cooper, M.A. and Hawthorne, F.C. (1995) Parakhinite, $Cu_3^{2+}Pb^{6+}Te^{6+}O_6(OH)_2$; crystal structure and revision of chemical formula. *The Canadian Mineralogist*, **33**, 33–40.

Burns, P.C., Ewing, R.C. and Hawthorne, F.C. (1997) The crystal chemistry of hexavalent uranium: polyhedron geometries, bond-valence parameters, and polymerization of polyhedra. *The Canadian Mineralogist*, **35**, 1551–1570.

Burns, P.C., Pluth, J.J., Smith, J.V., Eng, P., Steele, I. and Housley, R.M. (2000) Quetzalcoatlite: A new octahedral-tetrahedral structure from a $2 \times 2 \times 40$ μm^3 crystal at the Advanced Photon Source-GSE-CARS Facility. *American Mineralogist*, **85**, 604–607.

Byström, A., Hok, B. and Mason, B. (1942) The crystal structure of zinc metantimonate and similar compounds. *Arkiv för Kemi, Mineralogi och Geologi*, **154B4**, 1–8.

Cachau-Herreillat, D., Norbert, A., Maurin, M. and Philippot, E. (1981) Étude cristallochimique comparée et conductivité ionique des deux variétés $Li_2Te_2O_5$ α et β. *Journal of Solid State Chemistry*, **37**, 352–361.

https://doi.org/10.1180/minmag.2016.080.093 Published online by Cambridge University Press

Cachau-Herreillat, D., Norbert, A., Maurin, M., Fourcade, R. and Philippot, E. (1983) Synthèse, étude structurale par rayons X et par spectrometrie infrarouge et Raman du tellurite basique Li_2TeO_3, LiOH. *Revue de Chimie Minerale*, **20**, 129–139.

Carbone, C., Basso, R., Cabella, R., Martinelli, A., Grice, J.D. and Lucchetti, G. (2013) Mcalpineite from the Gambatesa mine, Italy, and redefinition of the species. *American Mineralogist*, **98**, 1899–1905.

Chabchoub, N., Darriet, J. and Khemakhem, H. (2006) Structural and conductivity studies of $CsKSO_4Te(OH)_6$ and $Rb_{1.25}K_{0.75}SO_4Te(OH)_6$ materials. *Journal of Solid State Chemistry*, **179**, 2164–2173.

Champarnaud-Mesjard, J.C., Blanchandin, S., Thomas, P., Mirgorodsky, A., Merle-Mejean, T. and Frit, B. (2000) Crystal structure, Raman spectrum and lattice dynamics of a new metastable form of tellurium dioxide: γ-TeO_2. *Journal of Physics and Chemistry of Solids*, **61**, 1499–1507.

Champarnaud-Mesjard, J.C., Frit, B., Chagraoui, A. and Taïri, A. (1996*a*) New anion-excess, fluorite-related, ordered structure: $Bi_2Te_2W_3O_{16}$. *Journal of Solid State Chemistry*, **127**, 248–255.

Champarnaud-Mesjard, J.C., Frit, B., Chagraoui, A. and Taïri, A. (1996*b*) Crystal structure of a new cation-ordered fluorite-related phase: $Bi_2Te_2WO_{10}$. *Zeitschrift für anorganische und allgemeine Chemie*, **622**, 1907–1912.

Charushnikova, I.A., Yusov, A.B., Fedoseev, A.M. and Polyakova, I.N. (2004) F-element complexes with tellurometallate anions: I. The crystal structure of $Eu_2TeMo_6O_{24} \cdot 18(H_2O)$. *Zhurnal Neorganicheskoi Khimii*, **49**, 1481–1487.

Charushnikova, I.A., Fedoseev, A.M., Yusov, A.B. and Auwer, C.D. (2005) Crystal structure of a new neodymium hexamolybdotellurate, $Nd_2TeMo_6O_{24} \cdot 19H_2O$. *Kristallografiya*, **52**, 223–225.

Chi, E.O., Ok, K.M., Porter, Y. and Halasyamani, P.S. (2006) $Na_2Te_3Mo_3O_{16}$: A new molybdenum tellurite with second-harmonic generating and pyroelectric properties. *Chemistry of Materials*, **18**, 2070–2074.

Choisnet, J., Bizo, L., Allix, M., Rosseinsky, M.J. and Raveau, B. (2007) Cation ordering in the fluorite-like transparent conductors $In_{4+x}Sn_{3-2x}Sb_xO_{12}$ and In_6TeO_{12}. *Journal of Solid State Chemistry*, **180**, 1002–1010.

Choisnet, J., Rulmont, A. and Tarte, P. (1988) Les tellurates mixtes Li_2ZrTeO_6 et Li_2HfTeO_6: un nouveau phenomène d'ordre dans la famille corindon. *Journal of Solid State Chemistry*, **75**, 124–135.

Choisnet, J., Rulmont, A. and Tarte, P. (1989) Ordering phenomena in the $LiSbO_3$ type structure: The new mixed tellurates Li_2TiTeO_6 and Li_2SnTeO_6. *Journal of Solid State Chemistry*, **82**, 272–278.

Christy, A.G. (1993) Multistage diffusionless pathways for reconstructive phase transitions: application to binary compounds and calcium carbonate. *Acta Crystallographica*, **B49**, 987–996.

Christy, A.G. (2015) Causes of anomalous mineralogical diversity in the Periodic Table. *Mineralogical Magazine*, **79**, 33–49.

Christy, A.G. and Mills, S.J. (2013) Effect of lone-pair stereoactivity on polyhedral volume and structural flexibility: application to $Te^{IV}O_6$ octahedra. *Acta Crystallographica*, **B69**, 446–456.

Christy, A.G., Kampf, A.R., Mills, S.J., Housley, R.M. and Thorne, B. (2014) Crystal structure and revised chemical formula for burckhardtite, $Pb_2(Fe^{3+}Te^{6+})[AlSi_3O_8]O_6$: a double-sheet silicate with intercalated phyllotellurate layers. *Mineralogical Magazine*, **78**, 1763–1773.

Christy, A.G., Mills, S.J., Kampf, A.R., Housley, R.M., Thorne, B. and Marty, J. (2016) The relationship between mineral composition, crystal structure and paragenetic sequence: the case of secondary Te mineralization at the Bird Nest drift, Otto Mountain, California, USA. *Mineralogical Magazine*, **80**, 291–310.

Churakov, A.V., Ustinova, E.A., Prikhodchenko, P.V., Tripol'skaya, T.A. and Howard, J.A.K. (2007) Synthesis and crystal structure of new alkali metal hydrogen tellurates. *Zhurnal Neorganicheskoi Khimii*, **52**, 1605–1612.

Ciobanu, C.L., Cook, N.J. and Spry, P.G. (2006) Preface – Special Issue: telluride and selenide minerals in gold deposits–how and why? *Mineralogy and Petrology*, **87**, 163–169.

Cohen-Addad, C. (1977) Étude structurale des hydroxystannates $CaSn(OH)_6$ et $ZnSn(OH)_6$ par diffraction neutronique, absorption infrarouge et résonance magnétique nucléaire. *Bullétin de la Société Française de Minéralogie et de Cristallographie*, **91**, 315–324.

Colville, A.A., Anderson, C.P. and Black, P.M. (1971) Refinement of the crystal structure of apophyllite: I. X-ray diffraction and physical properties. *American Mineralogist*, **56**, 1222–1233.

Cook, N.J. and Ciobanu, C.L. (2005) Tellurides in Au deposits: implications for modelling. Pp. 1387–1390 in: *Mineral Deposit Research: Meeting the Global Challenge* (J.W. Mao and F.P. Bierlein, editors). Springer, Berlin Heidelberg New York.

Cooper, M.A. and Hawthorne, F.C. (1996) The crystal structure of spiroffite. *The Canadian Mineralogist*, **34**, 821–826.

Cooper, M.A., Hawthorne, F.C. and Back, M.E. (2008) The crystal structure of khinite and polytypism in khinite and parakhinite. *Mineralogical Magazine*, **72**, 763–770.

Coppens, P. and Eibschütz, M. (1965) Determination of the crystal structure of yttrium orthoferrite and

https://doi.org/10.1180/minmag.2016.080.093 Published online by Cambridge University Press

refinement of the structure of gadolinium orthoferrite. *Acta Crystallographica*, **19**, 524–531.

Corella-Ochoa, M.N., Miras, H.N., Kidd, A., Long, D.L. and Cronin, L. (2011) Assembly of a family of mixed metal (Mo:V) polyoxometalates templated by $(TeO_3)^{2-}$: $(Mo_{12}V_{12}Te_3)$, $(Mo_{12}V_{12}Te_2)$ and $(Mo_{17}V_8Te)$. *Chemical Communications*, **47**, 8799–8801.

Crosnier, M.P., Delarue, E., Choisnet, J. and Fourquet, J. L. (1992) Li^+/H^+ exchange on Li_2TiTeO_6. *European Journal of Solid State and Inorganic Chemistry*, **29**, 321–332.

Dammak, M., Khemakhem, H., Mhiri, T., Kolsi, A.W. and Daoud, A. (1998) Structure and characterization of a mixed crystal $Rb_2SO_4 \cdot Te(OH)_6$. *Journal of Alloys and Compounds*, **280**, 107–113.

Dammak, M., Khemakhem, H., Mhiri, T., Kolsi, A.W. and Daoud, A. (1999) Structural and vibrational study of $K_2SeO_4 \cdot Te(OH)_6$ material. *Journal of Solid State Chemistry*, **145**, 612–618.

Dammak, M., Mhiri, T., Jaud, J. and Savariault, J.M. (2001) Structural study of the two new cesium sulfate and selenate tellurate $Cs_2SO_4.Te(OH)_6$ and Cs_2SeO_4. $Te(OH)_6$. *International Journal of Inorganic Materials*, **3**, 861–873.

Dammak, M., Ktari, L., Cousson, A. and Mhiri, T. (2005) Structural and conductivity study of a new protonic conductor $Cs_{0.86}(NH_4)_{1.14}(SO_4)(Te(OH)_6)$. *Journal of Solid State Chemistry*, **178**, 2109–2116.

Dammak, M., Mhiri, T. and Cousson, A. (2006) Neutron structural and vibrational studies of dipotassium selenate tellurate. *Journal of Alloys and Compounds*, **407**, 176–181.

Dammak, M., Litaiem, H., Gravereau, P., Mhiri, T. and Kolsi, A.W. (2007) X-ray and electrical conductivity studies in the rubidium selenate tellurate. *Journal of Alloys and Compounds*, **442**, 316–319.

Daniel, F., Moret, J., Philippot, E. and Maurin, M. (1977*a*) Étude structurale de Li_2TeO_4. Coordination du tellure VI et du lithium par les atomes d'oxygène. *Journal of Solid State Chemistry*, **22**, 113–119.

Daniel, F., Maurin, M., Moret, J. and Philippot, E. (1977*b*) Étude structurale d'un nouveau tellurate alcalin: Na_2TeO_4. Évolution de la coordination du tellure (VI) et du cation quand on passe du cation lithium au sodium. *Journal of Solid State Chemistry*, **22**, 385–391.

Daniel, F., Moret, J., Maurin, M. and Philippot, E. (1978) Structure cristalline d'un oxotellurate mixte, Te^{IV} et Te^{VI}: $K_2Te^{IV}Te_3^{VI}O_{12}$. Pentacoordination du tellure (IV) par les atomes d'oxygène. *Acta Crystallographica*, **B34**, 1782–1786.

Daniel, F., Moret, J., Maurin, M. and Philippot, E. (1981) Étude cristallographique du tellurite de sodium à deux molecules d'eau, $Na_2Te_2^{IV}O_5 \cdot 2H_2O$. *Acta Crystallographica*, **B37**, 1278–1281.

Daniel, F., Moret, J., Maurin, M. and Philippot, E. (1982) Étude du tellurite mixte de sodium et de potassium à trois molecules d'eau: $NaKTeO_2 \cdot 3H_2O$. *Acta Crystallographica*, **B38**, 703–706.

Daniel, P., Bulou, A., Rousseau, M., Nouet, J., Fourquet, J.L., Leblanc, M. and Burriel, R. (1990) A study of the structural phase transitions in AlF_3: X-ray powder diffraction, DSC and Raman scattering investigations of the lattice dynamics and phonon spectrum. *Journal of Physics: Condensed Matter*, **2**, 5663–5677.

Darriet, J. (1973) Structure cristalline de la phase $LiVTeO_5$. *Bulletin de la Societe Francaise de Mineralogie et de Cristallographie*, **96**, 97–99.

Darriet, J. and Galy, J. (1973) Tellurium (IV) vanadium (V) oxide, $Te_2V_2O_9$. *Crystal Structure Communications*, **2**, 237–238.

Dawson, B. (1953) The structure of the 9(18)-heteropoly anion in potassium 9(18)-tungstophosphate, $K_6(P_2W_{18}O_{62}) \cdot 14H_2O$. *Acta Crystallographica*, **6**, 113–126.

Deer, W.A., Howie, R.A. and Zussman, J. (1966) *An Introduction to the Rock-Forming Minerals.* Longman, London, 528 pp.

Delage, C., Carpy, A. and Goursolle, M. (1982) The TeO_2–SeO_2 system. Crystal structure of $Te_2Se_2O_8$. *Comptes Rendus Hebdomadaires des Séances de l'Academie des Sciences, Serie C*, **295**, 981–983.

Denes, G., Pannetier, J. and Lucas, J. (1980) About SnF_2 stannous fluoride. II. Crystal structure of β- and γ-SnF_2. *Journal of Solid State Chemistry*, **33**, 1–11.

Dewan, J.C., Edwards, A.J., Jones, G.R. and Young, I.M. (1978) Crystal structure of dilead tritellurate(IV). *Dalton Transactions*, **1978**, 1528–1532.

Dityat'yev, O.A., Berdonosov, P.S., Dolgikh, V.A., Aldous, D.W. and Lightfoot, P. (2006) On the crystal structures of $SrTeO_3$. *Solid State Sciences*, **8**, 830–835.

Djemel, M., Abdelhedi, M., Dammak, M. and Cousson, A. (2010) Synthesis and crystal structure of $(Cs_{3.5}Rb_{0.5})((Se_{0.85}S_{0.15})O_3)_2(Te(OH)_6)_3$. *X-ray structure analysis online*, **26**, 73–74.

Djemel, M., Abdelhedi, M., Zouari, N., Dammak, M. and Kolsi, A.W. (2012) Structural and conductivity studies of $CsK(SO_4)_{0.32}(SeO_4)_{0.68}Te(OH)_6$. *Journal of Solid State Chemistry*, **196**, 267–273.

Doi, Y., Suzuki, R., Hinatsu, Y. and Ohoyama, K. (2009) Magnetic and neutron diffraction study on quaternary oxides MTeMoO$_6$ (M = Mn and Zn). *Journal of Physics: Condensed Matter*, **21** 046006-1–046006-6.

Dolgikh, V.A., Kholodkovskaya, L.N. and Popovkin, B. A. (1996) Crystal structure of $Bi_5TeO_{8.5}Br_2$: coordination of Te(IV) atoms in layer Sillén phases. *Zhurnal Neorganicheskoi Khimii*, **41**, 970–975.

Dollase, W.A. (1965) Reinvestigation of the structure of low cristobalite. *Zeitschrift für Kristallographie*, **121**, 369–377.

https://doi.org/10.1180/minmag.2016.080.093 Published online by Cambridge University Press

Donnay, G., Stewart, J.M. and Preston, H. (1970) The crystal structure of sonoraite, $Fe^{3+}Te^{4+}O_3(OH) \cdot H_2O$. *Tschermaks mineralogische und petrographische Mitteilungen*, **14**, 27–44.

Downs, R.T. and Palmer, D.C. (1994) The pressure behavior of α cristobalite. *American Mineralogist*, **79**, 9–14.

Drewes, D. and Krebs, B. (2005) Synthesis and structure of a novel type of polyoxomolybdate lanthanide complex: $((Ln(H_2O)_6)_2(TeMo_6O_{24}))$ (Ln = Ho, Yb). *Zeitschrift für anorganische und allgemeine Chemie*, **631**, 2591–2594.

Drewes, D., Limanski, E.M. and Krebs, B. (2004*a*) A series of novel lanthanide polyoxometalates: condensation of building blocks dependent on the nature of rare earth cations. *Dalton Transactions*, **2004**, 2087–2091.

Drewes, D., Limanski, E.M. and Krebs, B. (2004*b*) The Anderson type anion $(TeMo_6O_{24})^{6-}$ – a multientate ligand for trivalent rare earth cations. *European Journal of Inorganic Chemistry*, **2004**, 4849–4853.

Driess, M., von Haenisch, C. and Merz, K. (1999) The first orthotelluric acid polysilylesters: synthesis and crystal structure of $((Me_3SiO)_8Te_2O_2)$ and $((Me_4Si_2O_2)_3Te)$. *Zeitschrift für anorganische und allgemeine Chemie*, **625**, 493–496.

Drits, V.A., Kashaev, A.A. and Sokolova, G.V. (1975) Crystal-structure of cymrite. *Kristallografiya*, **20**, 280–286.

Dubler, E., Vedani, A. and Oswald, H.R. (1983) New structure determination of murdochite, Cu_6PbO_8. *Acta Crystallographica*, **C39**, 1143–1146.

Durif, A. and Averbuch-Pouchot, M.T. (1981) Crystal structure of a silver phosphate-tellurate: $Te(OH)_6 \cdot 2Ag_2HPO_4$. *Zeitschrift für anorganische und allgemeine Chemie*, **472**, 129–132.

Durif, A., Averbuch-Pouchot, M.T. and Guitel, J.C. (1979) Structures de deux phosphotellurates: $Te(OH)_6 \cdot 2(NH_4)_2HPO_4$ et $Te(OH)_6 \cdot Na_2HPO_4 \cdot H_2O$. *Acta Crystallographica, B* **35**, 1444–1447.

Durif, A., Averbuch-Pouchot, M.T. and Guitel, J.C. (1982) $(NH_4)_4P_4O_{12} \cdot 2Te(OH)_6 \cdot 2H_2O$, the first example of a tetrametaphosphate-tellurate. *Journal of Solid State Chemistry*, **41**, 153–159.

Dušek, M. and Loub, J. (1988) X-ray powder diffraction data and structure refinement of TeO_3. *Powder Diffraction*, **3**, 175–176.

Dutreilh, M., Thomas, P., Champarnaud-Mesjard, J.C. and Frit, B. (2001) Crystal structure of a new gallium tellurite: $Ga_2Te_4O_{11}$. *Solid State Sciences*, **3**, 423–431.

Dytyatyev, O.A. and Dolgikh, V.A. (1999) On the crystal structure of a new binary oxide $Sr_3Te_4O_{11}$. *Materials Research Bulletin*, **34**, 733–740.

Effenberger, H. (1977) Verfeinerung der Kristallstruktur von synthetischem Teineit, $CuTeO_3 \cdot 2H_2O$. *Tschermaks mineralogische und petrographische Mitteilungen*, **24**, 287–298.

Effenberger, H. (1986) Die Kristallstrukturen von drei Modifikationen des $Cu(SeO_3)$. *Zeitschrift für Kristallographie*, **175**, 61–72.

Effenberger, H. and Tillmanns, E. (1993) The crystal structure of $K_2\{Cu[TeO_4(OH)_2]\} \cdot H_2O$. *Zeitschrift für Kristallographie*, **205**, 41–53.

Effenberger, H., Zemann, J. and Mayer, H. (1978) Carlfriesite; crystal structure, revision of chemical formula, and synthesis. *American Mineralogist*, **63**, 847–852.

Efremov, V.A., Tyulin, A.V. and Trunov, V.K. (1984) The structure of a new modification of Nd_2WO_6. *Kristallografiya*, **29**, 673–676.

Einstein, F.W. and Willis, A.C. (1981) Structure of tellurium (IV) pyrosulphate. *Acta Crystallographica*, **B37**, 218–220.

Elerman, Y. (1993) Crystal structure of two polymorphous types of $SrTeO_3$. *Turkish Journal of Physics*, **17**, 465–473.

Ercit, T.S., Hawthorne, F.C. and Černý, P. (1992) The crystal structure of alumotantite: its relationship to the structures of simpsonite. *The Canadian Mineralogist*, **30**, 653–662.

Evans, H.T. (1948) The crystal structures of ammonium and potassium molybdotellurates. *Journal of the American Chemical Society*, **70**, 1291–1292.

Evans, H.T. (1974) The molecular structure of the hexamolybdotellurate ion in the crystal complex with telluric acid $(NH_4)_6[TeMo_6O_{24}] \cdot Te(OH)_6 \cdot 7H_2O$. *Acta Crystallographica*, **B30**, 2095–2100.

Evstigneeva, M.A., Nalbandyan, V.B., Petrenko, A.A., Medvedev, B.S. and Kataev, A.A. (2011) A new family of fast sodium ion conductors: $Na_2M_2TeO_6$ (M = Ni, Co, Zn, Mg). *Chemistry of Materials*, **23**, 1174–1181.

Falck, L. and Lindqvist, O. (1978) X-ray refinement of the structure of cubic telluric acid. *Acta Crystallographica*, **B34**, 3145–3146.

Falck, L., Lindqvist, O. and Mark, W. (1978*a*) Tricopper(II) tellurate(VI). *Acta Crystallographica*, **B34**, 896–897.

Falck, L., Lindqvist, O., Mark, W., Philippot, E. and Moret, J. (1978*b*) The crystal structure of $CuTeO_4$. *Acta Crystallographica*, **B34**, 1450–1453.

Feger, C.R. and Kolis, J.W. (1998*a*) $Na_3Mn_4Te_2O_{12}$. *Acta Crystallographica*, **C54**, 1055–1057.

Feger, C.R. and Kolis, J.W. (1998*b*) V_2MnTeO_7. *Acta Crystallographica*, **C54**, 1217–1219.

Feger, C.R. and Kolis, J.W. (1998*c*) Synthesis and characterization of two new copper tellurites, $Ba_2Cu_4Te_4O_{11}Cl_4$ and $BaCu_2Te_2O_6Cl_2$, in supercritical H_2O. *Inorganic Chemistry*, **37**, 4046–4051.

Feger, C.R., Schimek, G.L. and Kolis, J.W. (1999) Hydrothermal synthesis and characterization of $M_2Te_3O_8$ (M = Mn, Co, Ni, Cu, Zn): a series

https://doi.org/10.1180/minmag.2016.080.093 Published online by Cambridge University Press

of compounds with the spiroffite structure. *Journal of Solid State Chemistry*, **143**, 246–253.

Fischer, R. and Pertlik, F. (1975) Verfeinerung der Kristallstruktur des Schafarzikits, $FeSb_2O_4$. *Tschermaks mineralogische und petrographische Mitteilungen*, **22**, 236–241.

Fischer, R., Pertlik, F. and Zemann, J. (1975) The crystal structure of mroseite, $CaTeO_2(CO_3)$. *The Canadian Mineralogist*, **13**, 383–387.

Fischer, W. and Koch, E. (2006) Symbols and properties of lattice complexes. Pp. 848–872 in: *International Tables for Crystallography, Volume A*. Chapter 14.2. International Union for Crystallography.

Fleet, M.E. (1972) The crystal structure of pararammelsbergite, $NiAs_2$. *American Mineralogist*, **57**, 1–9.

Folger, F. (1975*a*) Die Kristallstruktur von Li_2TeO_3. *Zeitschrift für anorganische und allgemeine Chemie*, **411**, 103–110.

Folger, F. (1975*b*) Die Kristallstruktur von $BaTeO_3$. *Zeitschrift für anorganische und allgemeine Chemie*, **411**, 111–117.

Forestier, P. and Goreaud, M. (1991) Structure cristalline de l'oxyde a valence mixte $TeMo_5O_{16}$ orthorombique. *Comptes Rendus Hebdomadaires des Seances de l'Academie des Sciences, Serie 2*, **312**, 1141–1145.

Frau, A.F., Kim, J.H. and Halasyamani, P.S. (2008) $Na_3Ga_3Te_2O_{12}$: Synthesis, single crystal structure and characterization. *Solid State Sciences*, **10**, 1263–1268.

Friauf, J.B. (1927) The crystal structures of two intermetallic compounds. *Journal of the American Chemical Society*, **49**, 3107–3114.

Friese, K., Halasyamani, P.S., Tolkiehn, M. and Grzechnik, A. (2011) A high-pressure single-crystal synchrotron diffraction study of $NH_4RbTe_4O_9 \cdot 2H_2O$: stability of three different TeO_x coordination polyhedra. *Acta Crystallographica*, **C67**, i45–i49.

Frit, B. (1975) Structure crystalline du tellurate d'indium In_2TeO_6. *Comptes Rendus Hebdomadaires des Seances de l'Academie des Sciences, Serie C*, **281**, 769–772.

Frit, B. and Jaymes, M. (1974) Synthese et étude structurale des tellurates de bismuth. *Bulletin de la Société Chimique de France*, **1974**, 402–406.

Frit, B. and Mercurio, D. (1980) Structure cristalline de Tl_2TeO_3 stéréochimie des éléments Tl(I) et Te(IV). *Revue de Chimie Minérale*, **17**, 192–201.

Frit, B., Pressigout, R. and Mercurio, D. (1975) Synthèse et étude structurale du tellurate(VI) de thallium(III) Tl_2TeO_6. *Materials Research Bulletin*, **10**, 1305–1312.

Frit, B., Roult, G. and Galy, J. (1983) Cristallochimie de $Tl^{III}_6Te^{VI}O_{12}$ et $Tl^{I}_6Te^{VI}O_6E_6$: un exemple original de l'activité stéréochimique de la paire éléctronique $6s^2$ (E) du thallium(I). *Journal of Solid State Chemistry*, **48**, 246–255.

Fu, W.T. and Ijdo, D.J.W. (2008) Chiolite-like $Ca_5Te_3O_{14}$: An X-ray and neutron diffraction study. *Journal of Solid State Chemistry*, **181**, 1236–1239.

Fu, W.T., Au, Y.S., Akerboom, S. and Ijdo, D.J.W. (2008) Crystal structures and chemistry of double perovskites $Ba_2M^{II}M'^{VI}O_6$ (M = Ca, Sr, M' = Te, W, U). *Journal of Solid State Chemistry*, **181**, 2523–2529.

Fuchs, J., Loederich, R. and Pickardt, J. (1982) Struktur und schwingungsspektrum des tetraguanidiniumditellurats, $[C(NH_2)_3]_4Te_2O_6(OH)_4$. *Zeitschrift für Naturforschung B*, **37**, 587–593.

Fujita, T., Kawada, I. and Kato, K. (1977) Raspite from Broken Hill. *Acta Crystallographica*, **B33**, 162–164.

Galuskina, I.O., Vapnik, Y., Lazic, B., Armbruster, T., Murashko, M. and Galuskin, E.V. (2014) Harmunite $CaFe_2O_4$: a new mineral from the Jabel Harmun, West Bank, Palestinian Autonomy, Israel. *American Mineralogist*, **99**, 965–975.

Galy, J. and Lindqvist, O. (1979) The crystal structure of $Te_3Nb_2O_{11}$. *Journal of Solid State Chemistry*, **27**, 279–286.

Galy, J. and Meunier, G. (1971) À propos de la cliffordite UTe_3O_8. Le système UO_3–TeO_2 à 700°C. Structure cristalline de UTe_3O_9. *Acta Crystallographica*, **B27**, 608–616.

Gao, B., Liu, S.X., Xie, L.H., Yu, M., Zhang, C.D., Sun, C.Y. and Cheng, H.Y. (2006) Hydrothermal assembly of (3,6)-connected networks with classical mineral structures constructed from Anderson-type heteropolymolybdate and metal cations. *Journal of Solid State Chemistry*, **179**, 1681–1689.

Gao, B., Liu, S.X., Zhang, C.D., Xie, L.H., Sun, C.Y. and Yu, M. (2007) Hydrothermal assembly of pyrite-related framework: $(NH_4)_2((Ni(H_2O)_3)_2(TeW_6O_{24}))(H_2O)$. *Journal of Coordination Chemistry*, **60**, 911–918.

Gao, J., Yan, J., Beeg, S., Long, D. and Cronin, L. (2012) Assembly of molecular "layered" heteropolyoxometalate architectures. *Angewandte Chemie International Edition*, **51**, 3373–3376.

Garavelli, A., Mitolo, D., Pinto, D. and Vurro, F. (2013) Lucabindiite, $(K,NH_4)As_4O_6(Cl,Br)$, a new fumarole mineral from the "La Fossa" crater at Vulcano, Aeolian Islands, Italy. *American Mineralogist*, **98**, 470–477.

Gaudin, E., Chaminade, J.P., El Abed, A. and Darriet, J. (2001) Indium tellurium trioxide chloride, $InTeO_3Cl$. *Acta Crystallographica*, **C57**, 1004–1005.

Gavarri, J.R. and Weigel, D. (1975) Oxydes de plomb. I. Structure cristalline du minium, Pb_3O_4, à température ambiante (293 K). *Journal of Solid State Chemistry*, **13**, 252–257.

Geller, S. (1967) Crystal chemistry of garnets. *Zeitschrift für Kristallographie*, **125**, 1–47.

Geller, S. (1971) Refinement of the crystal structure of cryolithionite, $\{Na_3\}[Al_2](Li_3)F_{12}$. *American Mineralogist*, **56**, 18–23.

https://doi.org/10.1180/minmag.2016.080.093 Published online by Cambridge University Press

Genkina, E.A. (1992) Accurate definition of $LiSbO_3$ crystal structure. *Kristallografiya*, **37**, 356–358.

Glazer, A.M. (1972) The classification of tilted octahedra in perovskites. *Acta Crystallographica*, **B28**, 3384–3392.

Goodey, J., Broussard, J. and Halasyamani, P.S. (2002) Synthesis, structure and characterization of a new second-harmonic-generating tellurite: $Na_2TeW_2O_9$. *Chemistry of Materials*, **14**, 3174–3180.

Goodey, J., Ok, K.M., Broussard, J., Hofmann, C., Escobedo, F.V. and Halasyamani, P.S. (2003) Syntheses, structures and second-harmonic generating properties in new quaternary tellurites: $A_2TeW_3O_{12}$ (A = K, Rb or Cs). *Journal of Solid State Chemistry*, **175**, 3–12.

Govett, G.J.S. (1983) *Rock Geochemistry in Mineral Exploration; Handbook of Exploration Geochemistry.* Elsevier, New York, 461 pp.

Grew, E.S., Locock, A.J., Mills, S.J., Galuskina, I.O., Galuskin, E.V. and Hålenius, U. (2013) Nomenclature of the garnet supergroup. *American Mineralogist*, **98**, 785–811.

Grice, J.D. (1989) The crystal structure of magnolite, $Hg_2^{1+}Te^{4+}O_3$. *The Canadian Mineralogist*, **27**, 133–136.

Grice, J.D. and Roberts, A.C. (1995) Frankhawthorneite, a unique HCP framework structure of a cupric tellurate. *The Canadian Mineralogist*, **33**, 649–654.

Grice, J.D., Groat, L.A. and Roberts, A.C. (1996) Jensenite, a cupric tellurate framework structure with two coordinations of copper. *The Canadian Mineralogist*, **34**, 55–59.

Grigor'ev, M.S., Struchkov, Yu.T., Fedoseev, A.M., Yusov, A.B. and Yanovskii, A.I. (1992) Synthesis, X-ray and luminescence study of some rare earths with iodo- and telluromolybdate-ions complexes. *Zhurnal Neorganicheskoi Khimii*, **37**, 2507–2514.

Grundler, P.V., Brugger, J., Meisser, N., Ansermet, S., Borg, S., Etschmann, B., Testemale, D. and Bolin, T. (2008) Xocolatlite, $Ca_2Mn_2^{4+}Te_2O_{12} \cdot H_2O$, a new tellurate related to kuranakhite: description and measurement of Te oxidation state by XANES spectroscopy. *American Mineralogist*, **93**, 1911–1920.

Grzechnik, A., Halasyamani, P.S., Chang, H.Y. and Friese, K. (2009) Twinned crystal structure and compressibility of $TlTeVO_4$. *Journal of Solid State Chemistry*, **182**, 1570–1574.

Grzechnik, A., Halasyamani, P.S., Kim, J.-H. and Friese, K. (2010) $(NH_4)_2WTe_2O_8$ at 5.09 GPa: A single-crystal study using synchrotron radiation. *Acta Crystallographica*, **C66**, i79–i81.

Gu, Q.H., Hu, C.L., Zhang, J.H. and Mao, J.G. (2011) A series of new phases in the alkali metal-Nb(V)/Ta(V)-Se(IV)/Te(IV)-O systems. *Dalton Transactions*, **40**, 2562–2569.

Guesdon, A. and Raveau, B. (2000) A series of Mo (VI) monophosphates involving the lone pair cation Te(IV): $A_2TeMo_2O_6(PO_4)_2$ (A = K, Rb, Tl, Cs). *Chemistry of Materials*, **12**, 2239–2243.

Haines, J. and Léger, J.M. (1997) X-ray diffraction study of the phase transitions and structural evolution of tin dioxide at high pressure: relationships between structure types and implications for other rutile-type dioxides. *Physical Review*, **B17**, 11144–11154.

Haines, J., Léger, J.M., Chateau, C. and Pereira, A.S. (2000) Structural evolution of rutile-type and $CaCl_2$-type germanium dioxide at high pressure. *Physics and Chemistry of Minerals*, **27**, 575–582.

Haley, M.J., Wallwork, S.C., Duffin, B., Logan, N. and Addison, C.C. (1997) Hexa-μ-nitrato-μ^4-oxo-tetraberyllium. *Acta Crystallographica*, **C53**, 829–830.

Hanke, K. (1967) Zinktellurit: Kristallstruktur und Beziehungen zu einigen Seleniten. *Naturwissenschaften*, **54**, 199–199.

Hanke, K., Kupcik, V. and Lindqvist, O. (1973) The crystal structure of $CuTe_2O_5$. *Acta Crystallographica*, **B29**, 963–970.

Harari, D., Bernier, J.C. and Poix, P. (1972) Contribution a l'étude de deux téllurates de type perovskite. *Journal of Solid State Chemistry*, **5**, 382–390.

Harrison, W.T.A. (2014) Crystal structure of ammonium divanadium(IV,V) tellurium(IV) heptaoxide. *Acta Crystallographica*, **E70**, 27–30.

Hawthorne, F.C. (1984) The crystal structure of mandarinoite, $Fe_2^{3+}Se_3O_9 \cdot 6H_2O$. *The Canadian Mineralogist*, **22**, 475–480.

Hawthorne, F.C. (2014) The structure hierarchy hypothesis. *Mineralogical Magazine*, **78**, 957–1027.

Hawthorne, F.C. and Ferguson, R.B. (1975) Refinement of the crystal structure of cryolite. *The Canadian Mineralogist*, **13**, 377–382.

Hawthorne, F.C., Ercit, T.S. and Groat, L.A. (1986) Structures of zinc selenite and copper selenite. *Acta Crystallographica*, **C42**, 1285–1287.

Hawthorne, F.C., Burns, P.C. and Grice, J.D. (1996) The crystal chemistry of boron. Pp. 41–115 in: *Boron: Mineralogy, Petrology, and Geochemistry* (L.M. Anovitz and E.S. Grew, editors) Reviews in Mineralogy & Geochemistry, **33**. Mineralogical Society of America, Washington, DC.

Hawthorne, F.C., Krivovichev, S.V. and Burns, P.C. (2000) The crystal chemistry of sulfate minerals. Pp. 1–112 in: *Sulfate Minerals: Crystallography, Geochemistry, and Environmental Significance* (C.N. Alpers, J.L. Jambor and D.K. Nordstrom, editors) Reviews in Mineralogy & Geochemistry, **40**. Mineralogical Society of America and the Geochemical Society, Chantilly, Virginia, USA.

Hazen, R.M., Finger, L.W. and Mariathasen, J.W.E. (1985) High-pressure crystal chemistry of

https://doi.org/10.1180/minmag.2016.080.093 Published online by Cambridge University Press

scheelite-type tungstates and molybdates. *Journal of Physics and Chemistry of Solids*, **46**, 253–263.

He, X.H., Huang, C.C., Sheng, L.D. and Qian, L.Z. (2010) Synthesis and characterization of new open-framework vanadium tellurite featuring an unprecedented (3,7)-connected network: $K_3((V^{V}O_4)(V^{IV}O)_4(TeO_3)_4) \cdot (H_2O)_4$. *Crystal Growth and Design*, **10**, 2021–2024.

Hector, A.L., Hill, N.J., Levason, W. and Webster, M. (2002) X-Ray crystal structures of hexa-oxotellurate complexes of ruthenium(VI) and silver(III): $Na_6[RuO_2\{TeO_4(OH)_2\}_2] \cdot 16H_2O$ and $Na_5[Ag\{TeO_4(OH)_2\}_2] \cdot 16H_2O$. *Zeitschrift für anorganische und allgemeine Chemie*, **628**, 815–818.

Helmholtz, L. (1936) The crystal structure of the low temperature modification of thallous iodide. *Zeitschrift für Kristallographie*, **95**, 129–137.

Hepworth, M.A., Jack, K.H., Peacock, R.D. and Westland, G.J. (1957) The crystal structures of the trifluorides of iron, cobalt, ruthenium, rhodium, palladium and iridium. *Acta Crystallographica*, **10**, 63–69.

Hesse, K.-F. and Liebau, F. (1980) Crystal chemistry of silica-rich barium silicates. III. Refinement of the crystal structures of the layer silicates $Ba_2[Si_4O_{10}]$ (l) (sanbornite) and $Ba_2[Si_4O_{10}]$ (h). *Zeitshcrift für Kristallografie*, **153**, 33–41.

Hill, R.J. (1985) Refinement of the structure of orthorhombic PbO (massicot) by Rietveld analysis of neutron powder diffraction data. *Acta Crystallographica*, **C41**, 1281–1284.

Hoekstra, H.R. and Marshall, R.H. (1967) Some uranium-transition metal double oxides. *Advances in Chemistry*, **71**, 211–227.

Hofmann, W. and Jäniche, W. (1935) Der Strukturtyp von Aluminiumborid, AlB_2. *Naturwissenschaften*, **23**, 851.

Höss, P. and Schleid, T. (2007*a*) Y_2TeO_6 with the La_2TeO_6-type structure. *Acta Crystallographica*, **E63**, i133–i135.

Höss, P. and Schleid, T. (2007*b*) $Sc_2Te_5O_{13}$ und Sc_2TeO_6: die ersten Oxotellurate des Scandiums. *Zeitschrift für anorganische und allgemeine Chemie*, **633**, 1391–1396.

Höss, P., Starkulla, G. and Schleid, T. (2005) Lutetium(III) oxotellurate(IV), $Lu_2Te_4O_{11}$. *Acta Crystallographica*, **E61**, i113–i115.

Höss, P., Osvet, A., Meister, E., Batentschuk, M., Winnacker, A. and Schleid, T. (2008) Synthesis, crystal structures and luminescence properties of the Eu^{3+}-doped yttrium oxotellurates(IV) $Y_2Te_4O_{11}$ and $Y_2Te_5O_{13}$. *Journal of Solid State Chemistry*, **181**, 2783–2788.

Hottentot, D. and Loopstra, B.O. (1979) Structures of calcium tellurate, $CaTeO_4$, and strontium tellurate, $SrTeO_4$. *Acta Crystallographica*, **B35**, 728–729.

Hottentot, D. and Loopstra, B.O. (1983) The structure of tribarium undecaoxotetratellurate (IV), $Ba_3Te_4O_{11}$. *Acta Crystallographica*, **C39**, 320–322.

Hou, J.-Y., Huang, C.-C., Zhang, H.-H., Yang, Q.-Y., Chen, Y.-P. and Xu, J.-F. (2005) Barium divanadium(V) tellurite(IV). *Acta Crystallographica*, **C61**, i59–i60.

Hou, J., Huang, C.C., Zhang, H., Tu, C., Sun, R. and Yang, Q. (2006) A new noncentrosymmetric tellurite: $BaMo_2Te_2O_{11}(H_2O)$ with $(Mo(1)Mo(2)O_{10})^n$ spiral chains. *Journal of Molecular Structure*, **785**, 37–42.

Housley, R.M., Kampf, A.R., Mills, S.J., Marty, J. and Thorne, B. (2011) The remarkable occurrence of rare secondary minerals at Otto Mountain near Baker, California – including seven new species. *Rocks & Minerals*, **86**, 132–142.

Howard, C.J. and Carpenter, M.A. (2010) Octahedral tilting in cation-ordered Jahn-Teller distorted perovskites – a group-theoretical analysis. *Acta Crystallographica*, **B66**, 40–50.

Howard, C.J., Sabine, T.M. and Dickson, F. (1991) Structural and thermal parameters for rutile and anatase. *Acta Crystallographica*, **B47**, 462–468.

Howard, C.J., Kennedy, B.J. and Woodward, P.M. (2003) Ordered double perovskites – a group-theoretical analysis. *Acta Crystallographica*, **B59**, 463–471.

Huminicki, D.M.C. and Hawthorne, F.C. (2001) Refinement of the crystal structure of swedenborgite. *The Canadian Mineralogist*, **39**, 153–158.

Hyde, B.G. and Andersson, S. (1989) *Inorganic Crystal Structures*. Wiley-Interscience. 430 pp.

Isasi, J. (2001) New $MM'O_4$ oxides derived from the rutile type: synthesis, structure and study of magnetic and electronic properties. *Journal of Alloys and Compounds*, **322**, 89–96.

IUPAC (1997) *Compendium of Chemical Terminology*, 2nd edition. [the "Gold Book"]. Compiled by A.D. McNaught and A. Wilkinson. Blackwell Scientific Publications, Oxford, UK. XML on-line corrected version: http://goldbook.iupac.org (2006–) created by M. Nic, J. Jirat, B. Kosata; updates compiled by A. Jenkins. ISBN 0-9678550-9-8. doi:10.1351/goldbook.

Ivanov, S.A., Nordblad, P., Mathieu, R., Tellgren, R. and Ritter, C. (2010*a*) Neutron diffraction studies and the magnetism of an ordered perovskite: Ba_2CoTeO_6. *Dalton Transactions*, **39**, 5490–5499.

Ivanov, S.A., Nordblad, P., Mathieu, R., Tellgren, R. and Ritter, C. (2010*b*) Structural and magnetic properties of the ordered perovskite Pb_2CoTeO_6. *Dalton Transactions*, **39**, 11136–11148.

Ivanov, S.A., Mathieu, R., Nordblad, P., Politova, E., Tellgren, R., Ritter, C. and Proidakova, V. (2012*a*) Structural and magnetic properties of $Mn_{3-x}Cd_xTeO_6$ ($x = 0$, 1, 1.5 and 2). *Journal of Magnetism and Magnetic Materials*, **324**, 1637–1644.

https://doi.org/10.1180/minmag.2016.080.093 Published online by Cambridge University Press

Ivanov, S.A., Tellgren, R., Ritter, C., Nordblad, P., Mathieu, R., Andre, G., Golubko, N.V., Politova, E. D. and Weil, M. (2012*b*) Temperature-dependent multi-*k* magnetic structure in multiferroic Co_3TeO_6. *Materials Research Bulletin*, **47**, 63–72.

Iwanaga, D., Inaguma, Y. and Itoh, M. (1999) Crystal structure and magnetic properties of B-site ordered perovskite-type oxides $A_2CuB'O_6$ (A = Ba, Sr; B' = W, Te). *Journal of Solid State Chemistry*, **147**, 291–295.

Iwanaga, D., Inaguma, Y. and Itoh, M. (2000) Structure and magnetic properties of Sr_2NiAO_6 (A = W, Te). *Materials Research Bulletin*, **35**, 449–457.

Jacoboni, C., Leble, A. and Rousseau, J.J. (1981) Détermination précise de la structure de la chiolite $Na_5Al_3F_{14}$ et étude par R.P.E. de $Na_5Al_3F_{14}$:Cr^{3+}. *Journal of Solid State Chemistry*, **36**, 297–304.

Jacobson, A.J., Scanlon, J.C., Poeppelmeier, K.R., Longo, J.M. and Cox, D.E. (1981) The preparation and characterization of $Ba_3Te_2O_9$: a new oxide structure. *Materials Research Bulletin*, **16**, 359–367.

Jeansannetas, B., Thomas, P., Champarnaud-Mesjard, J. C. and Frit, B. (1997) Crystal structure of $Tl_2Te_3O_7$. *Materials Research Bulletin*, **32**, 51–58.

Jeansannetas, B., Thomas, P., Champarnaud-Mesjard, J. C. and Frit, B. (1998) Crystal structure of α-$Tl_2Te_2O_5$. *Materials Research Bulletin*, **33**, 1709–1716.

Jensen, E.P. and Barton, M.D. (2000) Gold deposits related to alkaline magmatism. *Reviews in Economic Geology*, **13**, 279–314.

Jiang, H.-L. and Mao, J.-G. (2006*a*) $[Cd_2(Te_6O_{13})][Cd_2Cl_6]$ and $Cd_7C_{18}(Te_7O_{17})$: Novel tellurium(IV) oxide slabs and unusual cadmium chloride architectures. *Inorganic Chemistry*, **45**, 717–721.

Jiang, H.-L. and Mao, J.-G. (2006*b*) New members in the $Ni_{(n+1)}(QO_3)_nX_2$ family: unusual 3D network based on Ni_4ClO_3 cubane-like clusters in $Ni_7(TeO_3)_6Cl$. *Inorganic Chemistry*, **45**, 7593–7599.

Jiang, H. and Mao, J.-G. (2006*c*) Synthesis, crystal structure and characterization of the barium zinc tellurate disilicate: $Ba_3Zn_6[TeO_6][Si_2O_7]_2$. *Zeitschrift für anorganische und allgemeine Chemie*, **632**, 2053–2057.

Jiang, H. and Mao, J.-G. (2008) Syntheses, crystal structures and optical properties of the first strontium selenium(IV) and tellurium(IV) oxychlorides: $Sr_3(Se_3O_3)(Se_2O_5)Cl_2$ and $Sr_4(Te_3O_8)Cl_4$. *Journal of Solid State Chemistry*, **181**, 345–354.

Jiang, H., Feng, M.L. and Mao, J.-G. (2006) Synthesis, crystal structures and characterizations of BaZn $(SeO_3)_2$ and $BaZn(TeO_3)Cl_2$. *Journal of Solid State Chemistry*, **179**, 1911–1917.

Jiang, H.-L., Ma, E. and Mao, J.-G. (2007*a*) New luminescent solids in the Ln-W-(Mo)-Te-O (Cl) systems. *Inorganic Chemistry*, **46**, 7012–7023.

Jiang, H.-L., Xie, Z. and Mao, J.-G. (2007*b*) $Ni_3(Mo_2O_8)(XO_3)$ (X = Se, Te): The first nickel selenite- and tellurite-containing Mo_4 clusters. *Inorganic Chemistry*, **46**, 6495–6501.

Jiang, H., Kong, F. and Mao, J.-G. (2007*c*) Synthesis, crystal and band structures, and optical properties of a new lanthanide-alkaline earth tellurium(IV) oxide: $La_2Ba(Te_3O_8)(TeO_3)_2$. *Journal of Solid State Chemistry*, **180**, 1764–1769.

Jiang, H., Huang, S.P., Fan, Y., Mao, J.-G. and Cheng, W. D. (2008) Explorations of new types of second order nonlinear optical materials in Cd(Zn)-V^V-Te^{IV}-O systems. *Chemistry – A European Journal*, **14**, 1972–1981.

Johansson, G.B. (1978) Diammonium ditellurium (IV) pentaoxide dihydrate. *Acta Crystallographica*, **B34**, 2830–2832.

Johansson, G.B. and Lindqvist, O. (1976) The crystal structure of $Al_2(OH)_2TeO_3SO_4$. *Acta Crystallographica*, **B32**, 407–411.

Johansson, G.B. and Lindqvist, O. (1977) The crystal structure of ammine copper (II) tellurate (IV) monohydrate $Cu(NH_3)TeO_3 \cdot H_2O$. *Acta Crystallographica*, **B33**, 2418–2421.

Johansson, G.B. and Lindqvist, O. (1978) The crystal structure of dipotassium tellurate (IV) trihydrate, $K_2TeO_3 \cdot 3H_2O$. *Acta Crystallographica*, **B34**, 2959–2962.

Johansson, G.B., Lindqvist, O. and Moret, J. (1979) Diammonium tellurium (VI) dioxide tetrahydroxide. *Acta Crystallographica*, **B35**, 1684–1686.

Johnston, M.G. and Harrison, W.T. (2002) Manganese tellurite, β-$MnTe_2O_5$. *Acta Crystallographica*, **E58**, i59–i61.

Johnston, M.G. and Harrison, W.T.A. (2007) Li $(VO_2)_3(TeO_3)_2$. *Acta Crystallographica*, **C63**, i57–i59.

Johnsson, M. and Törnroos, K.W. (2003*a*) A synthetic zinc tellurium oxochloride, $Zn_2(TeO_3)Cl_2$. *Acta Crystallographica*, **C59**, i53–i54.

Johnsson, M. and Törnroos, K.W. (2003*b*) Synthesis and crystal structure of the layered compound $CuZn(TeO_3)Cl_2$. *Solid State Sciences*, **5**, 263–266.

Johnsson, M., Törnroos, K.W., Mila, F. and Millet, P. (2000) Tetrahedral clusters of copper(II): crystal structures and magnetic properties of $Cu_2Te_2O_5X_2$ (X = Cl, Br). *Chemistry of Materials*, **12**, 2853–2857.

Johnsson, M., Törnroos, K.W., Lemmens, P. and Millet, P. (2003) Crystal structure and magnetic properties of a new two-dimensional $S = 1$ quantum system $Ni_5(TeO_3)_3X_2$ (X = Cl, Br). *Chemistry of Materials*, **15**, 68–73.

Johnsson, M., Lidin, S., Törnroos, K.W., Bürgi, H.B. and Millet, P. (2004) Host-guest compounds in the family of tellurium-nickel oxohalogenides. *Angewandte Chemie International Edition*, **43**, 4292–4295.

Kalinina, I.V., Izarova, N.V. and Kortz, U. (2012) Bis [tetraruthenium(IV)]-containing polyoxometalates:

https://doi.org/10.1180/minmag.2016.080.093 Published online by Cambridge University Press

$[\{Ru_4^{IV}O_6(H_2O)_9\}_2Sb_2W_{20}O_{68}(OH)_2]^{4-}$ and $[\{Ru_4^{IV}O_6(H_2O)_9\}_2\{Fe(H_2O)_2\}_2\{\beta\text{-}TeW_9O_{33}\}_2H]^{-}$. *Inorganic Chemistry*, **51**, 7442–7444.

Kampf, A.R. and Mills, S.J. (2011) The role of hydrogen in tellurites: crystal structure refinements of juabite, poughite and rodalquilarite. *Journal of Geosciences*, **56**, 235–247.

Kampf, A.R., Housley, R.M., Mills, S.J., Marty, J. and Thorne, B. (2010*a*) Lead-tellurium oxysalts from Otto Mountain near Baker, California: I. Ottoite, Pb_2TeO_5, a new mineral with chains of tellurate octahedra. *American Mineralogist*, **95**, 1329–1336.

Kampf, A.R., Marty, J. and Thorne, B. (2010*b*) Lead-tellurium oxysalts from Otto Mountain near Baker, California: II. Housleyite, $Pb_6CuTe_4O_{18}(OH)_2$, a new mineral with Cu-Te octahedral sheets. *American Mineralogist*, **95**, 1337–1342.

Kampf, A.R., Housley, R.M. and Marty, J. (2010*c*) Lead-tellurium oxysalts from Otto Mountain near Baker, California: III. Thorneite, $Pb_6(Te_2^{6+}O_{10})(CO_3)Cl_2(H_2O)$, the first mineral with edge-sharing octahedral tellurate dimers. *American Mineralogist*, **95**, 1548–1553.

Kampf, A.R., Mills, S.J., Housley, R.M., Marty, J. and Thorne, B. (2010*d*) Lead-tellurium oxysalts from Otto Mountain near Baker, California: IV. Markcooperite, $Pb(UO_2)Te^{6+}O_6$, the first natural uranyl tellurate. *American Mineralogist*, **95**, 1554–1559.

Kampf, A.R., Mills, S.J., Housley, R.M., Marty, J. and Thorne, B. (2010*e*) Lead-tellurium oxysalts from Otto Mountain near Baker, California: V. Timroseite, $Pb_2Cu_5^{2+}(Te^{6+}O_6)_2(OH)_2$, and paratimroseite, $Pb_2Cu_4^{2+}(Te^{6+}O_6)_2(H_2O)_2$, two new tellurates with Te-Cu polyhedral sheets. *American Mineralogist*, **95**, 1560–1568.

Kampf, A.R., Mills, S.J., Housley, R.M., Marty, J. and Thorne, B. (2010*f*) Lead-tellurium oxysalts from Otto Mountain near Baker, California: VI. Telluroperite, $Pb_3Te^{4+}O_4Cl_2$, the Te analog of perite and nadorite. *American Mineralogist*, **95**, 1569–1573.

Kampf, A.R., Mills, S.J., Housley, R.M., Rumsey, M.S. and Spratt, J. (2012) Lead-tellurium oxysalts from Otto Mountain near Baker, California: VII. Chromschieffelinite, $Pb_{10}Te_6O_{20}(OH)_{14}(CrO_4)(H_2O)_5$, the chromate analog of schieffelinite. *American Mineralogist*, **97**, 212–219.

Kampf, A.R., Mills, S.J., Housley, R.M. and Marty, J. (2013*a*) Lead-tellurium oxysalts from Otto Mountain near Baker, California: VIII. Fuettererite, $Pb_3Cu_6^{2+}Te^{6+}O_6(OH)_7Cl_5$, a new mineral with double spangolite-type sheets. *American Mineralogist*, **98**, 506–511.

Kampf, A.R., Mills, S.J., Housley, R.M. and Marty, J. (2013*b*) Lead-tellurium oxysalts from Otto Mountain near Baker, California: IX. Agaite, $Pb_3Cu^{2+}Te^{6+}O_5(OH)_2(CO_3)$, a new mineral with CuO_5-TeO_6 polyhedral sheets. *American Mineralogist*, **98**, 512–517.

Kampf, A.R., Mills, S.J., Housley, R.M., Rossman, G.R., Marty, J. and Thorne, B. (2013*c*) Lead-tellurium oxysalts from Otto Mountain near Baker, California: X. Bairdite, $Pb_2Cu_4^{2+}Te_2^{6+}O_{10}(OH)_2(SO_4)(H_2O)$, a new mineral with thick HCP layers. *American Mineralogist*, **98**, 1315–1321.

Kampf, A.R., Mills, S.J., Housley, R.M., Rossman, G.R., Marty, J. and Thorne, B. (2013*d*) Lead-tellurium oxysalts from Otto Mountain near Baker, California: XI. Eckhardite, $(Ca,Pb)Cu^{2+}Te^{6+}O_5(H_2O)$, a new mineral with HCP stair-step layers. *American Mineralogist*, **98**, 1617–1623.

Kampf, A.R., Cooper, M.A., Mills, S.J., Housley, R.M. and Rossman, G.R. (2016) Lead–tellurium oxysalts from Otto Mountain near Baker, California: XII. Andychristyite, $PbCu^{2+}Te^{6+}O_5(H_2O)$, a new mineral with HCP stair-step layers. *Mineralogical Magazine*, DOI: 10.1180/minmag.2016.080.042.

Kashi, T., Yasiu, Y., Moyoshi, T., Sato, M., Kakurai, K., Iikubo, S. and Igawa, N. (2008) Crystal structure and magnetic properties of $CoZn(TeO_3)Br_2$. *Journal of the Physical Society of Japan*, **77**, 084707-1–084707-5.

Kasper, H.M. (1969) $LnCrTeO_6$ – a new series of compounds based on the $PbSb_2O_6$ structure. *Materials Research Bulletin*, **4**, 33–37.

Kear, B.H. and Wilsdorf, H.G.F. (1962) Dislocation configurations in plastically deformed polycrystalline Cu_3Au alloys. *Transactions of the AIME*, **224**, 382–386.

Keggin, J.F. (1934) The structure and formula of 12-phosphotungstic acid. *Proceedings of the Royal Society of London, Series A*, **144**, 75–100.

Kholodkovskaya, L.N., Dolgikh, V.A. and Popovkin, B. A. (1991) Crystal structure of bismuth-tellurium oxobromide $Bi_{0.97}TeO_3Br_{0.90}$. *Zhurnal Neorganicheskoi Khimii*, **36**, 2205–2209.

Kholodkovskaya, L.N., Dolgikh, V.A. and Popovkin, B. A. (1996) The crystal structure of the new pyroelectric phase $Bi_4Te_2O_9Br_2$. *Journal of Solid State Chemistry*, **116**, 406–408.

Kikuta, T., Hamatake, D., Yamazaki, T. and Nakatani, N. (2005) Crystal structure of telluric acid ammonium phosphate (TAAP) in the paraelectric phase. *Journal of the Korean Physical Society*, **46**, 211–216.

Kim, A.A., Zayakina, N.V. and Makhotko, V.F. (1990) Kuksite, $Pb_3Zn_3TeO_6(PO_4)_2$, and cheremnykhite, $Pb_3Zn_3TeO_6(VO_4)_2$, – new tellurates from the Kuranakh gold deposit (central Aldan, southern Yakutia [Sakha]). *Zapiski Rossiyskogo Mineralogicheskogo Obshchestva*, **119**, 50–57.

Kim, J.H. and Halasyamani, P.S. (2008) A rare multi-coordinate tellurite, $NH_4ATe_4O_9 \cdot 2H_2O$ (A = Rb or Cs): The occurence of TeO_3, TeO_4, and TeO_5

https://doi.org/10.1180/minmag.2016.080.093 Published online by Cambridge University Press

polyhedra in the same material. *Journal of Solid State Chemistry*, **181**, 2108–2112.

Kim, J.H., Baek, J. and Halasyamani, P.S. (2007*a*) $(NH_4)_2Te_2WO_8$: a new polar oxide with second-harmonic generating, ferroelectric, and pyroelectric properties. *Chemistry of Materials*, **19**, 5637–5641.

Kim, H., Cho, Y., Yun, H. and Do, J. (2007*b*) Hydrothermal synthesis of a new vanadium tellurate (VI) with a novel chain structure: $(NH_4)_4\{(VO_2)_2[Te_2O_8(OH)_2]\} \cdot 2(H_2O)$. *Zeitschrift für anorganische und allgemeine Chemie*, **633**, 473–477.

Kim, M.K., Kim, S.-H., Chang, H.-Y., Halasyamani, P.S. and Ok, K.M. (2010) New noncentrosymmetric tellurite phosphate material: synthesis, characterization, and calculations of $Te_2O(PO_4)_2$. *Inorganic Chemistry*, **49**, 7028–7034.

Kim, Y.H., Lee, D.W. and Ok, K.M. (2014*a*) Noncentrosymmetric $YVSe_2O_8$ and centrosymmetric $YVTe_2O_8$: macroscopic centricities influenced by the size of lone pair cation linkers. *Inorganic Chemistry*, **53**, 1250–1256.

Kim, Y.H., Lee, D.W. and Ok, K.M. (2014*b*) Strong second harmonic generation (SHG) originating from combined second-order Jahn-Teller (SOJT) distortive cations in a new noncentrosymmetric tellurite, InNb$(TeO_4)_2$. *Inorganic Chemistry*, **53**, 5240–5245.

Klein, W., Curda, J., Peters, E.M. and Jansen, M. (2005*a*) Disilberoxotellurat(VI), Ag_2TeO_4. *Zeitschrift für anorganische und allgemeine Chemie*, **631**, 723–727.

Klein, W., Curda, J., Peters, E.M. and Jansen, M. (2005*b*) Neue Silber(I)-oxotellurate(IV/VI). *Zeitschrift für anorganische und allgemeine Chemie*, **631**, 2893–2899.

Klein, W., Curda, J., Peters, E.M. and Jansen, M. (2006) $Ag_2Te_2O_7$, ein neues Silbertellurat mit Weberit-Struktur. *Zeitschrift für anorganische und allgemeine Chemie*, **632**, 1508–1513.

Klein, W., Curda, J. and Jansen, M. (2007) Crystal structure and properties of Ag_4CuTeO_6. *Zeitschrift für anorganische und allgemeine Chemie*, **633**, 231–234.

Kleppe, A.K., Welch, M.D., Crichton, W.A. and Jephcoat, A.P. (2012) Phase transitions in hydroxide perovskites: a Raman spectroscopic study of stottite, $FeGe(OH)_6$, to 21 GPa. *Mineralogical Magazine*, **76**, 949–962.

Knapp, M.C. (2006) *Investigations into structure and properties of ordered perovskites, layered perovskites, and defect pyrochlores*. Unpublished PhD Thesis, Ohio State University, USA, 161 pp.

Knop, O., Cameron, T.S. and Jochem, K. (1982) What is the true space group of weberite? *Journal of Solid State Chemistry*, **43**, 213–221.

Kocak, M., Platte, C. and Trömel, M. (1979*a*) Ueber verschiedene Formen von $BaTeO_3$. *Zeitschrift für anorganische und allgemeine Chemie*, **453**, 93–97.

Kocak, M., Platte, C. and Trömel, M. (1979*b*) Bariumhexaoxoditellurat (IV, VI): Sauerstoffkoordinationszahl fünf am vierwertigen Tellur. *Acta Crystallographica*, **B35**, 1439–1441.

Köhl, P. (1973) Die Kristallstruktur von Perowskiten $A_2^{II}Ni^{II}M^{VI}O_6$. II. Das Sr_2NiWO_6. *Zeitschrift für anorganische und allgemeine Chemie*, **401**, 121–131.

Köhl, P. and Reinen, D. (1974) Strukturelle und spektroskopische Untersuchungen am Ba_2CuTeO_6. *Zeitschrift für anorganische und allgemeine Chemie*, **409**, 257–272.

Kohn, K., Inoue, K., Horie, O. and Akimoto, S.I. (1976) Crystal chemistry of $MSeO_3$ and $MTeO_3$ (M = Mg, Mn, Co, Ni, Cu and Zn). *Journal of Solid State Chemistry*, **18**, 27–37.

Kondratyuk, I.P., Muradyan, L.A., Pisarevskii, Y.V. and Simonov, V.I. (1987) Precision X-ray structure investigation of acoustooptical single crystals of α-TeO_2. *Kristallografiya*, **32**, 354.

Kong, F., Jiang, H. and Mao, J.G. (2008) $La_4(Si_{5.2}Ge_{2.8}O_{18})(TeO_3)_4$ and $La_2(Si_6O_{13})(TeO_3)_2$: Intergrowth of the lanthanum(III) tellurite layer with the XO_4 (X = Si/Ge) tetrahedral layer. *Journal of Solid State Chemistry*, **181**, 263–268.

Kong, F., Hu, C., Hu, T., Zhou, Y. and Mao, J.G. (2009) Explorations of new phases in the Ga(III)/In(III)-Mo(VI)-Se(IV)/Te(IV)-O systems. *Dalton Transactions*, **2009**, 4962–4970.

Kong, F., Xu, X. and Mao, J.-G. (2010) A series of new ternary and quaternary compounds in the Li(I)-Ga(III)-Te(IV)-O System. *Inorganic Chemistry*, **49**, 11573–11580.

Kortz, U., Al-Kassem, N.K., Savelieff, M.G., Al Kadi, N. A. and Sadakane, M. (2001) Synthesis and characterization of copper, zinc, manganese and cobalt-substituted, dimeric heteropolyanions, $((\alpha\text{-}XW_9O_{33})_2M_3(H_2O)_3)^{n-}$ (n = 12, X = As^{III},Sb^{III}, M = Cu^{2+},Zn^{2+}; n = 10, X = Se^{IV}, Te^{IV}, M = Cu^{2+}). *Inorganic Chemistry*, **40**, 4742–4749.

Kramer, V. and Brandt, G. (1985) Structure of cadmium tellurate (IV), $CdTeO_3$. *Acta Crystallographica*, **C41**, 1152–1154.

Kramer, V. and Brandt, G. (1986) Structure of mercury tellurate (IV). *Acta Crystallographica*, **C42**, 917–918.

Kratochvil, B. (1986) The achieved results in the determination of the crystal structure of NaH_5TeO_6. *Sbornik Vysoke Skoly Chemicko – Technologicke v Praze, G: Mineralogie*, **22**, 53–69.

Kratochvil, B. and Jensovsky, L. (1977) The crystal structure of sodium metatellurate. *Acta Crystallographica*, **B33**, 2596–2598.

Kratochvil, B., Podlahova, J. and Jensovsky, L. (1978) Sodium potassium ditellurate(VI) hexahydrate. *Acta Crystallographica*, **B34**, 256–258.

https://doi.org/10.1180/minmag.2016.080.093 Published online by Cambridge University Press

Krishnan, K., Mudher, K.S. and Venugopal, V. (2000) Structural and thermal studies on $PuTe_2O_6$. *Journal of Alloys and Compounds*, **307**, 114–118.

Krivovichev, S.V. (2008) Minerals with antiperovskite structure: a review. *Zeitschrift für Kristallographie*, **223**, 109–113.

Krivovichev, S.V. and Brown, I.D. (2001) Are the compressive effects of encapsulation an artifact of the bond valence parameters? *Zeitschrift für Kristallographie*, **216**, 245–247.

Krivovichev, S.V., Mentré, O., Siidra, O.I., Colmont, M. and Filatov, S.K. (2013) Anion-centred tetrahedra in inorganic compounds. *Chemical Reviews*, **113**, 6459–6535.

Ktari, L., Dammak, M., Mhiri, T. and Kolsi, A.W. (2002) Characterization and structure determination of disordered rubidium ammonium sulfate tellurate $Rb_{1.12}(NH_4)_{0.88}SO_4{\cdot}(Te(OH)_6)$. *Physical Chemistry News*, **8**, 1–8.

Ktari, L., Dammak, M., Hadrich, A., Cousson, A., Nierlich, M., Romain, F. and Mhiri, T. (2004) Structural, vibrational and dielectric properties of the new mixed solution $K_{0.84}(NH_4)_{1.16}SO_4{\cdot}(Te(OH)_6)$. *Solid State Sciences*, **6**, 1393–1401.

Ktari, L., Abdelhedi, M., Bouhlel, N., Dammak, M. and Cousson, A. (2009) Synthesis, calorimetric, structural and conductivity studies in a new thallium selenate tellurate adduct compound. *Materials Research Bulletin*, **44**, 1792–1796.

Kunnmann, W., La Placa, S.J., Corliss, L.M., Hastings, J. M. and Banks, E. (1968) Magnetic structures of the ordered trirutiles Cr_2WO_6, Cr_2TeO_6 and Fe_2TeO_6. *Journal of Physics and Chemistry of Solids*, **29**, 1356–1364.

Kyung, K.M., Vinna, J., Woo, L.D. and Min, O.K. (2010) Anionic templating in a new layered bismuth tellurium oxychloride, $Bi_3Te_4O_{10}Cl_5$. *Dalton Transactions*, **39**, 6037–6042.

Lafuente, B., Yang, H. and Downs, R.T. (2015) Crystal structure of tetrawickmanite, $Mn^{2+}Sn^{4+}(OH)_6$. *Acta Crystallographica*, **E71**, 234–237.

Laligant, Y. (2001) X-ray and TEM studies of $CdTeMoO_6$ and $CoTeMoO_6$: a new superstructure of fluorite type with cation and anion deficiencies ($\square CoTeMo)(\square_2O_6$). *Journal of Solid State Chemistry*, **160**, 401–408.

Lam, A.E., Groat, L.A. and Ercit, T.S. (1998) The crystal structure of dugganite, $Pb_3Zn_3Te^{6+}As_2O_{14}$. *The Canadian Mineralogist*, **36**, 823–830.

Lam, A.E., Groat, L.A., Grice, J.D. and Ercit, T.S. (1999) The crystal structure of choloalite. *The Canadian Mineralogist*, **37**, 721–729.

Lammers, P. and Zemann, J. (1965) Beiträge zur Kenntnis der Alkalitellurate. I. Über ein neues Alkalitellurat und seinen Strukturtyp. *Zeitschrift für anorganische und allgemeine Chemie*, **334**, 225–234.

Larson, A.C. and Cromer, D.T. (1961) The crystal structure of $CeCu_2$. *Acta Crystallographica*, **14**, 73–74.

Laval, J.P. and Boukharrata, N.J. (2009) New vanadium (IV) and titanium(IV) oxyfluorotellurates(IV): $V_2Te_2O_7F_2$ and $TiTeO_3F_2$. *Acta Crystallographica*, **C65**, i1–i6.

Laval, J.P., Jennene Boukharrata, N. and Thomas, P. (2008) New oxyfluorotellurates(IV): $MTeO_3F$ (M = Fe (III), Ga(III) and Cr(III)). *Acta Crystallographica*, **C64**, i12–i14.

Lee, D.S. and Edmond, J.M. (1985) Tellurium species in seawater. *Nature*, **313**, 782–785.

Lee, D.W., Oh, S.-J., Halasyamani, P.S. and Ok, K.M. (2011) New quaternary tellurite and selenite: synthesis, structure, and characterization of centrosymmetric $InVTe_2O_8$ and noncentrosymmetric $InVSe_2O_8$. *Inorganic Chemistry*, **50**, 4473–4480.

Lee, D.W., Bak, D.-B., Kim, S.B., Kim, J. and Ok, K.M. (2012) Effect of the framework flexibility on the centricities in centrosymmetric $In_2Zn(SeO_3)_4$ and noncentrosymmetric $Ga_2Zn(TeO_3)_4$. *Inorganic Chemistry*, **51**, 7844–7850.

Léger, J.M., Haines, J. and Atouf, A. (1996) The high pressure behaviour of the cotunnite and post-cotunnite phases of $PbCl_2$ and $SnCl_2$. *Journal of Physics and Chemistry of Solids*, **57**, 7–16.

Levason, W. and Webster, M. (1998) Pentasodium bis [dihydroxytetraoxotellurium (VI)] gold (III) hexadecahydrate. *Acta Crystallographica*, **C54**, 1729–1731.

Levason, W., Spicer, M.D. and Webster, M. (1988) Coordination chemistry of higher oxidation states. Part 26. Spectroscopic studies of tellurate complexes of the trivalent group 1b metals. X-ray structure of $Na_5(Cu(TeO_4(OH)_2)_2).16(H_2O)$. *Dalton Transactions*, **5**, 1377–1381.

Levason, W., Spicer, M.D. and Webster, M. (1991) Coordination chemistry of higher oxidation states. Part 37. Tellurato complexes of palladium(IV) and platinum(IV). Crystal structures of $Na_8K_2H_4(Pd_2Te_4O_{24}H_2){\cdot}20H_2O$ and $K_6Na_2(Pt(OH)_2(HTeO_6)_2){\cdot}12H_2O$. *Inorganic Chemistry*, **30**, 967–971.

Levason, W., Oldroyd, R.D. and Webster, M. (1994) Extended x-ray absorption fine structure studies of transition-metal periodate and tellurate complexes. Crystal structure of $Rb_2Na_4(OsO_2(H_2TeO_6)_2).16(H_2O)$. *Dalton Transactions*, **20**, 2983–2988.

Levinson, A.A. (1974) *Introduction to Exploration Geochemistry.* Applied Publishing, Calgary, Canada, 611 pp.

Li, G., Xue, Y. and Xiong, M. (2014) Tewite, IMA 2014-053. CNMNC Newsletter No. 22, *Mineralogical Magazine*, **78**, 1241–1248.

https://doi.org/10.1180/minmag.2016.080.093 Published online by Cambridge University Press

Liebau, F. (1985) *Structural Chemistry of Silicates. Structure, Bonding and Classification.* Springer-Verlag, Berlin – Heidelberg, 347 pp.

Limanski, E.M., Drewes, D., Droste, E., Bohner, R. and Krebs, B. (2003) Syntheses and X-ray characterization of novel tellurium-substituted lacunary polyoxotungstates containing V^{IV}, Co^{II}, Ni^{II} and Zn^{II} as heteroatoms. *Journal of Molecular Structure*, **656**, 17–25.

Lin, W.-F., Xing, Q.-J., Ma, J., Zou, J.-P., Lei, S.-L., Luo, X.-B. and Guo, G.-C. (2013) Synthesis, band and crystal structures, and optical properties of the ternary compound $Mg_2Te_3O_8$. *Zeitschrift für anorganische und allgemeine Chemie*, **639**, 31–34.

Linda, D., Dutreilh-Colas, M., Loukil, M., Mirgorodsky, A., Masson, O., Duclere, J.R., Thomas, P. and Kabadou, A. (2010) Crystal structure and dynamical properties of a new tellurite: $AgTlTeO_3$. *Materials Research Bulletin*, **45**, 1883–1888.

Lindqvist, O. (1969) The crystal structure of the tellurate $Na_2K_4[Te_2O_8(OH)_2](H_2O)_{14}$. *Acta Chemica Scandinavica*, **23**, 3062–3070.

Lindqvist, O. (1970) The crystal structure of telluric acid, $Te(OH)_6$ (mon). *Acta Chemica Scandinavica*, **24**, 3178–3188.

Lindqvist, O. (1972*a*) The crystal structure of $CuTeO_3$. *Acta Chemica Scandinavica*, **26**, 1423–1430.

Lindqvist, O. (1972*b*) A redetermination of the crystal structure of $KTeO_3(OH)$. *Acta Chemica Scandinavica*, **26**, 4109–4120.

Lindqvist, O. and Moret, J. (1973) The crystal structure of a tellurium (IV, VI) oxyhydroxide, $H_2Te_2O_6$. *Acta Crystallographica*, **B29**, 956–963.

Lindqvist, O., Mark, W. and Moret, J. (1975) The crystal structure of Te_4O_9. *Acta Crystallographica*, **B31**, 1255–1259.

Ling, J., Ward, M. and Burns, P.C. (2011) Hydrothermal syntheses and structures of the uranyl tellurates $AgUO_2(HTeO_5)$ and $Pb_2UO_2(TeO_6)$. *Journal of Solid State Chemistry*, **184**, 401–404.

Lippmaa, E., Mägi, M., Samosan, A., Engelhardt, G. and Grimmer, A.-R. (1980) Structural studies of silicates by solid-state high resolution ^{29}Si NMR. *Journal of the American Chemical Society*, **102**, 4889–4893.

Litaiem, H., Dammak, M., Mhiri, T. and Cousson, A. (2005) Structural, conductivity and dielectric studies in $(NH_4)_2SeO_4 \cdot (Te(OH)_6)$. *Journal of Alloys and Compounds*, **396**, 34–39.

Liu, Y., Liu, S.X., Cao, R., Ji, H.M., Zhang, S. and Ren, Y. (2008) Hydrothermal assembly and luminescence property of lanthanide-containing Anderson polyoxometalates. *Journal of Solid State Chemistry*, **181**, 2237–2242.

Locock, A.J. and Burns, P.C. (2004) Revised Tl(I)–O bond valence parameters and the structures of thallous dichromate and thallous uranyl phosphate hydrate. *Zeitschrift für Kristallographie*, **219**, 259–266.

Loeksmanto, W., Moret, J., Maurin, M. and Philippot, E. (1980) Etude cristallochimique comparée et conductivité électrique de deux tellurates mixtes: $Ag_xNa_{2-x}Te_2^{IV}Te_3^{VI}O_{14}$ (X = 0, 4) et $K_2Te^{IV}Te_3^{VI}O_{12}$. *Journal of Solid State Chemistry*, **33**, 209–217.

Loopstra, B.O. and Goubitz, K. (1986) The structures of four caesium tellurates. *Acta Crystallographica*, **C42**, 520–523.

Lopez, M.L., Veiga, M.L., Jerez, A. and Pico, C. (1991) Synthesis and crystal structure of MTe_2O_6 (M = Ce, Th). *Journal of the Less-Common Metals*, **175**, 235–241.

Lopez, M.L., Jerez, A., Pico, C., Saez-Puche, R. and Veiga, M.L. (1993*a*) Synthesis, Crystal structure, and magnetic susceptibility of $MLnLiTeO_6$, M = Ca, Sr, Ba. *Journal of Solid State Chemistry*, **105**, 19–26.

Lopez, M.L., Alvarez, I., Gaitan, M., Jerez, A., Pico, C. and Veiga, M.L. (1993*b*) Structural study and magnetic measurements of some perovskites $MLnLiTeO_6$. *Solid State Ionics*, **63**, 599–602.

Lorenzo-Luis, P.A., Martin-Zarza, P., Gili, P., Saez-Puche, R., Jimenez-Jimenez, J., Rodriguez-Castellon, E., Ruiz Perez, C., Gonzalez-Platas, J. and Solans, X. (1997) Synthesis and characterisation of the molybdotellurates: $(M(H_2O)_6)_3 \cdot (TeMo_6O_{24})$: $M = Ni^{II}$ and Co^{II}. *European Journal of Solid State Inorganic Chemistry*, **34**, 1259–1271.

Ma, C., Tschauner, O., Beckett, J.R., Rossmann, G.R. and Liu, W.J. (2013) Kangite, $(Sc,Ti,Al,Zr,Mg,Ca,\square)_2O_3$, a new ultra-refractory scandia mineral from the Allende meteorite: synchrotron micro-Laue diffraction and electron backscatter diffraction. *American Mineralogist*, **98**, 870–878.

Ma, C., Beckett, J.R. and Rossman, G.R. (2014) Allendeite ($Sc_4Zr_3O_{12}$) and hexamolybdenum (Mo, Ru,Fe), two new minerals from an ultrarefractory inclusion from the Allende meteorite. *American Mineralogist*, **99**, 654–666.

Mahlmeister, D. and Irran, E. (2012) Synthesis and crystal structure of the new telluric acid adduct $(RbCl)_3 \cdot Te(OH)_6$. *Zeitschrift für Naturforschung, B: Chemical Sciences*, **67**, 1–4.

Mandarino, J.A., Williams, S.J. and Mitchell, R.S. (1963) Denningite, a new tellurite mineral from Moctezuma, Sonora, Mexico. *The Canadian Mineralogist*, **7**, 443–452.

Marezio, M. and Remeika, J.P. (1967) Bond lengths in the α-Ga_2O_3 structure and the high-pressure phase of $Ga_{2-x}Fe_xO_3$. *Journal of Chemical Physics*, **46**, 1862–1865.

Margison, S.M., Grice, J.D. and Groat, L.A. (1997) The crystal structure of leisingite, $(Cu^{2+},Mg,Zn)_2(Mg,Fe)Te^{6+}O_6 \cdot 6H_2O$. *The Canadian Mineralogist*, **35**, 759–763.

https://doi.org/10.1180/minmag.2016.080.093 Published online by Cambridge University Press

Marrot, J. and Savariault, J.M. (1996) Tricesium ditellurium tetravanadium chloride tetradecaoxide. *Acta Crystallographica*, **C52**, 2129–2132.

Marsh, R.E. (1988) The structure of $Te(OH)_6 \cdot Na_3P_3O_9 \cdot K_3P_3O_9$. *Acta Crystallographica*, **C44**, 774–774.

Martinez-Carrera, S., Sanz, J., Pico, C., Gaitan, M., Jerez, A. and Veiga, M.L. (1987) Mixed oxides of the system $M^{V}Te^{IV}O_2$ (M = Nb,Ta,Sb); II. Crystal structure of $Ta_2Te_2O_9$. *Materials Research Bulletin*, **22**, 1405–1412.

Martinez-Lope, M.J., Retuerto, M., Alonso, J.A., Sanchez-Benitez, J. and Fernandez-Diaz, M.T. (2011) High-pressure synthesis and neutron diffraction investigation of the crystallographic and magnetic structure of $TeNiO_3$ perovskite. *Dalton Transactions*, **40**, 4599–4604.

Masse, R., Guitel, J.C. and Trodjman, I. (1980) Preparation chimique et structure cristalline des tellurites de sodium et d'argent: Na_2TeO_3, Ag_2TeO_3. *Materials Research Bulletin*, **15**, 431–436.

Matzat, E. (1968) Die Kristallstruktur eines unbekannten zeolithartigen Telluritminerals, $(Zn,Fe)_2(TeO_3)_3Na_xH_{2-x} \cdot y(H_2O)$. *Tschermaks mineralogische und petrographische Mitteilungen*, **12**, 108–117.

Mayer, H. and Pupp, G. (1977) Synthese und Kristallstruktur von $Te_8O_{10}(PO_4)_4$. *Zeitschrift für Kristallographie*, **145**, 321–333.

Mayer, H. and Weil, M. (2003) Synthese und Kristallstruktur von $Te_3O_3(PO_4)_2$, einer Verbindung mit fünffach koordiniertem Tellur (IV). *Zeitschrift für anorganische und allgemeine Chemie*, **629**, 1068–1072.

McDonough, W.F. and Sun, S.-S. (1995) The composition of the Earth. *Chemical Geology*, **120**, 223–254.

Meagher, E.P. and Lager, G.A. (1979) Polyhedral thermal expansion in the TiO_2 polymorphs; refinement of the crystal structures of rutile and brookite at high temperature. *The Canadian Mineralogist*, **17**, 77–85.

Meier, S.F. and Schleid, T. (2002) Synthese und Kristallstruktur des Holmium(III)-chlorid- oxotellurats(IV) $HoClTeO_3$. *Zeitschrift für anorganische und allgemeine Chemie*, **628**, 526–528.

Meier, S.F. and Schleid, T. (2003*a*) $HoClTe_2O_5$: ein tellurdioxidreiches Holmium(III)-Chlorid-Oxotellurat (IV). *Zeitschrift für anorganische und allgemeine Chemie*, **629**, 1575–1580.

Meier, S.F. and Schleid, T. (2003*b*) Synthesis and crystal structure of Gd_2TeO_6. *Journal of Solid State Chemistry*, **171**, 408–411.

Meier, S.F. and Schleid, T. (2004) Oxotellurate(IV) der Lanthanide: I. Die isotype Reihe $M_2Te_4O_{11}$ (M = La-Nd, Sm-Yb). *Zeitschrift für Naturforschung, B: Chemical Sciences*, **59**, 881–888.

Meier, S.F. and Schleid, T. (2005) Oxotellurate(IV) der Lanthanide: II. Die isotype Reihe $M_2Te_5O_{13}$ (M = Dy-Lu). *Zeitschrift für Naturforschung, B: Chemical Sciences*, **60**, 720–726.

Meier, S.F. and Schleid, T. (2006*a*) $Ho_{11}ClTe_{16}O_{48}$: Ein extrem chlorarmes Chlorid-Oxotellurat(IV) des dreiwertigen Holmiums. *Zeitschrift für anorganische und allgemeine Chemie*, **632**, 1759–1767.

Meier, S.F. and Schleid, T. (2006*b*) $Na_2Te_2O_7$: Ein Natrium-Oxoditellurat (VI) mit eckenverknüpften $[TeO_6]^{6-}$-Oktaedern. *Zeitschrift für anorganische und allgemeine Chemie*, **632**, 2150–2150.

Meier, S.F., Höss, P. and Schleid, T. (2009) $Dy_2Te_3O_9$: The first representative of lanthanoid(III)-oxotellurates(IV) with composition $M_2Te_3O_9$. *Zeitschrift für anorganische und allgemeine Chemie*, **635**, 768–775.

Meisel, K. (1939) The crystal structure of thorium phosphides. *Zeitschrift für anorganische und allgemeine Chemie*, **240**, 300–312.

Mellini, M. and Merlino, S. (1981) Versiliaite and apuanite: derivative structures related to schafarzikite. *American Mineralogist*, **64**, 1235–1242.

Menzer, G. (1931) The crystal structure of eulytine. *Zeitschrift für Kristallographie*, **78**, 136–163.

Mercurio, D., Champarnaud-Mesjard, J.C., Gouby, I. and Frit, B. (1998) On the crystal structure of $Bi_2Te_2O_7$. *European Journal of Solid State and Inorganic Chemistry*, **35**, 49–65.

Mercurio, D., El Farissi, M., Frit, B. and Goursat, P. (1983) Étude structurale et densification d'un nouveau materiau piézoélectrique: Bi_2TeO_5. *Materials Chemistry and Physics*, **9**, 467–476.

Merlino, S. (1983) Okenite, $Ca_{10}Si_{18}O_{46} \cdot 18H_2O$, the first example of a chain and sheet silicate. *American Mineralogist*, **68**, 614–622.

Meunier, G. and Galy, J. (1971) Sur une déformation inédité du réseau de type fluorine. Structure cristalline des phases MTe_3O_8 (M = Ti, Sn, Hf, Zr). *Acta Crystallographica*, **B27**, 602–608.

Meunier, G., Darriet, J. and Galy, J. (1972) L'oxyde double $TeVO_4$. I. Synthèse et polymorphisme, structure cristalline de α-$TeVO_4$. *Journal of Solid State Chemistry*, **5**, 314–320.

Meunier, G., Darriet, J. and Galy, J. (1973) L'oxyde double $TeVO_4$. II. Structure cristalline de $TeVO_4$-β – Relations structurales. *Journal of Solid State Chemistry*, **6**, 67–73.

Meunier, G., Frit, B. and Galy, J. (1976) $Cr_2Te_4O_{11}$: une structure à anions complexes $(Cr_2O_{10})_{14}$. *Acta Crystallographica*, **B32**, 175–180.

Mikhaylov, A.A., Mel'nik, E.A., Churakov, A.V., Novotortsev, V.M., Howard, J.A.K., Sladkevich, S., Gun, J., Bharathi, S., Lev, O.and Prikhodchenko, P.V. (2011) Synthesis, crystal structure, and characterization of alkali metal hydroxoantimonates. *Inorganica Chemica Acta*, **378**, 24–29.

Miletich, R. (1991) Hydrothermalsynthese und Kristallstruktur von $MnCu(Te_2O_5)_2$ – ein Vertreter

https://doi.org/10.1180/minmag.2016.080.093 Published online by Cambridge University Press

des Denningit-Typs. *Österreische Akademie der Wissenschaften, Mathematich-Naturwissenschaftliche Klasse, Sitzungsberichte*, **128**, 31–34.

Miletich, R. (1993) Copper-substituted manganese-denningites, $Mn(Mn_{1-x}Cu_x)(Te_2O_5)_2$ ($0 < x < 1$): synthesis and crystal chemistry. *Mineralogy and Petrology*, **48**, 129–145.

Miletich, R. (1995*a*) Crystal chemistry of the microporous tellurite minerals zemannite and kinichilite, $Mg_{0.5}[Me^{2+}Fe^{3+}(TeO_3)_3] \cdot 4.5H_2O$, ($Me^{2+}$ = Zn; Mn). *European Journal of Mineralogy*, **7**, 509–523.

Miletich, R. (1995*b*) The synthetic microporous tellurites $Na_2[Me_2(TeO_3)_3] \cdot 3H_2O$ (Me = Zn, Co): Crystal structure, De- and rehydration, and ion exchange properties. *Monatshefte für Chemie/Chemical Monthly*, **126**, 417–430.

Miletich, R. and Pertlik, F. (1998) Crystal structure of $NaGaTe_2O_6$: Aspects of Te_nO_m polyhedral polymerization in a layer tellurite. *Journal of Alloys and Compounds*, **268**, 107–111.

Mills, S.J. and Christy, A.G. (2013) Revised values of the bond valence parameters for Te^{IV}–O, Te^{VI}–O and Te^{IV}–Cl. *Acta Crystallographica*, **B69**, 145–149.

Mills, S.J., Christy, A.G., Chen, E.C.C. and Raudsepp, M. (2009*a*) Revised values of the bond valence parameters for $^{[6]}$Sb(V)-O and $^{[3-11]}$Sb(III)-O. *Zeitschrift für Kristallographie*, **224**, 423–431.

Mills, S.J., Hatert, F., Nickel, E.H. and Ferraris, G. (2009*b*) The standardisation of mineral group hierarchies: application to recent nomenclature proposals. *European Journal of Mineralogy*, **21**, 1073–1080.

Mills, S.J., Kolitsch, U., Miyawaki, R., Groat, L.A. and Poirier, G. (2009*c*) Joëlbruggerite, $Pb_3Zn_3(Sb^{5+},Te^{6+})As_2O_{13}(OH,O)$, the Sb^{5+} analog of dugganite, from the Black Pine mine, Montana. *American Mineralogist*, **94**, 1012–1017.

Mills, S.J., Kampf, A.R., Kolitsch, U., Housley, R.M. and Raudsepp, M. (2010) The crystal chemistry and crystal structure of kuksite, $Pb_3Zn_3Te^{6+}P_2O_{14}$, and a note on the crystal structure of yafsoanite, $(Ca,Pb)_3Zn(TeO_6)_2$. *American Mineralogist*, **95**, 933–938.

Mills, S.J., Kartashov, P.M., Ma, C., Rossmann, G.R., Novgorodova, M.I., Kampf, A.R. and Raudsepp, M. (2011) Yttriaite-(Y): the natural occurrence of Y_2O_3 from the Bol'shaya Pol'ya River, Subpolar Urals, Russia. *American Mineralogist*, **96**, 1166–1170.

Mills, S.J., Christy, A.G., Génin, J.-M.R., Kameda, T. and Colombo, F. (2012) Nomenclature of the hydrotalcite supergroup: natural layered double hydroxides. *Mineralogical Magazine*, **76**, 1289–1336.

Mills, S.J., Kampf, A.R., Christy, A.G., Housley, R.M., Rossman, G.R., Reynolds, R.E. and Marty, J. (2014*a*) Bluebellite and mojaveite, two new minerals from the central Mojave Desert, California, USA. *Mineralogical Magazine*, **78**, 1325–1340.

Mills, S.J., Kampf, A.R., Christy, A.G., Housley, R.M., Thorne, B., Chen, Y.-S. and Steele, I.M. (2014*b*) Favreauite, a new selenite mineral from the El Dragón mine, Bolivia. *European Journal of Mineralogy*, **26**, 771–781.

Mills, S.J., Dunstan, M.A. and Christy, A.G. (2016) The first example of the $[Te(OH)_3]^+$ ion in a crystalline inorganic compound: the structure of $Na_{11}H[Te(OH)_3]_8[SO_4]_{10}(H_2O)_{13}$. *Dalton Transactions* (in press).

Minimol, M.P. and Vidyasagar, K. (2003) Hydrothermal synthesis and characterization of new one-dimensional tellurates, $A_2[Te_3O_8(OH)_4]$. *Indian Journal of Chemistry*, **42**, 2244–2249.

Minimol, M.P. and Vidyasagar, K. (2005) Syntheses and structural characterization of new mixed-valent tellurium oxides, $A_4[Te_5^{6+}Te_3^{4+}]O_{23}$ (A = Rb and K). *Inorganic Chemistry*, **44**, 9369–9373.

Mitchell, R.H. (2002) *Perovskites. Modern and Ancient.* Almaz Press, Thunder Bay, Ontario, Canada. 318 pp.

Moret, J., Philippot, E., Maurin, M. and Lindqvist, O. (1974) Structure cristalline de l'acide tetraoxotellurique H_2TeO_4. *Acta Crystallographica*, **B30**, 1813–1818.

Moret, J., Maurin, M. and Philippot, E. (1979) Étude du ternaire NH_3–TeO_3–H_2O. Synthèse et étude cristallochimique de $(NH_4)_2Te_3O_8(OH)_4$. *Revue de Chimie Minerale*, **16**, 39–47.

Morgenstern Badarau, I. and Michel, A. (1976) Sur l'existence d'un oxyhydroxyde double de fer(III) et d'étain(IV). *Journal of Inorganic and Nuclear Chemistry*, **38**, 1400–1402.

Mouron, P., Odier, P. and Choisnet, J. (1985) Titanates de cuivre substitués à structure bixbyite: les composés $Cu_{1-x}Ti_{1-x}Fe_{2x}O_3$ ($0.15 < x < 0.33$). *Journal of Solid State Chemistry*, **60**, 87–94.

Müller-Buschbaum, H. and Wedel, B. (1996) Zur Kristallchemie der Barium-Oxometallat-Tellurite $Ba_2Te_2M_6O_{21}$ (M = Niob und Tantal). *Zeitschrift für Naturforschung, Teil B*, **51**, 1411–1414.

Müller-Buschbaum, H. and Wedel, B. (1997) Über die Kristallchemie der Tellurate $Pb_3Fe_2Te_2O_{12}$ und Pb_2CoTeO_6. *Zeitschrift für Naturforschung, Teil B*, **52**, 35–39.

Müller-Buschbaum, H. and Wulff, L. (1997) Planare CuO_4-Polygone und eine einseitig offene $Te^{4+}O_3$ Koordination in $SrCuTe_2O_6$. *Zeitschrift für Naturforschung, B: Chemical Sciences*, **52**, 1341–1344.

Müller-Buschbaum, H. and Wulff, L. (1998) Zur Kristallchemie der Kupfer(II)-Zink-Tellurate $Cu_5Zn_4Te_3O_{18}$ und $Cu_{1.5}Zn_{1.5}TeO_6$, mit einer Notiz ueber $Cu_{1.5}Co_{1.5}TeO_6$. *Zeitschrift für Naturforschung, Teil B*, **53**, 53–57.

https://doi.org/10.1180/minmag.2016.080.093 Published online by Cambridge University Press

Nalbandyan, V.B., Avdeev, M. and Evstigneeva, M.A. (2013) Crystal structure of Li_4ZnTeO_6 and revision of $Li_3Cu_2SbO_6$. *Journal of Solid State Chemistry*, **199**, 62–65.

Nawash, J.M., Twamley, B. and Lynn, K.G. (2007) $ZnTe_6O_{13}$, a new ZnO-TeO_2 phase. *Acta Crystallographica*, **C63**, i66–i68.

Nguyen, S.D., Kim, S.-H. and Halasyamani, P.S. (2011) Synthesis, characterization, and structure-property relationships in two new polar oxides: $Zn_2(MoO_4)(SeO_3)$ and $Zn_2(MoO_4)(TeO_3)$. *Inorganic Chemistry*, **50**, 5215–5233.

Nielsen, B.R., Hazell, R.G. and Rasmussen, S.E. (1971) The crystal structure of barium tellurite monohydrate, $BaTeO_3H_2O$. *Acta Chemica Scandinavica*, **25**, 3037–3042.

Nikiforov, G.B., Kusainova, A.M., Berdonosov, P.S., Dolgikh, V.A. and Lightfoot, P. (1999) The crystal structure of the new REE-Te oxychlorides: $NdTe_2O_5Cl$ and $GdTe_2O_5Cl$. *Journal of Solid State Chemistry*, **146**, 473–477.

Noguera, O., Jouin, J., Masson, O., Jancar, B. and Thomas, P. (2012) Phase formation and crystal structure determination in the Y_2O_3–TeO_2 system prepared in an oxygen atmosphere. *Journal of the European Ceramic Society*, **32**, 4263–4269.

O'Callaghan, M.P., Powell, A.S., Titman, J.J., Chen, G.Z. and Cussen, E.J. (2008) Switching on fast lithium ion conductivity in garnets: the structure and transport properties of $Li_{3+x}Nd_3Te_{2-x}Sb_xO_{12}$. *Chemistry of Materials*, **20**, 2360–2369.

Oh, S.J., Lee, D.W. and Ok, K.M. (2012) $PbMSeO_6$ (M = Mo and W): New quaternary mixed metal selenites with asymmetric cationic coordination environments. *Dalton Transactions*, **41**, 2995–3000.

Ok, K.M. and Halasyamani, P.S. (2001) New tellurites: syntheses, structures, and characterization of $K_2Te_4O_9 \cdot 3.2(H_2O)$, $KGaTe_6O_{14}$, and $KGaTe_2O_6 \cdot 1.8(H_2O)$. *Chemistry of Materials*, **13**, 4278–4284.

Ok, K.M. and Halasyamani, P.S. (2002*a*) Synthesis, structure and characterization of a new tellurate: $NaBiTeO_5$. *Solid State Sciences*, **4**, 793–797.

Ok, K.M. and Halasyamani, P.S. (2002*b*) Anionic templating: synthesis, structure and characterization of novel three-dimensional mixed-metal oxychlorides $Te_4M_3O_{15} \cdot Cl$ ($M = Nb^{5+}$ or Ta^{5+}). *Inorganic Chemistry*, **41**, 3805–3807.

Ok, K.M. and Halasyamani, P.S. (2005) Mixed-metal tellurites: synthesis, structure, and characterization of $Na_{1.4}Nb_3Te_{4.9}O_{18}$ and $NaNb_3Te_4O_{16}$. *Inorganic Chemistry*, **44**, 3919–3925.

Ok, K.M. and Halasyamani, P.S. (2006) Synthesis, structure, and characterization of a new one-dimensional tellurite phosphate, $Ba_2TeO(PO_4)_2$. *Journal of Solid State Chemistry*, **179**, 1345–1350.

Ok, K.M., Zhang, L. and Halasyamani, P.S. (2003) Synthesis, characterization and dielectric properties of new unidimensional quaternary tellurites: $LaTeNbO_6$, $La_4Te_6Nb_2O_{23}$ and $La_4Te_6Ta_2O_{23}$. *Journal of Solid State Chemistry*, **175**, 264–271.

Ok, K.M., Orzechowski, J. and Halasyamani, P.S. (2004) Synthesis, structure, and characterization of two new layered mixed-metal phosphates, $BaTeMO_4(PO_4)$ ($M = Nb^{5+}$ or Ta^{5+}). *Inorganic Chemistry*, **43**, 964–968.

O'Keeffe, M. and Andersson, S. (1977) Rod packings and crystal chemistry. *Acta Crystallographica*, **A33**, 914–923.

O'Keeffe, M. and Hyde, B.G. (1981) The role of nonbonded forces in crystals. Pp. 227–254 in: *Structure and Bonding in Crystals I,* (M. O'Keeffe and A. Navrotsky, editors). Academic Press, New York, USA, 327 pp.

O'Keeffe, M. and Hyde, B.G. (1985) An alternative approach to non-molecular crystal structures with emphasis on the arrangements of cations. *Structure and Bonding*, **61**, 77–144.

O'Keeffe, M. and Hyde, B.G. (1996) *Crystal Structures. I. Patterns and Symmetry.* Mineralogical Society of America, Washington DC, 453 pp.

Olmi, F. and Sabelli, C. (1994) Brizziite, $NaSbO_3$, a new mineral from the Cetine mine (Tuscany, Italy): description and crystal structure. *European Journal of Mineralogy*, **6**, 667–672.

Olsson, C., Johansson, L.G. and Kazikowski, S. (1988) Structure of silver telluryl nitrate, $AgTeO_2NO_3$. *Acta Crystallographica*, **C44**, 427–429.

Oufkir, A., Dutreilh, M., Thomas, P., Champarnaud-Mesjard, J.C., Marchet, P. and Frit, B. (2001) The crystal structure of $PbTe_5O_{11}$. *Materials Research Bulletin*, **36**, 693–703.

Palenik, R.C., Abboud, K.A. and Palenik, G.J. (2005) Bond valence sums and structural studies of antimony complexes containing Sb bonded only to O ligands. *Inorganica chimica acta*, **358**, 1034–1040.

Papike, J.J. and Zoltai, T. (1967) Ordering of tetrahedral aluminum in prehnite, $Ca_2(Al,Fe^{3+})[AlSi_3O_{10}](OH)_2$. *American Mineralogist*, **52**, 974–984.

Park, K.T., Terakura, K. and Matsui, Y. (1988) Theoretical evidence for a new ultra-high-pressure phase of SiO_2. *Nature*, **336**, 670–672.

Pavlyuk, V.V., Dmytriv, G.S. and Bodak, O.I. (1993) Crystal structure of lithium calcium germanide ($LiCa_6Ge$). *Izvestiya Akademii Nauk SSSR, Neorganicheskie Materialy*, **29**, 727–728.

Park, J.-H. and Woodward, P.M. (2000) Synthesis, structure and optical properties of two new perovskites: $Ba_2Bi_{2/3}TeO_6$ and $Ba_3Bi_2TeO_9$. *International Journal of Inorganic Materials*, **2**, 153–166.

Park, J.-H., Woodward, P.M., Parise, J.B., Lubomirsky, I. and Stafsudd, O. (1999) Synthesis, structure and

https://doi.org/10.1180/minmag.2016.080.093 Published online by Cambridge University Press

dielectric properties of Na_2SnTeO_6. *Materials Research Society Symposia Proceedings*, **547**, 139–144.

Parker, R.L. (1967) Composition of the Earth's crust. In: *Data of Geochemistry*, 6th edition. U.S. Geological Survey Professional Paper **440-D**, 19 pp.

Pasero, M. and Perchiazzi, N. (1989) Chalcomenite from Baccu Locci, Sardinia, Italy: mineral data and structure refinement. *Neues Jahrbuch für Mineralogie, Monatshefte*, **1989**, 551–556.

Pauling, L. (1929) The principles determining the structure of complex ionic crystals. *Journal of the American Chemical Society*, **51**, 1010–1026.

Peacor, D.R. and Buerger, M.J. (1962) The determination and refinement of narsarsukite, $Na_2TiOSi_4O_{10}$. *American Mineralogist*, **47**, 539–556.

Pekov, I.V., Chukanov, N.V., Zadov, A.E., Roberts, A.C., Jensen, M.C., Zubkova, N.V. and Nikischer, A.J. (2010) Eurekadumpite, $(Cu,Zn)_{16}(TeO_3)_2(AsO_4)_3Cl(OH)_{18} \cdot 7H_2O$, a new hypergene mineral. *Zapiski Rossiyskogo Mineralogicheskogo Obshchestva*, **139**, 26–35 [in Russian, English translation: (2011) *Geology of Ore Deposits*, **53**, 575–582].

Pekov, I.V., Siidra, O.I., Vlasov, E.A., Yapaskurt, V.O., Lukina, E.A., Polekhovsky, Y.S. and Apletalin, A.V. (2015) Ilirneyite, IMA 2015–046. CNMNC Newsletter No. 27. *Mineralogical Magazine*, **79**.

Pekov, I.V., Vlasov, E.A., Zubkova, N.V., Yapaskurt, V.O., Chukanov, N.V., Belakovskiy, D.I., Lykova, I.S., Apletalin, A.V., Zolotarev, A.A. and Pushcharovsky, D.Y. (2016) Raisaite, $CuMg[Te^{6+}O_4(OH)_2] \cdot 6H_2O$, a new mineral from Chukotka, Russia. *European Journal of Mineralogy*, **28**, 459–466.

Perez, G., Lasserre, F., Moret, J. and Maurin, M. (1976) Structure cristalline des hydroxytellurites de nickel et de cobalt. *Journal of Solid State Chemistry*, **17**, 143–149.

Pertlik, F. (1972*a*) Die Kristallstruktur von $Fe_2Te_4O_{11}$. *Tschermaks mineralogische und petrographische Mitteilungen*, **18**, 39–55.

Pertlik, F. (1972*b*) Der Strukturtyp von Emmonsit, $\{Fe_2[TeO_3]_3 \cdot H_2O\} \cdot xH_2O$ ($x = 0-1$). *Tschermaks mineralogische und petrographische Mitteilungen*, **18**, 157–168.

Pertlik, F. (1987) Dimorphism of hydrothermal synthesized copper tellurite $CuTeO_3$: The structure of a monoclinic representative. *Journal of Solid State Chemistry*, **71**, 291–295.

Pertlik, F. and Gieren, A. (1977) Verfeinerung der Kristallstruktur von Mackayite, $Fe(OH)[Te_2O_5]$. *Neues Jahrbuch für Mineralogie Monatschefe*, **1977**, 145–154.

Pertlik, F. and Zemann, J. (1988*a*) Die Kristallstruktur von $Cu_7(OH)_6(TeO_3)_2(SO_4)_2$. *Monatshefte für Chemie/Chemical Monthly*, **119**, 311–317.

Pertlik, F. and Zemann, J. (1988*b*) The crystal structure of nabokoite, $Cu_7TeO_4(SO_4)_5 \cdot KCl$: The first example of a $Te(IV)O_4$ pyramid with exactly tetragonal symmetry. *Mineralogy and Petrology*, **38**, 291–298.

Phatak, R., Krishnan, K., Kulkarni, N.K., Achary, S.N., Banerjee, A. and Sali, S.K. (2010) Crystal structure, magnetic and thermal properties of $LaFeTeO_6$. *Materials Research Bulletin*, **45**, 1978–1983.

Philippot, E., Astier, R., Loeksmanto, W., Maurin, M. and Moret, J. (1978) Étude cristallochimique d'un tellurate (IV) d'indium $In_2Te_3O_9$. *Revue de Chimie Minerale*, **15**, 283–291.

Philippot, E., Benmiloud, L., Maurin, M. and Moret, J. (1979*a*) Pentacoordination de l'atome de tellure (IV) par les atomes d'oxygènej. Étude cristallochimique d'un oxotellurate mixte: $NH_4[Te^{IV}Te^{VI}O_5(OH)]$. *Acta Crystallographica*, **B35**, 1986–1989.

Philippot, E., Maurin, M. and Moret, J. (1979*b*) Étude cristallographique du tellurite de sodium a cinq molecules d'eau, $Na_2Te^{IV}O_3.5H_2O$. *Acta Crystallographica*, **B35**, 1337–1340.

Pico, C., Castro, A., Veiga, M.L., Gutiérrez-Puebla, E., Monge, M.A. and Ruiz-Valero, C. (1986) Synthesis, crystal structure, and some physico-chemical properties of Te_3SeO_8. *Journal of Solid State Chemistry*, **63**, 172–178.

Pitzschke, D. and Jansen, M. (2007) Hydrothermal synthesis and crystal structure of $AgVMO_5$ (M = Se, Te). *Zeitschrift für anorganische und allgemeine Chemie*, **633**, 1563–1567.

Pitzschke, D., Curda, J., Cakmak, G. and Jansen, M. (2008) $Ag_4I_2SeO_4$ and Ag_3ITeO_4 – two new silver solid electrolytes. *Zeitschrift für anorganische und allgemeine Chemie*, **634**, 1071–1076.

Platte, C. and Trömel, M. (1981) Nickelditellurat (IV): Sauerstoffkoordinationszahl Fünf am vierwertigen Tellur. *Acta Crystallographica*, **B37**, 1276–1278.

Podlahova, J., Loub, J., Pechar, F. and Petricek, V. (1984) Structure of the adduct of orthotelluric acid and potassium iodate, $Te(OH)_6 \cdot KIO_3$. *Acta Crystallographica*, **C40**, 1999–2001.

Pollitt, S. and Weil, M. (2014) Polymorphism of H_2SeO_3, $NaHSeO_4$ and $Na_5H_3(SeO_4)_4(H_2O)_2$, and re-refinement of the crystal structure of $Te_2O_4(OH)_2$. *Zeitschrift für anorganische und allgemeine Chemie*, doi: 10.1002/zaac.201400068.

Popova, V.I., Popov, N.S., Rudashevskiy, S.F., Polyakov, V.O. and Bushmakin, A.F. (1987) Nabokoite $Cu_7TeO_4(SO_4)_5 \cdot KCl$ and atlasovite $Cu_6Fe^{3+}Bi^{3+}O_4(SO_4)_5 \cdot KCl$. New minerals of volcanic exhalations. *Zapiski Rossiyskogo Mineralogicheskogo Obshchestva*, **116**, 358–367 [in Russian with English abstract].

Porter, Y. and Halasyamani, P.S. (2003) Syntheses, structures and characterization of new lead(II)-tellurium(IV)-oxide halides: $Pb_3Te_2O_6X_2$ and

https://doi.org/10.1180/minmag.2016.080.093 Published online by Cambridge University Press

$Pb_3TeO_4X_2$ (X = Cl or Br). *Inorganic Chemistry*, **42**, 205–209.

Porter, Y., Bhuvanesh, N.S.P. and Halasyamani, P.S. (2001) Synthesis and characterization of non-centrosymmetric $TeSeO_4$. *Inorganic Chemistry*, **40**, 1172–1175.

Pospelov, A.A., Nalbandyan, V.B., Serikova, E.I., Medvedev, B.S., Evstigneeva, M.A., Ni, E.V. and Lukov, V.V. (2011) Crystal structure and properties of a new mixed-valence compound $LiMn_2TeO_6$ and the survey of the Li$MM'XO_6$ family (X = Sb or Te). *Solid State Sciences*, **13**, 1931–1937.

Post, J.E., Bish, D.L. and Heaney, P.J. (2007) Synchrotron powder X-ray diffraction study of the structure and dehydration behavior of sepiolite. *American Mineralogist*, **92**, 91–97.

Prior, T.J., Couper, V.J. and Battle, P.D. (2005) Structural chemistry of the cation-ordered perovskites $Sr_2CaMo_{1-x}Te_xO_6$ ($0 \leq x \leq 1$). *Journal of Solid State Chemistry*, **178**, 153–157.

Qurashi, M.M. and Barnes, W.H. (1953) The structure of pucherite, $BiVO_4$. *American Mineralogist*, **38**, 489–500.

Ra, H.-S., Ok, K.M. and Halasyamani, P.S. (2003) Combining second-order Jahn-Teller distorted cations to create highly efficient SHG materials: synthesis, characterisation and NLO properties of $BaTeM_2O_9$ ($M = Mo^{6+}$ or W^{6+}). *Journal of the American Chemical Society*, **125**, 7764–7765.

Radtke, A.S., Dickson, F.W. and Slack, J.F. (1978) Occurrence and formation of avicennite, Tl_2O_3, as a secondary mineral at Carlin gold deposit, Nevada. *Journal of Research of the United States Geological Survey*, **6**, 241–246.

Raman, S. (1964) Crystal Structure of $KTeO(OH)_5 \cdot H_2O$. *Inorganic Chemistry*, **3**, 634–638.

Rastsvetaeva, R.K., Rekhlova, O.Yu, Andrianov, V.I. and Malinovskii, Yu.A. (1991) Crystal structure of hsianghualite. *Doklady Akademii Nauk SSSR*, **316**, 624–628.

Reimann, C. and de Caritat, P. (1998) *Chemical Elements in the Environment.* Factsheets for the geochemist and environmental scientist. Springer-Verlag, Berlin, 398 pp.

Robl, C. and Frost, M. (1993*a*) Water-rich molybdotellurates: preparation and crystal structure of $Li_6(TeMo_6O_{24}) \cdot 18H_2O$ and $Li_6(TeMo_6O_{24}) \cdot Te(OH)_6 \cdot 18H_2O$. *Zeitschrift für anorganische und allgemeine Chemie*, **619**, 1137–1146.

Robl, C. and Frost, M. (1993*b*) On the proton-acceptor properties of $Na_4(NH_4)_2(TeMo_6O_{24}) \cdot 16H_2O$. *Zeitschrift für anorganische und allgemeine Chemie*, **619**, 1132–1136.

Robl, C. and Frost, M. (1993*c*) $Cs_6(TeMo_6O_{24}) \cdot 2Te(OH)_6 \cdot 4H_2O$ – eine Tellursäure- reiche Einschlussverbindung. *Zeitschrift für anorganische und allgemeine Chemie*, **619**, 1624–1628.

Robl, C. and Frost, M. (1993*d*) $Na_6(TeMo_6O_{24}) \cdot 22H_2O$ – a layered heteropoly compound with the chain-like polycation $(Na_3(H_2O)_{11})_n^{3n+}$. *Zeitschrift für Naturforschung, B: Chemical Sciences*, **48**, 404–408.

Robl, C. and Frost, M. (1993*e*) Alkalimolybdotellurate: Darstellung und Kristallstruktur von $Rb_6(TeMo_6O_{24}) \cdot 10H_2O$ und $Rb_6(TeMo_6O_{24}) \cdot Te(OH)_6 \cdot 6H_2O$ eine Tellursäure- reiche Einschlussverbindung. *Zeitschrift für anorganische und allgemeine Chemie*, **619**, 1834–1840.

Rodewald, U.C., Hoffmann, R.D., Wu, Z. and Pöttgen, R. (2006) Structure refinement of $AuSn_2$. *Zeitschrift für Naturforschung B: Chemical Sciences*, **61**, 108–110.

Rossell, H.J., Leblanc, M., Ferey, G., Bevan, D.J.M., Simpson, D.J. and Taylor, M.R. (1992) On the crystal structure of $Bi_2Te_4O_{11}$. *Australian Journal of Chemistry*, **45**, 1415–1425.

Rozier, P., Vendier, L. and Galy, J. (2002) $KVTeO_5$ and a redetermination of the Na homologue. *Acta Crystallographica*, **C58**, i111–i113.

Rumsey, M.S., Welch, M.D., Mo, F., Kleppe, A.K., Spratt, J., Kampf, A.R. and Raanes, M.P. (2016) Millsite, IMA 2015-086. CNMNC Newsletter No. 29, February 2016, page 201; *Mineralogical Magazine*, **80**, 199–205.

Saalfeld, H. and Wedde, M. (1974) Refinement of the crystal structure of gibbsite, $Al(OH)_3$. *Zeitschrift für Kristallographie*, **139**, 129–135.

Sabelli, C. (1987) Structure refinement of elpasolite from Cetine mine, Tuscany, Italy. *Neues Jahrbuch für Mineralogie, Monatshefte*, **1987**, 481–487.

Schmidt, K.J., Schrobilgen, G.J. and Sawyer, J.F. (1986) Hexasodium hexatungstotellurate (VI) 22-hydrate. *Acta Crystallographica*, **C42**, 1115–1118.

Schuelke, U., Averbuch-Pouchot, M.T. and Durif, A. (1993) Chemical preparation and crystal structure of an adduct between potassium cyclooctaphosphate and telluric acid: $Te(OH)_6 \cdot K_8P_8O_{24} \cdot 2H_2O$. *Zeitschrift für Kristallographie*, **204**, 143–152.

Schulz, H. and Bayer, G. (1971) Structure determination of Mg_3TeO_6. *Acta Crystallographica*, **B27**, 815–821.

Sciau, P., Lapasset, J. and Moret, J. (1986) Structure de la phase quadratique de $PbTeO_3$. *Acta Crystallographica*, **C42**, 1688–1690.

Sedello, O. and Müller Buschbaum, H. (1996) Synthese und Kristallstruktur des Barium-Kupfer-Tellurit Tellurats $BaCu(TeO_3)(TeO_4)$. *Zeitschrift für Naturforschung, B: Chemical Sciences*, **51**, 465–468.

Semenova, T.F., Rozhdestvenskaya, I.V., Filatov, S.K. and Vergasova, L.P. (1992) Crystal structure and physical properties of sophiite, $Zn_2(SeO_3)Cl_2$, a new mineral. *Mineralogical Magazine*, **56**, 241–245.

Shan, Y.J., Yoshioka, Y., Wakeshima, M., Tezuka, K. and Imoto, H. (2014) Synthesis, structure, and magentic properties of the novel sodium cobalt tellurate $Na_5Co_{15.5}Te_6O_{36}$. *Journal of Solid State Chemistry*, **211**, 63–68.

https://doi.org/10.1180/minmag.2016.080.093 Published online by Cambridge University Press

Shen, Y.-L. and Mao, J.-G. (2005) Synthesis, crystal structures, and properties of six new lanthanide(III) transition metal tellurium(IV) oxyhalides with three types of structures. *Inorganic Chemistry*, **44**, 5328–5335.

Shen, Y.-L., Jiang, H.-L., Xu, J., Mao, J.-G. and Cheah, K. W. (2005) Luminescent lanthanide selenites and tellurites decorated by MoO_4 tetrahedra or MoO_6 octahedra: $Nd_2MoSe_2O_{10}$, $Gd_2MoSe_3O_{12}$, $La_2MoTe_3O_{12}$, and $Nd_2MoTe_3O_{12}$. *Inorganic Chemistry*, **44**, 9314–9321.

Shirkhanlou, M. and Weil, M. (2013) The Mg member of the isotypic series MTe_6O_{13}. *Acta Crystallographica*, **E69**, i18.

Sidey, V. (2009) Alternative presentation of the Brown-Wu bond-valence parameters for some s^2 cation/O^{2-} ion pairs. *Acta Crystallographica*, **B65**, 99–101.

Sivakumar, T., Ok, K.M. and Halasyamani, P.S. (2006) Synthesis, structure, and characterization of novel two- and three-dimensional vanadates: $Ba_{2.5}(VO_2)_3(SeO_3)_4.H_2O$ and $La(VO_2)_2(TeO_6).3H_2O$. *Inorganic Chemistry*, **45**, 3602–3605.

Smith, J.V. (1953) Reexamination of the crystal structure of melilite. *American Mineralogist*, **38**, 643–661.

Sokolov, M.N., Peresypkina, E.V., Kalinina, I.V., Virovets, A.V., Korenev, V.S. and Fedin, V.P. (2010) New cluster-polyoxometalate hybrids derived from the incorporation of $\{Mo_3S_4\}$ and $\{Mo_3CuS_4\}$ units into $\{EW_{15}\}$ cores (E = As(III), Sb(III), Te(IV)). *European Journal of Inorganic Chemistry*, **2010**, 5446–5454.

Song, S.Y., Lee, D.W. and Ok, K.M. (2014) Rich structural chemistry in scandium selenium/tellurium oxides: mixed-valent selenite-selenates, $Sc_2(SeO_3)_2(SeO_4)$ and $Sc_2(TeO_3)(SeO_3)(SeO_4)$, and ternary tellurite $Sc_2(TeO_3)_3$. *Inorganic Chemistry*, **53**, 7040–7046.

Spiridonov, E.M. and Tananeyva, O.I. (1982) Plumbotellurite, α-$PbTeO_3$, a new mineral. *Doklady Akademii Nauk SSSR*, **262**, 1231–1235.

Staack, M. and Müller-Buschbaum, H. (1997) Dicobaltoarsenat – $(CoAsO_7)$-Baugruppen im Cobaltoxid Tellurat $Co_6O_2(TeO_4(CoAsO_5)_2)$. *Zeitschrift für Naturforschung, Teil B*, **52**, 643–646.

Stöger, B. and Weil, M. (2012) The barium oxotellurate (IV) bromides $Ba_6Te_{10}O_{25}Br_2$ and $Ba_3Te_3O_8Br_2$ with channel structures. *Zeitschrift für anorganische und allgemeine Chemie*, **638**, 2150–2157.

Stöger, B. and Weil, M. (2013) The calcium oxotellurate (IV) nitrates $Ca_5Te_4O_{12}(NO_3)_2(H_2O)_2$ and $Ca_6Te_5O_{15}(NO_3)_2$: non-classic order/disorder polytypism and a rigid framework structure. *Mineralogy and Petrology*, **107**, 257–263.

Stöger, B., Weil, M., Zobetz, E. and Giester, G. (2009) Polymorphism of $CaTeO_3$ and solid solutions $Ca_xSr_{1-x}TeO_3$. *Acta Crystallographica*, **B65**, 167–181.

Stöger, B., Weil, M. and Zobetz, E. (2010) $SrTeO_6$ and $BaTeO_6$: Double perovskites with pronounced superstructures. *Zeitschrift für Kristallographie – Crystalline Materials*, **225**, 125–138.

Stöger, B., Weil, M., Baran, E.J., Gonzalez Baro, A.C., Malo, S., Rueff, J.M., Petit, S., Lepetit, M.B., Raveau, B. and Barrier, N. (2011*a*) The dehydration of $SrTeO_3(H_2O)$ – a topotactic reaction for preparation of the new metastable strontium oxotellurate(IV) phase ε-$Sr(TeO_3)$. *Dalton Transactions*, **40**, 5538–5548.

Stöger, B., Weil, M., Silich, K.A., Olenev, A.V., Berdonosov, P.S. and Dolgikh, V.A. (2011*b*) Synthesis and structural characterization of new phases in the cubic $M_3Te_2O_6X_2$ (M = Sr, Ba; X = Cl, Br) structure family. *Zeitschrift für anorganische und allgemeine Chemie*, **637**, 1322–1329.

Strunz, H. and Contag, B. (1960) Hexahydroxostannate Fe, Mn, Co, Mg, Ca $(Sn(OH)_6)$ und deren Kristallstruktur. *Acta Crystallographica*, **13**, 601–603.

Sullens, T.A. and Albrecht Schmitt, T.E. (2005) Structure and properties of the thorium vanadyl tellurate Th $(VO_2)_2(TeO_6)(H_2O)_2$. *Inorganic Chemistry*, **44**, 2282–2286.

Swainson, I.P. and Hammond, R.P. (2003) Hydrogen bonding in ikaite, $CaCO_3 \cdot 6H_2O$. *Mineralogical Magazine*, **67**, 555–562.

Swihart, G.H., Sen Gupta, P.K., Schlemper, E.O., Back, M.E. and Gaines, R.V. (1993) The crystal structure of moctezumite $[PbUO_2](TeO_3)_2$. *American Mineralogist*, **78**, 835–839.

Tagg, S.L., Huffmann, J.C. and Zwanziger, J.W. (1994) Crystal structure and sodium environments in sodium tetratellurite, $Na_2Te_4O_9$, and sodium tellurite, Na_2TeO_3, by X-ray crystallography and sodium-23 NMR. *Chemistry of Materials*, **6**, 1884–1889.

Tagg, S.L., Huffmann, J.C. and Zwanziger, J.W. (1997) Crystal structure of sodium ditellurite, $Na_4Te_4O_{10}$. *Acta Chemica Scandinavica*, **51**, 118–121.

Tait, K.T., DiCecco, V., Cooper, M.A., Ball, N.A. and Hawthorne, F.C. (2014) Backite, $Pb_2Al(TeO_6)Cl$, a new tellurate mineral from the Grand Central mine, Tombstone Hills, Cochise County, Arizona: description and crystal structure. *The Canadian Mineralogist*, **52**, 935–942

Takagi, R. and Johnsson, M. (2005) $Ca_2CuTe_4O_{10}Cl_2$, a new synthetic tellurium(IV) oxochloride. *Acta Crystallographica*, **C61**, i106–i108.

Takagi, R. and Johnsson, M. (2006) $Sr_2Cu_2TeO_6Br_2$: honeycomb layers of copper(II) ions. *Acta Crystallographica*, **C62**, i38–i40.

Takagi, R., Johnsson, M., Gnezdilov, V., Kremer, R.K., Brenig, W. and Lemmens, P. (2006*a*) Investigation of the oxohalide $Cu_4Te_5O_{12}Cl_4$ with weakly coupled Cu (II) tetrahedra. *Physical Review, Serie 3. B – Condensed Matter*, **74**, 014413-1–014413-8.

https://doi.org/10.1180/minmag.2016.080.093 Published online by Cambridge University Press

Takagi, R., Duc, F. and Johnsson, M. (2006*b*) Molybdenum (VI) tricopper(II) tellurium(IV) heptaoxide dichloride hemihydrate. *Acta Crystallographica*, **C62**, i16–i18.

Takagi, R. Johnsson, M., Kremer, R.K. and Lemmens, P. (2006*c*) Crystal structure and magnetic properties of the coupled spin dimer compound $SrCu_2(TeO_3)_2Cl_2$. *Journal of Solid State Chemistry*, **179**, 3763–3767.

Takagi, R., Torino Hjelmqvist, D. and Johnsson, M. (2007) The solid solution $Co_{3.6}Mg_{1.4}Cl_2(TeO_3)_4$. *Acta Crystallographica*, **E63**, i146–i147.

Takagi, R.F., Johnsson, M. and Lidin, S. (2008) Single-crystal x-ray study of $Ba_2Cu_2Te_4O_{11}Br_2$ and its incommensurately modulated superstructure companion. *Chemistry – A European Journal*, **14**, 3434–3441.

Takagi, R.F., Hjelmqvist, D.T., Johnsson, M. and Lidin, S. (2009) Helical chains of $[MO_5Cl]$ octahedra – Three compounds in the new family $AEM_2T_3O_8Cl_2$ (AE = Ca, Sr and M = Co, Ni). *Solid State Sciences*, **11**, 13–17.

Tang, Y., He, Z., Guo, W., Zhang, S. and Yang, M. (2014) Syntheses and magnetic properties of new tellurite-sulfate compounds $M_2(TeO_3)(SO_4)\cdot H_2O$ (M = Co, Mn) with a layer structure showing a distorted honeycomb spin-lattice. *Inorganic Chemistry*, **53**, 5862–5868.

Tarasov, I.V., Dolgikh, V.A., Aksel'rud, L.G., Berdonosov, P.S. and Ponovkin, B.A. (1996) $NdTe_2O_5Br$ is a new representative of the Bi_3O_4Br type structures. *Zhurnal Neorganicheskoi Khimii*, **41**, 1243–1247.

Taylor, S.R. and McLennan, S.M. (1985) *The Continental Crust: its Composition and Evolution. An Examination of the Geochemical Record Preserved in Sedimentary Rocks.* Blackwell Scientific, Oxford, UK, 312 pp.

Thomas, P., Jeansannetas, B., Champarnaud-Mesjard, J. C. and Frit, B. (1996) Crystal structure of a new mixed-valence bismuth oxotellurate $Bi_2Te^{IV}Te^{VI}O_8$. *European Journal of Solid State Inorganic Chemistry*, **33**, 637–646.

Thornber, M.R., Bevan, D.J.M. and Graham, J. (1968) Mixed oxides of the type MO_2 (fluorite) – M_2O_3. III. Crystal structures of the intermediate phases $Zr_5Sc_2O_{13}$ and $Zr_3Sc_4O_{12}$. *Acta Crystallographica*, **B24**, 1183–1190.

Thümmel, H.J. and Hoppe, R. (1974) Über die Tellurite der Alkalimetalle vom Typ M_2TeO_3. *Zeitschrift fuer Naturforschung, Teil B. Anorganische Chemie, Organische Chemie*, **29**, 28–31.

Tindemans-van Eijndhoven, J.C.M. and Verschoor, G.C. (1974) Redetermination of the crystal structure of $Cs_2AuAuCl_6$. *Materials Research Bulletin*, **9**, 1667–1670.

Trömel, V.M. and Scheller, T. (1976) Die kristallstruktur von $Co_6Te_5O_{16}$. *Zeitschrift für anorganische und allgemeine Chemie*, **427**, 229–234.

Trömel, M., Maetz, J. and Müllner, M. (1977) Berylliumtellurat Be_4TeO_7. *Acta Crystallographica*, **B33**, 3959–3961.

Trömel, M., Hötzler, F.W., Burckhardt, H.G., Platte, C. and Muench, E. (1987) Lanthanoidtellurate Ln_2TeO_6. *Zeitschrift für anorganische und allgemeine Chemie*, **551**, 95–100.

Troyanov, S.I., Tikhomirov, G.A., Znamenkov, K.O. and Morozov, I.V. (2000) Crystal structure of beryllium complexes $(NO)_2(Be(NO_3)_4)$ and $Be_4O(NO_3)_6$. *Zhurnal Neorganicheskoi Khimii*, **45**, 1941–1948.

Trudu, A.G. and Knittel, U. (1998) Crystallography, mineral chemistry and chemical nomenclature of goldfieldite, the tellurian member of the tetrahedrite solid-solution series. *The Canadian Mineralogist*, **36**, 1115–1137.

Ulku, D. (1967) Untersuchungen zur Kristallstruktur und magnetischen Struktur des Ferberits, $FeWO_4$. *Zeitschrift für Kristallographie*, **124**, 192–219.

Untenecker, H. and Hoppe, R. (1986*a*) Die Koordinationszahl 5 bei Telluraten: $Cs_2K_2[TeO_5]$. *Journal of the Less-Common Metals*, **124**, 29–40.

Untenecker, H. and Hoppe, R. (1986*b*) Neues über Oxotellurate: $K_3Li_3(TeO_6)$. *Journal of the Less-Common Metals*, **124**, 251–262.

Untenecker, H. and Hoppe, R. (1986*c*) Neue Oxotellurate (VI): $K_4Na_2(TeO_6)$. *Journal of the Less-Common Metals*, **125**, 223–231.

Untenecker, H. and Hoppe, R. (1987*a*) Ein neues oxotellurat, Na_4TeO_5, und eine revision der struktur von Li_4TeO_5. *Journal of the Less Common Metals*, **132**, 79–92.

Untenecker, H. and Hoppe, R. (1987*b*) Neue Oxotellurate (VI): $KNa_5(TeO_6)$. *Journal of the Less-Common Metals*, **132**, 93–105.

Vallar, S. and Goreaud, M. (1997) Crystal structure of a monoclinic form of $TeMo_5O_{16}$, a two-dimensional conductor mixed-valence oxide. *Journal of Solid State Chemistry*, **129**, 303–307.

van Bever, A.K. (1935) The crystal structure of calcium chloride, $CaCl_2$. *Zeitschrift fuer Kristallographie*, **90**, 374–376.

van der Lee, A. and Astier, R. (2007) Structural evolution in iron tellurates. *Journal of Solid State Chemistry*, **180**, 1243–1249.

Veblen, D.R. and Burnham, C.W. (1978) New biopyriboles from Chester, Vermont. II. The crystal chemistry of jimthompsonite, clinojimthompsonite, and chesterite and the amphibole-mica reactions. *American Mineralogist*, **63**, 1053–1073.

Viciu, L., Huang, Q., Morosan, E., Zandbergen, H.W., Greenbaum, N.I., McQueen, T. and Cava, R.J. (2007) Structure and basic magnetic properties of the honeycomb lattice compounds $Na_2Co_2TeO_6$ and $Na_3Co_2SbO_6$. *Journal of Solid State Chemistry*, **180**, 1060–1067.

https://doi.org/10.1180/minmag.2016.080.093 Published online by Cambridge University Press

von Dreele, R.B., Eyring, L., Bowman, A.L. and Yarnell, J.L. (1975) Refinement of the crystal structure of Pr_7O_{12} by powder neutron diffraction. *Acta Crystallographica*, **B31**, 971–974.

Walitzi, E.M. (1964) Die Kristallstruktur von Denningit, $(Mn,Ca,Zn)Te_2O_5$. *Naturwissenschaften*, **51**, 334–335.

Walitzi, E.M. (1965) Die Kristallstruktur von Denningit, $(Mn, Ca, Zn)Te_2O_5$. Ein Beispiel für die Koordination um vierwertiges Tellur. *Tschermaks mineralogische und petrographische Mitteilungen*, **10**, 241–255.

Wang, Z. and Becker, H. (2013) Ratios of S, Se and Te in the silicate Earth require a volatile-rich late veneer. *Nature*, **499**, 328–331.

Weber, F.A. and Schleid, T. (2000) $Pr_2Te_2O_7$: A praseodymium (III) oxide oxotellurate (IV) according to $Pr_2O(TeO_3)_2$ with pyrochlore-type crystal structure. *Zeitschrift für anorganische und allgemeine Chemie*, **626**, 1285–1287.

Wedel, B. and Müller-Buschbaum, H. (1996) Ueber ein Blei-Kupfer-Tellurat $PbCu_3TeO_7$ mit Cu^{2+} in deformiert tetragonal pyramidaler und tetraedrischer Sauerstoffkoordination. *Zeitschrift fuer Naturforschung, Teil B*, **51**, 1587–1590.

Wedel, B. and Sugiyama, K. (1999) A new tellurium compound with the garnet structure: $Na_3Te_2(Fe,Al)_3O_{12}$. *Zeitschrift für Kristallographie*, **214**, 151–152.

Wedel, B., Sugiyama, K. and Müller-Buschbaum, H. (1998) Verknüpfung von $(TeO_6)_6$ und $(TeO_6)_3(NiO_6)_3$ sechsringen durch $TeNiO_9$-Oktaederdoppel in $Pb_3Ni_{4.5}Te_{2.5}O_{15}$. *Zeitschrift für Naturforschung B: Chemical Sciences*, **53**, 527–531.

Weil, M. (2003*a*) Preparation, thermal behaviour and crystal structure of the basic mercury (II) tetraoxotellurate (VI), Hg_2TeO_5, and redetermination of the crystal structure of mercury (II) orthotellurate (VI), Hg_3TeO_6. *Zeitschrift für anorganische und allgemeine Chemie*, **629**, 653–657.

Weil, M. (2003*b*) Dimorphism in mercury(II) tellurite(IV) tellurate(VI): preparation and crystal structures of alpha- and beta-$(Hg_2Te_2O_7)$. *Zeitschrift für Kristallographie*, **218**, 691–698.

Weil, M. (2004*a*) Preparation and crystal structures of the hydrous mercury tellurates $Hg^{II}(H_4Te^{VI}O_6)$ and $Hg^{I}_2(H_4Te^{VI}O_6)(H_6Te^{VI}O_6) \cdot 2(H_2O)$. *Zeitschrift für anorganische und allgemeine Chemie*, **630**, 1048–1053.

Weil, M. (2004*b*) New phases in the systems Ca-Te-O and Cd-Te-O: the calcium tellurite(IV) $Ca_4Te_5O_{14}$ and the cadmium compounds $Cd_2Te_3O_9$ and $Cd_2Te_2O_7$ with mixed-valent oxotellurium(IV/VI) anions. *Solid State Sciences*, **6**, 29–37.

Weil, M. (2005*a*) $Ag_2Hg_2(TeO_4)_3$. *Acta Crystallographica*, **C61**, i103–i105.

Weil, M. (2005*b*) Redetermination of $MgTe_2O_5$. *Acta Crystallographica*, **E61**, i237–i239.

Weil, M. (2006*a*) Mn_3TeO_6. *Acta Crystallographica*, **E62**, i244–i245.

Weil, M. (2006*b*) Zn_3TeO_6. *Acta Crystallographica*, **E62**, 1246–1247.

Weil, M. (2007*a*) Redetermination of $Ag_2[TeO_2(OH)_4]$: a revised hydrogen-bonding scheme. *Acta Crystallographica*, **E63**, i77–i79.

Weil, M. (2007*b*) New silver tellurates – the crystal structures of a third modification of $Ag_2Te_2O_6$ and of Ag_4TeO_5. *Zeitschrift für anorganische und allgemeine Chemie*, **633**, 1217–1222.

Weil, M. (2014) Two modifications of $(TeO)(HAsO_4)$ and its dehydration product $(Te_3O_3)(AsO_4)_2$ – three more examples of tellurium (IV) with a fivefold oxygen coordination. *Zeitschrift für anorganische und allgemeine Chemie*, **640**, 128–135.

Weil, M. and Stöger, B. (2007*a*) Redetermination of $SrTe_3O_8$ from a hydrothermally grown single crystal. *Acta Crystallographica*, **E63**, i116–i118.

Weil, M. and Stöger, B. (2007*b*) Digallium(III) tris (tellurate(IV)) trihydrate. *Acta Crystallographica*, **E63**, i202–i202.

Weil, M. and Stöger, B. (2008*a*) $NaFe(TeO_3)_2$. *Acta Crystallographica*, **E64**, i3–i3.

Weil, M. and Stöger, B. (2008*b*) A non-twinned polymorph of $CaTe_2O_5$ from a hydrothermally grown crystal. *Acta Crystallographica*, **C64**, i79–i81.

Weil, M. and Stöger, B. (2010) $Pb_3Te_2O_6Br_2$. *Acta Crystallographica*, **E66**, i7–i7.

Weller, M.T., Pack, M.J., Binsted, N. and Dann, S.E. (1999) The structure of cesium tellurate(VI) by combined EXAFS and powder X-ray Diffraction. *Journal of Alloys and Compounds*, **282**, 76–78.

Wells, A.F. (1947) *Structural Inorganic Chemistry.* 1st edition. Oxford University Press, UK, 344 pp.

Wildner, M. (1993) Zemannite-type selenites – crystal structures of $K_2[Co_2(SeO_3)_3] \cdot 2H_2O$ and $K_2[Ni_2(SeO_3)_3] \cdot 2H_2O$. *Mineralogy and Petrology*, **48**, 215–225.

Wilk, P., Keller, H.L. and Wimbert, L. (1998) $BiTeO_3$ I – das erste Mitglied eines neuen Strukturtyps. *Zeitschrift für Kristallographie*, **15**, 64–64.

Williams, S.A. (1974) Cesbronite, a new copper tellurite from Moctezuma, Sonora. *Mineralogical Magazine*, **39**, 744–746.

Williams, S.A. (1975) Xocometatlite, $Cu_3TeO_4(OH)_4$, and tlalocite, $Cu_{10}Zn_6(TeO_3)(TeO_4)_2Cl(OH)_{25} \cdot 27H_2O$, two new minerals from Moctezuma, Sonora, Mexico. *Mineralogical Magazine*, **40**, 221–226.

Williams, S.A. (1979) Girdite, oboyerite, fairbankite and winstanleyite, four new tellurium minerals from Tombstone, AZ. *Mineralogical Magazine*, **43**, 453–457.

Wisser, T. and Hoppe, R. (1989) Neues über Oxotellurate (VI) der Alkalimetalle Zur Existenz und Konstitution

https://doi.org/10.1180/minmag.2016.080.093 Published online by Cambridge University Press

von Li_6TeO_6. *Zeitschrift für anorganische und allgemeine Chemie*, **573**, 133–142.

Wisser, T. and Hoppe, R. (1990*a*) Ein Oxotellurat (VI) neuen Typs: $Rb_6[TeO_5][TeO_4]$. *Zeitschrift für anorganische und allgemeine Chemie*, **584**, 105–113.

Wisser, T. and Hoppe, R. (1990*b*) Das erste quinquinäre Oxotellurat (VI): $K_3Na_2LiTeO_6$. *Zeitschrift für anorganische und allgemeine Chemie*, **586**, 125–135.

Woodward, J.D. and Albrecht-Schmitt, T.E. (2005) Molten salt flux synthesis and structure of the new layered uranyl tellurite, $K_4((UO_2)_5(TeO_3)_2O_5)$. *Journal of Solid State Chemistry*, **178**, 2922–2926.

Woodward, J.D., Almond, P.M. and Albrecht Schmitt, T.E. (2004) Synthesis and crystal structures of the layered uranyl tellurites $A_2((UO_2)_3(TeO_3)_2O_2)$ (A = K, Rb, Cs). *Journal of Solid State Chemistry*, **177**, 3971–3976.

Woodward, P.M., Sleight, A.W., Du, L.-S. and Grey, C.P. (1999) Structural studies and order-disorder phenomenon in a series of new quaternary tellurates of the type $A^{2+}M^{4+}Te^{6+}O_6$ and $A_2^{1+}M^{4+}Te^{6+}O_6$. *Journal of Solid State Chemistry*, **147**, 99–116.

Wulff, L. and Müller-Buschbaum, H. (1998) Isolierte trigonale SrO_6 – Prismen verknüpfen Kagome-Netze im Strontium-Manganat(IV)-Tellurat(VI): $SrMnTeO_6$. *Zeitschrift für Naturforschung*, **B53**, 283–286.

Wulff, L., Wedel, B. and Müller-Buschbaum, H. (1998) Zur Kristallchemie von Telluraten mit Mn^{2+} im kationischen und anionischen Teil der Kristallstruktur: $(Mn_{2.4}Cu_{0.6})TeO_6$, Ba_2MnTeO_6 und $Pb(Mn_{0.5}Te_{0.5})O_3$. *Zeitschrift für Naturforschung*, **B53**, 49–52.

Xiao, D., Wang, S., Wang, E., Hou, Y., Li, Y., Hu, C. and Xu, L. (2003) Hydrothermal synthesis and crystal structure of a three-dimensional vanadium tellurite $V_4Te_4O_{18}$. *Journal of Solid State Chemistry*, **176**, 159–164.

Xu, J., Assoud, A., Soheilnia, N., Derakhshan, S., Cuthbert, H.L., Greedan, J.E., Myungwhan, W. and Kleinke, H. (2005) Synthesis, structure, and magnetic properties of the layered copper(II) oxide $Na_2Cu_2TeO_6$. *Inorganic Chemistry*, **44**, 5042–5046.

Yablokova, S.V., Dubakina, L.S. Dmitrik, A.L. and Sokolova, G.V. (1975) Kuranakhite – a new supergene tellurium mineral. *Zapiski Rossiyskogo Mineralogicheskogo Obshchestva*, **104**, 310–313.

Yamanaka, T., Uchida, A. and Nakamoto, Y. (2013) Structural transition of post-spinel phases $CaMn_2O_4$, $CaFe_2O_4$ and $CaTi_2O_4$ under high pressures up to 80 GPa. *American Mineralogist*, **93**, 1874–1881.

Yan, X.H., Mo, S., Ju, Z.H., Wu, J.G. and Yao, K.L. (2008) Synthesis and structure of a series of Anderson-Evans type heteropolymolybdates: $(Ln(H_2O)_n)_2(TeMo_6O_{24}) \cdot 6(H_2O)$. *Synthesis and Reactivity in Inorganic, Metal-Organic and Nano-Metal Chemistry*, **38**, 529–533.

Yeon, J., Kim, S.-H., Hayward, M.A. and Halasyamani, P. S. (2011*a*) "*A*" cation polarity control in $ACuTe_2O_7$ ($A = Sr^{2+}$, Ba^{2+}, or Pb^{2+}). *Inorganic Chemistry*, **50**, 8663–8670.

Yeon, J.H., Kim, S.-H. and Halasyamani, P.S. (2011*b*) Crystal structure of a new quinternary oxide: $NaTl_3Cu_4Te_2O_{12}$. *Journal of Chemical Crystallography*, **41**, 328–331.

Yeon, J., Kim, S.-H., Green, M.A., Bhatti, K.P., Leighton, C. and Halasyamani, P.S. (2012*a*) Syntheses, crystal structures, and characterization of two new Tl^+-Cu^{2+}-Te^{6+} oxides: Tl_4CuTeO_6 and $Tl_6CuTe_2O_{10}$. *Journal of Solid State Chemistry*, **196**, 607–613.

Yeon, J., Kim, S.-H., Nguyen, S.D., Lee, H. and Halasyamani, P.S. (2012*b*) Two new noncentrosymmetric (NCS) polar oxides: syntheses, characterization, and structure-property relationships in $BaMTe_2O_7$ ($M = Mg^{2+}$ or Zn^{2+}). *Inorganic Chemistry*, **51**, 2662–2668.

Yin, Y. and Keszler, D.A. (1992) Crystal chemistry of colquiriite-type fluorides. *Chemistry of Materials*, **4**, 645–648.

Yu, Y., Ok, K.M. and Halasyamani, P.S. (2004) Synthesis and characterization of two novel mixed metal tellurates: $KGaTeO_5 \cdot H_2O$ and $K_3GaTe_2O_8(OH)_2 \cdot H_2O$. *Dalton Transactions*, **2004**, 392–396.

Yun, G., Hwang, Y., Yun, H., Do, J. And Jacobson, A.J. (2010) A vanadium tellurate, $(NH_4)_2[VO_2]_2[TeO_4(OH)_2]$, containing two edge-shared square-pyramidal VO_5 groups. *Inorganic Chemistry*, **49**, 229–233.

Zachariasen, W. (1928) On the crystal structure of bixbyite and of synthetic Mn_2O_3. *Zeitschrift für Kristallographie*, **67**, 455–464.

Zalkin, A. and Templeton, D.H. (1964) X-ray diffraction refinement of the calcium tungstate structure. *Journal of Chemical Physics*, **40**, 501–504.

Zavodnik, V.E., Ivanov, S.A. and Stash, A.I. (2007) The alpha-phase of $SrTeO_3$ at 295 K. *Acta Crystallographica*, **E63**, i75–i76.

Zavodnik, V.E., Ivanov, S.A. and Stash, A.I. (2008) alpha-Lead tellurite from single-crystal data. *Acta Crystallographica*, **E64**, i16–i16.

Zhang, D. and Johnsson, M. (2008) $Zn_2(TeO_3)Br_2$. *Acta Crystallographica*, **E64**, i26–i26.

Zhang, D. and Johnsson, M. (2009) Nickel vanadium tellurium oxide, $NiV_2Te_2O_{10}$. *Acta Crystallographica*, **C65**, i9–i10.

Zhang, D., Johnsson, M., Berger, H., Kremer, R.K., Wulferding, D. and Lemmens, P. (2009*a*) Separation of the oxide and halide part in the oxohalide $Fe_3Te_3O_{10}Cl$ due to high Lewis acidity of the cations. *Inorganic Chemistry*, **48**, 6599–6603.

Zhang, D., Johnsson, M. and Kremer, R.K. (2010*a*) Two new layered oxohalides in the system Cu-Yb-Te-O-Cl. *Solid State Sciences*, **12**, 536–540.

Zhang, D., Kremer, R.K., Lemmens, P., Choi, K.-Y., Liu, J., Wnagbo, M., Berger, H., Skourski, Yu. and Johnsson, M. (2011*a*) Crystal structure and magnetic

https://doi.org/10.1180/minmag.2016.080.093 Published online by Cambridge University Press

properties of two new antiferromagnetic spin dimer compounds: $FeTe_3O_7X$ (X = Cl, Br). *Inorganic Chemistry*, **50**, 12877–12885.

Zhang, J.J., Zhang, Z.H., Zhang, W.G., Zheng, Q.X., Sun, Y.X., Zhang, C.Q. and Tao, X.T. (2011*b*) Polymorphism of $BaTeMo_2O_9$: a new polar polymorph and the phase transformation. *Chemistry of Materials*, **23**, 3752–3761.

Zhang, J.J., Zhang, Z.H., Sun, Y.X., Zhang, C.Q., Zhang, S.J., Liu, Y. and Tao, X.T. (2012*a*) $MgTeMoO_6$: A neutral layered material showing strong second-harmonic generation. *Journal of Materials Chemistry*, **19**, 9921–9927.

Zhang, S., Jiang, H., Sun, C.F. and Mao, J.G. (2009*b*) Syntheses, crystal structures, and properties of five new transition metal molybdenum(VI) selenites and tellurites. *Inorganic Chemistry*, **48**, 11809–11820.

Zhang, S., Hu, C., Sun, C.F. and Mao, J.G. (2010*b*) Syntheses and crystal structures of a series of alkaline earth vanadium selenites and tellurites. *Inorganic Chemistry*, **49**, 11627–11636.

Zhang, S., Hu, C. and Mao, J. (2011*c*) New mixed metal selenites and tellurites containing Pd^{2+} ions in a square planar geometry. *Dalton Transactions*, **41**, 2011–2017.

Zhang, S., Hu, C., Li, P., Jiang, H. and Mao, J. (2012*b*) Syntheses, crystal structures and properties of a new lead(II) or bismuth(III) selenites and tellurite. *Dalton Transactions*, **41**, 9532–9542.

Zhou, Y., Hu, C., Hu, T., Kong, F. and Mao, J.G. (2009) Explorations of new second-order NLO materials in the Ag(I)-Mo(VI)/W(VI)-Te(IV)-O systems. *Dalton Transactions*, **2009**, 5747–5754.

Zikmund, Z. (1967) On the crystal structure of orthorhombic $K_2TeO_3(OH)_2(H_2O)_{2.5}$. *Czechoslovak Journal of Physics*, **17**, 196–198.

Zilber, R., Durif, A. and Averbuch-Pouchot, M.T. (1980*a*) Structure of potassium sulfate tellurate: $Te(OH)_6K_2SO_4$. *Acta Crystallographica*, **B36**, 2743–2745.

Zilber, R., Tordjman, I. and Guitel, J.C. (1980*b*) Structure of sodium sulfate tellurate. *Acta Crystallographica*, **B36**, 2741–2743.

Zilber, R., Durif, A. and Averbuch-Pouchot, M.T. (1981) Structure of ammonium sulfate tellurate $Te(OH)_6 \cdot (NH_4)_2SO_4$. *Acta Crystallographica*, **B37**, 650–652.

Zilber, R., Durif, A. and Averbuch-Pouchot, M.T. (1982) Structure of thallium sulfate tellurate $Te(OH)_6 \cdot Tl_2SO_4$. *Acta Crystallographica*, **B38**, 1554–1556.

Zimmermann, I., Kremer, R.K. and Johnsson, M. (2011) crystal structure and magnetic properties of the open framework compound $Co_3Te_2O_2(PO_4)_2(OH)_4$. *Journal of Solid State Chemistry*, **184**, 3080–3084.

Zitzer, S. and Schleid, T. (2009) Ein neues Selten-Erd-Metall(III)-Oxidchlorid-Oxotellurat(IV): $Nd_5O_4Cl_3[TeO_3]_2$. *Zeitschrift für Naturforschung, B: Chemical Sciences*, **64**, 197–203.

Zitzer, S. and Schleid, T. (2010) The first alkali-metal lanthanoid(III) iodide oxotellurate(IV): $Na_2Lu_3I_3[TeO_4]_3$. *Zeitschrift für anorganische und allgemeine Chemie*, **636**, 1050–1055.

Zoltai, T. (1960) Classification of silicates and other minerals with tetrahedral structures. *American Mineralogist*, **45**, 960–973.

https://doi.org/10.1180/minmag.2016.080.093 Published online by Cambridge University Press